**CENTRO DE INVESTIGACIÓN Y DE ESTUDIOS AVANZADOS DEL INSTITUTO POLITÉCNICO NACIONAL**

**UNIDAD ZACATENCO**

**DEPARTAMENTO DE TOXICOLOGÍA**

**"Efecto de la exposición a manganeso en el control traduccional en células gliales"**

Tesis que presenta:
**M. en C. JAZMÍN SOTO VERDUGO**

Para obtener el grado de
**Doctora en Ciencias**

En la especialidad de
**Toxicología**

Director de tesis:
**Dr. Arturo Ortega Soto**

Ciudad de México                                          Febrero de 2023

**DEDICATORIA**

*A mi familia*

## AGRADECIMIENTOS

A Dios.

A mis padres, Martha Verdugo y Luis Soto, que con su ejemplo de disciplina, perseverancia y trabajo duro han forjado la persona que ahora soy. Gracias por sus palabras de aliento, comprensión y todo el amor que me han dado en cada momento de mi vida. Les agradezco por creer en mí y brindarme su apoyo incondicional.

A mis hermanas, Brisa y Luisa, por todos los momentos que hemos vivido juntas. Gracias por enseñarme a compartir y por inspirarme con su ejemplo a ser yo misma.

A toda mi familia, por sus oraciones y palabras de aliento. En especial a mi tía Griselda Rábago.

A Manuel Viveros, gracias por brindarme tu amor, compresión y cariño, incluso en los momentos no tan gratos.

A mis compañeros y amigos de generación de doctorado, por todos los momentos que compartimos durante este tiempo, les deseo éxito en todo lo que se propongan.

Al colegio de profesores del departamento de Toxicología, agradezco sus enseñanzas y apoyo en mi formación académica. De la misma manera, agradezco al personal administrativo del departamento, en especial a Lucina González.

A mis compañeros del laboratorio 31, gracias por compartir tantos buenos y malos momentos juntos. Por sus enseñanzas dentro y fuera del laboratorio, gracias por su amistad.

A todos los estudiantes de verano de investigación que tuve el honor de instruir y que me asistieron durante el desarrollo de este proyecto.

A Luisa Hernández, Luis Cid y Blanca Ibarra del departamento de Toxicología gracias por su asesoría técnica en los métodos realizados en este trabajo.

A mis asesores, la Dra. Libia Vega; la Dra. Esther López-Bayghen; el Dr. Bulmaro Cisneros y el Dr. Gabriel Roldán por todas sus observaciones, sugerencias y tiempo invertido en el enriquecimiento de este proyecto.

A la Dra. Babette Fuss, muchas gracias por darme la confianza de aportar mi granito de arena en su laboratorio, por compartir su conocimiento y tiempo conmigo. Así como a Sati Afshari y la Dra. Edna Suárez gracias por su brindarme su amistad, consejos y asistencia técnica durante mi estancia académica.

A la persona que hizo posible este proyecto, Dr. Ortega, le agradezco por permitirme formar parte de su grupo de trabajo y compartirme de su experiencia. Por su confianza, paciencia y palabras de aliento durante los últimos seis años. Gracias por guiarme en el andar científico.

Al CONACyT, por la beca otorgada durante el desarrollo de este proyecto.

Al Cinvestav, por acogerme durante mis estudios de posgrado.

## RESUMEN

El manganeso ($Mn^{2+}$) es un elemento esencial en el funcionamiento correcto de múltiples procesos celulares. Sin embargo, la exposición a grandes concentraciones de este metal está asociada a la etiología de enfermedades neurodegenerativas. El $Mn^{2+}$ atraviesa la barrera hematoencefálica a través de diversos transportadores de metales y se acumula en células gliales y neuronas. Dentro de los mecanismos de toxicidad activados por la exposición a $Mn^{2+}$, la excitotoxicidad es uno de los más importantes. En nuestro grupo de trabajo se ha descrito que el tratamiento con glutamato (Glu) a concentraciones excitotóxicas, es capaz de modular la maquinaria traduccional alterando el proceso de síntesis de proteínas en células gliales. La traducción tiene un costo alto de energía, por lo que en situaciones de estrés energético este proceso es ralentizado para conservar la homeostasis celular. Además, la disrupción del metabolismo energético es uno de los mecanismos de toxicidad asociados a la exposición a este metal. Por lo anterior, el objetivo de este proyecto fue determinar el efecto de la exposición a $Mn^{2+}$ en la maquinaria traduccional en células gliales de Bergmann (CGB).

El tratamiento con $MnCl_2$ no disminuye la viabilidad celular en términos de actividad metabólica. Aumenta la fosforilación de Akt en forma dependiente de la dosis y del tiempo de exposición a $MnCl_2$, este efecto es modulado por la cinasa de fosfatidilinositol 3 (PI3K). Al inhibir al intercambiador de $Na^+/Ca^{2+}$ (NCX) el efecto inducido por $MnCl_2$ fue abatido. El tratamiento con $MnCl_2$ aumenta la fosforilación de la proteína de unión al factor de inicio de la traducción 4E (4E-BP1) y este efecto está modulado por el complejo 1 del blanco mecanístico de la rapamicina (mTOR), el regulador maestro de la traducción. De manera relevante, observamos que el tratamiento con $Mn^{2+}$ incrementa la síntesis global de proteínas a partir de los 10 min de exposición manteniéndose elevada por al menos una hora. Por otro lado, el patrón de fosforilación de la proteína AMPK, también es modificado por el tratamiento con $MnCl_2$, apoyando la idea de que el $Mn^{2+}$ promueve un déficit energético después de la activación de la síntesis de proteínas. Estos resultados sugieren que la exposición a $Mn^{2+}$ promueve un cambio en la tasa traducción de proteínas, el cual podría estar relacionado con los niveles de ATP, provocando un cambio en el repertorio proteico de las células gliales vía PI3K/Akt/mTOR. Nuestros hallazgos resaltan la importancia de las células gliales en la neurotoxicidad ocasionada por la exposición a $Mn^{2+}$.

*Palabras clave: Manganeso, Control traduccional, PI3K/Akt, Células gliales, AMPK, 4E -BP1*

## ABSTRACT

Manganese ($Mn^{2+}$) is an essential trace element for the proper functioning of multiple cellular processes. However, exposure to high concentrations of this metal is associated with the etiology of neurodegenerative diseases. $Mn^{2+}$ permeates the blood-brain barrier through various metal transporters and accumulates in glial cells and neurons. Among the mechanisms of toxicity activated by $Mn^{2+}$ exposure, excitotoxicity is the most important. In our lab group, it has been reported that treatment with glutamate (Glu) at excitotoxic concentrations can modulate the translational machinery and alter the process of protein synthesis in glial cells. Translation has a high energy cost; therefore, in situations of energy stress, this process is slowed down to preserve cellular homeostasis. In addition, the disruption of energy metabolism is one of the mechanisms of toxicity associated with exposure to this metal. Therefore, this study aimed to determine the effect of $Mn^{2+}$ exposure on the translational machinery of radial glial cells. Treatment with $MnCl_2$ did not decrease cell viability in terms of metabolic activity. An increase in Akt phosphorylation in a dose- and time-dependent manner upon exposure to $MnCl_2$ was observed, which was modulated by phosphatidylinositol kinase 3 (PI3K). However, by inhibiting the $Na^+/Ca^{2+}$ (NCX) exchanger, the effect induced by $MnCl_2$ was abated. $MnCl_2$ treatment increased the phosphorylation of eukaryotic translation initiation factor 4E-binding protein 1 (4E-BP1), and this effect was modulated by the mechanistic target of rapamycin (mTOR) complex 1, the master regulator of protein translation. $Mn^{2+}$ treatment increased global protein synthesis after 10 min of exposure and remained elevated for at least one hour. In contrast, the phosphorylation pattern of AMPK protein was also modified by treatment with $MnCl_2$, supporting the idea that $Mn^{2+}$ promotes an energy deficit after the activation of protein synthesis. These results suggest that exposure to $Mn^{2+}$ promotes a change in the protein translation rate, which could be related to ATP levels, causing a change in the protein repertoire of glial cells via the PI3K/Akt/mTOR pathway. Our findings highlight the importance of glial cells in neurotoxicity caused by exposure to $Mn^{2+}$.

*Keywords: Manganese, Translational Control, PI3K7Akt, Glial Cells, AMPK, 4E-BP1*

## ABREVIATURAS

**4E-BP1** • Proteína de unión 1 al factor del inicio de la traducción 4E
**ADAM** • Desintegrina y metaloproteinasa
**ADP** • Adenosín difosfato
**Akt** • Proteína cinasa B
**AMP** • Adenosín monofosfato
**AMPA** • Ácido α-amino-3-hidroxi-5-metilo-4-isoxazolpropiónico
**AMPK** • Proteína cinasa dependiente del adenosín monofosfato
**ANOVA** • Análisis de varianza
**ATD** • Dominio amino-terminal extracelular
**ATP** • Adenosín trifosfato
**CaMKII** • $Ca^{2+}$/Calmodulina proteína cinasa II
**CGB** • Células gliales de Bergmann
**CPM** • Cuentas por minuto
**CRD** • Dominio rico en cisteína
**CTD** • Dominio carboxilo terminal intracelular
**DA** • Dopamina
**DAG** • Diacilglicerol
**DMSO** • Dimetilsulfóxido
**EAAT** • Transportador de aminoácidos excitadores
**eEF1A** • Factor eucariótico de elongación 1A
**eEF1B** • Factor eucariótico de elongación 1B
**eEF2** • Factor eucariótico de elongación 2
**eEF2K** • Cinasa del factor de eucariotico de elongación 2
**eIF1** • Factor de inicio de la traducción 1
**eIF2** • Factor de inicio de la traducción 2
**eIF2** • Factor eucariótico del inicio de la traducción 2
**eIF3** • Factor de inicio de la traducción 3
**eIF4E** • Factor de inicio de la traducción 4E
**eIF4E** • Factor eucariótico del inicio de la traducción 4E
**eIF5** • Factor de inicio de la traducción 5
**eRF1** • Factor eucariótico de liberación 1
**eRF3** • Factor eucariótico de liberación 3
**ERK 1/2** • Proteína cinasa regulada por señales extracelulares 1/2
**GABA** • Ácido γ-aminobutírico
**GCN** • Cinasa de control general no-deprimible
**GDP** • Guanosín bifosfato
**GLAST** • Transportador de Glutamato-Aspartato (EAAT1)
**Gln** • Glutamina
**GLT1** • Transportador de Glu 1 (EAAT2)
**Glu** • Glutamato
**GluR** • Receptor de glutamato
**GS** • Glutamina sintetasa
**GTP** • Guanosín trifosfato
**HRI** • Cinasa inhibidora hemo-regulada
**IGFR** • Receptor del Factor de Crecimiento similar a la Insulina tipo I
**iGluR** • Receptor de glutamato ionotrópico
**IP3** • 1,4,5-trifosfato
**IR** • Receptor de insulina
**JNK** • cinasa c-Jun N-terminal
**KA** • Kainato
**LBD** • Dominio de unión a ligando
**LKB1** • Cinasa hepática B1
**MAPK** • Proteína cinasa activada por mitógenos
**MCU** • Uniporte de $Ca^{2+}$ mitocondrial
**mGluR** • Receptor de glutamato metabotrópico

**MLK1** • Cinasa de MAPKK
**MMP** • Metaloproteinasa de matriz extracelular
**MMT** • Metilciclopentadienil tricarbonil manganeso
**MNK** • Cinasas que interactúan con las MAPK
**mPTP** • Poro de transición de permeabilidad mitocondrial
**MRI** • Imagen de resonancia magnética
**mRNA** • Ácido ribonucleico mensajero
**mTOR** • Objetivo mecanístico de la rapamicina
**MTT** • Bromuro de 3-[4,5-dimetiltiazol-2-il]-2,5-difeniltetrazolio
**NCX** • Intercambiador de $Na^+/Ca^{2+}$
**NMDA** • *N*-metil-D-aspartato
**OPC** • Células progenitoras de oligodendrocitos (NG2)
**p70S6K** • Cinasa de la proteína ribosomal S6
**PABP** • Proteína de unión a secuencias de poliadenilación
**PAGE** • Gel de poliacrilamida
**PD** • Enfermedad de Parkinson
**PDK** • Cinasa dependiente de fosfoinositol
**PERK** • Cinasa de retículo endoplásmico similar a PKR
**PI3K** • Cinasa de fosfatidilinositol 3
**PIC** • Complejo de preinicio
**PIP2** • Fosfatidilinositol 4,5-bifosfato
**PIP3** • Fosfatidilinositol 3,4,5-trifosfato
**PKC** • Proteína cinasa C
**PKR** • Proteína cinasa R
**PLP** • Fosfolipasa C
**PMSF** • Fenilmetilsulfonilo
**PTC** • Centro peptidil transferasa ribosomal
**PTEN** • Proteína fosfatasa homóloga de tensina
**Rheb** • Homólogo de Ras enriquecido en cerebro
**RSK** • Cinasa ribosomal S6 (p90RSK)
**RTK** • Receptor tirosina cinasa
**S6K** • Cinasa ribosomal S6 (p70S6)
**SDS** • Dodecil sulfato de $Na^+$
**SFB** • Suero Fetal Bovino
**Slc1** • Familia acarreadora de solutos 1
**SNC** • Siatema nervioso central
**SNP** • Sistema nervioso periférico
**SOD2** • Superóxido dismutasa 2
**TAK1** • Cinasa activada de TGF-β
**TC** • Complejo ternario
**TMD** • Dominio transmembranal
**tRNA** • Ácido ribonucleico de transferencia
**TSC1** • Complejo de esclerosis tuberosa 1
**TSC2** • Complejo de esclerosis tuberosa 2
**VFT** • Dominio venus fly-trap

# ÍNDICE GENERAL

## I.  INTRODUCCIÓN

### 1.1. Las células gliales: su importancia en el sistema nervioso central

El sistema nervioso central (SNC) está construido principalmente de dos tipos de células: neuronas y glía. Las neuronas se encargan directamente de la transmisión y el procesamiento de información, mientras las últimas llevan a cabo funciones tales como: mantener la barrera hematoencefálica, regular el flujo sanguíneo regional, proveer de soporte antioxidante, trófico y metabólico a las neuronas, además del reciclaje de neurotransmisores y regular la sinaptogénesis, así como la transmisión sináptica [1].

Existen diversos tipos de células gliales, en el sistema nervioso periférico (SNP) podemos encontrar a las células de Schwann, las cuales se encargan de producir mielina y se encuentran relacionadas de manera importante con la propagación de impulsos nerviosos, y a las células satélites que envuelven el soma neuronal [2].

Por otro lado, en el SNC tenemos dos principales tipos de glía: microglía y macroglía. La microglía, es reconocida como los macrófagos del encéfalo dada su especializada actividad inmune. La macroglía, cuenta con funciones tan variadas como sus tipos celulares y está conformada por: glía radial, astrocitos, células progenitoras de oligodendrocitos (OPCs, también conocidas como células NG2) y oligodendrocitos [3,4] (**Figura 1**).
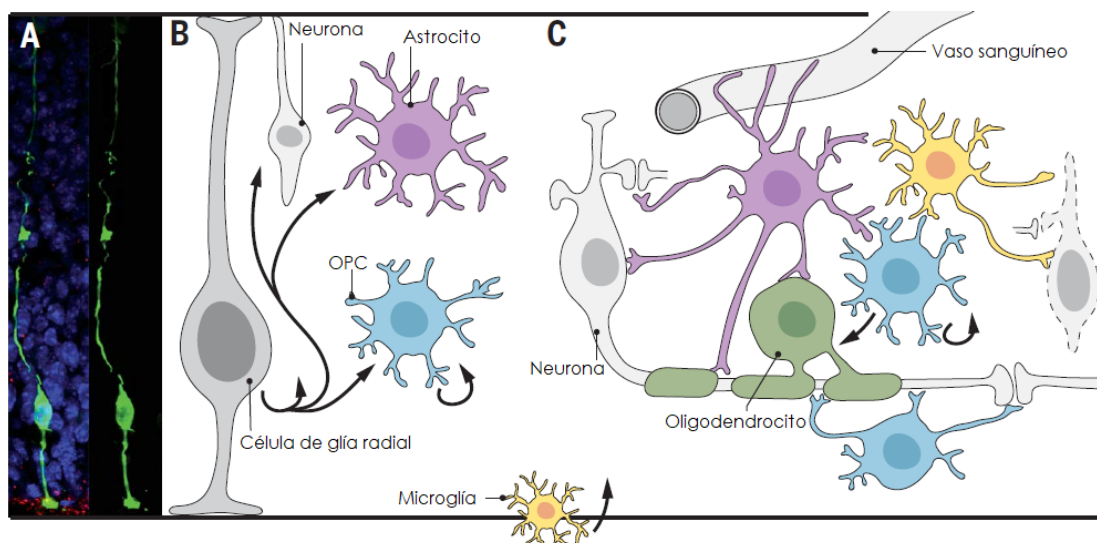


*Figura 1. Células gliales del sistema nervioso central. A) Imagen confocal de una célula de glía radial. B) Las células de glía radial son las principales células progenitoras neuroepiteliales del SNC. C) Interacción entre las neuronas y las células gliales. OPCs: células progenitoras de oligodendrocitos. Modificada de* [3].

La glía radial, por ejemplo, actúa como progenitora de la mayoría de las neuronas y células gliales, ya sea de manera directa o por medio de progenitores intermediarios como las OPCs. Las OPCs son las células más proliferativas del SNC generando oligodendrocitos mielinizantes, y probablemente cuentan con múltiples papeles en la formación y función de circuitos neuronales [5].

Los oligodendrocitos maduros, por su parte, generan la envoltura de mielina que agiliza la conducción de impulsos nerviosos y provee de soporte metabólico a los axones, donde la regulación dinámica de la mielinización puede regular la sincronización de la propagación de información y la comunicación a través de circuitos funcionales [6].

Finalmente, los astrocitos son las células de forma estrellada que interactúan con cientos de procesos en el SNC, y exhiben un amplio rango de actividades que colaboran con el desarrollo del sistema nervioso y diseñan su actividad [3].

### 1.1.1. Células gliales de Bergmann

Las células gliales de Bergmann (CGBs) son un tipo de glía radial específica del cerebelo. Sin duda, el cerebelo es reconocido por su papel en el procesamiento de la función motora, sin embargo, cada vez hay más evidencias acerca de su importante participación en funciones cognitivas superiores. La corteza cerebelar adulta es una estructura trilaminar (**Figura 2**), conformada por la capa granular interna, compuesta como su nombre lo denota de células granulares, la capa intermedia donde reside el soma de las CGBs y las neuronas de Purkinje, extendiendo sus procesos hasta la capa molecular externa.

De manera similar a los astrocitos protoplásmicos en otras partes del cerebro, los procesos de las CGBs cubren las sinapsis de las dendritas de las neuronas de Purkinje, lo cual sugiere un importante papel en la regulación de la transmisión sináptica [7].

Las CGBs son esenciales en la migración y la correcta estratificación de las células granulares en el desarrollo temprano del cerebelo. Sin embargo, estas células permanecen como parte del circuito cerebelar adulto, donde llevan a cabo importantes actividades como la homeostasis de iones extracelulares, la estabilidad sináptica, la plasticidad, la neuroprotección y la función metabólica. Por lo cual se les considera como la unidad canónica computacional del cerebelo, ya que no sólo se encargan de funciones esenciales de mantenimiento sino también del procesamiento de información llevado a cabo en el cerebelo [8].

Los tipos celulares del cerebelo surgen de dos regiones germinales principales del cerebelo embrionario: el labio rómbico anterior, localizado en la región dorsal del cerebelo posterior, que da lugar a neuronas glutamatérgicas (neuronas nucleares y granulares) y la zona ventricular, que produce neuronas de Purkinje GABAérgicas (Ácido γ-aminobutírico), interneuronas GABAérgicas y células gliales. Por su sencilla conformación celular, el cerebelo es un excelente paradigma experimental para estudiar la neurotransmisión glutamatérgica/GABAérgica [9].
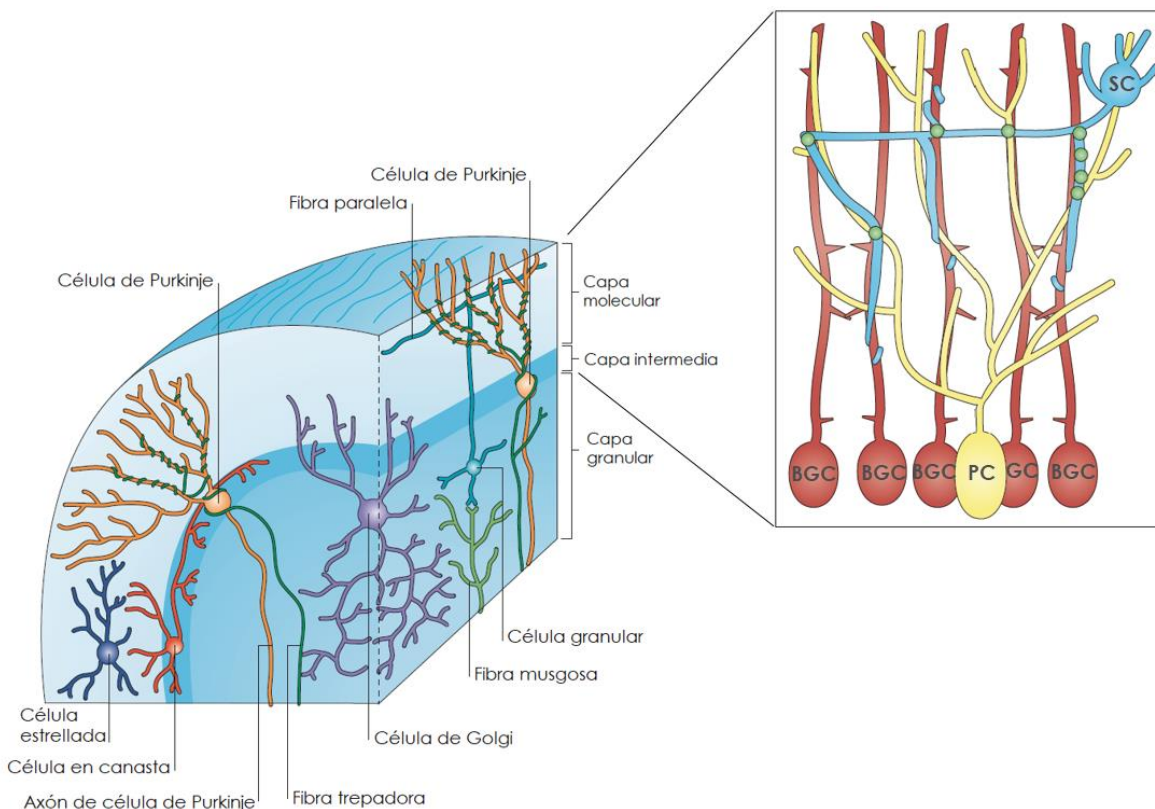


*Figura 2. Arquitectura de la corteza cerebelar. Imagen de un corte transversal de un lóbulo cortical individual, indicando la presencia de las tres capas distintivas del córtex cerebelar. Modificado de* [10,11].

### 1.2. El glutamato como neurotransmisor

El glutamato (Glu) es el principal neurotransmisor excitador del SNC. Además de ser un neurotransmisor, el Glu tiene un papel importante como intermediario metabólico en todos los órganos y tejidos, uniendo el metabolismo de aminoácidos con el metabolismo de carbohidratos a través del ciclo de los ácidos tricarboxílicos [12].

3

Las concentraciones de Glu en el medio extracelular y el líquido cefalorraquídeo se encuentran alrededor de 4 y 10 µM, respectivamente. En el SNC, el Glu se sintetiza a partir de α-cetoglutarato al añadirle un grupo amino, acción mediada por la enzima glutamato deshidrogenasa, o al remover un grupo amino de la glutamina (Gln) a través de la enzima glutaminasa [13]. El Glu funge un papel esencial en el desarrollo del SNC, en la inducción y terminación de sinapsis, así como en la migración, la diferenciación y la muerte celular.

### 1.2.1. Receptores glutamatérgicos

Con el fin de satisfacer los complejos papeles del Glu como neurotransmisor, neuromodulador y gliotransmisor, una variedad de receptores de Glu (GluRs) se encuentran a lo largo del SNC. El Glu ejerce sus acciones al activar receptores específicos de membrana, los cuales se clasifican en dos principales subtipos: los receptores ionotrópicos (iGluRs) los cuales funcionan como canales iónicos activados por ligando y los receptores metabotrópicos (mGluRs) que son receptores acoplados a proteínas G [14].

### 1.2.1.1. Receptores ionotrópicos

Los iGluRs son canales iónicos activados por ligando que permiten en influjo de cationes tras la unión de Glu. Cada canal está conformado por cuatro subunidades que cuentan con cuatro dominios conservados (**Figura 3A**), que incluyen: dominio amino-terminal extracelular (ATD), de unión a ligando (LBD), transmembranal (TMD) y un carboxilo terminal intracelular (CTD) [15].

Se han identificado tres familias de iGluRs: receptores AMPA (ácido α-amino-3-hidroxi-5-metil-4-isoxazolpropiónico), KA (kainato) y NMDA (*N*-metil-D-aspartato). Los receptores AMPA están conformados por una combinación de productos génicos individuales conocidos como GRIA1-4. Los receptores KA están conformados por 5 subunidades que se encuentran subdivididos en dos grupos, GRIK1-3 de baja afinidad y GRIK 4 y 5 que se consideran las subunidades de mayor afinidad. Los receptores NMDA están formados por combinaciones heterodiméricas de tres subfamilias; GRIN1, GRIN2A-GRIN2D y GRIN3A-3D (**Figura 3B**) [16]. Las subunidades GRIA y GRIK forman receptores homo- o heterotetraméricos que son rápidamente activados al unir el Glu al LBD, lo cual a su vez promueve su desensibilización. Los NMDARs forman

heterotetrámeros estrictos de dos subunidades GRIN1 que se unen a glicina o D-serina y dos subunidades GRIN2 que unen al Glu. Otra familia de iGluRs son los receptores δ (GLUD1 y GLUD2), los cuales no son activados directamente por ligando sin embargo son importantes para la organización transináptica y la plasticidad [17].
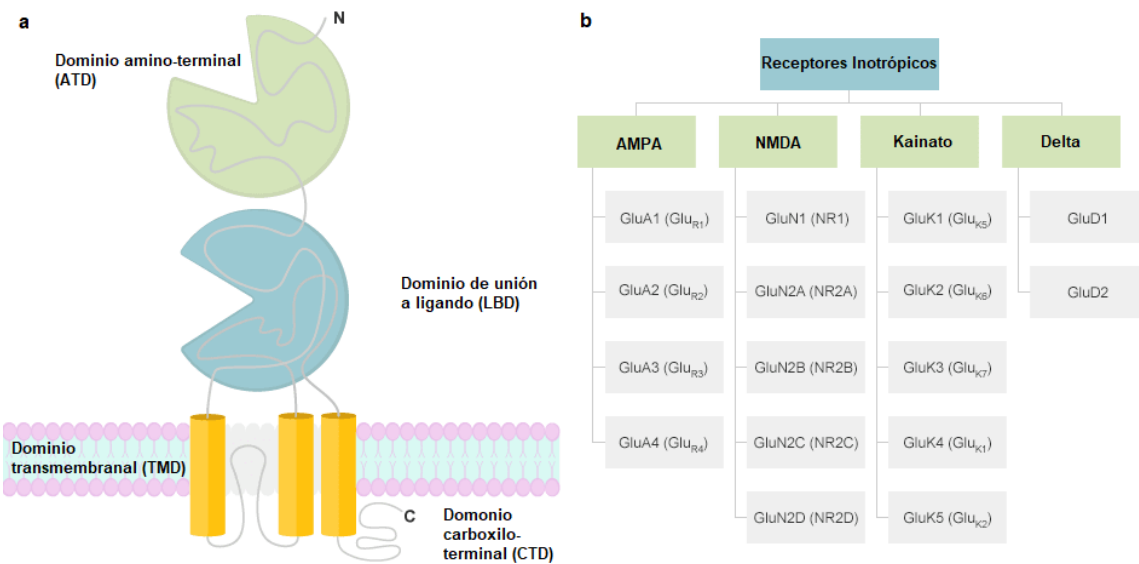


*Figura 3. Receptores inotrópicos de glutamato. **A)** Estructura básica de los receptores ionotrópicos, cuentan con 4 dominios principales: dominio amino-terminal (ATD), dominio de unión al ligando (LBD), dominio transmembranal (TMIID) y un dominio carboxilo terminal (CTD). **B)** Clasificación molecular de los receptores ionotrópicos. Modificada de* [18].

### 1.2.1.2. Receptores metabotrópicos

Los receptores metabotrópicos son receptores acoplados a proteínas G que existen como dímeros constitutivos. Todos los mGluRs comparten una estructura básica (**Figura 4A**), conformada por diferentes dominios que incluyen al ATD, que también es conocido como el dominio *venus fly-trap* (VFT) debido a su estructura particular, el dominio rico en cisteína (CRD) crítico en la dimerización y activación del receptor, así como el clásico dominio de siete segmentos transmembranales alfa-hélice (TMD) y el dominio CTD [15].

Los mGluRs están organizados en tres subfamilias basados en sus secuencias homólogas y sus proteínas G afines (**Figura 4B**). El grupo I (GRM1 y GRM5) está acoplado principalmente a proteínas $G_q$, que inician cascadas de señalización relacionadas a la vía de fosfolipasa C (PLC)/Inositol 1, 4, 5-trifosfato (IP3)/diacilglicerol (DAG). Los grupos II (GRM2 y GRM3) y III

(GRM6, GRM7 y GRM8) se encuentran acoplados a proteínas $G_{i/o}$, cuya señalización reduce los niveles de adenosín monofosfato cíclico (cAMP) [14].

Las isoformas del receptor difieren en el CTD. Algunas isoformas del grupo I (GRM1a Y GRM5a) contienen un amplio dominio rico en prolina, el cual ha sido estudiado por sus intricadas interacciones proteína-proteína y sus configuraciones complejas. Tal dominio, facilita el acople de los mGluRs con los receptores NMDA y otras proteínas [15].
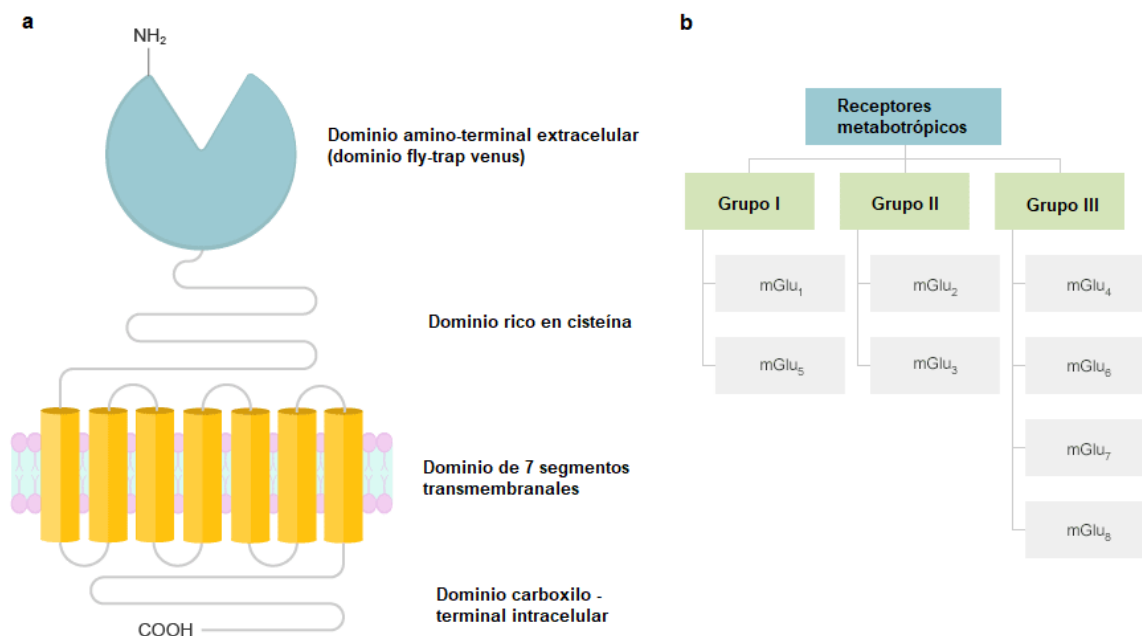


**Figura 4. Receptores metabotrópicos de glutamato.** *A) Estructura básica de los receptores metabotrópicos, cuentan con 4 dominios principales: dominio amino-terminal extracelular o venus fly-trap, dominio rico en cisteína, dominio de siete segmentos transmembranales y un dominio carboxilo terminal intracelular.* **B)** *Clasificación molecular de los receptores metabotrópicos. Modificada de* [19].

### 1.2.2. Transportadores de glutamato

La terminación de la transmisión glutamatérgica y la reducción de los niveles excesivos de Glu en el espacio sináptico se encuentra finamente regulado. Debido a que no hay enzimas que degraden el Glu de manera extracelular, la homeostasis del Glu se encuentra regulada por un sistema de captura de alta afinidad. Las proteínas transportadoras encargadas de esta actividad se localizan en la superficie celular de células gliales y neuronas, y se les ha denominado transportadores de aminoácidos excitadores (EAAT) [20].

Los EAATs pertenecen a la familia de acarreadores de solutos 1 (*Slc1*) y cinco subtipos de estos transportadores de Glu han sido identificados (EAAT1-5). Originalmente, estos transportadores fueron clonados en cerebro de rata, y fueron denominados de la siguiente manera: transportador de Glu/aspartato (GLAST) [21], transportador de Glu 1 (GLT1) [22], y el transportador de Glu neuronal EAAC1 [23]. Los cuales fueron identificados pocos años después en humano como EAAT1-3, respectivamente [24]. Otros dos transportadores fueron identificados en los siguientes años: EAAT4 [25] y EAAT5 [26]. Tales transportadores se expresan de manera diferencial en el SNC, siendo EAAT1 (**Figura 5**) y EAAT2 expresados casi exclusivamente en células gliales, mientras que EAAT3 se encuentra presente en células neuronales. EAAT4 ha sido hallado en células de Purkinje cerebelares y EAAT5 se encuentra en células fotoreceptoras de bastón y en células ganglionares de la retina [2].

El modelo estructural más aceptado de estos transportadores es el que muestra 8 segmentos transmembranales y dos bucles de horquilla (**Figura 5A**) [27]. La estequiometría del transporte de los EAATs es de 3 moléculas de $Na^+$ más una de $H^+$ por cada molécula de Glu transportada, mientras que una molécula de $K^+$ es liberada (**Figura 5B**) [28]. Estudios recientes han evidenciado el papel de los EAATs como transductores de señales, lo cual tiene una gran importancia no sólo en la función glial sino también en las interacciones glía/neurona, indispensables para llevar a cabo una correcta neurotransmisión [29].
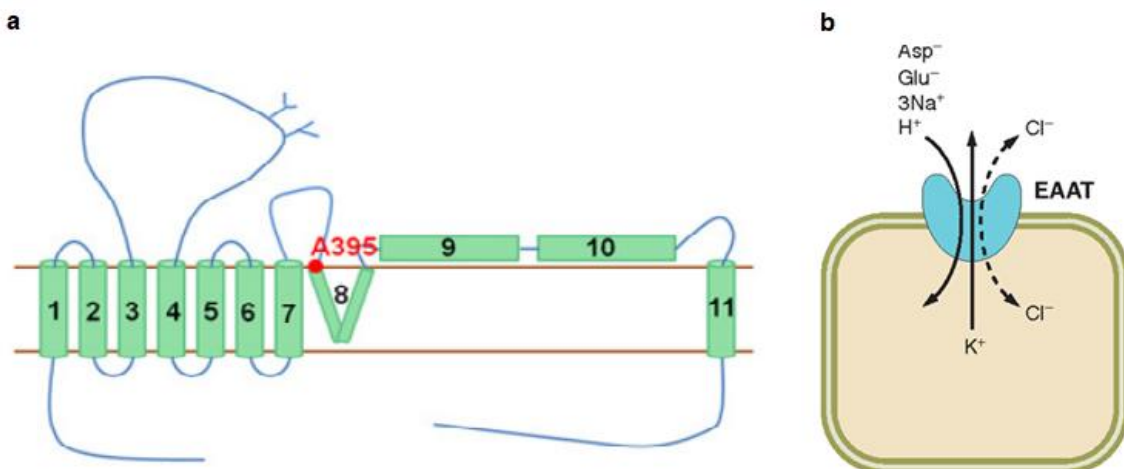


*Figura 5. Transportador de glutamato GLAST/EAAT1. A) Modelo estructural topológico del transportador EAAT1 (GLAST). B) Estequiometría del transporte de Glu, El transportador EAAT puede transportar una molécula de Glu junto con 3 moléculas de $Na^+$ y una de $H^+$ y en contraflujo una de $K^+$. Modificado de* [27,30]*.*

### 1.2.3. Lanzadera Glu/Gln

A la localización estrecha de las células gliales con las estructuras pre y postsinápticas neuronales se le conoce como sinapsis tripartita [31]. Las células gliales son capaces de detectar los niveles locales de actividad neural y, en respuesta, liberar sustancias que modulan tales sinapsis [32]. El Glu liberado a la hendidura sináptica es capturado por las células gliales gracias a los EAATs, específicamente EAAT1/GLAST en células gliales, para convertirse en Gln por la enzima glutamina sintetasa (GS). La Gln se transporta fuera de la célula glial hacia las neuronas, donde se utiliza para re-sintetizar Glu con la ayuda de la enzima glutaminasa y de esta manera continuar con la neurotransmisión [32,33].

Evidencia reciente ha demostrado que se requiere Gln extracelular para mantener los niveles máximos de la transmisión sináptica excitadora [34,35]. Esto, aunado a que la principal enzima productora de Gln (GS) se encuentra expresada mayormente en glía [36], delineó la noción de que debe existir un ciclo Glu/Gln. Originalmente se propuso que este ciclo funcionase de manera estequiométrica, estudios recientes lo cuestionan seriamente ya que una parte del Glu capturado experimenta un metabolismo oxidativo [37]. Por lo que podemos concluir que la lanzadera Glu/Gln no opera de manera estequiométrica estricta.

### 1.3. Manganeso

El manganeso ($Mn^{2+}$) es un elemento del grupo 7 de la Tabla Periódica, siendo el 5° metal y el 12° elemento más abundante en la biósfera. Se encuentra ampliamente distribuido en la corteza terrestre, alrededor del 0.1% de ésta. Su forma más común es la inorgánica, con 11 estados de oxidación de $Mn^{3-}$ a $Mn^{7+}$ [38]. Sin embargo, en sistemas biológicos, los estados predominantes de oxidación son $Mn^{2+}$ y $Mn^{3+}$ [39].

Debido sus características físicas y químicas, el $Mn^{2+}$ es usado en una gran variedad de actividades industriales; en la agricultura, el $Mn^{2+}$ está presente en varios pesticidas y fungicidas, como el Maneb y el Mancozeb. En el consumo de energía, se utiliza como antidetonante en el MMT (metilciclopentadienil tricarbonil manganeso) como aditivo de gasolina, induce la liberación de fosfato de $Mn^{2+}$ en la atmósfera tras la combustión del hidrocarburo. Por sus propiedades paramagnéticas, el $Mn^{2+}$ sirve como agente de contraste en imágenes de resonancia magnética (MRI) en medicina. En manufactura, el $Mn^{2+}$ es utilizado en la producción de baterías, cerámica,

acero, cosméticos y vidriería. Concentraciones considerablemente altas de este metal han sido encontradas en fórmula láctea infantil (69.8-741.0 µg/L), así como en nutrición parenteral total (310 µg/L) [40]. Recientemente, se ha descrito la presencia de $Mn^{2+}$ en drogas psicoestimulantes derivadas de la pseudoefedrina (600 mg/L), la cual utiliza permanganato de potasio como agente oxidante en su síntesis [41].

### 1.3.1. La dualidad del $Mn^{2+}$: toxicidad versus esencialidad

El $Mn^{2+}$ es un metal de transición esencial, debido a que es requerido en la función inmune, la apropiada regulación de la glucosa en la sangre y energía celular, la reproducción, la digestión, el crecimiento óseo, la coagulación sanguínea, y en la defensa contra las especies reactivas de oxígeno [42]. Esta variedad de funciones fisiológicas es posible gracias a la incorporación de este metal a metaloproteínas, enzimas como la arginasa, la glutamina sintetasa, la fosfoenolpiruvato decarboxilasa, la piruvato carboxilasa y la $Mn^{2+}$ superóxido dismutasa (SOD) [42]. Además, estudios recientes han identificado que el $Mn^{2+}$ tiene un papel importante en el metabolismo de la urea y en el proceso de autofagia [43].

Sin embargo, a pesar de ser un elemento esencial, la exposición crónica a este metal puede tener efectos deletéreos en el sistema respiratorio, reproductivo y el SNC. La afección característica tras la exposición crónica a $Mn^{2+}$ es la enfermedad neurodegenerativa denominada manganismo, la cual presenta síntomas similares a los de la enfermedad de Parkinson [44,45]; esta enfermedad se reporta principalmente en personal ocupacionalmente expuesto de las industrias minera y del acero, expuestos de manera crónica al polvos o aerosoles que contienen el metal [42,43].

### 1.3.2. Toxicocinética

Dadas las diversas fuentes de exposición al $Mn^{2+}$, las principales rutas de absorción en el organismo pueden ser tanto gastrointestinal (3-5%) como inhalatoria, aunque la exposición por administración intravenosa, *in utero* y dérmica no deben descartarse. Una vez que este metal ha ingresado al organismo es absorbido en el torrente sanguíneo a través de transporte activo o por difusión pasiva, lo cual es mediado por transportadores de $Mn^{2+}$ y proteínas que se unen a este metal [40,46,47].

Una vez que ha entrado al torrente sanguíneo el $Mn^{2+}$ es rápidamente distribuido a diferentes tejidos, como el hígado (1.2-1.3 mg/kg), el páncreas (1.04 mg/kg), los huesos (1 mg/kg), los riñones (0.98 mg/kg) y el encéfalo (0.15-0.46 mg/kg) son los órganos en los cuales se encuentran mayores niveles de $Mn^{2+}$[40]. Diversos estudios epidemiológicos han reportado efectos tóxicos neuronales, reproductivos y respiratorios. Sin embargo, aunque el encéfalo no es el tejido con mayor acumulación de $Mn^{2+}$, es el principal blanco de los efectos tóxicos que este metal ocasiona. Finalmente, la eliminación del $Mn^{2+}$ es llevada a cabo principalmente mediante excreción hepatobiliar (80%), donde el exceso de $Mn^{2+}$ es conjugado en la bilis y excretado en heces fecales. En menor proporción, el $Mn^{2+}$ también puede ser excretado mediante orina, leche materna y sudor [40].

### 1.3.3. Mecanismos de toxicidad del $Mn^{2+}$

Los mecanismos por los cuales el $Mn^{2+}$ puede llevar a cabo procesos de neurodegeneración siguen sin ser completamente elucidados. Sin embargo, diversos estudios establecen como posibles mecanismos de acción del $Mn^{2+}$ principales: a) a la disfunción mitocondrial y metabolismo energético alterado, b) la alteración en los niveles de neurotransmisores y excitotoxicidad y, c) la activación de proteasas y muerte apoptótica [46].

#### 1.3.3.1. Disfunción mitocondrial y metabolismo energético

Las mitocondrias son cruciales en múltiples procesos celulares, como la síntesis de ATP, el metabolismo energético, la óxido-reducción y la muerte celular. Su funcionamiento se encuentra regulado por una red integrada de vías de señalización relacionadas con la biogénesis y dinámica mitocondrial, así como la mitofagia [48]. Cualquier disrupción en este sistema de control mitocondrial puede conducir a la degeneración neuronal y el desarrollo de múltiples enfermedades neurodegenerativas [49,50]. El $Mn^{2+}$ es un importante cofactor de la enzima SOD2, una enzima antioxidante de gran importancia localizada en la mitocondria. Sin embargo, la acumulación de $Mn^{2+}$ en la mitocondria interrumpe la homeostasis y, por ende, daña la función mitocondrial (**Figura 6**) [51–53]. Diversos estudios han demostrado que el $Mn^{2+}$ es capaz de inhibir a los complejos I y II de la cadena respiratoria además de inducir la transición de la permeabilidad mitocondrial [54–56]. La interferencia en el proceso de fosforilación oxidativa y la inhibición de

la actividad mitocondrial eventualmente llevará a la depleción de ATP, comprometiendo el metabolismo energético de la célula [46]. Este colapso bioenergético es particularmente deletéreo para las neuronas, sobre todo durante la activación neural ya que dependen de manera específica de la respiración mitocondrial para funcionar apropiadamente [57].
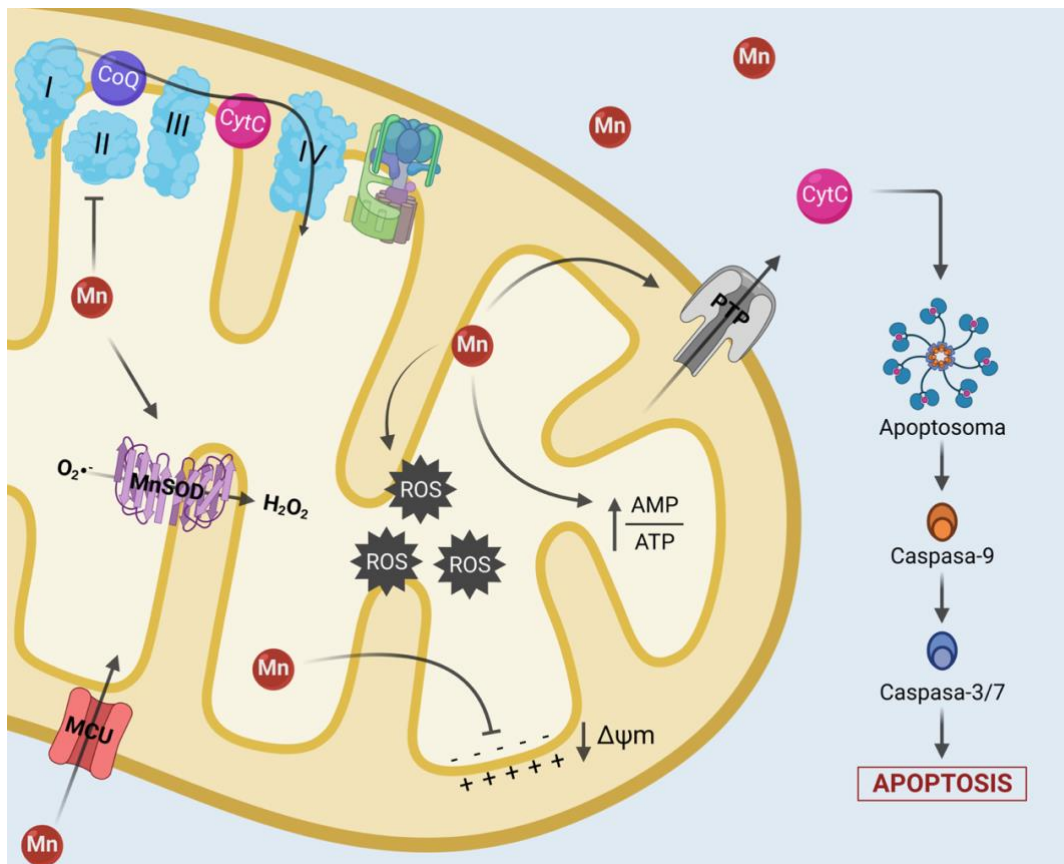


*Figura 6. Efecto del Mn$^{2+}$ en la función mitocondrial.*

La inhibición de la cadena transportadora de electrones resultante del tratamiento con Mn$^{2+}$ puede promover la fuga de electrones de la cadena respiratoria, lo cual lleva a la producción de especies reactivas de oxígeno, dañando directamente a la mitocondria [58]. Además, el aumento excesivo de estrés oxidante, aunado a la despolarización de la membrana mitocondrial a causa del exceso de Mn$^{2+}$ y Ca$^{2+}$ en el interior de la mitocondria, resulta en la apertura del poro de transición de permeabilidad mitocondrial (mPTP), liberando citocromo c (**Figura 6**) y favoreciendo a la activación de cascadas apoptóticas mediadas por caspasas [59]. De manera interesante, en estudios recientes, se ha propuesto a la autofagia mitocondrial como un mecanismo estratégico de las

células para disminuir los efectos deletéreos del $Mn^{2+}$, al eliminar las mitocondrias dañadas o indeseables [57,60].

### 1.3.3.2. Alteración en los niveles de neurotransmisores y excitotoxicidad

Diversos estudios han demostrado que la exposición a $Mn^{2+}$ altera los niveles de neurotransmisores como la dopamina (DA), el Glu y el GABA [42,61]. Enfocándonos específicamente en la neurotransmisión glutamatérgica (**Figura 7**), el $Mn^{2+}$ (30 mg/kg vía intraperitoneal, 3 semanas) incrementa la liberación sináptica de Glu e inhibe la conductancia de los receptores NMDA bloqueando el canal iónico de este receptor en ratas Sprague-Dawley [62].

Estudios en astrocitos corticales han mostrado como el $Mn^{2+}$ (*in vivo*: 30 mg/kg vía instilación intranasal, 21 días e *in vitro*: 250 μM, 6 h) disminuye la captura de Glu al disminuir la expresión de mRNA y proteína de GLAST/EAAT1 y GLT-1/EAAT2 en ratones C57BL/6J y en la línea celular astrocítica H4 [63,64]. En nuestro grupo de trabajo hemos descrito como la exposición a $Mn^{2+}$ (200 μM, 30 min) en un modelo de CGB modifica la actividad del transportador GLAST/EAAT1, en conjunto con una disminución en la captura de glucosa [65]. Además, la exposición a $Mn^{2+}$ (0.1-1 mM, 4-24 h) disminuye los niveles de mRNA y de proteína de los principales transportadores de Gln, con un comportamiento dependiente de la dosis en cultivo primario de astrocitos [66–68]. La enzima GS tiene una alta especificidad por el $Mn^{2+}$ ($K_d \approx 1$ μM) [69] y la exposición a $Mn^{2+}$ (125-500 μM, 24 h) lleva a una disminución en la actividad de esta enzima, así como una reducida expresión de su mRNA y proteína en cultivo primario de astrocitos [70].

En resumen, la exposición a $Mn^{2+}$ altera el funcionamiento de los principales efectores de la lanzadera Glu/Gln (**Figura 7**) [71]. La hiperactivación de los receptores glutamatérgicos debido a la incorrecta remoción de Glu de la hendidura sináptica ocasiona un tipo de muerte neuronal conocida como excitotoxicidad [72]. En breve, una vez que la concentración de $Mn^{2+}$ ha sobrepasado el umbral fisiológico en el SNC (incremento de 3 veces la concentración normal) [73], el Glu tiende a acumularse debido a la disminución de la expresión de los EAATs, principalmente por la activación de PKC, disminuyendo la captura de Glu. Lo que lleva al derrame de este neurotransmisor fuera de la hendidura sináptica y sobreactiva no solamente a los GluRs de la sinapsis, sino también a aquellos que se encuentran en el espacio extra-sináptico. Específicamente a los NMDARs que contienen la subunidad GRIN2B, cuya activación induce la

acción de vías de señalización de muerte celular y de un influjo excesivo de iones a la célula, principalmente de calcio, lo cual promueve la activación de proteasas, fosfolipasas y endonucleasas, concluyendo en la muerte neuronal por excitotoxicidad [74]. Por otra parte, la actividad de GS es abatida junto con la regulación a la baja del transporte de Gln, afectando gravemente todos los niveles del ciclo Glu/Gln, concluyendo en una neurotransmisión glutamatérgica defectuosa.
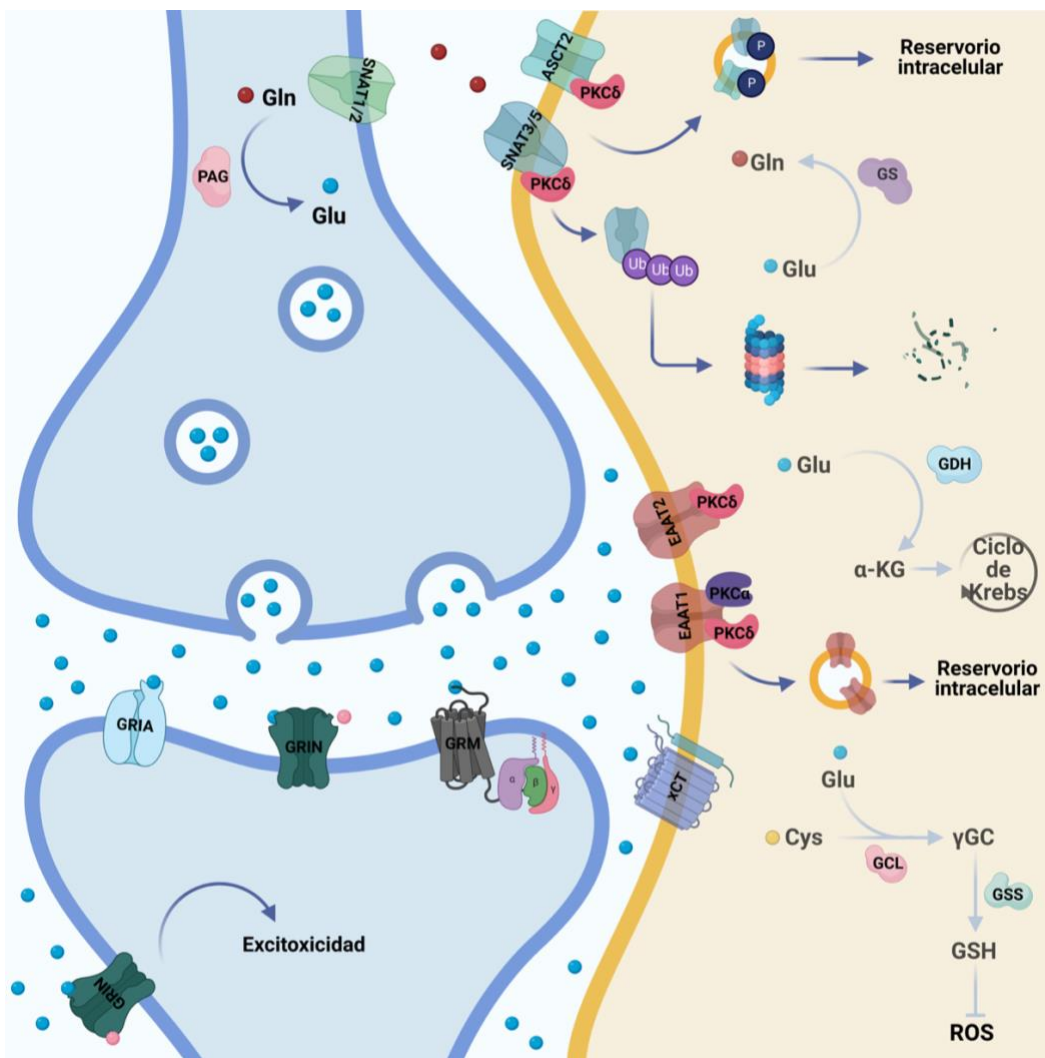


*Figura 7. Efectos del Mn$^{2+}$ en el ciclo Glu-Gln en astrocitos corticales.*

### 1.4. Traducción de proteínas

La traducción de proteínas es un fenómeno celular fundamental, cuya regulación determina el destino celular tanto de forma temporal como espacial. Es un mecanismo postranscripcional de

control génico que tiene un papel importante en múltiples procesos biológicos, incluidos el crecimiento y desarrollo celular, respuesta al estrés, plasticidad sináptica, entre otros [75].

Tras la acción de estímulos extracelulares y/o intracelulares, la maquinaria de traducción puede ajustar rápidamente el traductoma (mRNA en ribosomas) de un grupo de mRNAs preexistentes antes de que haya repercusiones en el transcriptoma (**Figura 8**). La desregulación de la traducción es un mecanismo común en la transformación celular y el desarrollo tumorogénico, entre otros muchos procesos celulares, tales como la regulación sináptica, la cual tiene repercusiones en la potenciación a largo plazo y por lo tanto en el aprendizaje y memoria [76].
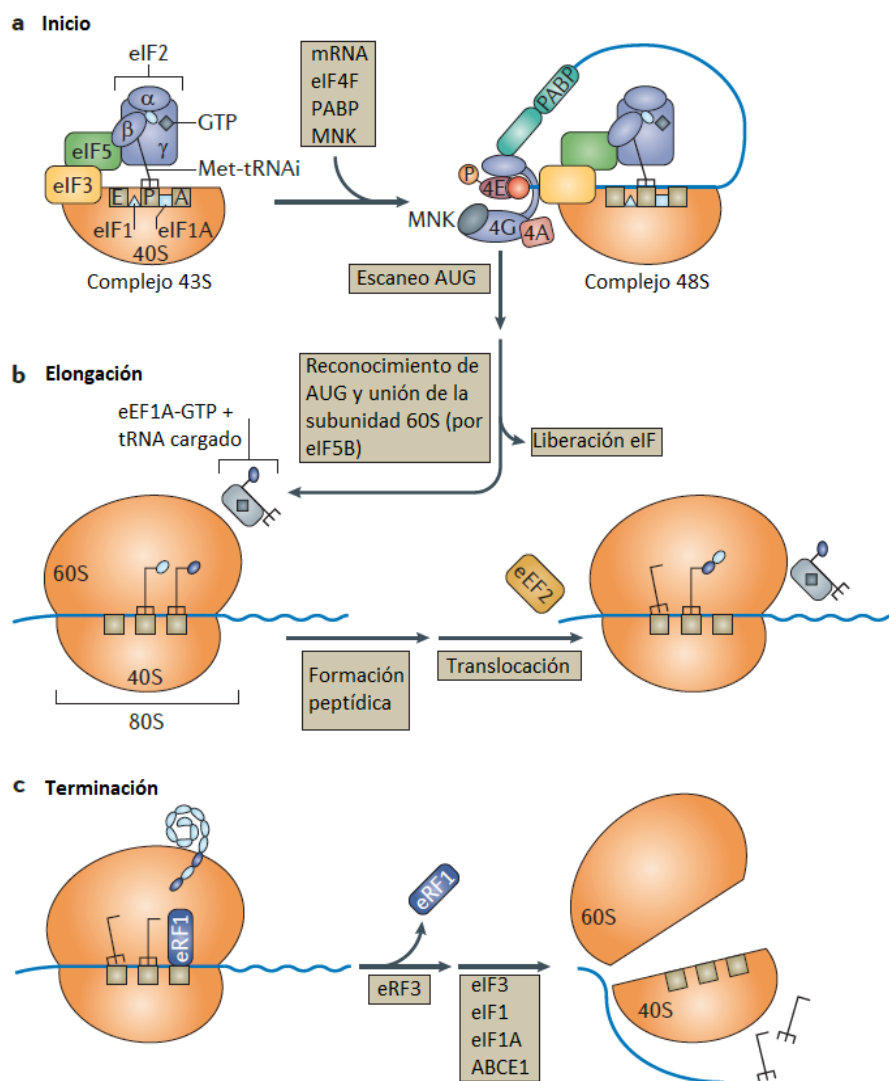


**Figura 8. Traducción de mRNA en eucariontes.** *El proceso de traducción tiene tres fases: **A)** inicio, **B)** elongación y **C)** terminación. Cada fase requiere de factores de traducción específicos. Modificado de* [75].

### 1.4.1. Control traduccional

Alteraciones en los mecanismos del control de la traducción han sido relacionados con el desarrollo de enfermedades neurodegenerativas y problemas en el neurodesarrollo [77]. El control traduccional es un importante mecanismo por el cual las células gestionan la expresión génica, proveyendo de una rápida respuesta sin involucrar vías nucleares de síntesis y transporte de proteínas [78]. El proceso de síntesis de proteínas puede ser dividido entre tres fases principales: inicio, elongación y terminación (**Figura 8**).

En el inicio de la traducción, la subunidad ribosomal 40S se une a un RNA de transferencia iniciador específico (Met-tRNA) y a un mRNA. La fase de inicio finaliza cuando la subunidad 40S selecciona un codón de inicio y la subunidad 60S se une para formar un ribosoma funcional [79]. La fase de elongación de la síntesis de proteínas se encarga de la adición de aminoácidos (dependiente del codón) a la cadena polipeptídica naciente y finalmente la terminación implica la liberación de la cadena polipeptídica completa del ribosoma, terminando con la disociación del ribosoma y el tRNA desacetilado del mRNA [80].

### 1.4.1.1. Inicio de la traducción

El inicio de la traducción es el paso más controlado y probablemente el más estudiado de la síntesis de proteínas. Previo al reclutamiento del mRNA, el factor de inicio de la traducción 2 (eIF2) unido a GTP se vincula al tRNA de inicio (Met-tRNA$_i$) conformando el complejo ternario (TC), el cual se asocia con la subunidad 40S junto con los factores eIF1, eIF3 y eIF5, formando el complejo de preinicio (PIC) 43S [80]. La fosforilación de la subunidad α en el residuo de 51 de serina desactiva a eIF2, tal acción es llevada a cabo por diferentes cinasas como, la cinasa de control general no-deprimible (GCN), la cinasa inhibidora hemo-regulada (HRI), la cinasa de retículo endoplásmico similar a PKR (PERK) y la proteína cinasa R (PKR); que son activadas por eventos de estrés discreto. Cuando eIF2 se fosforila previene el intercambio de nucleótidos de GTP por GDP, inactivando su reciclaje y disminuyendo la tasa de inicio de la traducción [79,81]. Por otro lado, la preparación de la unión del mRNA al PIC 43S para formar el PIC 48S es llevado a cabo por el factor de inicio eucariótico 4E de unión a cap 7-metilguanosina (eIF4E), la helicasa de RNA eIF4A, el factor de anclaje eIF4G y el factor eIF4B (**Figura 9**). La unión de eIF4E a eIF4G es un paso crucial en el ensamblaje de eIF4F y por ende del inicio de la traducción [80].

La proteína 1 de unión al factor 4E (4E-BP1), como se puede inferir, se une al eIF4E, reprimiendo su ensamblaje con el eIF4F. La hiperfosforilación de 4E-BP1 promueve la liberación de eIF4E de 4E-BP1 permitiendo su unión a eIF4G, lo cual lleva a la fosforilación de eIF4E por proteínas asociadas al eIF4G y el reclutamiento del complejo 43S [80,82].
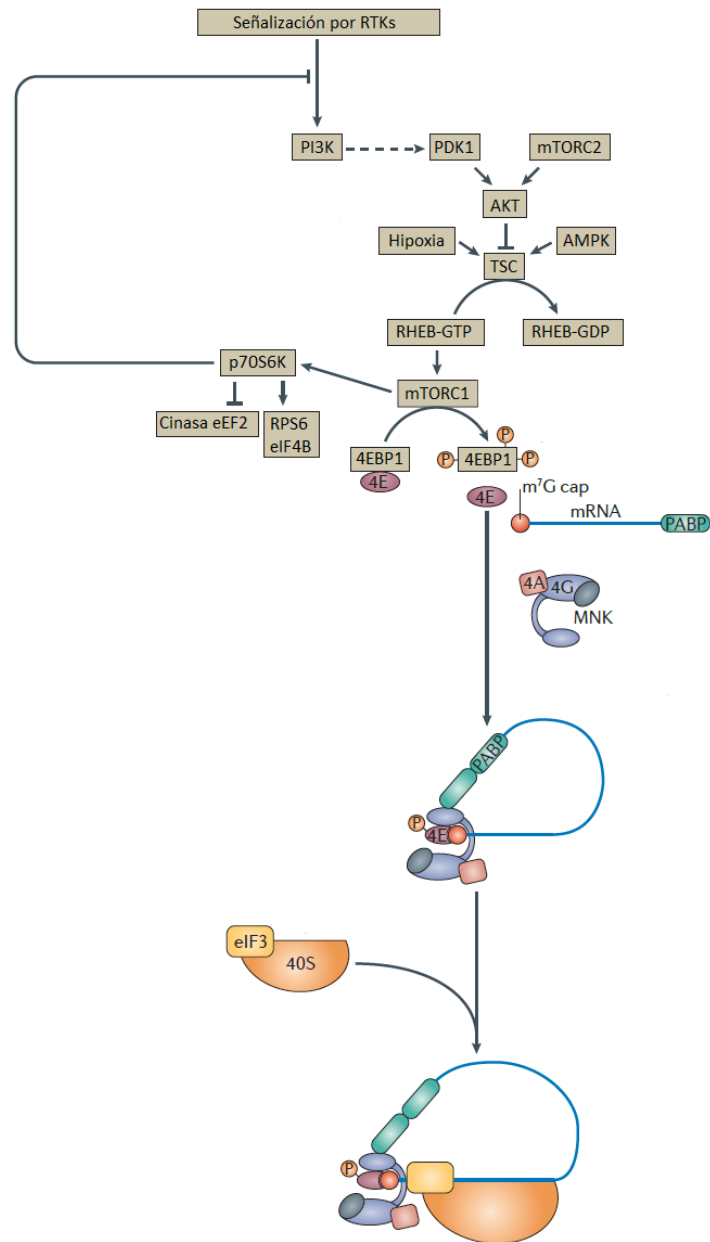


**Figura 9. Control de la traducción dependiente de cap.** *El inicio de la traducción es regulado por el correcto ensamblaje del complejo de inicio 4F. Modificado de* [75].

La proteína de unión a secuencias de poliadenilación (PABP) se une a la secuencia de poliadenilación (poli-A) en el extremo 3', asociándose con eIF4G, estimulando la traducción dependiente de cap (**Figura 9**) [75]. Una vez unido al sitio 5' terminal del mRNA, el complejo ribosomal hace un escaneo en busca del codón de inicio AUG. La selección del sitio de inicio de la traducción es acompañada por la hidrólisis de GTP llevada a cabo por eIF2 y la consecuente liberación de los factores de inicio para ser recicladas. El eIF5B promueve la unión a la subunidad 60S para formar el ribosoma 80S mediante la hidrólisis de GTP que lleva a la liberación del monosoma 80S, lo cual es el parteaguas para iniciar la fase de elongación de la traducción [80].

### 1.4.1.2. Elongación de la traducción

El ribosoma es la unidad de procesamiento central, durante de la elongación. En esta fase se decodifica el mRNA y se recluta la maquinaria necesaria (factores de elongación: EFs) para obtener una proteína correctamente plegada. La elongación ocurre a un rango aproximado de 4-6 aminoácidos por segundo en eucariontes, aunque los transcritos suelen tener diferentes tiempos de elongación [82].

De manera general, un eEF1A-GTP-aa-tRNA se une al sitio-A del ribosoma. El reconocimiento del codón por el tRNA activa la hidrolisis y liberación de eEF1A-GDP, lo cual permite que el aa-tRNA sea acomodado en el sitio-A. El centro peptidil transferasa ribosomal (PTC) posiciona el aa-tRNA en el sitio-A y al peptidil-tRNA en el sitio-P, para permitir una rápida formación del enlace peptídico. La unión y la hidrólisis de GTP, que es llevada a cabo por el eEF2, promueve la traslocación del anticodón tRNA en los sitios-E y -P, respectivamente. El tRNA desacetilado es liberado del sitio-E y el siguiente eEF1A-GTP-aa-tRNA se une al sitio-A. El ciclo continúa hasta que se encuentra un codón sinsentido. El reciclaje del eEF1A-GDP a eEF1A-GTP entre cada ciclo requiere del intercambiador de nucleótidos de guanina eEF1B [80].

### 1.4.1.3.Terminación de la traducción

La elongación termina cuando la translocación posiciona uno de los tres codones de paro (UAA, UGA o UAG) en el sitio-A del ribosoma, iniciando la fase de terminación, lo que conduce al desacople del péptido del ribosoma. Existen dos factores de liberación eucarióticos (eRF1 y eRF3) [82]. La estructura de eRF1 se asemeja a la de un tRNA, lo cual permite que el dominio N-terminal

del factor de liberación se ancle al sitio-A del ribosoma e interaccione directamente con el codón de paro. La alta fidelidad de esta unión acoplada con la actividad GTPasa del eRF3 promueve la hidrolisis del peptidil-tRNA necesaria para liberar el polipéptido del sitio-P y del ribosoma. Finalmente, la unidad 80S es desmantelada en sus subunidades 40S y 60S [80,82].

### 1.4.2. Vías de señalización participantes en el control de la traducción

La traducción es el proceso con más alto costo energético en la célula. Además, juega un papel importante en la regulación de la expresión génica, por lo cual debe ser un proceso finamente regulado. Al modular la fosforilación de ciertos componentes de la maquinaria traduccional se pueden inducir cambios cuantitativos y cualitativos en la traducción de mRNA. Además, es un hecho que la composición proteica en la célula no es equivalente a los niveles de mRNA, lo cual nos indica que la regulación de la expresión génica mediante mecanismos postranscripcionales tiene un papel especialmente importante en la formación del proteoma [83,84].

Diversas vías de señalización convergen en la regulación de la maquinaria traduccional en respuesta a múltiples estímulos. Dos rutas de señalización altamente implicadas en la regulación de la síntesis de proteínas son: la vía de las proteínas cinasas activadas por mitógenos (MAPK) y la ruta de la cinasa de fosfatidilinositol 3 (PI3K)/proteína cinasa B (Akt). Ambas vías regulan la homeostasis de la síntesis proteica, su desregulación resulta en una traducción de proteínas aberrante, la cual puede llevar al desarrollo de condiciones patológicas tales como el cáncer, la diabetes y desórdenes neurológicos [83].

#### 1.4.2.1.PI3K/Akt/mTOR en la traducción de proteínas

La vía de señalización PI3K/Akt/mTOR (**Figura 10**) tiene un papel vital en la regulación de la supervivencia celular, el crecimiento, la proliferación, la angiogénesis, el metabolismo y la traducción de proteínas [85]. La interacción de RTKs o de receptores acoplados a proteínas G con sus ligandos específicos, induce la fosforilación de los dominios activos de sus enzimas intracelulares y la activación de la señalización por parte de proteínas adaptadoras (ejemplo: IRS1), llevando a la activación de PI3K [85,86]. Consecuentemente, PI3K fosforila el carbono 3 del fosfatidilinositol 4,5-bifosfato (PIP2) para producir fosfatidilinositol 3,4,5-trifosfato (PIP3). PIP3, funge como sitio de anclaje de diversas proteínas intracelulares, para formar complejos de

señalización [86–88]. Tal es el caso de PDK1 y Akt, donde una vez reclutadas en la membrana, PDK1 fosforila a Akt en su dominio cinasa (Thr[308]) y PDK2 (mTORC2) lo fosforila en el dominio carboxilo terminal (Ser[473]). PIP3 permanece en la membrana plasmática hasta su desfosforilación mediada por la proteína fosfatasa homóloga de tensina (PTEN). PTEN desfosforila el anillo de inositol de PIP3, generando PIP2 [87,89,90].
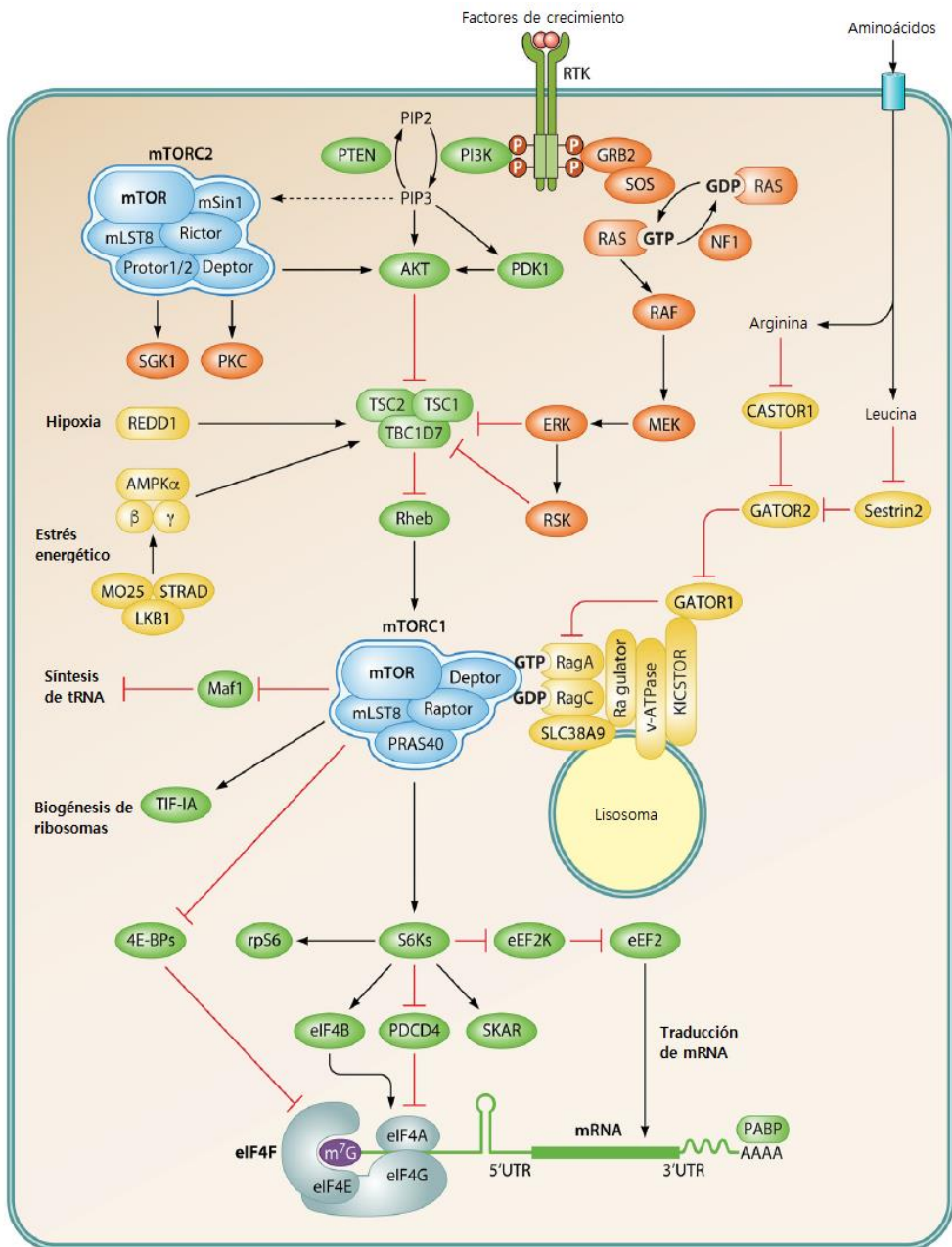


**Figura 10. Papel de las vías de señalización PI3K/Akt/mTOR y AMPK en la síntesis de proteínas.** *Modificada de* [83].

Akt es capaz de activar directamente a mTORC1 al fosforilarlo en el residuo Ser[2448]. Asimismo, Akt puede llevar a la activación indirecta de mTORC1 a través de la fosforilación del complejo 2 de esclerosis tuberosa (TSC2), causando la inhibición del complejo TSC1/TSC2. Cuando se encuentra activado este complejo promueve la conversión del homólogo de Ras enriquecido en cerebro-GTP (Rheb-GTP) al inactivo Rheb-GDP, dicha conversión lleva a la inactivación de mTORC1 [91]. Cuando mTORC1 se encuentra activado fosforila a las proteínas efectoras: S6K (cinasa de la proteína ribosomal S6) y 4E-BP1 [92]. La hiperfosforilación de 4E-BP1 libera el eIF4E, permitiendo su unión a eIF4G lo cual lleva a la fosforilación de eIF4E permitiendo el inicio de la traducción dependiente de 5'-cap [93,94].

La proteína S6K fosforila a eEF2K en el residuo Ser[366] tras la activación de mTOR, esta cinasa es un regulador negativo de la síntesis de proteínas al tener la capacidad de fosforilar e inhibir a eEF2 en el residuo Thr[56] [95,96]. El factor proapoptótico PDCD4 (muerte celular programada 4) es blanco de fosforilación (Ser[67] y Ser[457]) de S6K. PDCD4 bloquea la interacción entre eIF4G y eIF4A, lo cual inhibe el inicio de la traducción dependiente de cap [97]. Estudios recientes han descrito a la proteína 1 relacionada con La (LARP1) como un posible regulador de la traducción de mRNAs con un motivo 5'-TOP (tracto de oligopirimidina 5' terminal). LARP1 es fosforilado por mTOR (Ser[689] y Thr[692]), S6K (Ser[770]) y Akt (Ser[979]), aunque su papel exacto en la estabilización de 5'-TOP mRNAs en la síntesis de proteínas es aún controversial [83].

### 1.4.2.2. AMPK y la traducción de proteínas

AMPK, la proteína cinasa activada por adenosín monofosfato (AMP), también conocida como el sensor energético celular, es una proteína cinasa heterotrimérica de tipo Ser/Thr que es activada por alteraciones en la tasa intracelular de AMP: adenosín trifosfato (ATP) (**Error! Reference source not found.**). Se encuentra conformada por un complejo que incluye a una subunidad catalítica α (α1 y α2, una subunidad regulatoria β (β1 y β2) y una subunidad no-catalítica γ (γ1, γ2 y γ3) [98]. Tanto AMP como ATP se unen de manera competitiva a la subunidad γ. Cuando la molécula de ATP se une a la subunidad γ induce el cierre del trímero de AMPK y su consecuente inhibición. Por otro lado, la unión de AMP o adenosil bifosfato (ADP) a la subunidad γ induce un reordenamiento del dominio alostérico que en consecuencia promueve la fosforilación de AMPK en el residuo Thr[172] de la subunidad α llevada a cabo por cinasas río arriba de esta molécula [99]. La fosforilación en Thr[172] de AMPK es el sello distintivo de la activación de esta cinasa. La cinasa

hepática B1 (LKB1), la cinasa de cinasas de $Ca^{2+}$-calmodulina (CaMKK2), la cinasa activada de TGF-β (TAK1) y la cinasa de MAPKK (MLK1) son algunas de las cinasas descritas que fosforilan a AMPK en este residuo [100]. Tal como se mencionó, la síntesis de proteínas es un proceso con un alto costo energético en la célula, por lo que, durante fenómenos de estrés energético, este proceso es inhibido para conservar la homeóstasis de ATP en la célula. La AMPK inhibe la traducción dependiente de cap, tanto en la fase de inicio como en la fase de elongación [101].

Se ha descrito la inhibición indirecta de mTOR por esta cinasa, ya que AMPK fosforila de manera directa a TSC2 en los residuos $Thr^{1271}$ y $Ser^{1387}$, promoviendo su unión a TSC1 y formando el complejo GTPasa, TS2/TSC1, lo cual mantiene a Rheb (proteína activadora de mTOR) en unión con GDP, resultando en la inhibición de mTOR [102]. Además, AMPK también fosforila de manera directa a raptor en los residuos $Ser^{722/792}$, inhibiendo mTOR [103]. La inhibición de mTOR promueve la activación de 4E-BP1 e inhibe a p70S6K; previniendo el inicio de la traducción dependiente de cap e impidiendo la expresión de proteínas ribosomales, respectivamente. Además, AMPK disminuye la síntesis de RNA ribosomal al inducir la fosforilación inhibitoria de eIF1A [104].

El efecto de AMPK sobre la fase de elongación ha sido ampliamente descrito debido a que este paso de la síntesis de proteínas es el más costoso en términos de consumo de ATP [105]. Específicamente, AMPK fosforila a eEF2K en el residuo $Ser^{398}$, lo cual activa a esta cinasa. A su vez, eEF2K una vez activa, fosforila en el residuo $Thr^{56}$ a eEF2 inactivándolo y, por consecuencia, deteniendo la síntesis de proteínas en la fase de elongación [106].

Estudios recientes, proponen que AMPK desempeña estas funciones al cambiar de mecanismos dependientes de cap a mecanismos independientes de cap durante fenómenos de estrés energético, induciendo la expresión de genes críticos para la supervivencia celular [101,107].

### 1.5.Justificación

El $Mn^{2+}$ es un elemento esencial necesario en el correcto funcionamiento de múltiples procesos celulares. Sin embargo, la exposición a grandes concentraciones de este metal puede resultar en el desarrollo de una patología similar a la enfermedad de Parkinson, conocida como *manganismo*. El potencial neurotóxico del $Mn^{2+}$ lo hace un factor de riesgo importante en el desarrollo de múltiples enfermedades neurodegenerativas. El $Mn^{2+}$ es capaz de cruzar la barrera hematoencefálica a través de diversos transportadores de metales y de acumularse en neuronas y células gliales. Estudios

recientes sugieren que las células gliales son uno de los blancos principales de la toxicidad provocada por el $Mn^{2+}$, ya que este metal se acumula de manera preferente en éstas. Dentro de los mecanismos de toxicidad activados por la exposición a manganeso, la excitotoxicidad es uno de los principales y las células gliales son pieza clave en la remoción de Glu del espacio sináptico. En nuestro grupo de trabajo hemos descrito que el tratamiento con Glu a concentraciones excitotóxicas es capaz de modular la maquinaria traduccional, alterando el proceso de síntesis de proteínas en células gliales. La síntesis de proteínas tiene con un alto costo de energía, por lo que en situaciones de estrés energético este proceso es inhibido para conservar la homeostasis celular. Por lo tanto, consideramos que el estudio del efecto de la exposición a $Mn^{2+}$ en la maquinaria traduccional de células gliales de Bergmann –que rodean prácticamente solo sinapsis glutamatérgicas en el cerebelo– es de gran importancia para elucidar los mecanismos de neurotoxicidad inducidos por la exposición a este metal.

### 1.6. Hipótesis

La exposición de células gliales de Bergmann a $Mn^{2+}$ modificará efectores claves de la maquinaria traduccional, alterando la síntesis global de proteínas.

### 1.7. Objetivos
#### 1.7.1. Objetivo General

Determinar el efecto de la exposición a $MnCl_2$ en el control traduccional de células gliales de Bergmann.

#### 1.7.2. Objetivos específicos

- Evaluar la viabilidad de células gliales de Bergmann después de la exposición a $MnCl_2$ mediante la determinación de su actividad metabólica por medio del ensayo MTT.
- Caracterizar el papel de la ruta de señalización de PI3K/Akt/mTOR en el efecto inducido por la exposición a $MnCl_2$ en células gliales mediante la inhibición farmacológica de efectores claves esta vía.
- Evaluar si la exposición a $MnCl_2$ producen cambios en los patrones de fosforilación de 4E-BP1 en células gliales.

- Determinar si la exposición a MnCl$_2$ alterará la síntesis de proteínas en células gliales al evaluar el perfil de incorporación de [$^{35}$S]-metionina.

- Determinar los niveles de fosforilación de AMPK después de la exposición a MnCl$_2$ en células gliales.

## II.     MATERIALES Y MÉTODOS

### 2.1. Estrategia experimental
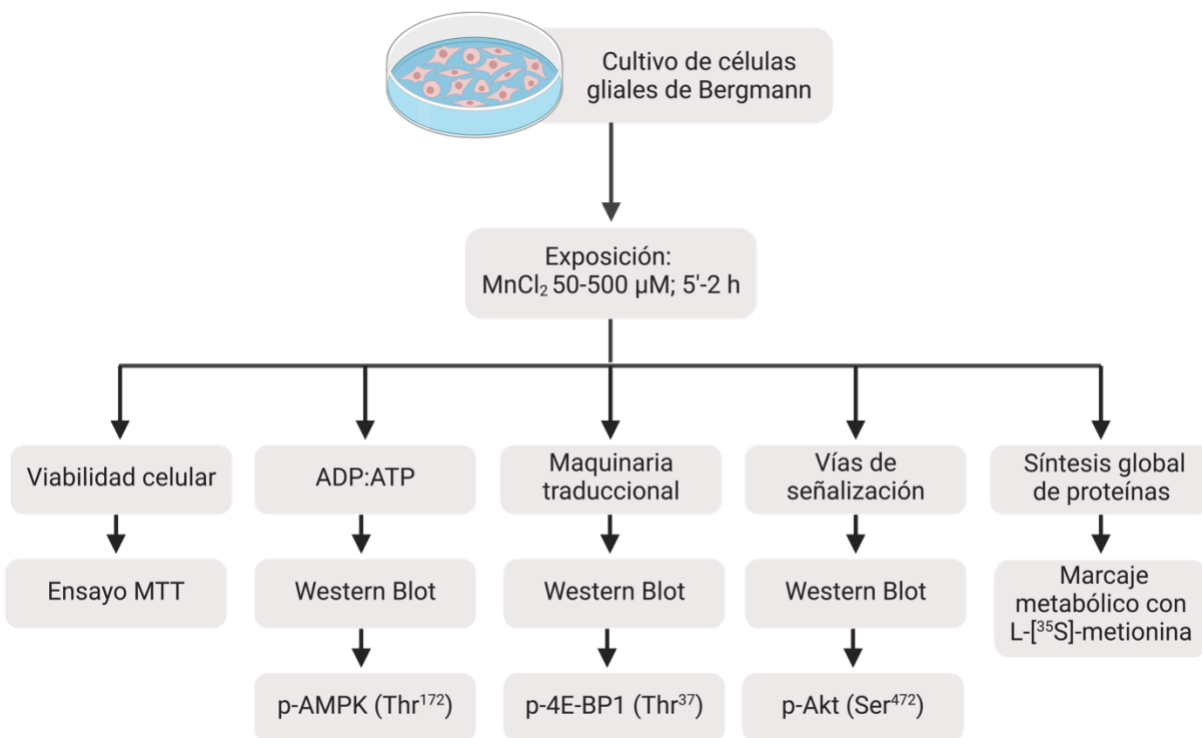


*Figura 11. Esquema experimental de trabajo.*

### 2.2. Reactivos

Los reactivos para realizar el cultivo primario de CGB se obtuvieron de GE Healthcare Life Sciences (Carlsbad, CA, EE. UU.). El ácido D-aspártico y bromuro de 3-[4,5-dimetiltiazol-2-il]-2,5-difeniltetrazolio (MTT) se adquirieron de Sigma-Aldrich (St. Louis, MO, EE. UU.). La L-[35S]-metionina se obtuvo de PerkinElmer (Waltham, MA, EE. UU.). El ácido L-glutámico fue adquirido de Tocris Biosciences (Ellisville, IL, EE. UU.) Los reactivos utilizados en la inmunodetección en fase sólida se adquirieron de Bio-Rad (Hercules, CA, EE. UU.). El resto de los agentes químicos se adquirieron de Sigma (St. Louis, MO, EE. UU.).

### 2.3. Material Biológico

Embriones de pollo de 10 días donados por Avi-Mex S.A. de C.V., se mantuvieron en incubación a 37 °C hasta el momento de la preparación del cultivo primario de CGB. Todos los procedimientos

se realizaron de acuerdo con las normas internacionales sobre el uso ético de animales en investigación y fueron aprobadas por el comité de ética animal del Cinvestav. Se hizo todo lo posible para reducir el número de embriones utilizados y su sufrimiento según lo sugerido por la American Veterinary Medical Association [108].

## 2.4. Cultivo primario de células gliales de Bergmann y protocolo de exposición

El cultivo primario de CGB fue elaborado conforme a la metodología previamente descrita por Ortega y colaboradores [109]. Partiendo de cerebelos de embriones de pollo de 14 días diseccionados y homogenizados de manera enzimática y mecánica, se sembraron $1 \times 10^6$ células/mL de medio DMEM (Medio de Cultivo Eagle Modificado de Dulbecco; Gibco) suplementado con 10% de suero fetal bovino (SFB) y 50 μg/mL de gentamicina. Las células fueron incubadas a 37 °C en una atmósfera con 5% de $CO_2$ y 95% de humedad, hasta alcanzar un 80-100% de confluencia (4-6 días *in vitro*).

Una vez confluentes, las células fueron privadas de suero (DMEM con SFB al 0.5%) durante 12 h, para luego ser tratadas con diferentes concentraciones de $MnCl_2$ en los periodos de tiempo indicados. Cada uno de los inhibidores farmacológicos utilizados fueron adicionados 30 min antes de la exposición a $MnCl_2$, tal como se muestra en las figuras correspondientes.

## 2.5. Ensayo de viabilidad celular MTT

### 2.5.1. Principio

Ensayo colorimétrico basado en la reducción metabólica del compuesto soluble amarillo bromuro de 3-(4,5-dimetiltiazol-2-ilo)-2,5-difeniltetrazol (MTT) llevada a cabo por la enzima mitocondrial succinato deshidrogenasa en un producto azul/púrpura insoluble. Se considera un índice de las células vivas, dado que las células muertas son incapaces de generar productos de formazán [110].

### 2.5.2. Procedimiento

Monocapas confluentes de CGB sembradas en cajas de cultivo celular de 96 pozos fueron tratadas con $MnCl_2$ en medio DMEM reducido en suero (0.5% de SFB) durante el tiempo indicado. Tres horas antes de concluir los tratamientos las células fueron incubadas con 20μL de solución de MTT (5 mg/mL) a 37 °C. Finalmente, se descartó el medio y los cristales formados fueron disueltos en 50μL de dimetilsulfóxido (DMSO) en agitación por 10 min. La densidad óptica de las muestras se

determinó por espectrofotometría a una longitud de onda de 570 nm en un lector de microplacas (Biotek Instruments, VT, EE. UU.). Los experimentos se realizaron por cuadruplicado en al menos tres cultivos independientes y los datos son presentados como porcentaje del control.

## 2.6. Marcaje metabólico de proteínas y determinación de síntesis global de proteínas
### 2.6.1. Principio

Es uno de los métodos mejor establecidos para medir la tasa de síntesis de proteínas en las células mediante la adición de aminoácidos radiomarcados, como la [$^{35}$S]-metionina y la [$^{35}$S]-cisteína, durante un lapso determinado de tiempo, para medir su incorporación en proteínas recién sintetizadas mediante la cuantificación de la radiactividad de esta molécula. Esto es debido a que el principal codón de inicio de la traducción es AUG, permitiendo la unión de la metionina radiomarcada junto con el tRNA de inicio de la síntesis de proteínas [111].

### 2.6.2. Procedimiento

Monocapas confluentes de CGB fueron marcadas durante 12 h con 1 µCi de [$^{35}$S]-metionina (Actividad específica: 1175.0 Ci/mmol) en DMEM libre de metionina (Gibco #21013024). Después de una serie lavados con solución salina de fosfatos fría (PBS: $K_2HPO_4/KH_2PO_4$ 10 mM, NaCl 150 mM, pH 7.4), las células fueron expuestas a 200 µM de $MnCl_2$ a diferentes periodos de tiempo. Consecuentemente, las células fueron lavadas en dos ocasiones con 1 mL de PBS frío y lisadas con solución amortiguadora de lisis (RIPA: Tris-HCl 20 mM, pH 7.4, EDTA 2 mM, EGTA 2 mM, KCl 50 mM, $MgCl_2$ 5 mM, NaCl 400 mM, aprotinina 1 mM, leupeptina 1 mM, fenilmetilsulfonilo 100 µM y NP-40 al 1%) y centrifugadas a 20,000xg durante 10 min. Con el fin de cuantificar la síntesis de proteínas total, una alícuota de ≈15µg de las muestras marcadas metabólicamente se aplicó a filtros de microfibra GF/C (Whatman, Clifton, NJ, USA). Los filtros fueron secados y después lavados durante 10 min en ácido tricloroacético (TCA) al 10%, seguido de tres lavados de 10 min con TCA al 5% frío. Finalmente, los filtros fueron secados a temperatura ambiente y colocados en viales con 3 mL de líquido de centelleo, así como con 10 µL de ácido acético glacial. La incorporación de [$^{35}$S]-metionina fue determinada mediante el conteo de centelleo radiactivo por minuto (CPM) en el contador de centelleo Tri-Carb 2810TR de PerkinElmer. Los experimentos fueron realizados por triplicado en al menos tres cultivos independientes y los datos presentados como porcentaje del control.

### 2.7. Obtención de extractos proteicos totales

Al finalizar la exposición a MnCl$_2$, las CGB se cosecharon mecánicamente en PBS con inhibidores de fosfatasas y proteasas (Na$_3$VO$_4$ 2 mM, NaF 25 mM, Na$_2$MoO$_4$ 10 mM, aprotinina 1 mg/mL, leupeptina 1 mg/mL, fenilmetilsulfonilo 1 mM). Para obtener los extractos totales, las células se centrifugaron a 20,000xg a 4 °C, durante 10 min. El precipitado fue homogenizado mecánicamente en solución RIPA. El homogenizado se centrifugó a 20,000xg durante 10 min a 4 °C, el sobrenadante fue colectado y se cuantificó el contenido proteico como se indica a continuación.

### 2.8. Determinación de proteínas por el método de Bradford y desnaturalización de las muestras

#### 2.8.1. Principio

Este método, introducido por Bradford en 1976, cuantifica residuos de aminoácidos básicos de arginina, lisina e histidina, los cuales contribuyen a la formación del complejo proteína-azul de Coomasie. La unión de moléculas proteicas al colorante azul de Coomassie bajo condiciones acídicas resulta en un cambio de coloración de café a azul [112].

#### 2.8.2. Procedimiento

Se determinó la concentración de proteína en las muestras a partir de una curva de calibración estándar, utilizando una solución de 10 mg/mL de γ-globulina, se prepararon diluciones de 1, 2, 3, 6 y 12 µg/mL en un volumen de 80 µL. Se añadió un volumen de 20 µL de cada muestra por triplicado en una microplaca y se les adicionó con 180 µL de reactivo de Bradford y se procedió a incubar la reacción a temperatura ambiente durante 5 min y posteriormente analizar sus absorbancias a 595 nm en un lector de microplacas (Biotek Instruments, VT, EE. UU.). Alrededor de 20-60 µg de proteínas totales se resuspendieron en solución amortiguadora de Laemmli (Tris-HCl pH 6.8 150 mM, SDS al 5%, β-mercaptoetanol al 5%, DTT 150 mM, azul de bromofenol al 3% y glicerol al 30%). Las muestras fueron sometidas a ebullición durante 5 min y se les provocó un choque térmico en hielo durante 5 min. Estas muestras se reservaron para realizar la inmunodetección en fase sólida.

### 2.9. Inmunodetección en fase sólida

#### 2.9.1. Principio

También conocida como Western blot, esta técnica se describió por primera vez en 1979, y se utiliza para separar y detectar proteínas. El método se basa en la construcción de un complejo antígeno-anticuerpo, dada por la unión de anticuerpos específicos a proteínas que se encuentran inmovilizadas en una membrana y su consecuente detección mediante un segundo anticuerpo acoplado a un marcador quimioluminiscente [113].

#### 2.9.2. Procedimiento

Las muestras de proteína previamente desnaturalizadas en la solución amortiguadora de Laemmli fueron separadas mediante electroforesis en un gel de poliacrilamida al 10% en presencia de dodecil sulfato de sodio (SDS-PAGE) a 80 V durante 90 min aproximadamente y, posteriormente, fueron transferidas a membranas de nitrocelulosa a 180 mA durante 2 h. Las membranas se tiñeron con 5 mL de rojo de Ponceau S durante 5 min, para confirmar el contenido proteico de las mismas. Las membranas se lavaron en PBS para remover el exceso de rojo de Ponceau S y ser incubadas en PBS y Tween 20 al 0.1% con leche semidescremada al 5% durante 2 h, con el fin de bloquear el exceso de sitios de unión de proteína inespecíficos. Posteriormente, las membranas fueron incubadas durante la noche a 4 °C con los anticuerpos primarios indicados (1:1000), seguidos de sus anticuerpos secundarios (1:4000) correspondientes acoplados a peroxidasa de rábano durante 2 h (**Tabla 1**). Los polipéptidos inmunorreactivos fueron detectados por quimioluminiscencia en foto-documentador MicroChemi DNR o Li-COR Odyssey y fueron procesadas en el software Image J (NIH; Bethesda, Maryland, USA) o Image Studio Lite (Li-COR, Lincoln, NE), respectivamente, para finalmente cuantificar la intensidad total de las bandas. Los datos son presentados como porcentaje del control de al menos 3 experimentos independientes.

### 2.10. Análisis estadístico

Los datos han sido expresados como medias ± el error estándar, de por lo menos tres cultivos independientes. Una vez que la distribución de los datos fue analizada mediante la prueba de normalidad de Shapiro-Wilk, los análisis estadísticos se realizaron mediante análisis de varianza de una *vía* (one-way ANOVA) de medidas repetidas, y comparaciones *post hoc* mediante el método de Dunnet y/o Bonferroni, según fuera el caso, se consideraron diferencias

estadísticamente significativas con valores de p<0.05. Todos los análisis se realizaron con el programa GraphPad Prism 9 (La Jolla, CA, EE. UU.).

*Tabla 1. Lista de anticuerpos utilizados en el presente trabajo.*

| ANTICUERPO | CAT# | RRID | COMPAÑÍA |
|---|---|---|---|
| Anti-pAkt | sc-514032 | AB_2861344 | Santa Cruz Biotechnology (Dallas, TX, EE. UU.) |
| Anti-Akt | sc-81434 | AB_1118808 | |
| Anti-p4E-BP1 | sc-23768-R | AB_2095599 | |
| Anti-4E-BP1 | sc-9977 | AB_626621 | |
| Anti-pAMPK | 2535 | AB_331250 | Cell Signaling Technology (Danvers, MA, EE. UU.) |
| Anti-AMPK | 2532 | AB_330331 | |
| Anti-conejo | 81-6120 | AB_87750 | Invitrogen Corporation (Carlsbad, CA, EE. UU.) |
| Anti-mouse | 81-6520 | AB_87763 | |

*\*Todos los anticuerpos primarios se utilizaron a una concentración de 1:1000, mientras que los secundarios a una concentración 1:4000.*

## III. RESULTADOS

### 3.1. La exposición a $Mn^{2+}$ no afecta la viabilidad de CGB

La concentración basal de $Mn^{2+}$ en células gliales del cerebelo es de 75 µM [114] Según las consideraciones propuestas por Aschner y Bowman para estudios *in vitro* sobre los efectos del $Mn^{2+}$ [73], donde un factor de 3 veces la concentración basal (≈200 µM) representa una concentración de toxicidad relevante de estudio, elegimos un rango que tomara en cuenta valores normales y patológicos (50-500 µM). Por lo que como primer acercamiento evaluamos la viabilidad de CGB mediante la determinación de la actividad metabólica por medio del ensayo MTT, con el fin de establecer las condiciones de trabajo no citotóxicas. Utilizamos concentraciones de 50 a 500 µM de $MnCl_2$ a diferentes tiempos de exposición: 3, 6, 12, y 24 h y Tritón al 1% como control de muerte celular (**Figura 12**).
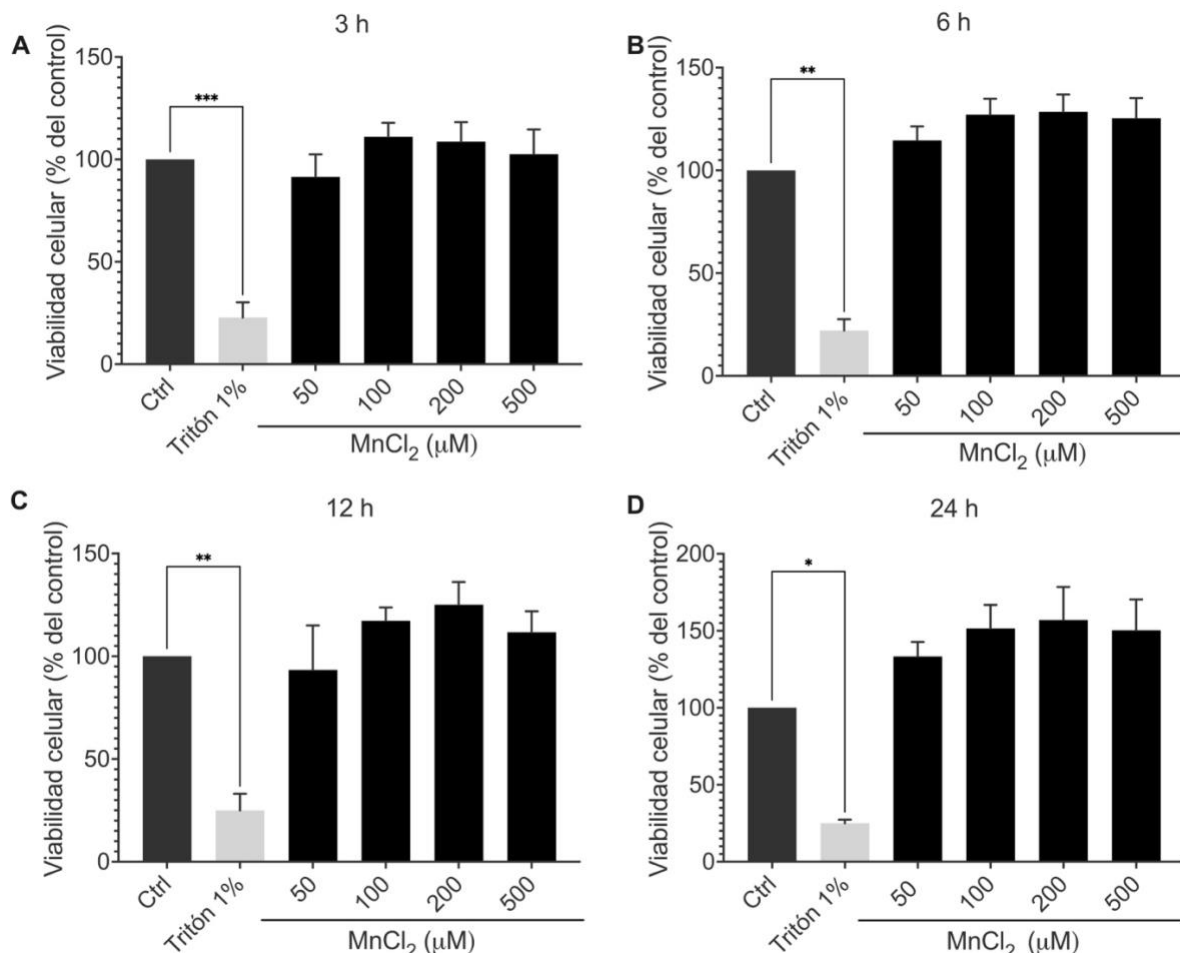


*Figura 12. Efecto del $Mn^{2+}$ en la viabilidad celular de CGB. A)3 h, B)6 h, C)12 h, D)24 h. Tritón al 1% fue utilizado como control. Los datos están expresados como media ± error estándar, n≥3. ANOVA de medidas repetidas y prueba post hoc de Dunnet, \*p<0.05, \*\*p<0.01, \*\*\*p<0.001.*

Los resultados que se encuentran en la **Figura 12** muestran que, en las CGB, la exposición a $Mn^{2+}$ a los diferentes tiempos (3-24 h) y concentraciones (50-500 µM) evaluadas, no hubo efecto en la actividad mitocondrial, incluso en las concentraciones más altas. Mientras que la exposición a Tritón a 1% tuvo un efecto severo en la viabilidad de CGB, como era de esperarse. Así mismo, podemos observar un incremento en la reducción de MTT en la mayoría de los tratamientos, lo cual sugiere un posible incremento de la actividad metabólica en respuesta al estrés oxidante ocasionado por la exposición al $Mn^{2+}$. Por lo que con estos resultados decidimos continuar utilizando el rango de 50-500 µM de $MnCl_2$ durante el estudio.

### 3.2. La exposición a $Mn^{2+}$ incrementa la fosforilación de Akt en CGB

En un estudio previo hemos demostrado que la exposición a $MnCl_2$ incrementa la captura de Glu mediada por GLAST en CGB [115], y teniendo en cuenta que la capacidad señalizadora de GLAST ha sido reportada ampliamente [116], decidimos estudiar la activación de la vía de señalización de PI3K/Akt por la exposición a $MnCl_2$ en CGB. Para lo cual, examinamos los patrones de fosforilación de Akt en el residuo $Ser^{473}$, residuo conocido como un potenciador de la actividad cinasa de Akt [117]. En la **Figura 13A** podemos observar que después de 30 min de exposición a $MnCl_2$ hay un incremento en la fosforilación de Akt dependiente de la concentración. Debido a que la concentración de 200 µM de $Mn^{2+}$ mostró un incremento significativo en la fosforilación de Akt y que, como se mencionó antes, ésta es una concentración toxicológicamente relevante en CGB, decidimos utilizar esta concentración en los siguientes experimentos. Al realizar un curso temporal de esta modificación post-traduccional observamos un rápido incremento en la fosforilación de Akt en respuesta a la exposición a $MnCl_2$ 200 µM, el cual presentó su pico máximo a los 5 min de exposición, regresando a niveles basales a los 60 min (**Figura 13B**). Como control positivo de la fosforilación de Akt, las células fueron expuestas a Glu 1 mM durante 15 min, donde podemos observar resultados similares a los que hemos reportado previamente [118]. Por lo que podemos concluir que la exposición a $Mn^{2+}$ induce la fosforilación de Akt.
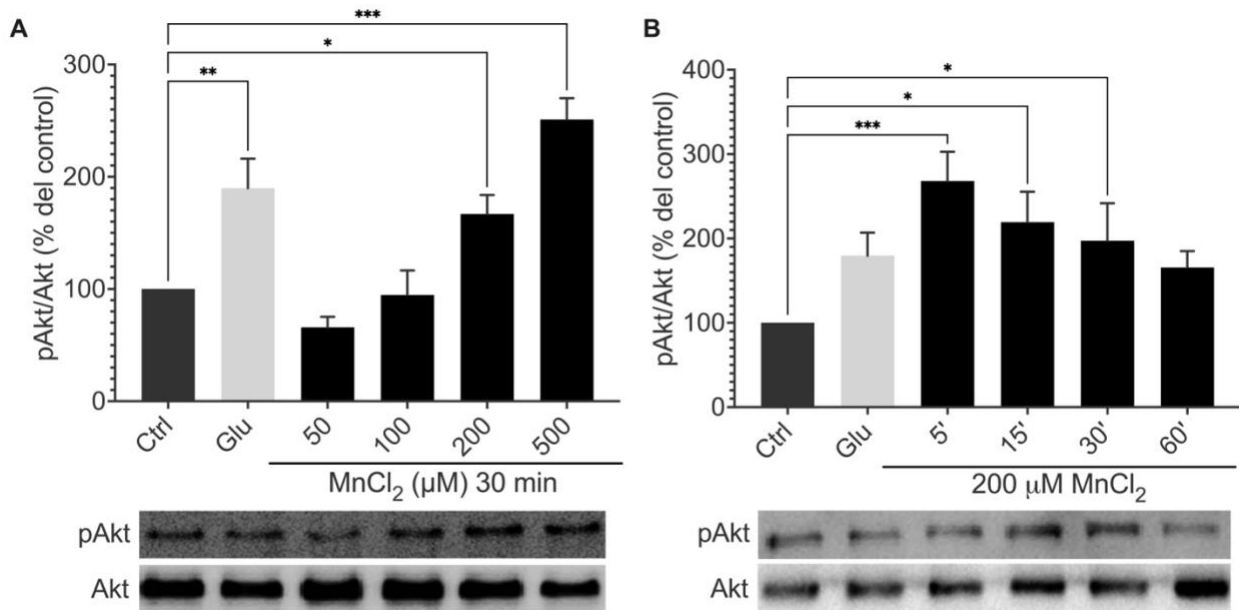
*Figura 13. La exposición a Mn²⁺ incrementa la fosforilación en el residuo Ser⁴⁷³ de Akt. **A**) Dosis-respuesta, **B**) Curso temporal. Glu 1 mM durante 15 min fue utilizado como control. Los datos están expresados como media ± error estándar, n≥3. ANOVA de medidas repetidas y prueba post hoc de Dunnet, \*p<0.05, \*\*p<0.01, \*\*\*p<0.001.*

### 3.3. El efecto de Mn²⁺ sobre Akt es mediado por la activación de PI3K

La fosforilación de Akt es mediada de manera canónica mediante la activación de PI3K, esta cinasa se encarga de fosforilar a $PIP_2$ convirtiéndole en $PIP_3$, dicha modificación permite la localización tanto de Akt como de PDK1, posibilitando la fosforilación de Akt [83]. Con el fin de disecar la señalización suscitada por la exposición a Mn2+ río arriba de Akt optamos por la inhibición farmacológica de PI3K mediante el pretratamiento con Wortmanina 100 nM durante 30 min. Dicho pretratamiento inhibió el efecto inducido por la exposición de 5 min con $MnCl_2$ 200 µM sobre la fosforilación de Akt (**Figura 14**, barras negras). Asimismo, podemos observar en las barras grises nuestro control interno de Glu 1 mM también fue disminuido por el pretratamiento con Wortamina, acorde a nuestros estudios previos [118]. Lo cual confirma que la vía de señalización de PI3K/Akt es activada por la exposición a Mn²⁺.
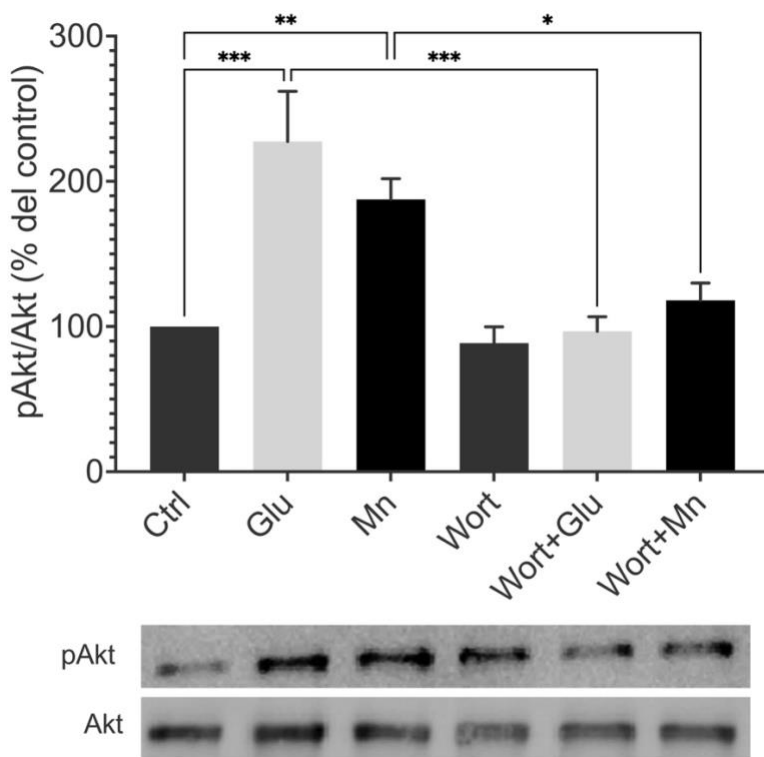
*Figura 14. PI3K modula el efecto inducido por $Mn^{2+}$ en la fosforilación de Akt ($Ser^{473}$). 30 min antes de la exposición a $MnCl_2$ se agregó wortmanina 100 nM. Glu 1mM durante 15 min fue utilizado como control. Los datos están expresados como media ± error estándar, n≥3. ANOVA de medidas repetidas y prueba post hoc de Bonferroni, \*p<0.05, \*\*p<0.01, \*\*\*p<0.001.*

### 3.4. La fosforilación de Akt inducida por $Mn^{2+}$ involucra al intercambiador NCX

Con el fin de obtener más información sobre la señalización involucrada en la fosforilación de Akt mediada por la exposición a $Mn^{2+}$ y tomando en consideración que este metal incrementa la eficiencia catalítica del transportador GLAST en nuestro modelo celular [115], decidimos explorar la posibilidad de que el intercambiador de $Na^+/Ca^{2+}$ (NCX) participe en los efectos inducidos por la exposición a $Mn^{2+}$, ya que el incremento en el transporte de Glu implica un aumento en el $Na^+$ intracelular, el cual ha sido relacionado con la activación de NCX para mantener la homeostasis de iones en la célula. Por lo que utilizamos el inhibidor farmacológico de NCX, KBR7943 15 µM, 30 min antes de los tratamientos con $Mn^{2+}$. Los resultados en la **Figura 15** muestran que la inhibición del NCX previene la fosforilación inducida por la exposición a $Mn^{2+}$ sugiriendo que la exposición a $Mn^{2+}$ incrementa el $Ca^{2+}$ intracelular debido a la activación del NCX, abriendo a la posibilidad de activación de múltiples vías de señalización activadas por $Ca^{2+}$ que a su vez inducen la fosforilación de Akt.
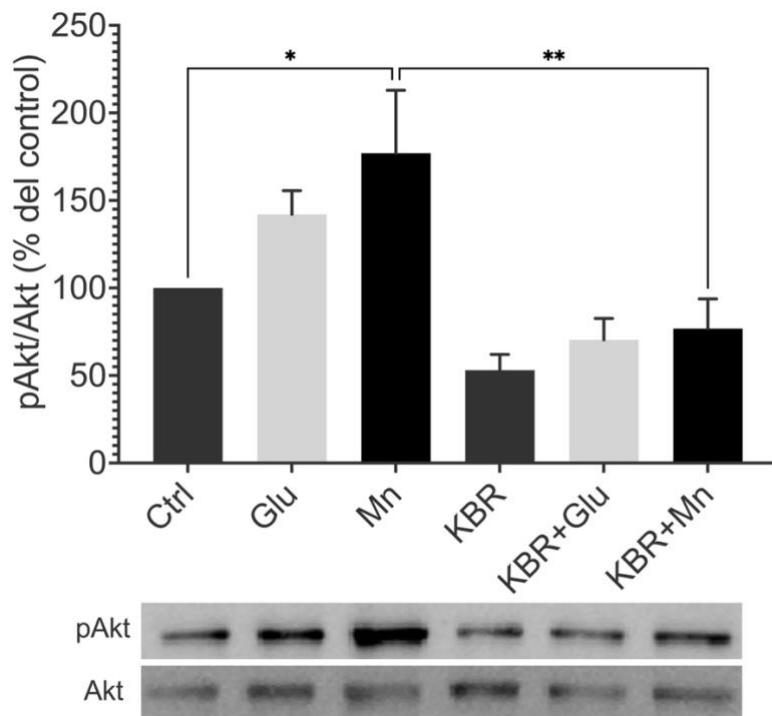
*Figura 15. La inhibición del intercambiador NCX disminuye la fosforilación de Akt inducida por Mn$^{2+}$. 30 min antes de la exposición a MnCl$_2$ se agregó 15 μM de KBR7943. Glu 1 mM durante 15 min fue utilizado como control. Los datos están expresados como media ± error estándar, n≥3. ANOVA de medidas repetidas y prueba post hoc de Bonferroni, \*p<0.05, \*\*p<0.01.*

### 3.5. La exposición a Mn$^{2+}$ induce la fosforilación de 4E-BP1 mediante mTOR y regula la síntesis *de novo* de proteínas

mTOR, el control maestro de la traducción es una proteína efectora río abajo de PI3K/Akt y su activación promueve la traducción de proteínas dependiente de cap a través de la fosforilación de 4E-BP1 [83], por lo que decidimos evaluar los niveles de fosforilación de esta proteína en respuesta a la exposición a 200 μM de MnCl$_2$ durante un curso temporal de 5-30 min, en esta ocasión utilizamos Asp 1 mM durante 15 como control positivo de fosforilación, ya que es un análogo no-metabolizable de Glu que en nuestro modelo de CGB incrementa la fosforilación de 4E-BP1 [119]. Nuestros hallazgos muestran un incremento significativo en la fosforilación de 4E-BP1 en el residuo Thr$^{70}$ después de 10 y 15 min de exposición (**Figura 16A**). Tal efecto demostró ser mediado por mTOR, ya que al utilizar al inhibidor de mTORC1 (100 nM de rapamicina), 30 min antes de la exposición a 200 μM de MnCl$_2$ durante 15 min, la fosforilación de 4E-BP1 inducida

por el Mn$^{2+}$ fue abatida (**Figura 16B**). Estos resultados indican que la exposición a MnCl$_2$ 200 μM regula la fase de inicio de la traducción dependiente de cap en CGB, sin embargo, tal efecto parece disminuir a partir de los 30 min de exposición.
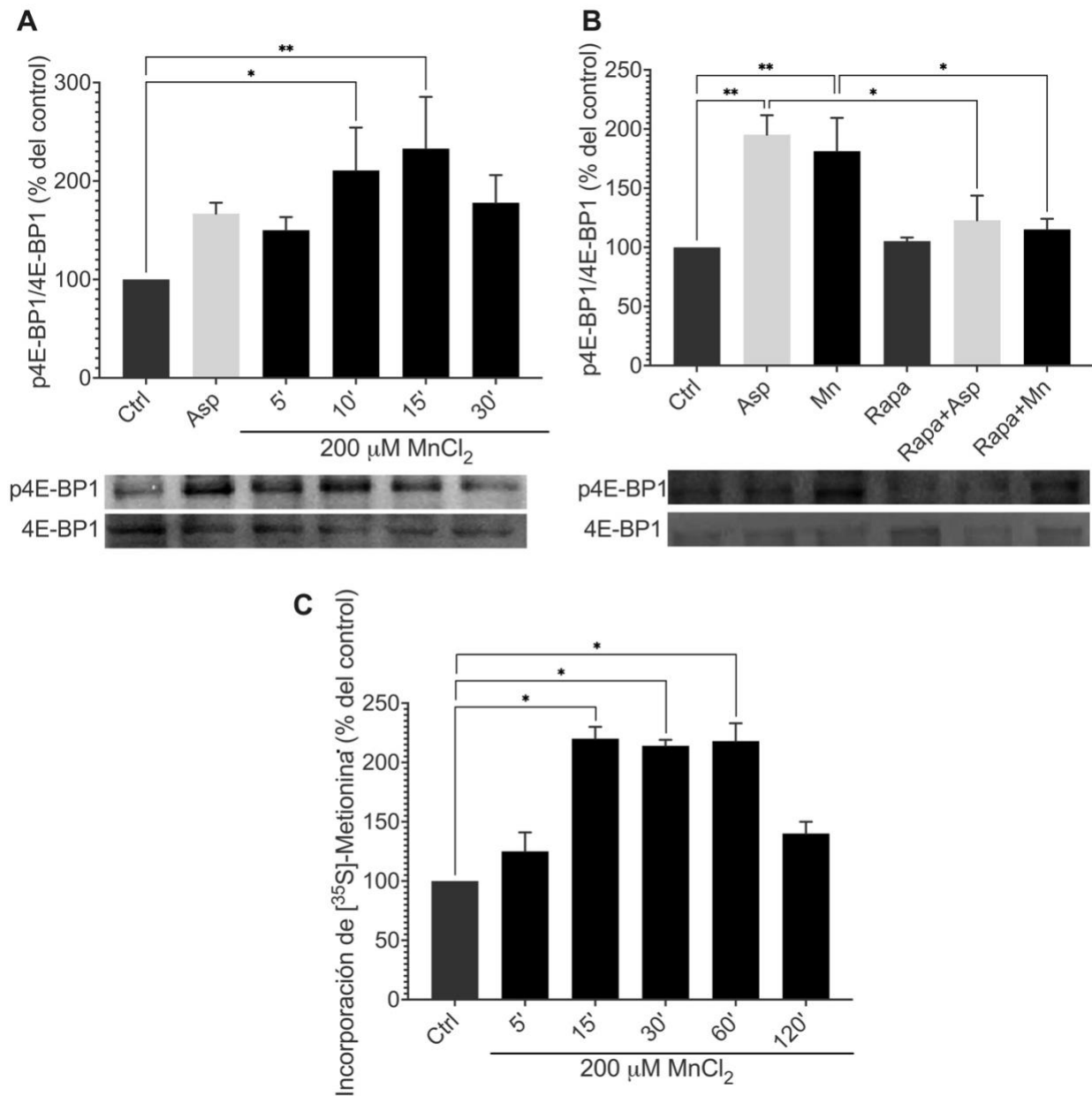


*Figura 16. La exposición a Mn$^{2+}$ incrementa la fosforilación de 4E-BP1 (Thr$^{70}$) a través de mTORC1 y altera la síntesis de proteínas. A) Curso temporal. B) Inhibición de mTORC1. 30 min antes de la exposición a MnCl$_2$ añadimos rapamicina 100 nM. C) Curso temporal de incorporación de [$^{35}$S]-Metionina en nuevas cadenas de polipéptidos. Asp 1 mM durante 15 min fue utilizado como control. Los datos están expresados como media ± error estándar, n≥3. ANOVA de medidas repetidas y prueba post hoc de Bonferroni, \*p<0.05, \*\*p<0.01.*

Con el fin de establecer la consecuencia funcional de la activación de dicha vía de señalización, decidimos evaluar la síntesis global de proteínas. Incubamos CGB confluentes con 1 µCi de [$^{35}$S]-metionina durante 12 h previo a los tratamientos con MnCl$_2$ 200 µM a diferentes tiempos de exposición (5-120 min). Las cadenas de polipéptidos fueron precipitadas con TCA y se cuantificaron las CPM de cada una de las muestras y los resultados se presentaron como porcentaje del control. De manera interesante, encontramos que después de 15 min de exposición a MnCl$_2$ hay un incremento en la incorporación de [$^{35}$S]-metionina en las cadenas nacientes de polipéptidos (**Figura 16C**), en concordancia con los resultados de la fosforilación de 4E-BP1. El efecto sobre la síntesis global de proteínas se mantuvo hasta los 60 min de exposición a MnCl$_2$, lo cual demuestra un efecto transiente de este metal sobre el proceso de traducción de proteínas en CGB donde observamos un incremento en la síntesis de proteínas a los 15 min de exposición al Mn$^{2+}$ debido al incremento en el inicio de la traducción de proteínas posiblemente para mediar los efectos tóxicos del Mn$^{2+}$, sin embargo a partir de los 120 min este efecto disminuye debido a que la síntesis de proteínas es un proceso con un gran costo energético y las CGB se encuentran además bajo estrés oxidante por la exposición al Mn$^{2+}$, por lo que es posible que la célula en ese punto comience a disminuir los procesos catabólicos con el fin de conservar energía.

### 3.6. La exposición a Mn$^{2+}$ induce la fosforilación de AMPK

Los efectos dañinos del Mn$^{2+}$ sobre la mitocondria han sido ampliamente descritos en diferentes modelos de estudio [120], además la exposición a Mn$^{2+}$ reduce la captura de glucosa en nuestro modelo de CGB [115], y teniendo en cuenta que la síntesis de global de proteínas mostró un incremento a los 15 min de exposición a Mn$^{2+}$ y una disminución de dicho efecto después de los 120 min de exposición a este metal (**Figura 16**); nos preguntamos si era posible que los niveles de ATP estuvieran desregulados debido a la exposición a Mn$^{2+}$. Por lo que evaluamos al sensor de ATP activado por el aumento en los niveles de ADP dentro de la célula, AMPK. La fosforilación de esta cinasa en el residuo Thr$^{172}$ es considerada como su marca de activación [121]. Al evaluar los niveles de fosforilación de AMPK tras la exposición a Mn$^{2+}$ a diferentes tiempos (5-60 min) y concentraciones (50-500 µM), encontramos que la exposición a MnCl$_2$ 200 y 500 µM aumenta la fosforilación de AMPK después de 30 min de exposición (**Figura 17**A), dicho efecto fue estadísticamente significativo solo a los 30 min de exposición (**Figura 17**B), aunque a los 60 min de exposición la fosforilación de AMPK aún se encuentra a la alza.
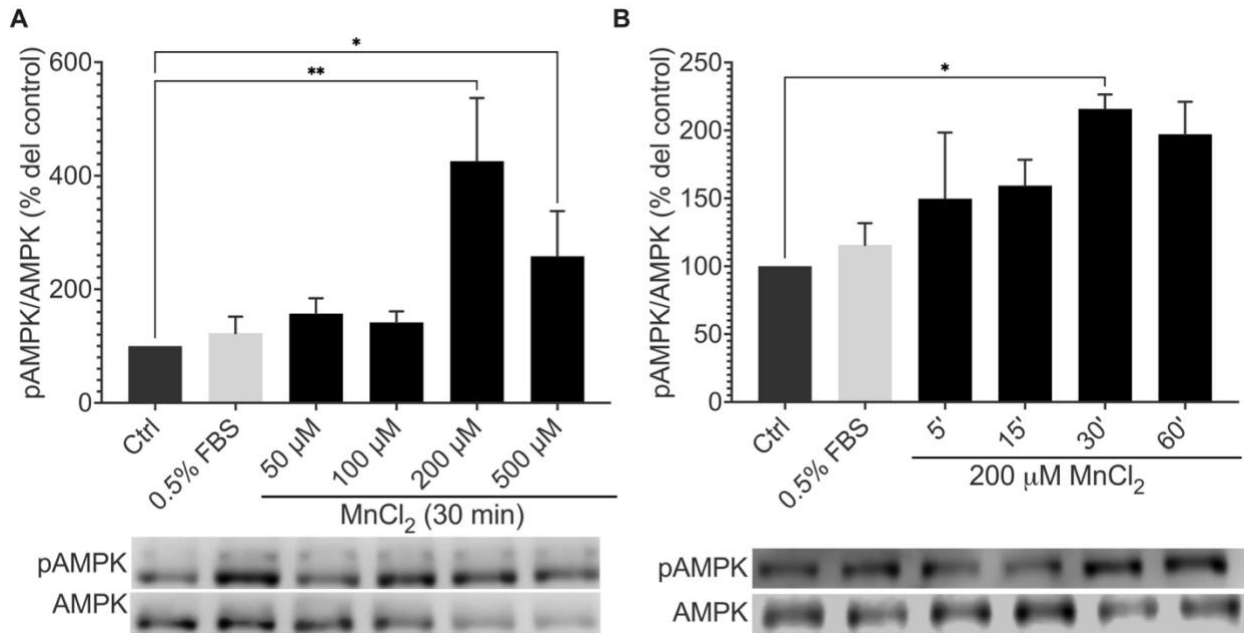
***Figura 17. La exposición a Mn²⁺ incrementa la fosforilación de AMPK en Thr¹⁷². A) Dosis-***
*respuesta. **B)** Curso temporal. Glu 1 mM durante 15 min fue utilizado como control. Los datos*
*están expresados como media ± error estándar, n≥3. ANOVA de medidas repetidas y prueba post*
*hoc de Dunnet, \*p<0.05, \*\*p<0.01.*

Estudios recientes han descrito la comunicación cruzada entre el sensor energético AMPK y Akt
[122,123]. Por esta razón decidimos evaluar si la inhibición farmacológica con Akt IV 15 µM, 30
min antes de la exposición de 30 min de $MnCl_2$ 200µM, altera la fosforilación de AMPK inducida
por $Mn^{2+}$. La inhibición de Akt disminuye el efecto inducido por el $Mn^{2+}$ a los 30 min (**Figura
18A**). Sin embargo, a los 5, 15 y 60 min de exposición no se presentó ningún efecto (**Figura 18B
y C**). Estos resultados sugieren una posible comunicación cruzada entre el sensor energético
AMPK y la vía PI3K/Akt. Es posible que tanto la comunicación entre estas dos vías, así como la
fosforilación de 4E-BP1, estén relacionadas al efecto del $Mn^{2+}$ en la cinética de la síntesis global
de proteínas, aunque no hay que descartar la participación de otros componentes reguladores de la
traducción y el déficit energético.
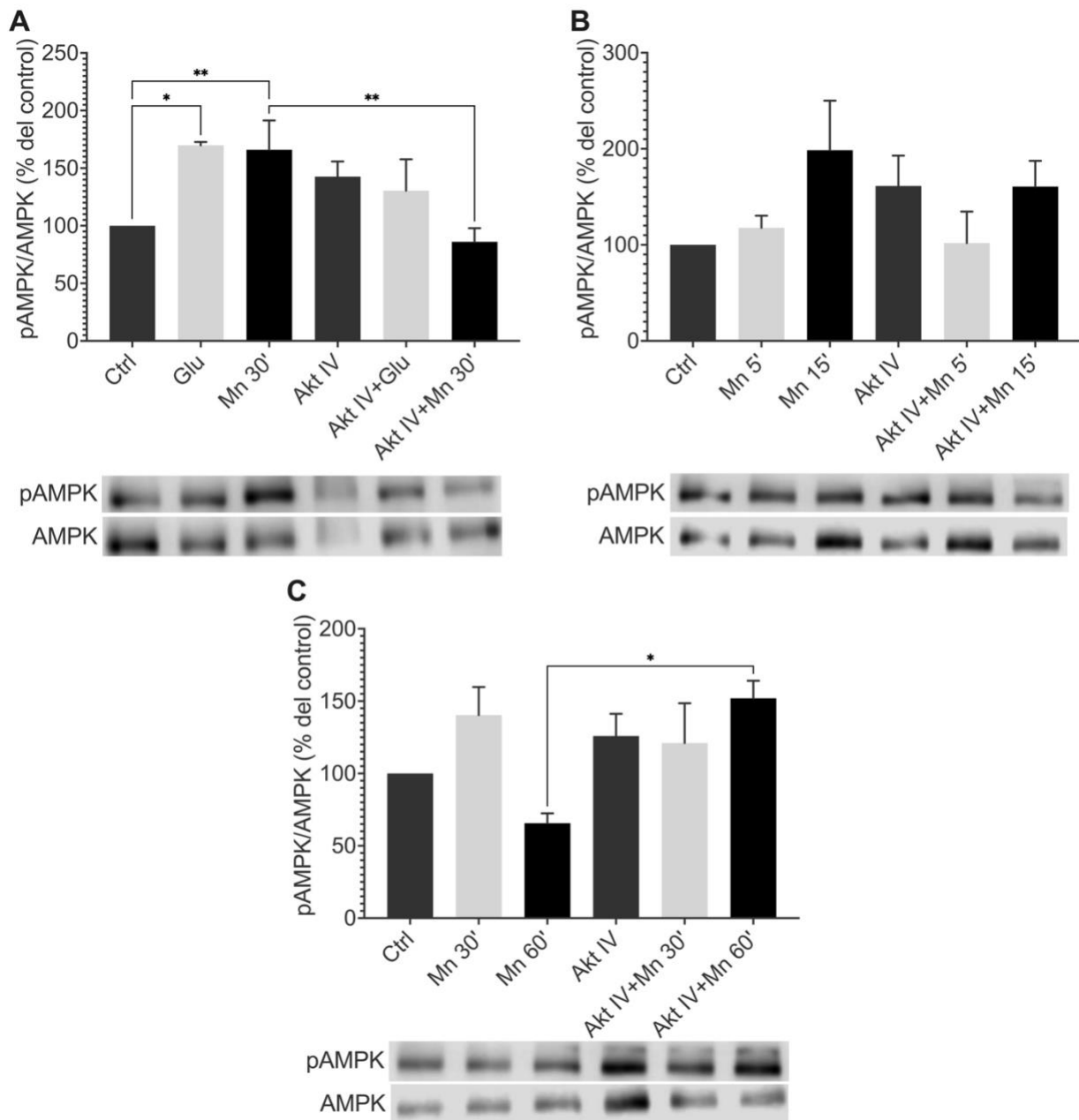
**Figura 18. El efecto de Mn sobre AMPK es modificado por el estado activación de Akt. A)** *30 min antes de la exposición a MnCl₂ 200 μM (30 min) se agregó Akt IV 15 μM. Glu 1 mM durante 15 min fue utilizado como control.* **B)** *MnCl₂ 200 μM durante 5 y 15 min, y* **C)** *30 y 60 min. Los datos están expresados como media ± error estándar, n≥3. ANOVA de medidas repetidas y prueba post hoc de Bonferroni, \*p<0.05, \*\*p<0.01.*

## IV. DISCUSIÓN

La dualidad del $Mn^{2+}$ como un elemento traza esencial, así como un potente agente neurotóxico, ha sido objeto de discusión en la comunidad científica desde hace años, ya que tanto la deficiencia como el exceso pueden ocasionar efectos deletéreos en el SNC. Dado que la mayoría de los estudios *in vitro* de los efectos de la exposición a Mn utilizan concentraciones que sobrepasan las fisiológicamente relevantes [73], en el presente trabajo utilizamos concentraciones que representan una exposición aguda en individuos [71].

A pesar de que el $Mn^{2+}$ se acumula en los ganglios basales y el cerebelo [124], no hay estudios que se enfoquen en el efecto del $Mn^{2+}$ en este órgano. Aunado a esto, el $Mn^{2+}$ se acumula de manera preferencial en células gliales [125]. Además, diversos estudios han mostrado que las células gliales son más resistentes a los efectos citotóxicos del $Mn^{2+}$, en comparación con las neuronas [126,127]. Las CGB son el tipo celular más abundante no-neuronal en el cerebelo, lo cual las hace un excelente modelo para estudiar las interacciones glía-neurona en este órgano [128]. Las CGB envuelven por completo las sinapsis entre las fibras paralelas y las células de Purkinje y tienen una parte activa en la denominada lanzadera Glu/Gln, asegurando el suministro suficiente de neurotransmisores neuronales y, por ende, una correcta neurotransmisión glutamatérgica. Además, las CGB son fundamentales para prevenir el desarrollo de excitotoxicidad debido a la activación de receptores de Glu extrasinápticos [129].

Diversos estudios han descrito que el $Mn^{2+}$ afecta los principales componentes del ciclo Glu/Gln conduciendo a una neurotransmisión glutamatérgica deficiente [130]. Por otro lado, una gran cantidad de estudios acerca del papel del $Mn^{2+}$ en la desregulación del ciclo Glu/Gln se han enfocado principalmente en los efectos a nivel transcripcional [130]. Sin embargo, estudios previos sugieren que el $Mn^{2+}$ puede alterar procesos anabólicos, tales como la síntesis de proteínas [131–133]. El control de la maquinaria de traducción provee de un mecanismo inmediato en respuesta a señales ambientales [82].

Nuestro grupo de investigación y otros, hemos descrito que los transportadores de Glu pueden ser regulados post-transcripcionalmente, al nivel de síntesis de proteínas [2,134]. Sin embargo, hasta donde sabemos, no hay estudios que relacionen los efectos del $Mn^{2+}$ sobre la regulación de la neurotransmisión glutamatérgica a nivel de la traducción.

Se ha descrito que la exposición a $Mn^{2+}$ puede alterar diversas proteínas importantes en la señalización celular, dado que la mayoría de las cinasas son dependientes de $Mn^{2+}$ o $Mg^{2+}$

[135,136]. ERK, Akt, mTOR, JNK, entre otras proteínas pueden ser activadas por el Mn$^{2+}$ *in vivo* e *in vitro* [137]. Akt tiene un papel importante en el control del metabolismo, el crecimiento, la proliferación y la supervivencia celular y, su fosforilación es inducida por la exposición a Mn$^{2+}$ en diferentes modelos [137,138]. Debido a lo anterior, fue de nuestro interés dilucidar los mecanismos desencadenados por Mn$^{2+}$ específicamente en la vía de señalización PI3K/Akt y su posible participación en la traducción de proteínas mediante la activación de proteínas efectoras río abajo de Akt. Hemos demostrado que la exposición a Mn$^{2+}$ induce una rápida fosforilación de Akt en el residuo Ser$^{473}$, es conocido como el sitio regulador de la activación de Akt, y su fosforilación es llevada a cabo por mTORC2 [90]. La activación de Akt es controlada río arriba por un proceso de múltiples etapas e involucra la activación de PI3K, y en el presente trabajo encontramos que la activación de Akt inducida por Mn$^{2+}$ precisa de la actividad de PI3K.

La vía de señalización de PI3K/Akt es activada de manera canónica como consecuencia de la activación de receptores tirosina cinasa (RTK) en la membrana plasmática, tales como los de factores de crecimiento y de insulina, entre otros. Estudios recientes han demostrado que la exposición a Mn$^{2+}$ incrementa la fosforilación del Receptor del Factor de Crecimiento similar a la Insulina tipo I (IGFR-1) y el Receptor de Insulina (IR), lo cual podría explicar que la activación de PI3K/Akt es inducida por la exposición a Mn$^{2+}$ mediante un efecto directo sobre estos receptores [138]. Otra posibilidad es que el Mn$^{2+}$ esté afectando de manera indirecta a los RTKs, ya que se sabe que la activación de ciertos receptores membranales es capaz de transactivar a IGFR-1/IR. Este fenómeno ha sido ampliamente descrito en consecuencia de la activación de GPCRs y de receptores de neurotransmisores [139].

Específicamente, estudios previos en nuestro laboratorio sugieren que la activación de los receptores AMPA transactivan a IGFR-1 [140]. Los receptores AMPA de las CGB son permeables a iones de Ca$^{2+}$ y están vinculados con la activación de cinasa II de Ca$^{2+}$-calmodulina (CaMKII), PKC y Src, las cuales inducen la fosforilación de tirosinas cinasas y por consecuencia la activación de RTKs. Por otro lado, el mismo influjo de Ca$^{2+}$ puede inducir la activación de proteasas, como la metaloproteinasa de matriz extracelular (MMPs), y/o la desintegrina y metaloproteinasa (ADAM), las cuales escinden y liberan agonistas que activan a sus respectivos receptores [141]. Src tiene un papel importante en la activación de MMP y ADAM [142], lo cual la hace una proteína interesante para analizar la posible transactivación de IGFR/IR mediada por la exposición a Mn$^{2+}$.

Previamente hemos demostrado que el cotransporte de Glu y $Na^+$ por medio de los transportadores GLAST conduce a la activación del NCX [119,143]. La activación de este intercambiador conlleva al influjo de $Ca^{2+}$ a causa del incremento en los niveles intracelulares de $Na^+$ ocasionados por el transporte de Glu en CGB. Además, el incremento en el $Ca^{2+}$ intracelular está ligado a la activación de mTOR [119,143]. Es este trabajo, hemos demostrado que el intercambiador NCX está involucrado en la fosforilación de Akt inducida por $Mn^{2+}$ y estudios recientes indican que el transporte de $Mn^{2+}$ a células del SNC puede estar influenciado por el transporte de $Ca^{2+}$ y las moléculas señalizadoras de este catión, tales como: calmodulina, calbindina, calretinina, entre otras [136].

Tomando en cuenta que la exposición a $Mn^{2+}$ incrementa el influjo de $Ca^{2+}$ y que el uniporte de $Ca^{2+}$ mitocondrial (MCU) tiene afinidad por el transporte de $Mn^{2+}$ [144], éste último puede cambiar la morfología e integridad de la membrana plasmática mitocondrial interrumpiendo la cadena respiratoria. Por lo tanto, el daño mitocondrial ocasionado por la exposición a $Mn^{2+}$ puede llevar a un deterioro en la síntesis de proteínas, simplemente porque este proceso es la función celular que más energía consume. En este contexto, los resultados de la **Figura 18**, panel C pueden parecer a primera vista contradictorios con lo antes mencionado, ya que uno esperaría una marcada disminución en el proceso de traducción después de la exposición a $Mn^{2+}$, sin embargo, encontramos un aumento en la incorporación de [$^{35}S$]-Met en cadenas nacientes de polipéptidos. Es posible que esta respuesta esté relacionada con un esfuerzo de la célula para superar el daño causado por este metal, y que, en efecto, coincide con el curso temporal de la activación desencadenada por la exposición a $Mn^{2+}$ de la vía PI3K/Akt/mTOR/4E-BP1 y de AMPK. Es tentador especular que algunas de las proteínas sintetizadas en este periodo representan la línea de defensa celular contra la exposición a $Mn^{2+}$. Evidentemente, se deben realizar los experimentos pertinentes para comprender esta paradoja, los cuales quedan como perspectivas para continuar este estudio.

AMPK es una cinasa que censa los niveles energéticos celulares y cuando es activada promueve procesos catalíticos que ayudan a reabastecer los almacenes de ATP en la célula privada de energía, y de manera concomitante, detiene los procesos anabólicos, tales como la síntesis de proteínas con el fin de ahorrar energía para utilizarla en funciones vitales [121]. En este trabajo demostramos que la exposición a $Mn^{2+}$ incrementa la fosforilación de AMPK a partir de los 30 min y puede disminuir la traducción al inhibir la señalización de mTOR [98]. mTOR tiene un papel importante

en la regulación de diversos aspectos de la fisiología celular, tales como el metabolismo energético, el crecimiento celular, la diferenciación, así como la síntesis de proteínas. La AMPK inhibe a mTOR al activar a TSC2, el cual es un intermediario en la señalización entre Akt y mTOR. A su vez, 4E-BP1 es un blanco directo de mTOR, su fosforilación en el residuo $Thr^{70}$ previene la unión de 4E-BP1 a eIF4E [145]. En nuestro modelo de CGB, hemos encontrado que la exposición a $Mn^{2+}$ induce la fosforilación de 4E-BP1 y comprobamos que este efecto es dependiente de la activación de mTOR, que coincide con el aumento en la incorporación de $[^{35}S]$-Met.

El incremento en la fosforilación de 4E-BP1 promueve el inicio de la traducción [146]. La fosforilación de mTOR en el residuo $Ser^{2448}$ ha sido utilizado como indicador de su activación, sin embargo, el uso de este marcador ha sido puesto en tela de juicio ya que, la mutación de Ser por una Ala no afecta la fosforilación de los blancos de mTOR, 4E-BP1 entre ellos [147]. De manera interesante, la activación farmacológica de AMPK ha mostrado disminuir los niveles de fosforilación de Akt, mTOR, S6K y 4E-BP1 [103], lo cual es indicativo de la supresión de la traducción de proteínas [148]. En este punto es importante mencionar que el marco de tiempo de la activación de AMPK coincide con el inicio en la disminución de la fosforilación de 4E-BP1, así como de Akt después de los 30 min de exposición, aunque la síntesis global de proteínas aún se encuentra por encima de los niveles basales, es notable la naturaleza inversamente proporcional de estas vías de señalización después de la exposición a $Mn^{2+}$. Esto destaca el efecto transitorio en el control de la maquinaria traduccional glial en respuesta a la exposición a este metal divalente, como se ha demostrado con otros agentes neurotóxicos en CGB [2,149,150].

Hasta el momento, hemos demostrado que la exposición a $Mn^{2+}$ puede afectar el inicio de la traducción al alterar los patrones de fosforilación de 4E-BP1 a través de la señalización $Ca^{2+}$/PI3K/Akt/mTOR y la participación de AMPK. Interesantemente, las mismas vías de señalización tienen un papel importante en la regulación de la fase de elongación de síntesis de proteínas [83]. eEF2 es un blanco potencial de la exposición a $Mn^{2+}$, y es indirectamente regulado por mTOR a través de S6K. Además, es considerado el paso de la traducción que consume más energía. La fosforilación de eEF2 en el residuo $Thr^{56}$ es llevado a cabo mediante la cinasa específica eEF2K [95]. Mientras que S6K activa a eEF2 al fosforilar e inactivar a eEF2K, en contraste, AMPK induce la activación de eEF2K y la consecuente inactivación de eEF2 [106]. Además, existe otra pieza importante a tomar en consideración, y es la fosforilación en el residuo $Ser^{51}$, de eIF2a, que previene el intercambio de nucleótidos llevado a cabo por eIF2B y en

consecuencia la inhibición del complejo ternario de inicio de la traducción [81]. Existen 4 cinasas de eIF2α descritas: GCN1, HRI, PKR y PERK [151]. Estudios recientes ha mostrado que la exposición a $Mn^{2+}$ induce la activación de PERK, promoviendo la respuesta autofágica [152].

El modelo propuesto para explicar los efectos de la exposición a $Mn^{2+}$ en CGB es (**Figura 19**): la exposición de CGB a $Mn^{2+}$ induce la activación de la vía de señalización PI3K/Akt/mTOR, regulando el inicio de la traducción al hiperfosforilar a 4E-BP1 permitiendo el incremento de la síntesis global de proteínas, posiblemente traduciendo proteínas importantes para mediar el efecto tóxico del $Mn^{2+}$. Sin embargo, es probable que el incremento en la traducción provoque un déficit energético en la célula, por lo que sugerimos que la activación de AMPK está relacionada con la reducción en procesos catabólicos, como la traducción de proteínas. Pero ¿cómo la exposición a $Mn^{2+}$ induce la activación de PI3K/Akt/mTOR en CGB?, hay al menos tres posibilidades la primera es que el manganeso sea capaz de activar directamente a RTKs como IGFR-1 o IR; la segunda es la transactivación de RTKs por medio de MPP o ADAM debido a un incremento de $Ca^{2+}$ intracelular y como tercera posibilidad no podemos descartar que el $Mn^{2+}$ que haya ingresado a la célula sea capaz de interaccionar directamente con proteínas efectoras de estas vías de señalización.

En resumen, nuestros hallazgos sugieren que la alteración en la vía PI3K/Akt/mTOR representa un evento temprano en los mecanismos de toxicidad del $Mn^{2+}$ y que la síntesis de proteínas puede estar alterada por la exposición a este metal. Estos hallazgos fortalecen la idea del papel crítico que tienen las células gliales en el desarrollo de neurotoxicidad.
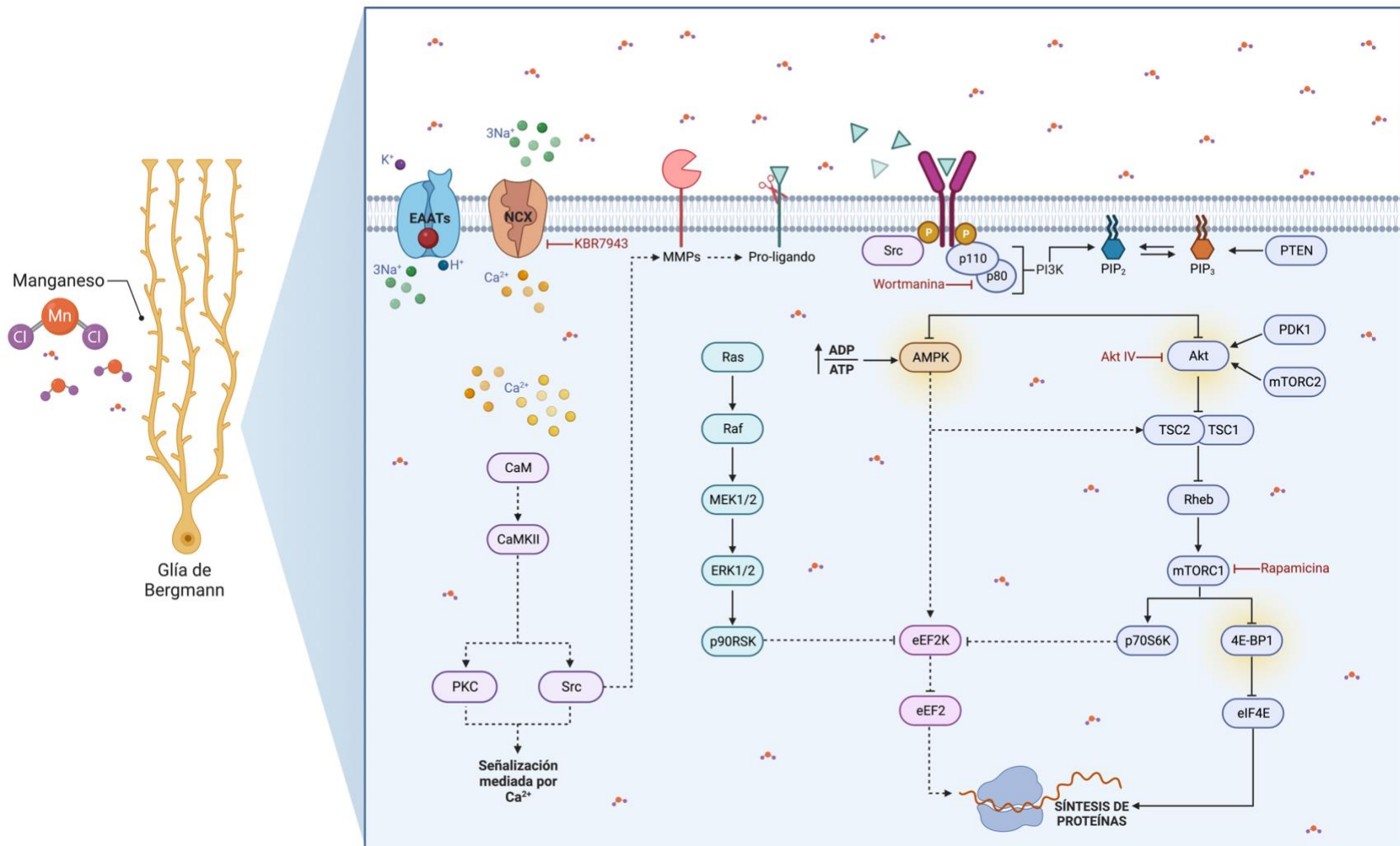
*Figura 19. Modelo propuesto de los efectos inducidos por la exposición aguda a Mn$^{2+}$ en la vía de señalización PI3K/Akt/mTOR/4E-BP1 en CGB*

## V.    CONCLUSIONES

- La exposición a MnCl$_2$ no afecta la viabilidad celular de CGB.

- La fosforilación de Akt (Ser$^{473}$) incrementa en CGB expuestas a MnCl$_2$ a partir de los 5 min de exposición y el efecto es dependiente de la dosis y de la activación de PI3K.

- El intercambiador NCX tiene un papel importante en la fosforilación de Akt (Ser$^{473}$) inducida por la exposición a MnCl$_2$ en CGB.

- La exposición a MnCl$_2$ incrementa la fosforilación de 4E-BP1 (Thr$^{70}$) a los 10 y 15 min de tratamiento, tal efecto es mediado por la actividad de mTOR.

- La exposición de CGB a MnCl$_2$ incrementa la incorporación de [$^{35}$S]-metionina en cadenas nascientes de polipétidos a partir de los 15 min y hasta los 60 min de exposición al metal.

- A partir de los 30 min de exposición a MnCl$_2$ se incrementa la fosforilación de AMPK (Thr$^{172}$), tal efecto se encuentra relacionado a la activación de Akt.

## VI.    PERSPECTIVAS

- Caracterizar la identidad de los mRNAs que se encuentran en la fracción polisomal durante el tratamiento con $MnCl_2$ en CGB mediante TRAP-seq (translating-ribosome affinity purification), para identificar y cuantificar los RNAs traducidos (traductoma) durante la exposición a $Mn^{2+}$.

- Analizar el estado bioenergético de las CGB después de la exposición a $MnCl_2$ mediante la cuantificación de la velocidad de consumo de oxígeno (OCR) y la de acidificación extracelular (ECAR) utilizando la técnica Seahorse para evaluar los cambios en la tasa de ATP en tiempo real en respuesta a la exposición a $Mn^{2+}$.

- Caracterizar el efecto de la exposición a $MnCl_2$ en el estado de fosforilación de las proteínas de la maquinaria traduccional eIF2$\alpha$, eEF2 y eEF2K en CGB, proteínas clave del control del inicio y la elongación de la traducción de proteínas.

- Evaluar el papel de las Ser/Thr fosfatasas mediante inhibición farmacológica en el efecto inducido por el tratamiento con $MnCl_2$ en la maquinaria traduccional de CGB ya que la actividad de las proteínas efectoras de la maquinaria traduccional también puede ser regulada por fosfatasas.

## VII.    REFERENCIAS

[1]     L. Ben Haim, D.H. Rowitch, Functional diversity of astrocytes in neural circuit regulation, Nat Rev Neurosci. (2016). https://doi.org/10.1038/nrn.2016.159.

[2]     M. Flores-Méndez, O.G. Mendez-Flores, A. Ortega, Glia plasma membrane transporters: Key players in glutamatergic neurotransmission, Neurochem Int. (2016). https://doi.org/10.1016/j.neuint.2016.04.004.

[3]     N.J. Allen, D.A. Lyons, Glia as architects of central nervous system formation and functionAllen, N. J., & Lyons, D. A. (2018). Glia as architects of central nervous system formation and function. Science. https://doi.org/10.1126/science.aat0473, Science (1979). (2018). https://doi.org/10.1126/science.aat0473.

[4]     L. Dimou, M. Götz, Glial cells as progenitors and stem cells: New roles in the healthy and diseased brain, Physiol Rev. (2014). https://doi.org/10.1152/physrev.00036.2013.

[5]     E. Taverna, M. Götz, W.B. Huttner, The Cell Biology of Neurogenesis: Toward an Understanding of the Development and Evolution of the Neocortex, Annu Rev Cell Dev Biol. (2014). https://doi.org/10.1146/annurev-cellbio-101011-155801.

[6]     R.G. Almeida, D.A. Lyons, On myelinated axon plasticity and neuronal circuit formation and function, Journal of Neuroscience. (2017). https://doi.org/10.1523/JNEUROSCI.3185-16.2017.

[7]     A.A. Chrobak, Z. Soltys, Bergmann Glia, Long-Term Depression, and Autism Spectrum Disorder, Mol Neurobiol. (2017). https://doi.org/10.1007/s12035-016-9719-3.

[8]     C.I. De Zeeuw, T.M. Hoogland, Reappraisal of Bergmann glial cells as modulators of cerebellar circuit function, Front Cell Neurosci. (2015). https://doi.org/10.3389/fncel.2015.00246.

[9]     A.W. Leung, J.Y.H. Li, The Molecular Pathway Regulating Bergmann Glia and Folia Generation in the Cerebellum, Cerebellum. (2018). https://doi.org/10.1007/s12311-017-0904-3.

[10]    R. Apps, M. Garwicz, Anatomical and physiological foundations of cerebellar information processing, Nat Rev Neurosci. (2005). https://doi.org/10.1038/nrn1646.

[11]    D.L. Chao, L. Ma, K. Shen, Transient cell–cell interactions in neural circuit formation. Nat Rev Neurosci 10, 262–271 (2009). https://doi.org/10.1038/nrn2594.

[12]    S. Magi, S. Piccirillo, S. Amoroso, The dual face of glutamate: from a neurotoxin to a potential survival factor—metabolic implications in health and disease, Cellular and Molecular Life Sciences. (2019). https://doi.org/10.1007/s00018-018-3002-x.

[13]    N.C. Danbolt, Glutamate uptake, Prog Neurobiol. (2001). https://doi.org/10.1016/S0301-0082(00)00067-8.

[14]    A. Reiner, J. Levitz, Glutamatergic Signaling in the Central Nervous System: Ionotropic and Metabotropic Receptors in Concert, Neuron. (2018). https://doi.org/10.1016/j.neuron.2018.05.018.

[15]    S.S. Willard, S. Koochekpour, Glutamate, glutamate receptors, and downstream signaling pathways, Int J Biol Sci. (2013). https://doi.org/10.7150/ijbs.6426.

[16]    G.T. Swanson, R. Sakai, Ligands for ionotropic glutamate receptors, Prog Mol Subcell Biol. 46 (2009) 123–157. https://doi.org/10.1007/978-3-540-87895-7_5.

[17]    M. Yuzaki, A.R. Aricescu, A GluD Coming-Of-Age Story, Trends Neurosci. (2017). https://doi.org/10.1016/j.tins.2016.12.004.

[18]    S.F. Traynelis, L.P. Wollmuth, C.J. McBain, F.S. Menniti, K.M. Vance, K.K. Ogden, K.B. Hansen, H. Yuan, S.J. Myers, R. Dingledine, Glutamate Receptor Ion Channels: Structure, Regulation, and Function, Pharmacol Rev. (2010). https://doi.org/10.1124/pr.109.002451.

[19]    P.J. Kenny, A. Markou, The ups and downs of addiction: Role of metabotropic glutamate receptors, Trends Pharmacol Sci. (2004). https://doi.org/10.1016/j.tips.2004.03.009.

[20]    Y. Zhou, N.C. Danbolt, Glutamate as a neurotransmitter in the healthy brain, J Neural Transm. (2014). https://doi.org/10.1007/s00702-014-1180-8.

[21]    T. Storck, S. Schulte, K. Hofmann, W. Stoffel, Structure, expression, and functional analysis of a Na(+)-dependent glutamate/aspartate transporter from rat brain, Proc Natl Acad Sci U S A. 89 (1992) 10955–10959. https://doi.org/10.1073/pnas.89.22.10955.

[22]    G. Pines, N.C. Danbolt, M. Bjørås, Y. Zhang, A. Bendahan, L. Eide, H. Koepsell, J. Storm-Mathisen, E. Seeberg, B.I. Kanner, Cloning and expression of a rat brain L-glutamate transporter, Nature. (1992). https://doi.org/10.1038/360464a0.

[23]    Y. Kanai, M.A. Hediger, Primary structure and functional characterization of a high-affinity glutamate transporter, Nature. (1992). https://doi.org/10.1038/360467a0.

[24] J.L. Arriza, W. a Fairman, J.I. Wadiche, G.H. Murdoch, M.P. Kavanaugh, S.G. Amara, Functional comparisons of three glutamate transporter subtypes cloned from human motor cortex., Journal of Neuroscience. (1994). https://doi.org/10.1016/j.jhg.2008.11.002.

[25] W.A. Fairman, R.J. Vandenberg, J.L. Arriza, M.P. Kavanaught, S.G. Amara, An excitatory amino-acid transporter with properties of a ligand-gated chloride channel, Nature. (1995). https://doi.org/10.1038/375599a0.

[26] J.L. Arriza, S. Eliasof, M.P. Kavanaugh, S.G. Amara, Excitatory amino acid transporter 5, a retinal glutamate transporter coupled to a chloride conductance, Proceedings of the National Academy of Sciences. (1997). https://doi.org/10.1073/pnas.94.8.4155.

[27] J. Jiang, S.G. Amara, New views of glutamate transporter structure and function: Advances and challenges, Neuropharmacology. (2011). https://doi.org/10.1016/j.neuropharm.2010.07.019.

[28] D. Chi-Castañeda, E. Suárez-Pozos, A. Ortega, Regulation of Glutamate Transporter Expression in Glial Cells BT - Glial Amino Acid Transporters, in: A. Ortega, A. Schousboe (Eds.), Springer International Publishing, Cham, 2017: pp. 199–224. https://doi.org/10.1007/978-3-319-55769-4_10.

[29] E. Suárez-Pozos, D. Chi-Castañeda, A. Ortega, Glial Glutamate Transporters as Signaling Molecules BT - Glial Amino Acid Transporters, in: A. Ortega, A. Schousboe (Eds.), Springer International Publishing, Cham, 2017: pp. 185–198. https://doi.org/10.1007/978-3-319-55769-4_9.

[30] R.J. Vandenberg, R.M. Ryan, Mechanisms of Glutamate Transport, Physiol Rev. (2013). https://doi.org/10.1152/physrev.00007.2013.

[31] G. Perea, M. Navarrete, A. Araque, Tripartite synapses: astrocytes process and control synaptic information, Trends Neurosci. (2009). https://doi.org/10.1016/j.tins.2009.05.001.

[32] M.C. Marx, D. Billups, B. Billups, Maintaining the presynaptic glutamate supply for excitatory neurotransmission, J Neurosci Res. (2015). https://doi.org/10.1002/jnr.23561.

[33] H. Tani, C.G. Dulla, Z. Farzampour, A. Taylor-Weiner, J.R. Huguenard, R.J. Reimer, A local glutamate-glutamine cycle sustains synaptic excitatory transmitter release, Neuron. (2014). https://doi.org/10.1016/j.neuron.2013.12.026.

[34] D. Billups, M.-C. Marx, I. Mela, B. Billups, Inducible Presynaptic Glutamine Transport Supports Glutamatergic Transmission at the Calyx of Held Synapse, Journal of Neuroscience. (2013). https://doi.org/10.1523/JNEUROSCI.1466-13.2013.

[35] C. Rae, N. Hare, W.A. Bubb, S.R. McEwan, A. Bröer, J.A. McQuillan, V.J. Balcar, A.D. Conigrave, S. Bröer, Inhibition of glutamine transport depletes glutamate and GABA neurotransmitter pools: Further evidence for metabolic compartmentation, J Neurochem. (2003). https://doi.org/10.1046/j.1471-4159.2003.01713.x.

[36] M.D. Norenberg, A. Martinez-Hernandez, Fine structural localization of glutamine synthetase in astrocytes of rat brain, Brain Res. (1979). https://doi.org/10.1016/0006-8993(79)90071-4.

[37] U. Sonnewald, A. Schousboe, In: Schousboe, A., Sonnewald, U. (eds) The Glutamate/GABA-Glutamine Cycle. Advances in Neurobiology, vol 13. Springer, Cham. https://doi.org/10.1007/978-3-319-45096-4_1.

[38] USEPA, Health Assessment Document for Manganese, Final Report, U.S. Environmental Protection Agency. EPA 600 (1984).

[39] A.W. Davidson, Advanced Inorganic Chemistry. A Comprehensive Text., J Am Chem Soc. (2005). https://doi.org/10.1021/ja00891a056.

[40] P. Chen, J. Bornhorst, M. Aschner, Manganese metabolism in humans, Frontiers in Bioscience - Landmark. (2018). https://doi.org/10.2741/4665.

[41] K. Sikk, S. Haldre, S.-M. Aquilonius, P. Taba, Manganese-Induced Parkinsonism due to Ephedrone Abuse., Parkinsons Dis. 2011 (2011) 865319. https://doi.org/10.4061/2011/865319.

[42] M. Aschner, K. Erikson, Manganese, Advances in Nutrition. 8 (2017) 520–521. https://doi.org/10.3945/an.117.015305.

[43] A.C. Pfalzer, A.B. Bowman, Relationships Between Essential Manganese Biology and Manganese Toxicity in Neurological Disease, Curr Environ Health Rep. (2017). https://doi.org/10.1007/s40572-017-0136-1.

[44] C. Olanow, Manganese-Induced Parkinsonism and Parkinson's Disease, Ann N Y Acad Sci. 1012 (2006) 209–223. https://doi.org/10.1196/annals.1306.018.

[45] Barbeau, A. (1984). Manganese and extrapyramidal disorders (a critical review and tribute to Dr. George C. Cotzias). Neurotoxicology, 5 1, 13-35.

[46] L. Quintanar, Manganese neurotoxicity: A bioinorganic chemist's perspective, Inorganica Chim Acta. 361 (2008) 875–884. https://doi.org/10.1016/J.ICA.2007.09.008.

[47]     J. Roth, S. Ponzoni, M. Aschner, Manganese Homeostasis and Transport, in: L. Banci (Ed.), Metallomics and the Cell, Springer Netherlands, Dordrecht, 2013: pp. 169–201. https://doi.org/10.1007/978-94-007-5561-1_6.

[48]     K. Palikaras, E. Lionaki, N. Tavernarakis, Balancing mitochondrial biogenesis and mitophagy to maintain energy metabolism homeostasis, Cell Death Differ. (2015). https://doi.org/10.1038/cdd.2015.86.

[49]     L. Dupuis, Mitochondrial quality control in neurodegenerative diseases, Biochimie. (2014). https://doi.org/10.1016/j.biochi.2013.07.033.

[50]     H.B. Suliman, C.A. Piantadosi, Mitochondrial Quality Control as a Therapeutic Target, Pharmacol Rev. (2015). https://doi.org/10.1124/pr.115.011502.

[51]     S. Zhang, Z. Zhou, J. Fu, Effect of manganese chloride exposure on liver and brain mitochondria function in rats, Environ Res. (2003). https://doi.org/10.1016/S0013-9351(03)00109-9.

[52]     S. Zhang, J. Fu, Z. Zhou, In vitro effect of manganese chloride exposure on reactive oxygen species generation and respiratory chain complexes activities of mitochondria isolated from rat brain, Toxicology in Vitro. (2004). https://doi.org/10.1016/j.tiv.2003.09.002.

[53]     S. Zhang, J. Fu, Z. Zhou, Changes in the brain mitochondrial proteome of male Sprague-Dawley rats treated with manganese chloride, Toxicol Appl Pharmacol. (2005). https://doi.org/10.1016/j.taap.2004.06.001.

[54]     E.A. Malecki, Manganese toxicity is associated with mitochondrial dysfunction and DNA fragmentation in rat primary striatal neurons, in: Brain Res Bull, 2001. https://doi.org/10.1016/S0361-9230(01)00456-7.

[55]     K. V. Rama Rao, M.D. Norenberg, Manganese induces the mitochondrial permeability transition in cultured astrocytes, Journal of Biological Chemistry. (2004). https://doi.org/10.1074/jbc.M402096200.

[56]     K. Sriram, G.X. Lin, A.M. Jefferson, J.R. Roberts, O. Wirth, Y. Hayashi, K.M. Krajnak, J.M. Soukup, A.J. Ghio, S.H. Reynolds, V. Castranova, A.E. Munson, J.M. Antonini, Mitochondrial dysfunction and loss of Parkinson's disease-linked proteins contribute to neurotoxicity of manganese-containing welding fumes, The FASEB Journal. (2010). https://doi.org/10.1096/fj.10-163964.

[57]     Q. Zhou, X. Fu, X. Wang, Q. Wu, Y. Lu, J. Shi, J.E. Klaunig, S. Zhou, Autophagy plays a protective role in Mn-induced toxicity in PC12 cells, Toxicology. (2018). https://doi.org/10.1016/j.tox.2017.12.001.

[58]     D.B. Zorov, M. Juhaszova, S.J. Sollott, Mitochondrial Reactive Oxygen Species (ROS) and ROS-Induced ROS Release, Physiol Rev. (2014). https://doi.org/10.1152/physrev.00026.2013.

[59]     Brustovetsky, N., Brustovetsky, T., Jemmerson, R. and Dubinsky, J.M. (2002), Calcium-induced Cytochrome c release from CNS mitochondria is associated with the permeability transition and rupture of the outer membrane. Journal of Neurochemistry, 80: 207-218. https://doi.org/10.1046/j.0022-3042.2001.00671.x.

[60]     H.T. Zhang, L. Mi, T. Wang, L. Yuan, X.H. Li, L.S. Dong, P. Zhao, J.L. Fu, B.Y. Yao, Z.C. Zhou, PINK1/Parkin-mediated mitophagy play a protective role in manganese induced apoptosis in SH-SY5Y cells, Toxicology in Vitro. (2016). https://doi.org/10.1016/j.tiv.2016.04.006.

[61]     V.A. Fitsanakis, C. Au, K.M. Erikson, M. Aschner, The effects of manganese on glutamate, dopamine and γ-aminobutyric acid regulation, Neurochem Int. (2006). https://doi.org/10.1016/j.neuint.2005.10.012.

[62]     L. Wang, F. HuanHuan, L. Bin, L. XiaoYan, C. WeiWei, Y. XiaoDan, The effect of postnatal manganese exposure on the NMDA receptor signaling pathway in rat hippocampus, J Biochem Mol Toxicol. 31 (2017) e21969. https://doi.org/10.1002/jbt.21969.

[63]     J. Johnson, E. Pajarillo, P. Karki, J. Kim, D.S. Son, M. Aschner, E. Lee, Valproic acid attenuates manganese-induced reduction in expression of GLT-1 and GLAST with concomitant changes in murine dopaminergic neurotoxicity, Neurotoxicology. 67 (2018) 112–120. https://doi.org/10.1016/j.neuro.2018.05.001.

[64]     Lee, E., Karki, P., Johnson, J., Hong, P., Aschner, M. (2017). Manganese Control of Glutamate Transporters' Gene Expression. In: Ortega, A., Schousboe, A. (eds) Glial Amino Acid Transporters. Advances in Neurobiology, vol 16. Springer, Cham. https://doi.org/10.1007/978-3-319-55769-4_1.

[65]     M. Escalante, J. Soto-Verdugo, L.C. Hernández-Kelly, D. Hernández-Melchor, E. López-Bayghen, T.N. Olivares-Bañuelos, A. Ortega, GLAST Activity is Modified by Acute Manganese Exposure in Bergmann Glial Cells, Neurochem Res. (2019). https://doi.org/10.1007/s11064-019-02848-8.

[66]     D. Milatovic, Z. Yin, R.C. Gupta, M. Sidoryk, J. Albrecht, J.L. Aschner, M. Aschner, Manganese Induces Oxidative Impairment in Cultured Rat Astrocytes, Toxicological Sciences. 98 (2007) 198–205. https://doi.org/10.1093/toxsci/kfm095.

[67]     M. Sidoryk-Wegrzynowicz, E. Lee, J. Albrecht, M. Aschner, Manganese disrupts astrocyte glutamine transporter expression and function, J Neurochem. (2009). https://doi.org/10.1111/j.1471-4159.2009.06172.x.

[68]    M. Sidoryk-Wegrzynowicz, E. Lee, N. Mingwei, M. Aschner, Disruption of astrocytic glutamine turnover by manganese is mediated by the protein kinase C pathway, Glia. (2011). https://doi.org/10.1002/glia.21219.

[69]    F.C. Wedler, B.W. Ley, Kinetic, ESR, and trapping evidence for in vivo binding of Mn(II) to glutamine synthetase in brain cells, Neurochem Res. (1994). https://doi.org/10.1007/BF00966808.

[70]    Y. Deng, Z. Xu, B. Xu, D. Xu, Y. Tian, W. Feng, The protective effects of riluzole on manganese-induced disruption of glutamate transporters and glutamine synthetase in the cultured astrocytes, Biol Trace Elem Res. (2012). https://doi.org/10.1007/s12011-012-9365-1.

[71]    J. Soto-Verdugo, A. Ortega, Critical Involvement of Glial Cells in Manganese Neurotoxicity, Biomed Res Int. 2021 (2021) 1596185. https://doi.org/10.1155/2021/1596185.

[72]    X.X. Dong, Y. Wang, Z.H. Qin, Molecular mechanisms of excitotoxicity and their relevance to pathogenesis of neurodegenerative diseases, Acta Pharmacol Sin. (2009). https://doi.org/10.1038/aps.2009.24.

[73]    A.B. Bowman, M. Aschner, Considerations on manganese (Mn) treatments for in vitro studies, Neurotoxicology. (2014). https://doi.org/10.1016/j.neuro.2014.01.010.

[74]    M. Brini, T. Calì, D. Ottolini, E. Carafoli, Neuronal calcium signaling: Function and dysfunction, Cellular and Molecular Life Sciences. (2014). https://doi.org/10.1007/s00018-013-1550-7.

[75]    D. Walsh, I. Mohr, Viral subversion of the host protein synthesis machinery, Nat Rev Microbiol. (2011). https://doi.org/10.1038/nrmicro2655.

[76]    S. Iwasaki, N.T. Ingolia, The Growing Toolbox for Protein Synthesis Studies, Trends Biochem Sci. (2017). https://doi.org/10.1016/j.tibs.2017.05.004.

[77]    W.S. Sossin, M. Costa-Mattioli, Translational Control in the Brain in Health and Disease, Cold Spring Harb Perspect Biol. 11 (2019). https://doi.org/10.1101/cshperspect.a032912.

[78]    M. Costa-Mattioli, N. Sonenberg, Chapter 5 Translational control of gene expression: A molecular switch for memory storage, Prog Brain Res. (2008). https://doi.org/10.1016/S0079-6123(07)00005-2.

[79]    N. Sonenberg, A.G. Hinnebusch, Regulation of Translation Initiation in Eukaryotes: Mechanisms and Biological Targets, Cell. (2009). https://doi.org/10.1016/j.cell.2009.01.042.

[80]    T.E. Dever, T.G. Kinzy, G.D. Pavitt, Mechanism and regulation of protein synthesis in Saccharomyces cerevisiae, Genetics. (2016). https://doi.org/10.1534/genetics.115.186221.

[81]    S.L. Moon, N. Sonenberg, R. Parker, Neuronal Regulation of eIF2α Function in Health and Neurological Disorders, Trends Mol Med. (2018). https://doi.org/10.1016/j.molmed.2018.04.001.

[82]    K.S. Browning, J. Bailey-Serres, Mechanism of Cytoplasmic mRNA Translation, Arabidopsis Book. (2015). https://doi.org/10.1199/tab.0176.

[83]    P.P. Roux, I. Topisirovic, Signaling Pathways Involved in the Regulation of mRNA Translation, Mol Cell Biol. (2018). https://doi.org/10.1128/mcb.00070-18.

[84]    P.P. Roux, I. Topisirovic, Regulation of mRNA translation by signaling pathways, Cold Spring Harb Perspect Biol. (2012). https://doi.org/10.1101/cshperspect.a012252.

[85]    M. Osaki, M. Oshimura, H. Ito, PI3K-Akt pathway: Its functions and alterations in human cancer, Apoptosis. (2004). https://doi.org/10.1023/B:APPT.0000045801.15585.dd.

[86]    B.T. Hennessy, D.L. Smith, P.T. Ram, Y. Lu, G.B. Mills, Exploiting the PI3K/AKT Pathway for Cancer Drug Discovery, Nat Rev Drug Discov. 4 (2005) 988–1004. https://doi.org/10.1038/nrd1902.

[87]    J.Á.F. Vara, E. Casado, J. de Castro, P. Cejas, C. Belda-Iniesta, M. González-Barón, PI3K/Akt signalling pathway and cancer, Cancer Treat Rev. 30 (2004) 193–204. https://doi.org/10.1016/j.ctrv.2003.07.007.

[88]    J.B. Park, C.S. Lee, J.H. Jang, J. Ghim, Y.J. Kim, S. You, D. Hwang, P.G. Suh, S.H. Ryu, Phospholipase signalling networks in cancer, Nat Rev Cancer. (2012). https://doi.org/10.1038/nrc3379.

[89]    A. Carnero, C. Blanco-Aparicio, O. Renner, W. Link, J. Leal, The PTEN/PI3K/AKT Signalling Pathway in Cancer, Therapeutic Implications, Curr Cancer Drug Targets. (2008). https://doi.org/10.2174/156800908784293659.

[90]    D.D. Sarbassov, D.A. Guertin, S.M. Ali, D.M. Sabatini, Phosphorylation and Regulation of Akt/PKB by the Rictor-mTOR Complex, Science (1979). 307 (2005) 1098 LP – 1101. https://doi.org/10.1126/science.1106148.

[91]    M.K. Ediriweera, K.H. Tennekoon, S.R. Samarakoon, Role of the PI3K/AKT/mTOR signaling pathway in ovarian cancer: Biological and therapeutic significance, Semin Cancer Biol. (2019). https://doi.org/10.1016/j.semcancer.2019.05.012.

[92]    N. Hay, N. Sonenberg, Upstream and downstream of mTOR, Genes Dev. (2004). https://doi.org/10.1101/gad.1212704.

[93] A.C. Gingras, B. Raught, S.P. Gygi, A. Niedzwiecka, M. Miron, S.K. Burley, R.D. Polakiewicz, A. Wyslouch-Cieszynska, R. Aebersold, N. Sonenberg, Hierarchical phosphorylation of the translation inhibitor 4E-BP1. Genes Dev. 2001 Nov 1;15(21):2852-64. doi: 10.1101/gad.912401.

[94] A.C. Gingras, S.P. Gygi, B. Raught, R.D. Polakiewicz, R.T. Abraham, M.F. Hoekstra, R. Aebersold, N. Sonenberg, Regulation of 4E-BP1 phosphorylation: A novel two step mechanism, Genes Dev. (1999). https://doi.org/10.1101/gad.13.11.1422.

[95] J.W. Kenney, C.E. Moore, X. Wang, C.G. Proud, Eukaryotic elongation factor 2 kinase, an unusual enzyme with multiple roles, Adv Biol Regul. (2014). https://doi.org/10.1016/j.jbior.2014.04.003.

[96] X. Wang, W. Li, M. Williams, N. Terada, D.R. Alessi, C.G. Proud, Regulation of elongation factor 2 kinase by p90RSK1 and p70 S6 kinase, EMBO Journal. (2001). https://doi.org/10.1093/emboj/20.16.4370.

[97] H.-S. Yang, A.P. Jansen, A.A. Komar, X. Zheng, W.C. Merrick, S. Costes, S.J. Lockett, N. Sonenberg, N.H. Colburn, The Transformation Suppressor Pdcd4 Is a Novel Eukaryotic Translation Initiation Factor 4A Binding Protein That Inhibits Translation, Mol Cell Biol. (2003). https://doi.org/10.1128/mcb.23.1.26-37.2003.

[98] R. Ke, Q. Xu, C. Li, L. Luo, D. Huang, Mechanisms of AMPK in the maintenance of ATP balance during energy metabolism, Cell Biol Int. 42 (2018) 384–392. https://doi.org/10.1002/cbin.10915.

[99] D.G. Hardie, D.R. Alessi, LKB1 and AMPK and the cancer-metabolism link - ten years after, BMC Biol. (2013). https://doi.org/10.1186/1741-7007-11-36.

[100] L. Luo, S. Jiang, D. Huang, N. Lu, Z. Luo, MLK3 phophorylates AMPK independently of LKB1, PLoS One. (2015). https://doi.org/10.1371/journal.pone.0123927.

[101] S.M. Jeon, Regulation and function of AMPK in physiology and diseases, Exp Mol Med. (2016). https://doi.org/10.1038/emm.2016.81.

[102] J. Huang, B.D. Manning, The TSC1-TSC2 complex: A molecular switchboard controlling cell growth, Biochemical Journal. (2008). https://doi.org/10.1042/BJ20080281.

[103] D.M. Gwinn, D.B. Shackelford, D.F. Egan, M.M. Mihaylova, A. Mery, D.S. Vasquez, B.E. Turk, R.J. Shaw, AMPK Phosphorylation of Raptor Mediates a Metabolic Checkpoint, Mol Cell. (2008). https://doi.org/10.1016/j.molcel.2008.03.003.

[104] S. Hoppe, H. Bierhoff, I. Cado, A. Weber, M. Tiebe, I. Grummt, R. Voit, AMP-activated protein kinase adapts rRNA synthesis to cellular energy supply, Proc Natl Acad Sci U S A. (2009). https://doi.org/10.1073/pnas.0909873106.

[105] G.J. Browne, C.G. Proud, Regulation of peptide-chain elongation in mammalian cells, Eur J Biochem. (2002). https://doi.org/10.1046/j.1432-1033.2002.03290.x.

[106] M. Johanns, S. Pyr dit Ruys, A. Houddane, D. Vertommen, G. Herinckx, L. Hue, C.G. Proud, M.H. Rider, Direct and indirect activation of eukaryotic elongation factor 2 kinase by AMP-activated protein kinase, Cell Signal. (2017). https://doi.org/10.1016/j.cellsig.2017.05.010.

[107] S. Mizrachy-Schwartz, N. Cohen, S. Klein, N. Kravchenko-Balasha, A. Levitzki, Up-regulation of AMP-activated protein kinase in cancer cell lines is mediated through c-Src activation, Journal of Biological Chemistry. (2011). https://doi.org/10.1074/jbc.M110.211813.

[108] AVMA, AVMA Guidelines for the Euthanasia of Animals: 2020 Edition and general comments, 2020.

[109] A. Ortega, N. Eshhar, V.I. Teichberg, Properties of kainate receptor/channels on cultured Bergmann glia, Neuroscience. (1991). https://doi.org/10.1016/0306-4522(91)90331-H.

[110] T. Mosmann, Rapid colorimetric assay for cellular growth and survival: Application to proliferation and cytotoxicity assays, J Immunol Methods. 65 (1983) 55–63. https://doi.org/https://doi.org/10.1016/0022-1759(83)90303-4.

[111] A.M. Esposito, T.G. Kinzy, Chapter Five - In Vivo [35 S]-Methionine Incorporation, in: J. Lorsch (Ed.), Methods Enzymol, Academic Press, 2014: pp. 55–64. https://doi.org/https://doi.org/10.1016/B978-0-12-420070-8.00005-2.

[112] M.M. Bradford, A rapid and sensitive method for the quantitation of microgram quantities of protein utilizing the principle of protein-dye binding, Anal Biochem. (1976). https://doi.org/10.1016/0003-2697(76)90527-3.

[113] H. Towbin, T. Staehelin, J. Gordon, Electrophoretic transfer of proteins from polyacrylamide gels to nitrocellulose sheets: procedure and some applications., Proceedings of the National Academy of Sciences. (1979). https://doi.org/10.1073/pnas.76.9.4350.

[114] G. Tholey, M. Ledig, P. Mandel, L. Sargentini, A.H. Frivold, M. Leroy, A.A. Grippo, F.C. Wedler, Concentrations of physiologically important metal ions in glial cells cultured from chick cerebral cortex, Neurochem Res. (1988). https://doi.org/10.1007/BF00971853.

[115] M. Escalante, J. Soto-Verdugo, L.C. Hernández-Kelly, D. Hernández-Melchor, E. López-Bayghen, T.N. Olivares-Bañuelos, A. Ortega, GLAST Activity is Modified by Acute Manganese Exposure in Bergmann Glial Cells, Neurochem Res. (2019). https://doi.org/10.1007/s11064-019-02848-8.

[116] Z. Martínez-Lozada, A. Ortega, Glutamatergic transmission: A matter of three, Neural Plast. (2015). https://doi.org/10.1155/2015/787396.

[117] J.S.L. Yu, W. Cui, Proliferation, survival and metabolism: the role of PI3K/AKT/mTOR signalling in pluripotency and cell fate determination, Development. 143 (2016) 3050 LP – 3060. https://doi.org/10.1242/dev.137075.

[118] M. Morales, M.E. González-Mejía, A. Bernabé, L.C.R. Hernández-Kelly, A. Ortega, Glutamate activates protein kinase B (PKB/Akt) through AMPA receptors in cultured bergmann glia cells, Neurochem Res. (2006). https://doi.org/10.1007/s11064-005-9034-2.

[119] Z. Martínez-Lozada, L.C. Hernández-Kelly, J. Aguilera, E. López-Bayghen, A. Ortega, Signaling through EAAT-1/GLAST in cultured Bergmann glia cells, Neurochem Int. 59 (2011) 871–879. https://doi.org/10.1016/J.NEUINT.2011.07.015.

[120] D.S. Harischandra, S. Ghaisas, G. Zenitsky, H. Jin, A. Kanthasamy, V. Anantharam, A.G. Kanthasamy, Manganese-induced neurotoxicity: New insights into the triad of protein misfolding, mitochondrial impairment, and neuroinflammation, Front Neurosci. (2019). https://doi.org/10.3389/fnins.2019.00654.

[121] S. Herzig, R.J. Shaw, AMPK: Guardian of metabolism and mitochondrial homeostasis, Nat Rev Mol Cell Biol. (2018). https://doi.org/10.1038/nrm.2017.95.

[122] O. El-Masry S., K. Al-Sakkaf, B. Brown L., P. Dobson R.M., Differential crosstalk between the AMPK and PI3K/Akt pathways in breast cancer cells of differing genotypes: Leptin inhibits the effectiveness of AMPK activation, Oncol Rep. 34 (2015) 1675–1680. https://doi.org/10.3892/or.2015.4198.

[123] S.A. Hawley, F.A. Ross, G.J. Gowans, P. Tibarewal, N.R. Leslie, D.G. Hardie, Phosphorylation by Akt within the ST loop of AMPK-α1 down-regulates its activation in tumour cells, Biochem J. 459 (2014) 275–287. https://doi.org/10.1042/BJ20131344.

[124] V. Blomlie, R. Sivanandan, P. Jynge, Manganese Uptake and Accumulation in the Human Brain, American Journal of Neuroradiology. (2020). https://doi.org/10.3174/ajnr.A6347.

[125] T. Ke, M. Sidoryk-Wegrzynowicz, E. Pajarillo, A. Rizor, F.A.A. Soares, E. Lee, M. Aschner, Role of Astrocytes in Manganese Neurotoxicity Revisited, Neurochem Res. (2019). https://doi.org/10.1007/s11064-019-02881-7.

[126] E.S.Y. Lee, Zz. Yin, D. Milatovic, H. Jiang, M. Aschner, Estrogen and tamoxifen protect against Mn-induced toxicity in rat cortical primary cultures of neurons and astrocytes, Toxicological Sciences. (2009). https://doi.org/10.1093/toxsci/kfp081.

[127] E.S.Y. Lee, M. Sidoryk, H. Jiang, Z. Yin, M. Aschner, Estrogen and tamoxifen reverse manganese-induced glutamate transporter impairment in astrocytes, J Neurochem. (2009). https://doi.org/10.1111/j.1471-4159.2009.06105.x.

[128] P. Somogyi, N. Eshhar, V.I. Teichberg, J.D.B. Roberts, Subcellular localization of a putative kainate receptor in Bergmann glial cells using a monoclonal antibody in the chick and fish cerebellar cortex, Neuroscience. (1990). https://doi.org/10.1016/0306-4522(90)90116-L.

[129] A.P.B. Araujo, R. Carpi-Santos, F.C.A. Gomes, The Role of Astrocytes in the Development of the Cerebellum, Cerebellum. (2019). https://doi.org/10.1007/s12311-019-01046-0.

[130] M. Sidoryk-Wegrzynowicz, M. Aschner, Impairment of glutamine/ glutamate-γ-aminobutyric acid cycle in manganese toxicity in the central nervous system, Issues in Toxicology. (2015).

[131] B.Y. Zhang, S. Chen, F.L. Ye, C.C. Zhu, H.X. Zhang, R.B. Wang, C.F. Xiao, T.C. Wu, G.G. Zhang, Effect of manganese on heat stress protein synthesis of new-born rats, World J Gastroenterol. (2002). https://doi.org/10.3748/wjg.v8.i1.114.

[132] M. Korc, Manganese action on pancreatic protein synthesis in normal and diabetic rats, Am J Physiol Gastrointest Liver Physiol. (1983). https://doi.org/10.1152/ajpgi.1983.245.5.g628.

[133] M.S. Bray, T.K. Lenz, J.W. Haynes, J.C. Bowman, A.S. Petrov, A.R. Reddi, N. V. Hud, L.D. Williams, J.B. Glass, Multiple prebiotic metals mediate translation, Proc Natl Acad Sci U S A. (2018). https://doi.org/10.1073/pnas.1803636115.

[134] G. Tian, L. Lai, H. Guo, Y. Lin, M.E.R. Butchbach, Y. Chang, C.L.G. Lin, Translational control of glial glutamate transporter EAAT2 expression, Journal of Biological Chemistry. (2007). https://doi.org/10.1074/jbc.M609822200.

[135]  R. Kamada, F. Kudoh, S. Ito, I. Tani, J.I.B. Janairo, J.G. Omichinski, K. Sakaguchi, Metal-dependent Ser/Thr protein phosphatase PPM family: Evolution, structures, diseases and inhibitors., Pharmacol Ther. (2020). https://doi.org/10.1016/j.pharmthera.2020.107622.

[136]  O.M. Ijomone, O.M. Aluko, C.O.A. Okoh, A.C. Martins, M. Aschner, Role for calcium signaling in manganese neurotoxicity, Journal of Trace Elements in Medicine and Biology. (2019). https://doi.org/10.1016/j.jtemb.2019.08.006.

[137]  T. V Peres, F.M. Cordova, M.W. Lopes, A.P. Costa, R.B. Leal, Chapter 7 Effect of Manganese on Signaling Pathways, in: Manganese in Health and Disease, The Royal Society of Chemistry, 2015: pp. 182–198. https://doi.org/10.1039/9781782622383-00182.

[138]  M.R. Bryan, A.B. Bowman, Manganese and the Insulin-IGF Signaling Network in Huntington's Disease and Other Neurodegenerative Disorders, in: Adv Neurobiol, 2017. https://doi.org/10.1007/978-3-319-60189-2_6.

[139]  Schafer AE, Blaxall BC. G Protein Coupled Receptor-mediated Transactivation of Extracellular Proteases. J Cardiovasc Pharmacol. 2017 Jul;70(1):10-15. doi: 10.1097/FJC.0000000000000475.

[140]  E. López-Bayghen, A. Aguirre, A. Ortega, Transcriptional Regulation Through Glutamate Receptors: Involvement of Tyrosine Kinases, J Neurosci Res. (2003). https://doi.org/10.1002/jnr.10807.

[141]  V. Di Liberto, G. Mudò, N. Belluardo, Crosstalk between receptor tyrosine kinases (RTKs) and G protein-coupled receptors (GPCR) in the brain: Focus on heteroreceptor complexes and related functional neurotrophic effects, Neuropharmacology. (2019). https://doi.org/10.1016/j.neuropharm.2018.11.018.

[142]  L.J. Watson, K.M. Alexander, M.L. Mohan, A.L. Bowman, S. Mangmool, K. Xiao, S. V. Naga Prasad, H.A. Rockman, Phosphorylation of Src by phosphoinositide 3-kinase regulates beta-adrenergic receptor-mediated EGFR transactivation, Cell Signal. (2016). https://doi.org/10.1016/j.cellsig.2016.05.006.

[143]  A.M. López-Colomé, Z. Martínez-Lozada, A.M. Guillem, E. López, A. Ortega, Glutamate Transporter-Dependent mTOR Phosphorylation in Müller Glia Cells, ASN Neuro. (2012). https://doi.org/10.1042/AN20120022.

[144]  J. Wettmarshausen, V. Goh, K.T. Huang, D.M. Arduino, U. Tripathi, A. Leimpek, Y. Cheng, A.A. Pittis, T. Gabaldón, D. Mokranjac, G. Hajnóczky, F. Perocchi, MICU1 Confers Protection from MCU-Dependent Manganese Toxicity, Cell Rep. (2018). https://doi.org/10.1016/j.celrep.2018.10.037.

[145]  J. Musa, M.F. Orth, M. Dallmayer, M. Baldauf, C. Pardo, B. Rotblat, T. Kirchner, G. Leprivier, T.G.P. Grünewald, Eukaryotic initiation factor 4E-binding protein 1 (4E-BP1): A master regulator of mRNA translation involved in tumorigenesis, Oncogene. (2016). https://doi.org/10.1038/onc.2015.515.

[146]  X. Qin, B. Jiang, Y. Zhang, 4E-BP1, a multifactor regulated multifunctional protein, Cell Cycle. (2016). https://doi.org/10.1080/15384101.2016.1151581.

[147]  V.C. Figueiredo, J.F. Markworth, D. Cameron-Smith, Considerations on mTOR regulation at serine 2448: implications for muscle metabolism studies, Cellular and Molecular Life Sciences. (2017). https://doi.org/10.1007/s00018-017-2481-5.

[148]  Y.-J. Liu, Y. Chern, Contribution of Energy Dysfunction to Impaired Protein Translation in Neurodegenerative Diseases, Front Cell Neurosci. 15 (2021). https://www.frontiersin.org/articles/10.3389/fncel.2021.668500.

[149]  M. Flores-Méndez, D. Ramírez, N. Alamillo, L.C. Hernández-Kelly, L.M. Del Razo, A. Ortega, Fluoride exposure regulates the elongation phase of protein synthesis in cultured Bergmann glia cells, Toxicol Lett. (2014). https://doi.org/10.1016/j.toxlet.2014.06.022.

[150]  A.G. Rodríguez-Campuzano, L.C. Hernández-Kelly, A. Ortega, Acute Exposure to SiO2 Nanoparticles Affects Protein Synthesis in Bergmann Glia Cells, Neurotox Res. (2020). https://doi.org/10.1007/s12640-019-00084-0.

[151]  S. Bond, C. Lopez-Lloreda, P.J. Gannon, C. Akay-Espinoza, K.L. Jordan-Sciutto, The integrated stress response and phosphorylated eukaryotic initiation factor 2α in neurodegeneration, J Neuropathol Exp Neurol. (2020). https://doi.org/10.1093/jnen/nlz129.

[152]  C. Liu, D.Y. Yan, C. Wang, Z. Ma, Y. Deng, W. Liu, B. Xu, Manganese activates autophagy to alleviate endoplasmic reticulum stress–induced apoptosis via PERK pathway, J Cell Mol Med. (2020). https://doi.org/10.1111/jcmm.14732.

## VIII. ANEXOS

**8.1. Artículo original.** <u>Soto-Verdugo J,</u> Silva-Parra J, Hernández-Kelly LC, Ortega A. Acute Manganese Exposure Modifies the Translation Machinery via PI3K/Akt Signaling in Glial Cells. ASN Neuro. 2022;14. doi:10.1177/17590914221131452. Factor de Impacto: 5.200

**8.2. Artículo original.** Spencer, S. A., Suárez-Pozos, E., <u>Soto-Verdugo, J.,</u> Wang, H., Afshari, F. S., Li, G., Manam, S., Yasuda, D., Ortega, A., Lister, J. A., Ishii, S., Zhang, Y., & Fuss, B. (2022). Lysophosphatidic acid signaling via LPA6: A negative modulator of developmental oligodendrocyte maturation. Journal of neurochemistry, 163(6), 478–499. https://doi.org/10.1111/jnc.15696. Factor de Impacto: 5.546

**8.3. Artículo original.** Escalante, M., <u>Soto-Verdugo, J.,</u> Hernández-Kelly, L.C. et al. GLAST Activity is Modified by Acute Manganese Exposure in Bergmann Glial Cells. Neurochem Res 45, 1365–1374 (2020). https://doi.org/10.1007/s11064-019-02848-8. Factor de Impacto: 4.414

**8.4. Revisión.** <u>Soto-Verdugo J</u>., Ortega A., Critical Involvement of Glial Cells in Manganese Neurotoxicity, BioMed Research International, vol. 2021, Article ID 1596185, 16 pages, 2021. https://doi.org/10.1155/2021/1596185. Factor de Impacto: 3.246

**8.5. Presentación de póster.** <u>J. Soto-Verdugo,</u> Luisa Clara Regina Hernández-Kelly, A. Ortega. "AMP-activated Protein Kinase Activation in Glial Cells Exposed to Manganese"
Presentado en la 4° Escuela Insignia de la International Society for Neurochemistry y el Journal of Neurochemistry titulada "Brain Metabolism in Health and Disease" en Schmerlenbach, Alemania. Llevada a cabo del 25 de septiembre al 2 de octubre del 2022.

**8.6. Presentación de póster.** <u>Soto-Verdugo J.,</u> Castillo-Montesinos M., Sánchez-Palestino L.M., Tovar-Ramírez J.G., Hernández-Kelly L.C.R., Ortega A. "Crosstalk between AMPK and Akt Signaling Pathways in Glial Cells after an Acute Neurotoxic Insult"
Presentado en la 52° conferencia anual de la American Society for Neurochemistry en Roanoke, Virginia, Estados Unidos. Llevada a cabo del 10-14 de abril del 2022.

**8.7. Presentación de póster.** <u>J. Soto-Verdugo,</u> M. Castillo-Montesinos, L. M. Sánchez-Palestino, J. G. Tovar-Ramírez, L. C. R. Hernández-Kelly, A. Ortega. "Short-term exposure to manganese modifies protein translation via PI3K/Akt signaling in glial cells"
Presentado en la 51° conferencia anual de la American Society for Neurochemistry en modalidad virtual. Llevada a cabo del 28 de junio al 1 de julio del 2021.

**8.8. Presentación de póster.** <u>Soto-Verdugo J.,</u> Castillo-Montesinos M., Sánchez-Palestino L.M., Tovar-Ramírez J.G., Hernández-Kelly L.C.R., Ortega A. "Exposure to Manganese induces PI3K/Akt signaling in Bergmann glial cells"
Presentado en la conferencia bienal de la International Society for Neurochemistry en Montreal, Quebec, Canadá. Llevada a cabo del 4-8 de agosto del 2019.

**8.9. Presentación de póster.** <u>Soto-Verdugo J.,</u> Hernández-Kelly L., López-Bayghen E., Ortega A. "Short-term exposure to manganese on Bergmann glial cells: relevance to the Glu/Gln cycle"
Presentado en la 48° conferencia anual de la Society for Neuroscience en San Diego, California, Estados Unidos. Llevada a cabo del 3-7 de noviembre del 2018.

**8.10.    Ficha de datos de seguridad del Manganeso.**

*Original Papers*

# Acute Manganese Exposure Modifies the Translation Machinery *via* PI3K/Akt Signaling in Glial Cells

Jzmín Soto-Verdugo [ID], Janisse Siva-Parra, Luisa C Hernández-Kelly and Arturo Ortega [ID]

## Abstract

Manganese (Mn) exerts serious neurotoxic effects, among which, the disruption of the glutamate/glutamine (Glu/Gln) cycle, leads to an excitotoxic insult. The molecular mechanisms mediating Mn-induced neurotoxicity, have not yet been fully understood. Glu, the major excitatory neurotransmitter in the nervous system, activates a variety of signal transduction cascades involved in protein synthesis regulation. Although protein translation is an exquisitely regulated process, translational dysregulation has been observed in many neurodegenerative disorders. Hence, we investigated the effect of a short-term Mn exposure in signaling pathways critically involved in protein synthesis, such as the phosphatidylinositol 3 kinase (PI3K)/protein kinase B (Akt) cascade. To this end, we used the well-characterized chick cerebellar Bergmann glial cells (BGC) primary culture. Confluent BGC monolayers were exposed to different $MnCl_2$ concentrations (50–500 μM) for different time periods. The phosphorylation patterns of Akt, the eukaryotic translation initiation factor 4E-binding protein 1 (4E-BP1) as well as the adenosine monophosphate-dependent protein kinase (AMPK) were measured. A time and dose-dependent increase in the phosphorylation status of these proteins was found, thus the involvement of a $Ca^{2+}$/PI3K/mTOR pathway could be demonstrated. Accordingly, a modulation of [$^{35}$S]-methionine incorporation into newly synthesized polypeptides was found upon Mn acute exposure. These results demonstrate that Mn exerts triggers a change in the protein *repertoire* of glia cells that support their involvement in Mn neurotoxicity.

## Summary Statement

We demonstrate herein that short-term exposure of radial glia cells to Manganese, a neurotoxic metal, induces an effect on protein synthesis, altering the protein *repertoire* of these cells.

## Introduction

Mn is a transition metal naturally occurring in the earth's crust. More importantly, is an essential element critical for development, reproduction, antioxidant defense, energy metabolism, immune response, and regulation of brain function (Chen et al., 2018). Mn functions as a cofactor for a variety of enzymes, including arginase, glutamine synthetase (GS), pyruvate carboxylase, and Mn superoxide dismutase (Mn-SOD) (Bjørklund et al., 2020). Alterations in Mn homeostasis are associated with altered neuronal physiology and cognition in humans, and either overexposure or less likely insufficiency can cause neurological dysfunctions (Balachandran et al., 2020). The main pathology due to Mn-overexposure is known as *Manganism*, which shares several pathological features of Parkinson's disease (PD)

Departamento de Toxicología, Centro de Investigación y de Estudios Avanzados del Instituto Politécnico Nacional, México City, México

**Corresponding Author:**
Arturo Ortega, Departamento de Toxicología, Centro de Investigación y de Estudios Avanzados del Instituto Politécnico Nacional, México City, México, 07360.
Email: arortega@cinvestav.mx

55

(Chen et al., 2018), and it is considered an important risk factor for the development of several neurodegenerative diseases. The proposed mechanisms of Mn neurotoxicity range from functional changes in neurotransmission, to mitochondrial damage, and oxidative stress (Aschner and Erikson, 2017). Regarding the effects on neurotransmitter regulation, numerous studies have documented that Mn induces neurotoxicity *via* Glu-mediated signaling (Escalante et al., 2019; Lee et al., 2017). Glu is the main excitatory neurotransmitter in the central nervous system, and its concentrations in the synaptic cleft are tightly regulated by a family of high-affinity transporters. The dysregulation of any of the main components of glutamatergic neurotransmission leads to excitotoxic cell death (Danbolt, 2001). Multiple studies implicate Glu signaling in changes in the protein synthesis machinery, influencing local translation in the axons (Hsu et al., 2015; Martínez-Lozada and Ortega, 2015).

Translation is one of the most energy-consuming cellular processes and several signaling pathways are involved in the regulation of its biochemical machinery (Moon et al., 2018). The dysregulation of these pathways results in anomalous protein synthesis which leads to the development of neurological diseases. The PI3K/Akt cascade engages with the mechanistic target of rapamycin (mTOR), known as the master regulator of protein synthesis (Roux and Topisirovic, 2018). mTOR serves an important role in neural plasticity (Cho et al., 2018). Canonically, growth factors activate receptor tyrosine kinases (RTKs) in the plasma membrane that become tyrosine phosphorylated and by these means serve as scaffold proteins for the recruiting of components of their signaling cascade that harbor the *so-called* SH2 (Src homology domain 2) domain. PI3K is one of these proteins, that once recruited to the growth factor receptor, phosphorylates phosphatidylinositol 4,5-bisphosphate ($PIP_2$) producing phosphatidylinositol-3,4,5-trisphosphate ($PIP_3$). $PIP_3$ recruits phosphoinositide-dependent kinase 1 (PDK1) and AKT to the plasma membrane where PDK1 phosphorylates and activates Akt ($Thr^{308}$). mTORC2 increases Akt activity by phosphorylating its $Ser^{473}$ residue (Ediriweera et al., 2019). Then, Akt phosphorylates the Tuberous sclerosis complex 2 (TSC2) and inhibits its GTPase activity, resulting in increased Rheb-GTP levels and the activation of the serine/threonine kinase mTORC1 which phosphorylates 4E-BPs and the 70-kDa ribosomal S6 kinases (S6Ks) 1 and 2, critically involved in mRNA translation regulation (Roux and Topisirovic, 2018). Furthermore, Mn exposure results in its accumulation in the mitochondria (Chen et al., 2018). Once inside, Mn impairs superoxide dismutase (SOD) generating ROS, which inhibits several metabolic enzymes, and disrupts the respiratory chain, particularly complexes I and II (Warren et al., 2020). All these biochemical reactions lead to a sustained energy deficit that shuts down most of the ATP-consuming functions in the cell. Alterations in cellular energetics are sensed by the AMP-activated protein kinase (AMPK). To ameliorate the ATP deficit, AMPK downregulates anabolic processes, such as protein synthesis by inhibiting mTORC1 (Roux and Topisirovic, 2018).

It is broadly known that Mn accumulates preferentially in glial cells (Ke et al., 2019). BGC is a well-established model of radial glia that enwraps glutamatergic synapses, contributing to the recycling of Glu from the synaptic cleft (Glu/Gln shuttle) and the metabolic coupling with the surrounding neurons (astrocyte-neuron lactate shuttle) (Martínez-Lozada et al., 2013; Mendez-Flores et al., 2016). Moreover, Mn activates the PI3K/Akt pathway and promotes an energy deficit due to its interaction with the mitochondria (Peres et al., 2015; Warren et al., 2020). Currently, no studies have linked the effects of Mn on glutamatergic neurotransmission to translational control. Therefore, it is plausible that the translation process could be affected by Mn exposure, contributing to the neurotoxicity effects triggered by this metal. Hence, we decided to investigate herein the effect of Mn short-term exposure in signaling pathways involved in protein synthesis, such as the PI3K/Akt signaling cascade, in a model of chick cerebellar BGC.

## Materials and Methods

### Materials

Tissue culture reagents were obtained from GE Healthcare (Carlsbad, CA, USA). $MnCl_2$, D-Aspartic, and the MTT reagent were purchased from Sigma-Aldrich (St. Louis, MO, USA). L-Glutamate was obtained from Tocris Biosciences (Ellisville, IL, USA). L-[$^{35}$S]-Methionine (Cat# NEG009A, specific activity 1175 Ci/mmol) was purchased from PerkinElmer (Waltham MA, USA). Bradford and sodium dodecyl sulfate-polyacrylamide gel electrophoresis (SDS-PAGE) reagents were obtained from Bio-Rad (Hercules, CA, USA). Anti-pAkt (Cat# sc-514032, RRID: AB_2861344), anti-Akt (Cat# sc-81434, RRID:AB_1118808), anti-p4E-BP1 (Cat# sc-23768-R, RRID: AB_2095599), anti-4E-BP1 (Cat# sc-9977, RRID: AB_626621) were purchased from Santa Cruz Biotechnology (Dallas, TX, USA); anti-pAMPK (Cat# 2535, RRID: AB_331250), anti-AMPK (Cat# 2532, RRID:AB_330331), anti-ERK1/2 (Cat# 9102, RRID:AB_330744) were purchased from Cell Signaling (Danvers, MA USA). Secondary antibodies were from Abcam. Horseradish peroxidase–linked secondary antibodies and the enhanced chemiluminescence reagent (ECL) were obtained from GE Healthcare (Carlsbad, CA, USA). All other chemicals were from Sigma (St. Louis, MO, USA).

### Animals

Chicken embryos were kindly donated by Avimex, S.A de C.V. (Mexico City, Mexico) and maintained at 37°C until usage. All experiments were performed according to the International Guidelines on the Ethical Use of Animals in Research and were approved by the Cinvestav Animal

Ethics Committee. Every effort was made to reduce the number of embryos used and their suffering.

## Bergmann Glial Cell Culture and Stimulation Protocol

Primary cultures of cerebellar BGC were prepared from 14-days-old chick embryos as previously described and characterized (Ortega et al., 1991). Chicken embryonic cerebella were dissected and dissociated by brief trituration and incubated in Puck's medium supplemented with trypsin (0.25 mg/mL) and DNase (0.08 mg/mL) for 15 min. The supernatant media was removed and, the sediment was resuspended in reduced-serum Minimal Essential Medium (Opti-MEM) containing 2.5% fetal bovine serum (FBS), 2 mM glutamine, and gentamicin (50 µg/mL) for mechanical dissociation. Cells were recovered by repeated removal of dissociated cells and seeded in plastic culture dishes at a density of $1 \times 10^6$ cells/mL. The cultures were maintained at 37°C and 95% air/5% $CO_2$ in a humidified incubator. For the experiments, cells were used 4–7 days post-isolation and serum-starved (DMEM with 0.5% FBS) for 12 h and then treated with different $MnCl_2$ concentrations at the indicated time periods. All inhibitors were added 30 min before the $MnCl_2$ treatments.

## Cell Viability Assay

Cell viability was measured using the 3-(4,5-dimethylthiazol-2-yl)-2,5-diphenyltetrazolium bromide (MTT) assay. The cells were seeded in 96-well culture plates and treated with different $MnCl_2$ concentrations for 3, 6, 12, and 24 h. Then, 3 h before the end of each treatment, the cells were incubated with 5 mg/mL of MTT stock solution and maintained at 37°C. At the end of the treatments, the media was discarded and, 100 µL of dimethyl sulfoxide (DMSO) were added to each well to dissolve the formazan crystals formed in the MTT reaction. Absorbance was measured with a microplate reader (BioTek Instruments, VT, USA) at 570 nm. Experiments were performed in quadruplicates in three independent cultures. A 1% Triton X-100 was used as a positive control of cell death.

## SDS-PAGE and Western Blots

Confluent monolayers were harvested with phosphate-buffered solution (10 mM $K_2HPO_4/KH_2PO_4$, 150 mM NaCl, pH 7.4) containing phosphatase inhibitors (10 mM NaF, 1 mM $Na_2MoO_4$, and 1 mM $Na_3VO_4$) and 1 mM of the protease inhibitor phenylmethylsulphonyl fluoride (PMSF). The cells were lysed with RIPA buffer (50 mM Tris-HCl, 1 mM EDTA, 150 mM NaCl, 1 mM PMSF, 1 mg/mL aprotinin, 1 mg/mL leupeptin, 1% NP-40, 0.25% sodium deoxycholate, 10 mM NaF, 1 mM $Na_2MoO_4$, and 1 mM $Na_3VO_4$, pH 7.4). Total cell lysates were denaturized in Laemmli's sample buffer, and equal amounts of protein (approximately 50 µg of total protein as determined by the Bradford method) were resolved through 10% SDS-PAGE

slab gels and then electroblotted to nitrocellulose membranes. Blots were stained with Ponceau S stain to confirm equal protein content in all lanes. Membranes were soaked in PBS to remove the Ponceau S and incubated in TBS containing 5% dried skimmed milk and 0.1% Tween 20 for 2 h to block the excess of nonspecific protein binding sites. Then, the membranes were incubated overnight at 4°C with the primary antibodies indicated in each figure, followed by their respective secondary antibodies. The detection of the immunoreactive polypeptides was conducted using a MicroChemi DNR Bio-Imaging System imager or a Li-COR Odyssey Imaging System and processed by the Image J software (NIH; Bethesda, Maryland, USA) or the Image Studio Lite (Li-COR, Lincoln, NE) to quantify the total intensity of the bands.

## Metabolic Labelling and Assessment of Overall Protein Synthesis

Confluent BGC monolayers were labelled for 12 h with 1 µCi of L-[$^{35}$S] Methionine in methionine-free DMEM. The cells were extensively washed and treated for the indicated time points with 200 µM $MnCl_2$. The monolayers were washed twice with ice-cold PBS and lysed with cold RIPA buffer. An aliquot containing approximately 15 µg of protein was spotted onto GF/C microfiber filters (Whatmann). The filters were air-dried and washed for 10 min in ice-cold 10% trichloroacetic acid (TCA) followed by three 10 min washes in cold 5% TCA. After drying at room temperature, the filters were placed in scintillation vials with 3 ml of scintillation liquid containing 10 µl of glacial acetic acid. [$^{35}$S]-Methionine incorporation was determined *via* liquid scintillation counting in a PerkinElmer Tri-Carb 2810TR scintillation counter.

## Statistical Analysis

Data are presented as the mean ± SD from at least three independent experiments. Data with a normal distribution (evaluated by the Shapiro-Wilk test) was analyzed by repeated-measures ANOVA followed by Dunnett's or Bonferroni's *post hoc* tests. Otherwise, non-parametric Friedman's test was used, and data were presented as median ± interquartile range. Differences with a $p \leq 0.05$ value were considered statistically significant. All statistical analyses were performed using GraphPad 9.0 software (GraphPad Software, La Jolla, California, USA).

## Results

### Mn Increases Akt Phosphorylation in BGC via PI3K

Within the cerebellum, BGCs actively participate in information processing, through the effective recycling of the major excitatory amino acid transmitter, glutamate. Interestingly, it has been documented that Mn significantly accumulates in the cerebellum (Pajarillo et al., 2020; Sepúlveda et al.,
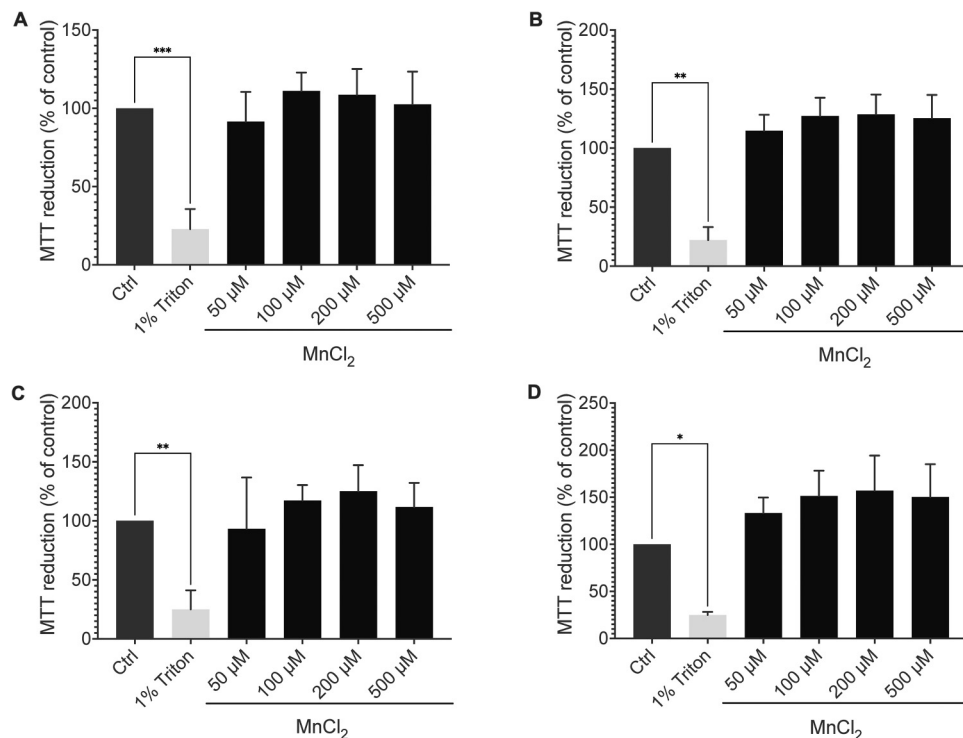
**Figure 1.** Mn effect on cell viability. Bergmann glial cells were treated with several concentrations of $MnCl_2$ (50, 100, 200, or 500 µM) for different time of exposure (A) 3 h (n = 3), (B) 6 h (n = 4), (C) 12 h (n = 4) and (D) 24 h (n = 3), and the reduction of MTT to formazan was evaluated. Control (Ctrl), 1% Triton X-100 was used as a control of cell death at each of the times. Data are expressed as the mean ± SD of at least three independent experiments. A repeated-measures analysis of variance (ANOVA) and Dunnett's *post hoc* test were performed. Statistically significant differences are indicated by *p < 0.05, **p < 0.01 and ***p < 0.001.

2012; Ye and Kim, 2015). Several studies have indicated that astrocytes are more resistant to Mn insults when compared to neurons (Lee et al., 2009). To gain insight into the cytotoxic effect of $MnCl_2$ exposure on cultured Bergmann glia cells, we performed MTT assays. Confluent BGC monolayers were treated with $MnCl_2$ concentrations ranging from 50 to 500 µM exposed for 3, 6, 12, and 24 h. The results are presented in Figure 1. BGCs are resilient to the cytotoxic effects of Mn since there was no apparent cell death at any of the time points evaluated, even at the maximum concentration used (500 µM). As expected, the exposure to a 1% Triton X-100 solution reduced cell viability.

Previous findings from our group have demonstrated that $MnCl_2$ exposure increases the catalytic efficacy of the sodium-dependent glutamate/aspartate transporter (GLAST) (Escalante et al., 2019). Taking into consideration that we and others have demonstrated the signaling capabilities of this transporter (reviewed in (Martínez-Lozada and Ortega, 2015)), we decided to explore the signaling transactions activated by $MnCl_2$. To evaluate the activation of the PI3K/PKB/Akt pathway we evaluated the $Ser^{473}$ PKB/Akt phosphorylation patterns since it is established that this specific phosphorylation is a requirement for its kinase activity (Yu and Cui, 2016). A dose-dependent increase in PKB/Akt phosphorylation was found after 30 min of exposure to $MnCl_2$ (Figure 2A). The time-course

of this post-translational modification shows a rapid response to the exposure to 200 µM Mn (Figure 2B), reaching its peak just after 5 min of treatment and then decreasing to normal conditions at 60 min. Accordingly, the inhibition of PI3K with a 100 nM concentration of Wortmannin 30 min prevents the Mn effect (Figure 3). As control of these experiments, cells were exposed for 30 min to 1 mM glutamate (Glu) (Morales et al., 2006).

## Mn-Induced Akt Phosphorylation Involves the Activation of NCX

To gain insight into the signaling mechanisms involved in the recorded Mn-mediated Akt phosphorylation and taking into account that this metal increases the catalytic efficacy of the sodium-dependent glutamate/aspartate transporter GLAST in our culture model (Escalante et al., 2019), we decided to explore the possibility that the $Na^+/Ca^{2+}$ exchanger (NCX) could be involved in Akt phosphorylation. To this end, we used the NCX inhibitor KBR7943. The results are presented in Figure 4. Preincubation with the exchanger blocker prevents the Mn-induced Akt phosphorylation, suggesting that manganese exposure augments $[Ca^{2+}]_i$, opening the possibility of the activation of several signal transduction cascades associated with the exposure to this metal.
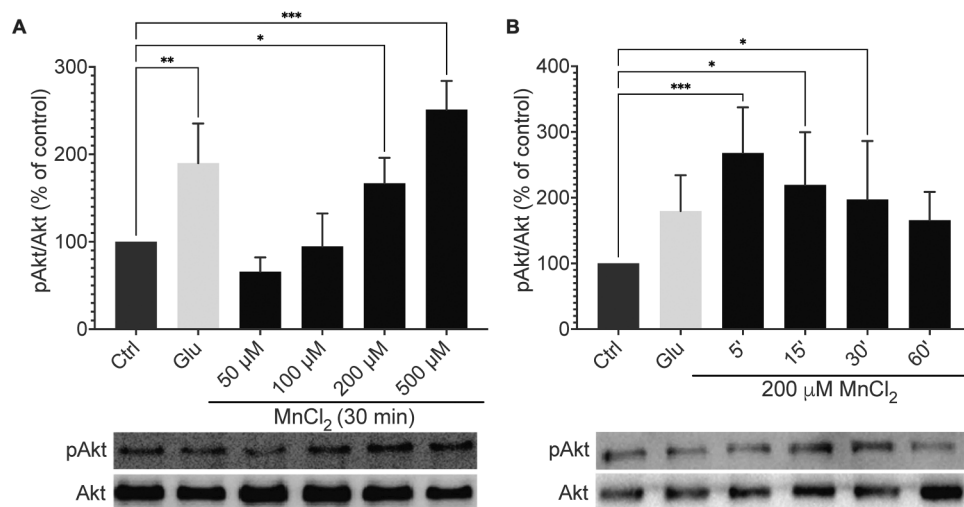
**Figure 2.** Mn treatment increases $Ser^{473}$ Akt phosphorylation. (A) Dose-response curve of the effect of Mn on Akt phosphorylation in BGC. Bergmann glia was treated for 30 min with $MnCl_2$ (50, 100, 200, or 500 µM), n = 4. (B) Time course of the response of BGC to Mn in the phosphorylation of Akt. Bergman glia was treated with $MnCl_2$ 200 µM, for up to 60 min. Control (Ctrl), Glutamate (Glu) 1 mM (30 min) was used as a positive control, n = 3. A representative blot is presented below each graph. Data are expressed as the mean $\pm$ SD of at least three independent experiments. A repeated-measures analysis of variance (ANOVA) and Dunnett's *post hoc* test were performed. Statistically significant differences are indicated by *$p < 0.05$, **$p < 0.01$ and ***$p < 0.001$.
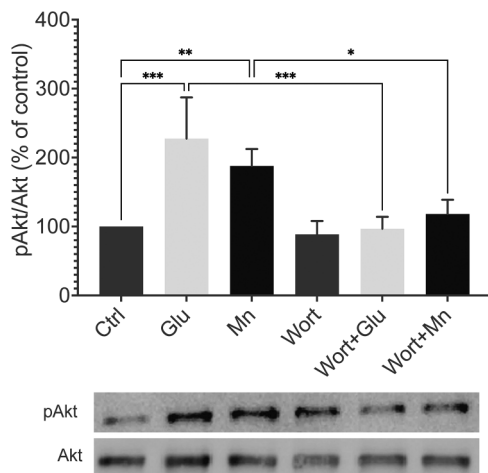


**Figure 3.** Phosphatidylinositol 3 kinase (PI3K) modulates the Mn effect on Akt phosphorylation ($Ser^{473}$). Bergmann glial cells were treated with Wortmannin (Wort) 100 nM 30 min before the treatment with $MnCl_2$ 200 µM for 5 min. Control (Ctrl), Glutamate (Glu) 1 mM (30 min) was used as a positive control, n = 3. A representative blot is presented below each graph. Data are expressed as the mean $\pm$ SD of at least three independent experiments. A repeated-measures analysis of variance (ANOVA) and Bonferroni's *post hoc* test were performed. Statistically significant differences are indicated by *$p < 0.05$, **$p < 0.01$ and ***$p < 0.001$.



**Figure 4.** Inhibition of the $Na^+/Ca^{2+}$ exchanger (NCX) diminishes Mn-induced $Ser^{473}$ Akt phosphorylation. 30 min before the treatment with $MnCl_2$ 200 µM (5 min), KBR7943 (KBR) was added to the Bergmann glial cells culture at a concentration of 15 µM. Glu 1 mM (15 min) was used as a control. Control (Ctrl), Glutamate (Glu) 1 mM (30 min) was used as a positive control, n = 4. A representative blot is presented below each graph. Data are expressed as the mean $\pm$ SD of at least three independent experiments. A repeated-measures analysis of variance (ANOVA) and Bonferroni's *post hoc* test were performed. Statistically significant differences are indicated by *$p < 0.05$ and **$p < 0.01$.

## Mn Induces 4E-BP1 Phosphorylation via mTORC1 and Regulates de novo Protein Synthesis

An important downstream effector of the PI3K/Akt signaling pathway is the mechanistic target of rapamycin (mTOR) complex 1, the master regulator of protein synthesis (Roux and Topisirovic, 2018). Moreover, mTOR activity promotes cap-dependent translation through 4E-BP1 phosphorylation (Santini and Klann, 2011). To explore the effect of Mn treatment on mTORC1 activity we measured phospho-4E-BP1 levels. Treatment with Aspartate 1 mM for 15 min was used
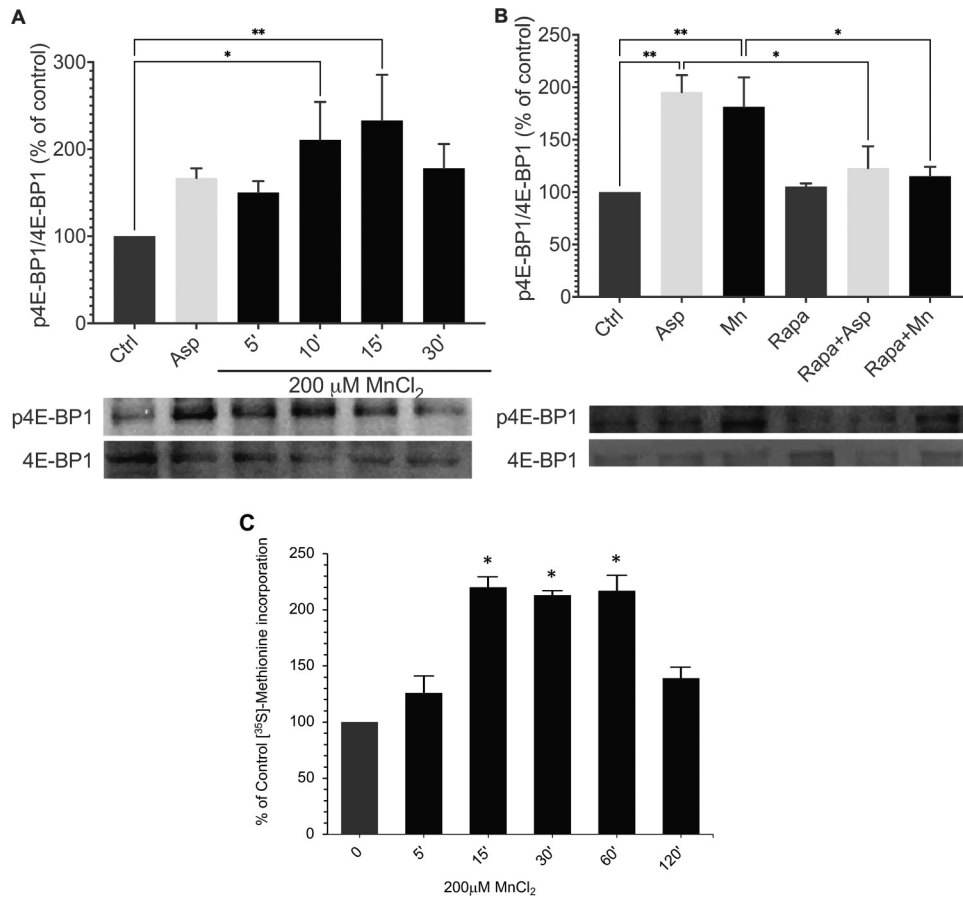
**Figure 5.** Mn treatment increases 4E-BP1 phosphorylation (Thr[70]) through mTORC1 and regulates protein synthesis. (A) Time course of the response to Mn treatment on 4E-BP1phosphorylation in BGC. Bergmann glial cells were treated with $MnCl_2$ 200 μM from 5 to 30 min of exposure. Friedman's test was performed, n = 3. (B) Participation of mTORC1 in the Mn-induced 4E-BP1 phosphorylation. 30 min before the treatment with $MnCl_2$ 200 μM (15 min), Rapamycin (Rapa) was added at 100 nM. (C) Time-dependent [35S]-Methionine incorporation into TCA precipitable polypeptides after exposure to 200 μM. A repeated-measures analysis of variance (ANOVA) and Bonferroni's *post hoc* test was performed. Control (Ctrl), Aspartate (Asp) 1 mM (15 min) was used as a positive control, n = 4. A representative blot is presented below each graph. Data are expressed as the mean ± SD of at least three independent experiments. Statistically significant differences are indicated by *p < 0.05 and **p < 0.01.

as a control for these experiments (Martínez-Lozada et al., 2011). A significant increase in the phosphorylation of 4E-BP1 in its Thr[70] residue was statistically significant after 15 min of $MnCl_2$ treatment (Figure 5A), after 30 min the effect is not significant. This effect is mediated by mTORC1 since the rapamycin abolished the Mn effect (Figure 5B). When phosphorylated, 4E-BP1 releases the eIF4E which is a cap-binding subunit of the eIF4F translation initiation complex that facilitates the recruitment of mRNAs to the ribosome (Qin et al., 2016). These results indicate that the initiation of cap-dependent translation is being upregulated after a 15 min of exposure to Mn, from then the effect returns to its basal levels. In order to establish a functional consequence of this signaling pathway triggered by Mn, we decided to evaluate overall protein synthesis. To this end, we labeled confluent BGC cultures with 1 μCi of [35S]-Methionine for 12 h in methionine-free medium. Cells were then exposed for different time periods to 200 μM

$MnCl_2$, and the polypeptides precipitated with TCA. An increase in [35S]-Methionine incorporation into polypeptides was found after 15 min and lasted for up to 60 min of Mn exposure, returning to basal levels after 2 h (Figure 5, panel C). These results demonstrate a transient effect of this metal in the translation process.

## Mn Induces AMPK Phosphorylation (Thr[172])

The well-established mitochondrial deleterious effects of Mn exposure in different model systems (Harischandra et al., 2019), the fact that Mn reduces glucose uptake in our model system (Escalante et al., 2019), and the return to basal translation levels after 120 min of Mn, prompted us to evaluate the ATP sensor, the adenosine monophosphate protein kinase (AMPK). It has been established that phosphorylation in its Thr[172] residue is well-correlated with its enzymatic activity (Herzig and Shaw, 2018). Given the fact that the
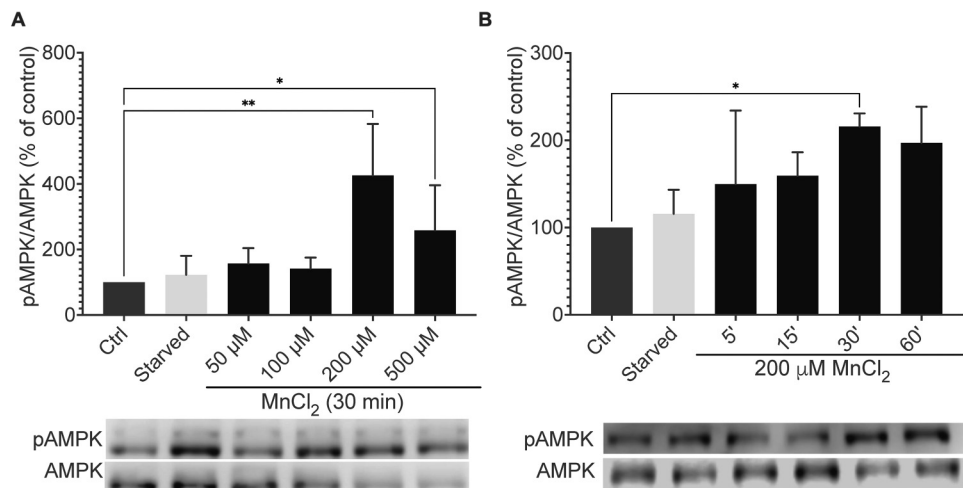
**Figure 6.** Mn treatment increases Thr$^{172}$ AMPK phosphorylation. (A) Dose-response curve of the effect of Mn on AMPK phosphorylation in BGC. Bergmann glia was treated for 30 min with MnCl$_2$ (50, 100, 200, or 500 μM), n = 3. (B) Time course of the response of BGC to Mn treatment over the phosphorylation of AMPK. A repeated-measures analysis of variance (ANOVA) and Dunnett's *post hoc* test was performed. Control (Ctrl), Serum-starved cells were used as a control, n = 3. A representative blot is presented below each graph. Data are expressed as the mean $\pm$ SD of at least three independent experiments. Statistically significant differences are indicated by *p < 0.05 and **p < 0.01.

results described above demonstrate a Mn effect in protein synthesis, and that this is the most energy-consuming cellular process, we explored AMPK phosphorylation after different periods of Mn exposure. The results are presented in Figure 6, a 200 μM concentration of the metal increased the AMPK Thr$^{172}$ phosphorylation levels after a 30 min of exposure (Figure 6A) that remain augmented after 60 min of Mn (Figure 6B). Moreover, these effects appear to be regulated by the PI3K/Akt pathway since PKB/Akt inhibition prevents AMPK phosphorylation at 30 min of exposure to Mn (Figure 7A), but after a 60 min exposure, an opposite effect is detected (Figure 7C) with no effects at shorter exposure times (5 and 15 min) (Figure 7B), suggesting a differential crosstalk between the AMPK and PI3K/Akt pathways as proposed for other models (El-Masry S. et al., 2015; Hawley et al., 2014). The Mn-induced increase of AMPK phosphorylation at 30 min and then a diminished AMPK phosphorylation after 60 min of Mn together with the kinetics of 4E-BP1 phosphorylation (Figure 5) correlate well with the recorded Mn effect in protein synthesis, in that its return to basal levels is most possibly linked to a reduction in ATP levels and the resulting change in the protein *repertoire* of these cells as shown in panel D of Figure 5.

## MAPK ERK 1/2 Signaling Pathway Involvement in Mn-Mediated Effects in Bergmann glia

The mitogen-activated protein kinases (MAPKs) are Ser/Thr kinases also known for their involvement in translational control along with the PI3K/Akt pathway (Roux and Topisirovic, 2018). Therefore, we decided to explore the phosphorylation status of the extracellular signal-regulated protein kinases 1/2 (ERK1/2) after the exposure to different MnCl$_2$ concentrations (50–500 μM) for different time periods (10–120 min). A non-monotonic effect in response to the treatment with increasing concentrations of MnCl$_2$ at 120 min of exposure was found, with an increase in ERK 1/2 phosphorylation up to 200 μM but at 500 μM such effect was not present (Figure 8A). On the other hand, the increase in ERK1/2 phosphorylation at 100 μM MnCl$_2$ was time-dependent (Figure 8B and C). These results confirm that the ERK1/2 pathway is activated in BGC treated after MnCl$_2$ exposure. Since ERK1/2 has several downstream effector proteins such as the p90 ribosomal S6 kinases (RSK) and the MAPK-interacting kinases (MNCs) (Roux and Topisirovic, 2018) these enzymes might be implicated in the regulation of mRNA translation. These and other possibilities will be addressed in our lab in the near future. In panel C, the treatment with 1 mM, Glu was used as a positive control (López-Colomé and Ortega, 1997).

## Discussion

The duality of Mn as an essential trace element and a potent neurotoxic metal has been the object of discussion for the last few years. Since most of the *in vitro* studies have used Mn concentrations far from the ones physiologically relevant (Bowman and Aschner, 2014), in this work we focused on the use of Mn concentrations that result in acute neurotoxic effects. More importantly, Mn accumulates preferentially in glial cells in the CNS (Ke et al., 2019), and it can be found in the cerebellum (Blomlie et al., 2020). BGC is the most abundant non-neuronal cell type in the cerebellum which
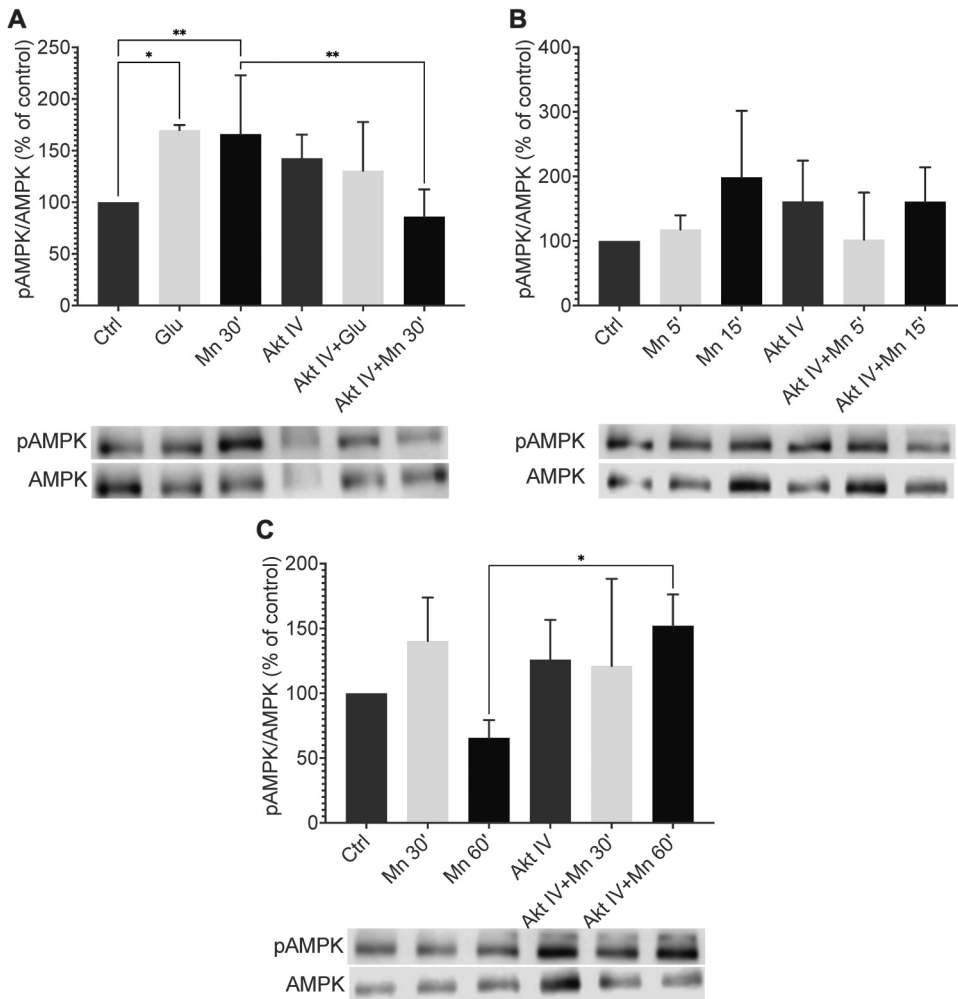
**Figure 7.** Inhibition of Akt downregulates Mn-induced AMPK phosphorylation (Thr[172]). (A) 30 min before the treatment with MnCl$_2$ 200 μM (30 min), Akt IV was added to the Bergmann glial cells culture at a concentration of 15 μM. Glutamate (Glu) 1 mM (15 min) was used as a positive control (n = 4). After the 30 min of pretreatment with Akt IV BGC were also treated with MnCl$_2$ 200 μM at (B) 5 and 15 min (n = 4), or (C) 30 and 60 min of exposure to assess different points of regulation (n = 4). Control (Ctrl). A representative blot is presented at the right of each graph. Data are expressed as the mean ± SEM of at least three independent experiments. A repeated-measures analysis of variance (ANOVA) and Bonferroni's *post hoc* test was performed. Statistically significant differences are indicated by *p < 0.05 and **p < 0.01.

makes these cells an excellent model to study neuron-glia interactions (Somogyi et al., 1990). BGC completely enwraps the parallel fiber-Purkinje cell synapses and takes an active part in the *so-called* Glu/Gln shuttle, ensuring sufficient neuronal neurotransmitter supply and thus, proper glutamatergic neurotransmission. Moreover, BGC are fundamental in preventing excitotoxicity insults linked to the activation of extra-synaptic receptors (Araujo et al., 2019). Several studies, mostly performed in cortical astrocytes, have established that Mn affects glutamate turnover through the impairment of the Glu/Gln cycle. A Mn dysregulation of the transcription of several of its components, like neutral amino acid transporters, has been reported (Sidoryk-Wegrzynowicz and Aschner, 2014). Other studies have demonstrated that Mn is capable to disturb anabolic metabolic pathways, such as protein synthesis (Bray et al., 2018; Korc, 1983; Zhang et al., 2002). The

control of the translation machinery provides an immediate mechanism of response to environmental signals (Browning and Bailey-Serres, 2015). We and others have described that Glu transporters can be regulated post-transcriptionally at the level of protein synthesis (Flores-Méndez et al., 2016; Tian et al., 2007). However, to our knowledge, no studies have linked Mn effects on glutamatergic neurotransmission resulting from the mentioned increase in GLAST catalytic activity, to translational control.

Mn exposure has been described to alter several signaling proteins, and this is not surprising since most kinases are either Mn or Mg-dependent (Ijomone et al., 2019; Kamada et al., 2020). ERK, Akt, mTOR, c-Jun N-terminal kinase (JNK), and more can be activated by Mn both *in vitro* and *in vivo* (Peres et al., 2015). Since Akt is known to play a major role in the control of cell metabolism, growth,
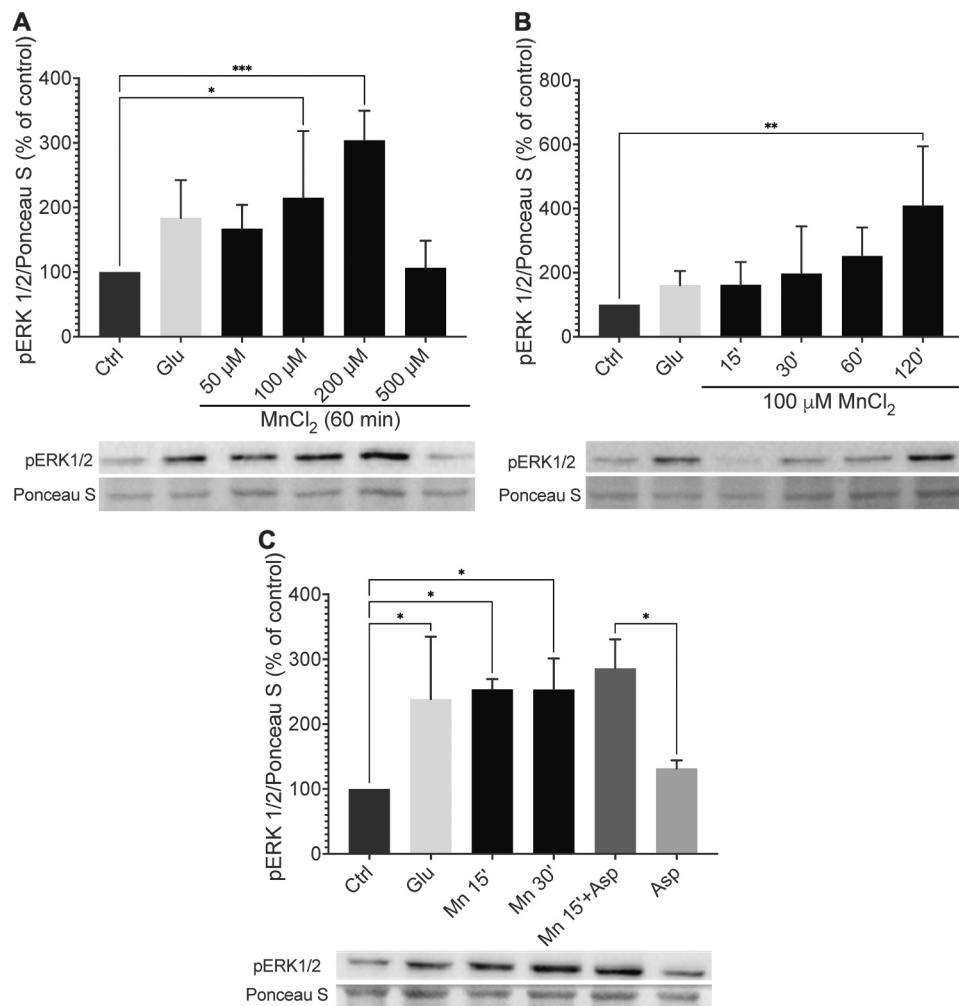
**Figure 8.** Mn treatment induces ERK 1/2 phosphorylation. (A) Dose-response curve of the effect of Mn on ERK 1/2 phosphorylation in BGC (n = 4). Bergmann glia was treated for 120 min with $MnCl_2$ (50, 100, 200, or 500 μM). (B) Time course of the response of BGC to Mn treatment over the phosphorylation of ERK 1/2. A repeated-measures analysis of variance (ANOVA) and Dunnett's *post hoc* test was performed (n = 4). (C) Glutamate transport and Mn mediated ERK 1/2 phosphorylation. Co-exposure of $MnCl_2$ 200 μM and Aspartate 60 μM for 15 min. A repeated-measures analysis of variance (ANOVA) and Bonferroni's *post hoc* test was performed. Control (Ctrl), Glutamate (Glu) 1 mM (15 min), and Aspartate (Asp) 60 μM (15 min) were used as a positive control (n = 3). A representative blot is presented below each graph. Data are expressed as the mean ± SD of at least three independent experiments. Statistically significant differences are indicated by n.s. not significant, *$p < 0.05$, **$p < 0.01$ and ***$p < 0.001$.

proliferation, and survival, its phosphorylation is induced by Mn in different models (Bryan and Bowman, 2017; Peres et al., 2015), it was of our interest to elucidate the mechanisms triggered by Mn specifically in the PI3K/Akt pathway and its possible involvement in the translation process through the activation of effector molecules downstream of Akt. We demonstrate here that Mn treatment induces $Ser^{473}$ Akt phosphorylation rapidly in BGC (Figure 2). The phosphorylation in the $Ser^{473}$ residue is known as the regulatory site of Akt activation and this phosphorylation is carried out by mTORC2 (Sarbassov et al., 2005). Akt activation is controlled upstream by a multi-step process that involves PI3K activation, and we precisely observed that Mn-induced Akt activation involves PI3K activation (Figure 3).

The PI3K/Akt pathway is canonically activated downstream of plasma membrane tyrosine kinase receptors (i.e., growth factor, insulin receptors). Recent studies have shown that Mn exposure increases the Insulin-like growth factor 1 receptor (IGFR)/Insulin receptor (IR) phosphorylation and thus, the described signaling results from a direct Mn effect on these receptors (Bryan and Bowman, 2017). Another possibility is that Mn is indirectly affecting the tyrosine kinase receptors since it is known that the activation of certain membrane receptors is capable of transactivating IGFR/IR. This phenomenon has been largely described for GPCRs and neurotransmitter receptors (Schafer and Blaxall, 2017). Specifically, previous work from our lab has suggested that Glu receptors (α-amino-3-hydroxy-5-methyl-4-isoxazole
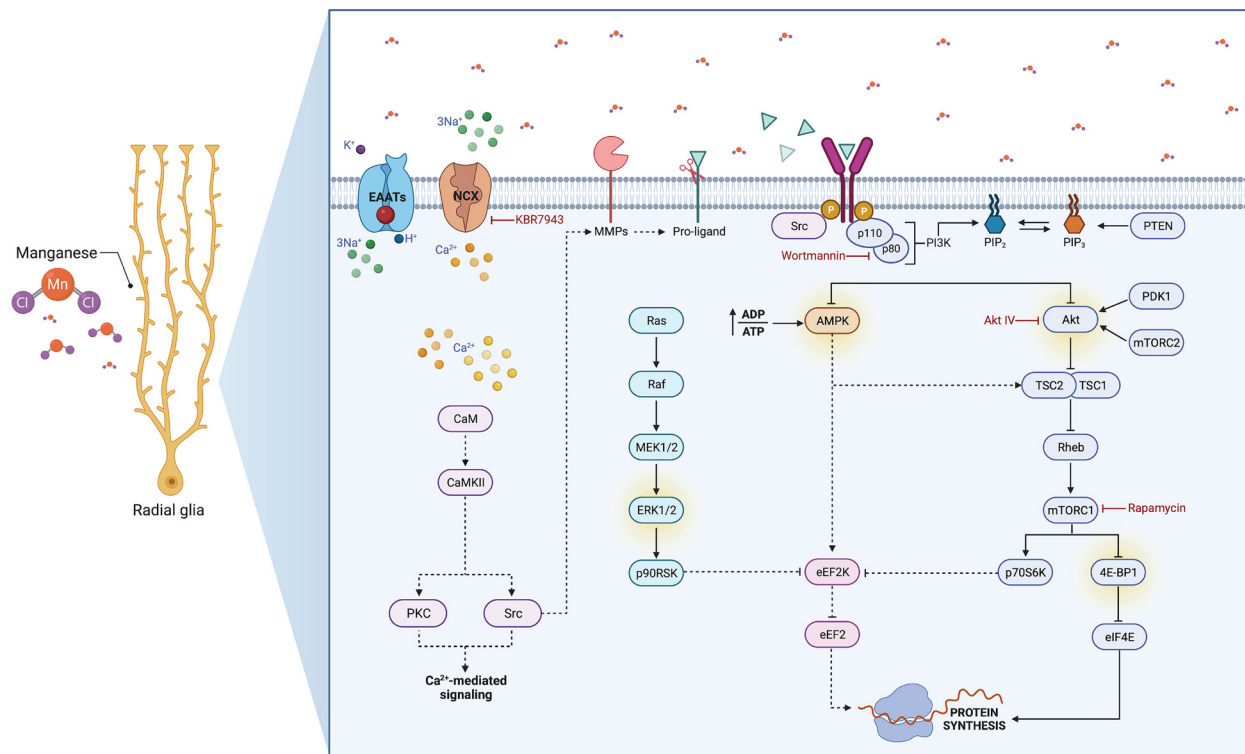
**Figure 9.** Proposed model for the effects of acute Mn exposure on PI3K/Akt/mTOR/4E-BP1 signaling pathway in BGC. For a detailed description please refer to the discussion section of this manuscript.

propionic acid: AMPA) transactivate IGFR (López-Bayghen et al., 2003). BGC AMPA receptors are $Ca^{2+}$-permeable and are linked to the activation of the $Ca^{2+}$/calmodulin-dependent multiprotein kinase II (CaMKII), the $Ca^{2+}$/diacylglycerol-dependent protein kinase C (PKC), and the non-receptor tyrosine kinases (i.e., Src), that result in augmented tyrosine phosphorylation and RTK activation. On the other hand, the same $Ca^{2+}$ influx may induce the activation of proteases such as matrix metalloproteases (MMPs) and/or A Disintegrin and Metalloprotease (ADAM), which cleave and release agonists that activate their respective receptors (Di Liberto et al., 2019). Src also plays a critical role in the activation of MMP and ADAM (Watson et al., 2016), which makes it an interesting protein to analyze due to its plausible involvement in Mn-mediated IGFR/IR transactivation.

We have previously demonstrated that the co-transport of Glu and $Na^+$ leads to the activation of NCX (López-Colomé et al., 2012; Martínez-Lozada et al., 2011). The activation of this exchanger leads to $Ca^{2+}$ influx driven by the Glu transport increased $Na^+$ levels in BGC. The increase in intracellular $Ca^{2+}$ is linked to the mTORC1 activation (López-Colomé et al., 2012; Martínez-Lozada et al., 2011). The present work demonstrates that NCX is involved in the Mn-induced Akt phosphorylation (Figure 4). Moreover, recent studies have indicated that Mn transport into the CNS cells may be influenced by $Ca^{2+}$ transport and some of its downstream signaling proteins

(Ijomone et al., 2019). Taking into consideration that Mn exposure increases $Ca^{2+}$ influx and knowing that the mitochondrial $Ca^{2+}$ uniporter (MCU) is capable of Mn transport (Wettmarshausen et al., 2018), this metal may change the morphology and integrity of the mitochondrial plasma membrane disrupting the respiratory chain. Therefore, Mn-dependent mitochondrial damage could lead to impairment in protein synthesis because this process is the most energy-consuming cell function. In this context, the results presented in panel C of Figure 5, might appear to be contradictory at first sight, meaning that one would expect a sharp decraese in the translation process after Mn exposure, and in fact, an increase in [$^{35}$S]-Methionine polypeptide incorporation was found for up to 60 min. This response could be linked to a cellular effort to overcome the metal insult, and in fact matches with the time course of the Mn-triggered activation of the PI3K/Akt/mTORC1/4EBP1 cascade and the final AMPK phosphorylation. It is tempting to speculate that some of the proteins synthesized in this period represent the cell defense against $MnCl_2$ exposure, clearly, other experiments that are beyond the scope of this communication have to be done to gain insight into this paradox.

AMPK is an energy-sensing kinase that promotes catalytic processes that favor the replenishment of ATP stores in the energy-deprived cells while concomitantly shutting down anabolic processes, such as protein synthesis (Herzig and Shaw, 2018). We demonstrate here that short-term Mn exposure increases AMPK phosphorylation as early as 30 min of

exposure (Figures 6 and 7). The Thr[172] AMPK phosphorylation is its hallmark of activation, that can disrupt translation by inhibiting the mTORC1 signaling (Ke et al., 2018). mTOR plays a pivotal role in the regulation of diverse aspects of cellular physiology such as energy metabolism, cell growth, and differentiation as well as protein synthesis. AMPK inhibits mTOR by activating TSC2, which is a signaling intermediate between Akt and mTOR. 4E-BP1 is a downstream target of mTOR, its Thr[70] phosphorylation prevents the binding of 4E-BP1 to eIF4E (Musa et al., 2016). In our model of BGC, we show that after the treatment with Mn there is an increase in 4E-BP1 phosphorylation (Figure 5A) that is dependent on the activation of mTOR (Figure 5B) that matches with an increase in [$^{35}$S]-Methionine incorporation into newly synthesized polypeptide (Figure 5C). The increase in 4E-BP1 phosphorylation enhances mRNA translation (Qin et al., 2016). Although phosphorylation of mTOR in the Ser[2448] residue has been used as an indicator of its activation, the usefulness of this measurement has been a controversial topic since the mutation of Ser to Ala does not affect the mTOR-induced 4E-BP1 phosphorylation (Figueiredo et al., 2017). Interestingly, pharmacological activation of AMPK has shown to decrease phosphorylation of Akt, mTOR, S6K, and 4E-BP1 (Gwinn et al., 2008), which are indicative of suppressed protein translation. At this point is important to mention that the time frame for the activation of AMPK overlaps with the decrease in the phosphorylation of 4E-BP1 as well as Akt after the 20 min of treatment, although [$^{35}$S] methionine incorporation is still above control levels, nevertheless it is remarkable the inversely proportional nature of these signaling pathways upon Mn. This data highlights the transient effect in glial translational control in response to the exposure to this metal, as it has been shown for other neurotoxicants (Flores-Méndez et al., 2013, 2014; Rodríguez-Campuzano et al., 2020).

At this point, we show herein that Mn affects translation through a signal transduction cascade that changes the phosphorylation patterns of 4E-PB1 *via* the Ca$^{2+}$/PI3K/Akt/mTOR pathway and AMPK, with the possible involvement of ERK 1/2 (Figure 8). Interestingly, these same signaling pathways have also an important role in the elongation phase of the protein synthesis (Johanns et al., 2017). The eukaryotic elongation factor 2 (eEF2) is a potential target of Mn exposure (Figure 9), eEF2 is indirectly regulated by mTOR through S6K and ERK 1/2 through RSK. It is the most energy-consuming step in the protein translation process. The phosphorylation of eEF2 at Thr[56] is carried out by the Eukaryotic Elongation Factor 2 Kinase (eEF2K) (Kenney et al., 2014). While S6K activates eEF2 by phosphorylating and inactivating eEF2K, AMPK induces the activation of eEF2K and the consequent eEF2 deactivation (Johanns et al., 2017). There is another important piece in the translation machinery that we need to take into consideration, the eukaryotic initiation factor 2 (eIF2), the phosphorylation of its alpha subunit (eIF2α) in Ser[51] prevents the nucleotide exchange of eIF2B and thus the formation of

the ternary complex of the initial translation step (Moon et al., 2018). There are four eIF2α kinases: general control non-depressible 2 kinases (GCN2), heme-regulated inhibitor kinase (HRI), double-stranded RNA-dependent protein kinase (PKR), and PKR-like endoplasmic reticulum kinase (PERK) (Bond et al., 2020). Evidence has revealed that Mn exposure induces eIF2α phosphorylation through PERK, activating the autophagic response (Liu et al., 2020). Work in progress in our lab is also aimed at this direction.

In summary, our findings suggest that an altered intracellular PI3K/Akt/mTOR signaling represent an early event in Mn toxicity mechanisms and that protein synthesis is altered by Mn exposure. These findings strengthen the idea of the critical role of glial cells in neurotoxicity processes. A summary of our findings is depicted in Figure 9.

## Author Contribution

JSV and AO conceptualized the experiments. JSV, JSP, and LHK performed the experiments, analyzed data, and prepared the figures. JSV wrote the first draft manuscript. AO supervised, obtained the funding, and wrote the final manuscript. All authors have approved the final manuscript.

## Compliance with Ethical Standards

All experiments were performed according to the International Guidelines on the Ethical Use of Animals in Research and approved by the Cinvestav Animal Ethics Committee.

## Declaration of Conflicting Interests

The authors declare that they do not have conflicts of interest regarding this article's research, authorship, and/or publication.

## ORCID iDs

Jzmín Soto-Verdugo https://orcid.org/0000-0002-7050-4015
Arturo Ortega https://orcid.org/0000-0002-9594-8114

## References

Araujo, A. P. B., Carpi-Santos, R., & Gomes, F. C. A. (2019). The role of astrocytes in the development of the cerebellum. *Cerebellum*, 18(6), 1017–1035. https://doi.org/10.1007/s12311-01046-0

Aschner, M., & Erikson, K. (2017). Manganese. *Advances in Nutrition*, 8(3), 520–521. https://doi.org/10.3945/an.117.0115305

Balachandran, R. C., Mukhopadhyay, S., McBride, D., Veevers, J., Harrison, F. E., Aschner, M., Haynes, E. N., & Bowman, A. B.

(2020). Brain manganese and the balance between essential roles and neurotoxicity. *Journal of Biological Chemistry*, *295*(19), 6312–6329. https://doi.org/10.1074/jbc.REV119.009453

Bjørklund, G., Dadar, M., Peana, M., Rahaman, M. S., & Aaseth, J. (2020). Interactions between iron and manganese in neurotoxicity. *Archives of Toxicology*, *94*(3), 725–734. https://doi.org/10.1007/s00204-020-02652-2

Blomlie, V., Sivanandan, R., & Jynge, P. (2020). Manganese uptake and accumulation in the human brain. *American Journal of Neuroradiology*, *41*(1), E3. https://doi.org/10.3174/ajnr.A6347

Bond, S., Lopez-Lloreda, C., Gannon, P. J., Akay-Espinoza, C., & Jordan-Sciutto, K. L. (2020). The integrated stress response and phosphorylated eukaryotic initiation factor 2α in neurodegeneration. *Journal of Neuropathology and Experimental Neurology*, *79*(2), 123–143. https://doi.org/10.1093/jnen/nlz129

Bowman, A. B., & Aschner, M. (2014). Considerations on manganese (Mn) treatments for in vitro studies. *NeuroToxicology*, *41*, 141–142. https://doi.org/10.1016/j.neuro.2014.01.010

Bray, M. S., Lenz, T. K., Haynes, J. W., Bowman, J. C., Petrov, A. S., Reddi, A. R., Hud N, V., Williams, L. D., & Glass, J. B. (2018). Multiple prebiotic metals mediate translation. *Proceedings of the National Academy of Sciences of the United States of America*, *115*(48), 12164–12169. https://doi.org/10.1073/pnas.1803636115

Browning, K. S., & Bailey-Serres, J. (2015). Mechanism of cytoplasmic mRNA translation. *The Arabidopsis Book*, *13*, e0176. https://doi.org/10.1199/tab.0176

Bryan, M. R., & Bowman, A. B. (2017). Manganese and the insulin-IGF signaling network in Huntington's disease and other neurodegenerative disorders. *Advances in Neurobiology*, *18*, 113–142. https://doi.org/10.1007/978-3-319-60189

Chen, P., Bornhorst, J., & Aschner, M. (2018). Manganese metabolism in humans. *Frontiers in Bioscience - Landmark*, *23*, 1655–1679. https://doi.org/10.2741/1665

Cho, C., Michailidis, V., & Martin, L. J. (2018). Revealing brain mechanisms of mTOR-mediated translational regulation: implications for chronic pain. *Neurobiology of Pain*, *4*, 27–34. https://doi.org/10.1016/j.ynpai.2018.03.002

Danbolt, N. C. (2001). Glutamate uptake. *Progress in Neurobiology*, *65*(1), 1–105. https://doi.org/10.1016/s0301-0082(00)00067-8

Di Liberto, V., Mudò, G., & Belluardo, N. (2019). Crosstalk between receptor tyrosine kinases (RTKs) and G protein-coupled receptors (GPCR) in the brain: focus on heteroreceptor complexes and related functional neurotrophic effects. *Neuropharmacology*, *152*, 67–77. https://doi.org/10.1016/j.neuropharm.2018.11.018

Ediriweera, M. K., Tennekoon, K. H., & Samarakoon, S. R. (2019). Role of the PI3K/AKT/mTOR signaling pathway in ovarian cancer: biological and therapeutic significance. *Seminars in Cancer Biology*, *59*, 147–160. https://doi.org/10.1016/j.semcancer.2019.05.012

El-Masry, S. O., Al-Sakkaf, K., Brown, L. B., & Dobson, R. M. P. (2015). Differential crosstalk between the AMPK and PI3K/akt pathways in breast cancer cells of differing genotypes: leptin inhibits the effectiveness of AMPK activation. *Oncology Reports*, *34*, 1675–1680. https://doi.org/10.1007/or.2015.4198

Escalante, M., Soto-Verdugo, J., Hernández-Kelly, L. C., Hernández-Melchor, D., López-Bayghen, E., Olivares-Bañuelos, T. N., & Ortega, A. (2019). GLAST Activity is modified by acute manganese exposure in bergmann glial cells. *Neurochemical Research*, *45*(6), 1365–1374. https://doi.org/10.1007/s11064-019-02848-8

Figueiredo, V. C., Markworth, J. F., & Cameron-Smith, D. (2017). Considerations on mTOR regulation at serine 2448: Implications for muscle metabolism studies. *Cellular and Molecular Life Sciences*, *74*(14), 2537–2545. https://doi.org/10.1007/s00018-017-2481-5

Flores-Méndez, M., Mendez-Flores, O. G., & Ortega, A. (2016). Glia plasma membrane transporters: key players in glutamatergic neurotransmission. *Neurochemistry International*, *98*, 46–55. https://doi.org/10.1016/j.neuit.2016.04.004

Flores-Méndez, M., Ramírez, D., Alamillo, N., Hernández-Kelly, L. C., Del Razo, L. M., & Ortega, A. (2014). Fluoride exposure regulates the elongation phase of protein synthesis in cultured Bergmann glia cells. *Toxicology Letters*, *229*(1), 126–133. https://doi.org/10.1016/j.yoxlet.2014.06.022

Flores-Méndez, M. A., Martínez-Lozada, Z., Monroy, H. C., Hernández-Kelly, L. C., Barrera, I., & Ortega, A. (2013). Glutamate-dependent translational control in cultured bergmann glia cells: EIF2α phosphorylation. *Neurochemical Research*, *38*(7), 1324–1332. https://doi.org/10.1007/s11064-013-1024-1

Gwinn, D. M., Shackelford, D. B., Egan, D. F., Mihaylova, M. M., Mery, A., Vasquez, D. S., Turk, B. E., & Shaw, R. J. (2008). AMPK Phosphorylation of raptor mediates a metabolic checkpoint. *Molecular Cell*, *30*(2), 214–226. https://doi.org/10.1016/j.molcel.2008.03.003

Harischandra, D. S., Ghaisas, S., Zenitsky, G., Jin, H., Kanthasamy, A., Anantharam, V., & Kanthasamy, A. G. (2019). Manganese-induced neurotoxicity: new insights into the triad of protein misfolding, mitochondrial impairment, and neuroinflammation. *Frontiers in Neuroscience*, *13*, 654. https://doi.org/10.3389/fnins.2019.00654

Hawley, S. A., Ross, F. A., Gowans, G. J., Tibarewal, P., Leslie, N. R., & Hardie, D. G. (2014). Phosphorylation by Akt within the ST loop of AMPK-α1 down-regulates its activation in tumour cells. *Biochemical Journal*, *459*(2), 275–287. https://doi.org/10.1042/BJ20131344

Herzig, S., & Shaw, R. J. (2018). AMPK: guardian of metabolism and mitochondrial homeostasis. *Nature Reviews Molecular Cell Biology*, *19*(2), 121–135. https://doi.org/10.1038/nrm.2017.95

Hsu, W. L., Chung, H. W., Wu, C. Y., Wu, H. I., Lee, Y. T., Chen, E. C., Fang, W., & Chang, Y. C. (2015). Glutamate stimulates local protein synthesis in the axons of rat cortical neurons by activating α-amino-3-hydroxy-5-methyl-4-isoxazolepropionic acid (AMPA) receptors and metabotropic glutamate receptors. *Journal of Biological Chemistry*, *290*(34), 20748–20760. https://.doi.org/jbc.M115.638023

Ijomone, O. M., Aluko, O. M., Okoh, C. O. A., Martins, A. C., & Aschner, M. (2019). Role for calcium signaling in manganese neurotoxicity. *Journal of Trace Elements in Medicine and Biology*, *56*, 146–155. https://doi.org/10.1016/jtemb.2019.08.006

Johanns, M., Pyr dit Ruys, S., Houddane, A., Vertommen, D., Herinckx, G., Hue, L., Proud, C. G., & Rider, M. H. (2017). Direct and indirect activation of eukaryotic elongation factor 2 kinase by AMP-activated protein kinase. *Cellular Signalling*, *36*, 212–221. https://doi.org/10.1016/j.cellsig.2017.05.010

Kamada, R., Kudoh, F., Ito, S., Tani, I., Janairo, J. I. B., Omichinski, J. G., & Sakaguchi, K. (2020). Metal-dependent Ser/Thr protein phosphatase PPM family: evolution, structures, diseases and inhibitors. *Pharmacology & Therapeutics*, *215*, 107622. https://doi.org/j.pharmthera.2020.107622

Ke, R., Xu, Q., Li, C., Luo, L., & Huang, D. (2018). Mechanisms of AMPK in the maintenance of ATP balance during energy metabolism. *Cell Biology International*, *42*(4), 384–392. https://doi.org/10.1002/cbin.10915

Ke, T., Sidoryk-Wegrzynowicz, M., Pajarillo, E., Rizor, A., Soares, F. A. A., Lee, E., & Aschner, M. (2019). Role of astrocytes in manganese neurotoxicity revisited. *Neurochemical Research*, *44*(1), 2449–2459. https://doi.org/10.1007/s11064-019-02881-7

Kenney, J. W., Moore, C. E., Wang, X., & Proud, C. G. (2014). Eukaryotic elongation factor 2 kinase, an unusual enzyme with multiple roles. *Advances in Biological Regulation*, *55*, 15–27. https://doi.org/10.1016/j.bior.2014.04.003

Korc, M. (1983). Manganese action on pancreatic protein synthesis in normal and diabetic rats. *American Journal of Physiology - Gastrointestinal and Liver Physiology*, *245*(5 Pt), G628–34. https://10.1152/ajpgi.1983.245.5.G628

Lee, E., Karki, P., Johnson, J., Hong, P., & Aschner, M. (2017). Manganese control of glutamate transporters' gene expression. *Advances in Neurobiology*, *16*, 1–12. https://doi.org/10.1007/978-3-319-55769-4_1

Lee, E.-S. Y., Yin, Z., Milatovic, D., Jiang, H., & Aschner, M. (2009). Estrogen and tamoxifen protect against Mn-induced toxicity in rat cortical primary cultures of neurons and astrocytes. *Toxicological Sciences*, *110*(2), 156–167. https://doi.org/10.1111/j.1471-4159.2009.06105.x

Liu, C., Yan, D. Y., Wang, C., Ma, Z., Deng, Y., Liu, W., & Xu, B. (2020). Manganese activates autophagy to alleviate endoplasmic reticulum stress–induced apoptosis via PERK pathway. *Journal of Cellular and Molecular Medicine*, *24*(1), 328–341. https://doi.org/10.1111/jcmm.14732

López-Bayghen, E., Aguirre, A., & Ortega, A. (2003). Transcriptional regulation through glutamate receptors: involvement of tyrosine kinases. *Journal of Neuroscience Research*, *74*(5), 717–725. https://doi.org/10.1002/jnr.10807

López-Colomé, A. M., Martínez-Lozada, Z., Guillem, A. M., López, E., & Ortega, A. (2012). Glutamate transporter-dependent mTOR phosphorylation in Müller Glia cells. *ASN Neuro*, *4*(5), e00095. https://doi.org/10.1042/AN20120022

López-Colomé, A. M., & Ortega, A. (1997). Activation of p42 mitogen-activated protein kinase by glutamate in cultured Radial Glia. *Neurochemical Research*, *22*(6), 679–685. https://doi.org/10.1023/A:1027345808746

Martínez-Lozada, Z., Guillem, A. M., Flores-Méndez, M., Hernández-Kelly, L. C., Vela, C., Meza, E., Zepeda, R. C., Caba, M., Rodríguez, A., & Ortega, A. (2013). GLAST/EAAT1-induced glutamine release via SNAT3 in Bergmann glial cells: evidence of a functional and physical coupling. *Journal of Neurochemistry*, *125*(4), 545–554. https://doi.org/10.1111/jnc.12211

Martínez-Lozada, Z., Hernández-Kelly, L. C., Aguilera, J., López-Bayghen, E., & Ortega, A. (2011). Signaling through EAAT-1/GLAST in cultured Bergmann glia cells. *Neurochemistry International*, *59*(6), 871–879. https://doi.org/10.1016/jneuit.2011.07.015

Martínez-Lozada, Z., & Ortega, A. (2015). Glutamatergic transmission: A matter of three. *Neural Plasticity*, *2015*, 787396. https://doi.org/10.1155/2015/7877396

Mendez-Flores, O. G., Hernández-Kelly, L. C., Suárez-Pozos, E., Najimi, M., & Ortega, A. (2016). Coupling of glutamate and glucose uptake in cultured Bergmann glial cells. *Neurochemistry International*, *98*, 72–81. https://doi.org/10.1016/j.neuit.2016.05.001

Moon, S. L., Sonenberg, N., & Parker, R. (2018). Neuronal regulation of eIF2α function in health and neurological disorders. *Trends in Molecular Medicine*, *24*(6), 575–589. https://doi.org/j.molmed.2018.04.001

Morales, M., González-Mejía, M. E., Bernabé, A., Hernández-Kelly, L. C. R., & Ortega, A. (2006). Glutamate activates protein kinase B (PKB/Akt) through AMPA receptors in cultured bergmann glia cells. *Neurochemical Research*, *31*(3), 423–429. https://doi.org/10.1007/s11064-005-9034-2

Musa, J., Orth, M. F., Dallmayer, M., Baldauf, M., Pardo, C., Rotblat, B., Kirchner, T., Leprivier, G., & Grünewald, T. G. P. (2016). Eukaryotic initiation factor 4E-binding protein 1 (4E-BP1): A master regulator of mRNA translation involved in tumorigenesis. *Oncogene*, *35*(36), 4675–4688. https://doi.org/10.1038/onc.2015-515

Ortega, A., Eshhar, N., & Teichberg, V. I. (1991). Properties of kainate receptor/channels on cultured Bergmann glia. *Neuroscience*, *41*(2-3), 336–349. https://doi.org/10.1016/0306-4522(91)90331-h

Pajarillo, E., Johnson, J., Rizor, A., Nyarko-Danquah, I., Adinew, G., Bornhorst, J., Stiboller, M., Schwerdtle, T., Son, D. S., Aschner, M., & Lee, E. (2020). Astrocyte-specific deletion of the transcription factor yin yang 1 in murine substantia nigra mitigates manganese-induced dopaminergic neurotoxicity. *Journal of Biological Chemistry*, *295*(46), 15662–15676. https://doi.org/10.1074/jbc.RA120.015552

Peres, T. V., Cordova, F. M., Lopes, M. W., Costa, A. P., & Leal, R. B. (2015). Chapter 7 Effect of manganese on signaling pathways. In *Manganese in health and disease* (pp. 182–198). The Royal Society of Chemistry. https://doi.org/10.1007/978-94-007-7500-8 7

Qin, X., Jiang, B., & Zhang, Y. (2016). 4E-BP1, A multifactor regulated multifunctional protein. *Cell Cycle*, *15*(6), 781–786. https://doi.org/10.1080/155384101.2016.1151581

Rodríguez-Campuzano, A. G., Hernández-Kelly, L. C., & Ortega, A. (2020). Acute exposure to SiO2 nanoparticles affects protein synthesis in Bergmann Glia cells. *Neurotoxicity Research*, *37*(2), 366–379. https://doi.org/10.1007/s12640-019-00084-0

Roux, P. P., & Topisirovic, I. (2018). Signaling pathways involved in the regulation of mRNA translation. *Molecular and Cellular Biology*, *38*(12), e00070–18. https://doi.org/10.1128/MCB.00070-18

Santini, E., & Klann, E. (2011). Dysregulated mTORC1-dependent translational control: from brain disorders to psychoactive drugs. *Frontiers in Behavioral Neuroscience*, *5*(76), 76. https://doi.org/10.3389/fnbeh.2011.00076

Sarbassov, D. D., Guertin, D. A., Ali, S. M., & Sabatini, D. M. (2005). Phosphorylation and regulation of akt/PKB by the rictor-mTOR Complex. *Science*, *307*(5712), 1098–1101 (1979). https://doi.org/10.1126/science.1106148

Schafer, A. E., & Blaxall, B. C. (2017). G protein coupled receptor-mediated transactivation of extracellular proteases. *Journal of Cardiovascular Pharmacology*, *70*(1), 10–16. https://doi.org/10.1097/FJC.0000000000000475

Sepúlveda, M. R., Dresselaers, T., Vangheluwe, P., Everaerts, W., Himmelreich, U., Mata, A. M., & Wuytack, F. (2012). Evaluation of manganese uptake and toxicity in mouse brain during continuous MnCl2 administration using osmotic pumps. *Contrast Media and Molecular Imaging*, *7*(4), 426–434. https://doi.org/10.1002/cmmi.1469

Sidoryk-Wegrzynowicz, M., & Aschner, M. (2014). Impairment of glutamine/ glutamate-γ-aminobutyric acid cycle in manganese toxicity in the central nervous system. *Folia Neuropathol*, 52(4), 377–382. https://doi.org/10.5114/fn.2014.47838

Somogyi, P., Eshhar, N., Teichberg, V. I., & Roberts, J. D. B. (1990). Subcellular localization of a putative kainate receptor in bergmann glial cells using a monoclonal antibody in the chick and fish cerebellar cortex. *Neuroscience*, 35(1), 9–30. https://doi.org/10.1016/0306-4522(90)90116-I

Tian, G., Lai, L., Guo, H., Lin, Y., Butchbach, M. E. R., Chang, Y., & Lin, C. L. G. (2007). Translational control of glial glutamate transporter EAAT2 expression. *Journal of Biological Chemistry*, 282(3), 1727–1737. https://doi.org/10.1074/jbc.M609822200

Warren, E. B., Bryan, M. R., Morcillo, P., Hardeman, K. N., Aschner, M., & Bowman, A. B. (2020). Manganese-induced mitochondrial dysfunction is not detectable at exposures below the acute cytotoxic threshold in neuronal cell types. *Toxicological Sciences*, 176(1), 446–459. https://doi.org/10.1093/toxsci/kfaa079

Watson, L. J., Alexander, K. M., Mohan, M. L., Bowman, A. L., Mangmool, S., Xiao, K., Naga Prasad, S. V., & Rockman, H. A. (2016). Phosphorylation of Src by phosphoinositide 3-kinase regulates beta-adrenergic receptor-mediated EGFR transactivation. *Cellular Signalling*, 28(10), 1580–1592. https://doi.org/10.1016/j.cellsig.2016.05.006

Wettmarshausen, J., Goh, V., Huang, K. T., Arduino, D. M., Tripathi, U., Leimpek, A., Cheng, Y., Pittis, A. A., Gabaldón, T., Mokranjac, D., Hajnóczky, G., & Perocchi, F. (2018). MICU1 Confers protection from MCU-dependent manganese toxicity. *Cell Reports*, 25(6), 1425–1435.e7. https://doi.org/10.1016/j.celrep.2018.10.037

Ye, Q., & Kim, J. (2015). Effect of olfactory manganese exposure on anxiety-related behavior in a mouse model of iron overload hemochromatosis. *Environmental Toxicology and Pharmacology*, 40(1), 333–341. https://doi.org/10.1016/j.etap.2015.06.016

Yu, J. S. L., & Cui, W. (2016). Proliferation, survival and metabolism: The role of PI3K/AKT/mTOR signalling in pluripotency and cell fate determination. *Development*, 143(17), 3050–3060. https://doi.org/10.1242/dev.137075

Zhang, B. Y., Chen, S., Ye, F. L., Zhu, C. C., Zhang, H. X., Wang, R. B., Xiao, C. F., Wu, T. C., & Zhang, G. G. (2002). Effect of manganese on heat stress protein synthesis of new-born rats. *World Journal of Gastroenterology*, 8(1), 114–118. https://doi.org/10.3748/wjg.v8.i1.114

## List of Abbreviations

| | |
|---|---|
| 4E-BP1 | Eukaryotic translation initiation factor 4E (eIF4E)-binding protein 1 |
| ADAM | A Disintegrin and Metalloprotease |
| Akt | Protein kinase B |
| AMPA | α-amino-3-hydroxy-5-methyl-4-isoxazolepropionic acid receptor |
| AMPK | Adenosine monophosphate-dependent protein kinase |
| BGC | Bergmann glial cells |
| $Ca^{2+}$ | Calcium |
| CaMKII | $Ca^{2+}$/calmodulin-dependent multiprotein kinase II |
| DMSO | Dimethyl sulfoxide |
| eEF2 | Eukaryotic elongation factor 2 |
| eEF2K | Eukaryotic Elongation Factor 2 Kinase |
| eIF2 | Eukaryotic initiation factor 2 |
| eIF4E | Eukaryotic translation initiation factor 4E |
| ERK 1/2 | Extracellular signal-regulated protein kinases 1/2 |
| FBS | Fetal bovine serum |
| GCN2 | General control non-depressible 2 kinases |
| GLAST | Glutamate/aspartate transporter |
| Gln | Glutamine |
| Glu | Glutamate |
| GS | Glutamine synthetase |
| HRI | Heme-regulated inhibitor kinase |
| IGFR | Insulin-like growth factor 1 receptor |
| IR | Insulin receptor |
| JNK | c-Jun N-terminal kinase |
| MAPK | Mitogen-activated protein kinase |
| MCU | Mitochondrial $Ca^{2+}$ uniporter |
| MMP | Matrix metalloproteases |
| Mn | Manganese |
| MNC | MAPK-interacting kinases |
| mTOR | Mechanistic target of rapamycin |
| MTT | 3-(4,5-dimethylthiazol-2-yl)-2,5-diphenyltetrazolium bromide |
| NCX | $Na^+$/$Ca^{2+}$ exchanger |
| Opti-MEM | Reduced-serum Minimal Essential Medium |
| PD | Parkinson's disease |
| PDK1 | Phosphoinositide-dependent kinase 1 |
| PERK | PKR-like endoplasmic reticulum kinase |
| PI3K | phosphatidylinositol 3 kinase |
| $PIP_2$ | Phosphatidylinositol 4,5-bisphosphate |
| $PIP_3$ | Phosphatidylinositol-3,4,5-trisphosphate |
| PKC | $Ca^{2+}$/diacylglycerol-dependent protein kinase C |
| PKR | Double-stranded RNA-dependent protein kinase |
| PMSF | Phenylmethylsulphonyl fluoride |
| RSK | Ribosomal S6 kinases |
| RTK | Receptor tyrosine kinases |
| S6K | Ribosomal S6 kinase |
| SH2 | Src homology domain 2 |
| SOD | Superoxide dismutase |
| TSC2 | Tuberous sclerosis complex 2 |

ORIGINAL ARTICLE

# Lysophosphatidic acid signaling via LPA$_6$: A negative modulator of developmental oligodendrocyte maturation

Samantha A. Spencer[1] | Edna Suárez-Pozos[1] | Jazmín Soto-Verdugo[1,2] |
Huiqun Wang[3] | Fatemah S. Afshari[1] | Guo Li[3] | Susmita Manam[1] | Daisuke Yasuda[4] |
Arturo Ortega[2] | James A. Lister[5] | Satoshi Ishii[4] | Yan Zhang[3] | Babette Fuss[1]

[1]Department of Anatomy and Neurobiology, Virginia Commonwealth University School of Medicine, Virginia, USA

[2]Departamento de Toxicología, Centro de Investigación y de Estudios Avanzados del IPN, Ciudad de México, México

[3]Department of Medicinal Chemistry, Virginia Commonwealth University School of Pharmacy, Virginia, USA

[4]Department of Immunology, Akita University Graduate School of Medicine, Akita, Japan

[5]Department of Human and Molecular Genetics, Virginia Commonwealth University School of Medicine, Virginia, USA

**Correspondence**
Babette Fuss, Department of Anatomy and Neurobiology, Virginia Commonwealth University School of Medicine, 1101 East Marshall Street, Richmond, VA 23298, USA.
Email: babette.fuss@vcuhealth.org

## Abstract

The developmental process of central nervous system (CNS) myelin sheath formation is characterized by well-coordinated cellular activities ultimately ensuring rapid and synchronized neural communication. During this process, myelinating CNS cells, namely oligodendrocytes (OLGs), undergo distinct steps of differentiation, whereby the progression of earlier maturation stages of OLGs represents a critical step toward the timely establishment of myelinated axonal circuits. Given the complexity of functional integration, it is not surprising that OLG maturation is controlled by a yet fully to be defined set of both negative and positive modulators. In this context, we provide here first evidence for a role of lysophosphatidic acid (LPA) signaling via the G protein-coupled receptor LPA$_6$ as a negative modulatory regulator of myelination-associated gene expression in OLGs. More specifically, the cell surface accessibility of LPA$_6$ was found to be restricted to the earlier maturation stages of differentiating OLGs, and OLG maturation was found to occur precociously in *Lpar6* knockout mice. To further substantiate these findings, a novel small molecule ligand with selectivity for preferentially LPA$_6$ and LPA$_6$ agonist characteristics was functionally characterized in vitro in primary cultures of rat OLGs and in vivo in the developing zebrafish. Utilizing this approach, a negative modulatory role of LPA$_6$ signaling in OLG maturation could be corroborated. During development, such a functional role of LPA$_6$ signaling likely serves to ensure timely coordination of circuit formation and myelination. Under pathological conditions as seen in the major human demyelinating disease multiple sclerosis (MS), however, persistent LPA$_6$ expression and signaling in OLGs can be seen as an inhibitor of myelin repair. Thus, it is of interest that LPA$_6$ protein levels appear

**478** | | wileyonlinelibrary.com/journal/jnc | *Journal of Neurochemistry.* 2022;163:478–499.

elevated in MS brain samples, thereby suggesting that LPA$_6$ signaling may represent a potential new druggable pathway suitable to promote myelin repair in MS.

**KEYWORDS**
computational ligand-protein docking, lipid signaling, multiple sclerosis, myelination, oligodendrocyte, small molecule ligands

# 1 | INTRODUCTION

Myelination in the central nervous system (CNS) of higher vertebrates has evolved to allow rapid and efficient signal propagation within the physical constraints imposed by the skull and vertebrae (Zalc, 2016; Zalc et al., 2008). During development, this process is defined by a tightly regulated differentiation program during which CNS myelinating cells, namely oligodendrocytes (OLGs), undergo a stepwise progression, from lineage committed progenitor cells and through stages of maturing OLGs, to ultimately convert into myelinating and then myelin maintaining OLGs (Elbaz & Popko, 2019; Emery & Lu, 2015; Sock & Wegner, 2021). In this scenario, each of the OLG maturation stages is characterized by a distinct gene expression profile that is determined by both intrinsic mechanisms and extrinsic factors (Adams et al., 2021; Baydyuk et al., 2020; Liu et al., 2016; Mitew et al., 2014; Wheeler & Fuss, 2016). Despite the critical importance of this process for the functional acuity of neuronal signal propagation in the CNS, the regulatory molecular pathways are still not fully understood.

Notably, our previous studies identified signaling initiated by the extracellular lipid signaling molecule lysophosphatidic acid (LPA) as a critical regulator of the transcriptional program regulating OLG maturation (Wheeler et al., 2015; Wheeler & Fuss, 2016; Yuelling et al., 2012). In general, LPA exerts its biological effects via activation of a family of G protein-coupled receptors with currently six members identified in mammals, namely LPA$_{1-6}$ encoded by *Lpar1-6* (Hecht et al., 1996; Kano et al., 2021; Kihara et al., 2014; Yung et al., 2014). With the exception of *Lpar5*, all of these receptors are, at least to some extent, expressed by cells of the mammalian OLG lineage, whereby at more mature stages the expression of *Lpar1* and *Lpar6* prevails (Cahoy et al., 2008; Marisca et al., 2020; Marques et al., 2016; Nogaroli et al., 2009; Stankoff et al., 2002; Suckau et al., 2019; Weiner et al., 1998; Wheeler et al., 2015; Yu et al., 2004; Zhang et al., 2014). Loss-of-function of *Lpar1* has only in the Malága variant of *Lpar1* null mice been described to affect CNS myelination by causing defects in protein trafficking without affecting the transcriptional regulation of OLG maturation (Anliker et al., 2013; Estivill-Torrus et al., 2008; Garcia-Diaz et al., 2015; Gennero et al., 2011). Thus, we focused our studies here on LPA$_6$, the most recently identified member of the LPA receptor family (Pasternack et al., 2008; Shimomura et al., 2008; Yanagida et al., 2009), for which a role in OLG maturation and CNS myelination had, to the best of our knowledge, not yet been explored. Our findings presented here uncover LPA$_6$ signaling as a new modulator that attenuates gene expression

associated with OLG maturation, and they introduce a novel small molecule ligand with preferential selectivity for LPA$_6$ and functional applicability in an in vitro as well as in vivo model of OLG maturation. Interestingly, our data also provide initial evidence for dysregulated LPA$_6$ signaling in the major human demyelinating disease multiple sclerosis (MS), in which alterations in OLG gene expression profiles have been associated with pathology and disease progression (Chang et al., 2002; Duncan et al., 2017; Falcão et al., 2018; Jäkel et al., 2019; Kuhlmann et al., 2008; Schirmer et al., 2019). Thus, taken together, our studies identify LPA$_6$ signaling as a novel mechanism modulating OLG maturation, and they suggest LPA$_6$ as a potential new druggable target for treating CNS diseases associated with myelin deficits.

# 2 | MATERIALS AND METHODS

## 2.1 | Reagents

LPA (LPA 18:1, 1-oleoyl-LPA) was purchased from Avanti Polar Lipids (Cat. No 857130) and stored at −20°C (10 mg/ml in chloroform). (2S)-OMPT (L-sn-1-O-oleoyl-2-O-methylglyceryl-3-phosphothionate) was purchased from Echelon Biosciences (Cat. No L-9418) and stored at −20°C (10 mM in dimethyl sulfoxide [DMSO]). GL-8-28 (Figure 3) was synthesized by us and stored at −20°C (10 mM in DMSO). Unless otherwise stated, all other reagents were purchased from Sigma-Aldrich or Thermo Fisher Scientific. Details to antibodies and PCR primers are shown in Tables 1 and 2.

## 2.2 | Chemical synthesis and characterization of compound GL-8-28

All reagents were purchased from Sigma-Aldrich or as otherwise stated. Melting points were obtained with a Fisher Scientific micro melting point apparatus and are uncorrected. All infrared (IR) spectra were recorded on a Nicolet Avatar 360 FT-IR Instruments. Proton (300 MHz) and Carbon-13 (75 MHz) nuclear magnetic resonance (NMR) spectra were recorded at ambient temperature with tetramethylsilane as the internal standard on either a Varian Gemini-300 MHz "Tesla" spectrometer or Varian Mercury-300 MHz NMR spectrometer. Gas chromatography/mass spectrometry (GC/MS) analysis was performed on a Hewlett Packard 6890 column. Thin layer chromatography (TLC) analyses were carried out on

**TABLE 1** Antibody RRIDs and concentrations or dilutions used in the assays listed

| | RRID | Assay (concentration or dilution) |
|---|---|---|
| **Primary antibodies** | | |
| A2B5 (clone 105) | CVCL_7946 | Immunopanning (15 µg/ml) Immunocytochemistry (undiluted hybridoma supernatant) |
| Anti-APC (CC-1) | AB_2057371 | Immunohistochemistry (1:100) |
| Anti-CD16/CD32 (clone 93) | AB_467133 | Flow cytometry (1:100) |
| Anti-GAPDH | AB_2107445 | Western blot (1:10000) |
| Anti-LPA$_4$ | AB_2340992 | Flow cytometry (1:100) Western blot (1:100) |
| Anti-LPA$_6$ | AB_2340993 | Flow cytometry (1:100) Western blot (1:100) Immunocytochemistry (1:100) |
| Anti-MBP (SMI99P) | AB_2314772 | Immunocytochemistry (1:100) |
| O4 (clone O4) | CVCL_Z932 | Immunocytochemistry (undiluted hybridoma supernatant) |
| Anti-Olig2 | AB_10807410 | Immunohistochemistry (1:100) |
| Rabbit IgG isotype control | AB_2811130 | Flow cytometry (1:100) |
| **Secondary antibodies** | | |
| Goat anti-rabbit IgG, AlexaFluor 488 conjugated | AB_143165 | Flow cytometry (1:100) Immunocytochemistry (1:500) Immunohistochemistry (1:500) |
| Goat anti-Mouse IgG2b, AlexaFluor 568 conjugated | AB_2535780 | Immunohistochemistry (1:500) |
| Goat anti-Mouse IgG2b, AlexaFuor 594 conjugated | AB_2535781 | Immunocytochemistry (1:500) |
| Goat anti-Mouse IgM, AlexaFluor 633 conjugated | AB_2535715 | Immunocytochemistry (1:500) |
| Goat anti-Mouse IgG2a, AlexaFluor 633 conjugated | AB_2535775 | Immunohistochemistry (1:500) |
| Goat anti-Mouse IgG, IRDye 680 | AB_621840 | Western blot (1:10000) |
| Goat anti-Rabbit IgG, IRDye 800CW conjugated | AB_10796098 | Western blot (1:10000) |

**TABLE 2** List of primer sequences used for RT-qPCR analysis

| | Forward primer (5′-3′) | Reverse primer (5′-3′) |
|---|---|---|
| **Mouse genes** | | |
| *Olig2* | ACCGTTAACACGAGGGGCAA | TTAGGAAGCGGCGCAGTACA |
| *Cnp* | ATGCCCAACAGGATGTGGTG | AGGGCTTGTCCAGGTCACTT |
| *Ugt8* | AGGAGCTCTGGGGAGATTGC | TTTGAATGGCCAAGCAGGTCA |
| *Egr1* | CCTGACCACAGAGTCCTTTTCT | AAAGTGTTGCCACTGTTGGG |
| **Mouse reference genes** | | |
| *Ppia* | GGAGACGAACCTGTAGGACG | GATGCTCTTTCCTCCTGTGC |
| *Pgk1* | ATGCAAAGACTGGCCAAGCTAC | AGCCACAGCCTCAGCATATTTC |
| *Rpl13a* | GCGCCTCAAGGTGTTGGATG | CGCCCCAGGTAAGCAAACTTTC |
| **Zebrafish genes** | | |
| *cldnk* | TGGCATTTCGGCTCAAGCTCTGGA | GGTACAGACTGGGCAATGGACCTGA |
| *plp1b* | TGCCATGCCAGGGGTTGTTTGTGGA | TGGCGACCATGTAAACGAACAGGGC |
| **Zebrafish reference genes** | | |
| *ef1a* | GTACTACTCTTCTTGATGCCC | GTACAGTTCCAATACCTCCA |
| *actb2* | CCCTGTTCCAGCCATCCTT | TTGAAAGTGGTCTCGTGGATACC |
| *rpl13a* | TCTGGAGGACTGTAAGAGGTATGC | AGACGCACAATCTTGAGAGCAG |

Abbreviations: *actb2*, beta actin; *cldnk*, claudin k; *Cnp*, 2′,3′ cyclic nucleotide phosphodiesterase; *ef1a*, elongation factor 1-alpha; Egr1, early growth response 1; *Olig2*, oligodendrocyte transcription factor 2; *Pgk1*, phosphoglycerate kinase 1; *plp1b*, proteolipid protein 1b; *Ppia*, peptidylprolyl isomerase A (cyclophilin A); *Rpl13a*, ribosomal protein L13a; *Ugt8*, UDP glycosyltransferase 8.

Analtech Uniplate F254 plates. Chromatographic purification was carried out on silica gel columns (230~400 mesh, Merck). Yields were not maximized.

Compound GL-8-28 was prepared in four steps. First, 3-tri methylsilanyloxy-propylamine was prepared following a previously reported method (Mormann & Leukel, 1988). The mixture of 3-amino-1-propanol (1.50 g, 20 mmol), hexamethyldisilazane (1.78 g, 11 mmol), and trimethylsilane chloride (catalytic amount) was heated at 140°C for 2 h. After cooldown, the mixture was concentrated under vacuum to give 2.09 g light yellow oil, in 68% yield. $^1$H NMR (300 MHz, DMSO): $\delta$ 3.70(t, $J = 7.5$ Hz, 2 H), 2.80(t, $J = 6.6$ Hz, 2 H), 1.69(m, 2 H), 0.14 (s, 9 H). Second, octadec-9(Z)-enoic acid (3-trime thylsianyloxy-propyl)-amide was prepared. The mixture of octadec-9(Z)-enoic acid (3.59 g, 12.6 mmol) and thionyl chloride (3.0 g, 25.2 mmol) in chlorobenzene (40 ml) was heated to reflux overnight. After concentrated to remove solvent and the excess thionyl chloride, the residue was dissolved in dry dichloromethane (10 ml). Then, the resulting solution was added into a solution of 3-trimethylsilan yloxy-propylamine (1.16 g, 6.3 mmol) in dry dichloromethane (90 ml) at 0°C. The mixture was stirred overnight. The dichloromethane layer was washed with water (30 ml × 3), brine and dried over sodium sulfate. After filtered and concentrated, the resulting residue was purified by silica gel column, hexane, and ethyl acetate (4: 1) to give 1.4 g product in 61% yield. $^1$H NMR (300 MHz, CDCl$_3$): $\delta$ 5.76 (br, 1 H), 5.37 (m, 2 H), 4.17 (t, $J = 6.0$ Hz, 2 H), 3.33 (t, $J = 6.6$ Hz, 2 H), 2.34 (t, $J = 7.2$ Hz, 2 H), 2.19 (m, 2 H), 2.05 (m, 2 H), 1.86 (m, 2 H), 1.65 (m, 2 H), 1.29 (m, 16 H), 0.90 (t, $J = 6.6$ Hz, 3 H), 0.13 (s, 9 H); $^{13}$C NMR (75 MHz, CDCl$_3$) $\delta$: 172.74, 129.59, 129.31, 61.23, 36.47, 35.71, 33.88, 31.49, 31.48, 29.35, 29.34, 29.27, 29.11, 29.10, 28.91, 28.90, 28.73, 28.72, 28.45, 26.80, 25.35, 24.55, 22.27, 13.71. Third, octadec-9(Z)-enoic acid (3-hydroxy-propyl)-amide was prepared. In an ice-water bath, the solution of octadecanoic acid (3-trimethylsilanyloxy-prop yl)-amide (500 mg, 1.2 mmol) in ethanol (10 ml) was added 1 N HCl (5 ml). The mixture was allowed to stir at 20°C for 5 hrs. Filtration gave 380 mg white powder in 93% yield. $^1$H NMR (300 MHz, CDCl$_3$): $\delta$ 6.05 (br, 1 H), 5.36 (m, 2 H), 3.63 (m, 2 H), 3.43 (q, $J = 6.0$ Hz, 2 H), 2.21 (m, 2 H), 2.03 (m, 4 H), 1.70 (m, 4 H), 1.30 (m, 20 H), 0.90 (t, $J = 6.9$ Hz, 3 H); $^{13}$C NMR (75 MHz, CDCl$_3$) $\delta$: 174.18, 129.57, 129.28, 58.68, 36.29, 35.68, 31.92, 31.47, 29.34, 29.28, 29.09, 28.89, 28.88, 28.84, 28.83, 28.71, 26.79, 26.74, 25.40, 22.26, 13.70. Last, sulfuric acid mono-(3-octadec-9(Z)-enoylamino-propyl) ester (GL-8-28) was prepared based on a reported method (Pogorevc & Faber, 2002). To a suspension of sodium hydride (16.3 mg, 0.67 mmol) in dimethylfor-mamide (DMF) (2 ml), octadecanoic acid (3-hydroxy-propyl)-amide (105 mg, 0.31 mmol) was added. After being stirred at 20°C for 1 hour, the resulting mixture was added to the solution of sulfur trioxide triethylamine complex (67 mg, 0.37 mmol) in DMF (1 ml). The reaction mixture was stirred overnight. After concentrated under vacuum to remove DMF, the residue was purified by silica gel column, dichloromethane, and methanol (10:1) to give 65 mg gum, in 50% yield. $^1$H NMR (300 MHz, CDCl$_3$): $\delta$ 5.37 (m, 2 H), 4.06 (t, $J = 6.6$ Hz, 2 H), 3.23 (m, 2 H), 2.21 (t, $J = 7.5$ Hz, 2 H), 2.04 (m, 2 H), 1.87 (m, 2 H), 1.62 (m, 2 H), 1.34 (m, 20 H), 0.93 (t, $J = 6.6$ Hz, 3 H);

$^{13}$C NMR (75 MHz, CD$_3$OD) $\delta$: 174.34, 128.92, 128.81, 64.75, 46.03, 35.27, 31.14, 28.92, 28.91, 28.69, 28.53, 28.42, 28.41, 28.33, 28.26, 26.21, 25.15, 21.82, 12.57, 7.34; MS (ESI) m/z: 420.3(M + H)$^+$.

## 2.3 | Experimental animals

$Lpar_6$ KO mice (Accession No. CDB0977K: http://www.clst.riken.jp/arg/mutant%20mice%20list.html) were generated as previously described (Hata et al., 2016); these mice were housed at Akita University (Japan) under temperature-controlled conditions with ad libitum access to food and water in a 12 h dark/light cycle, and kept on a C57BL/6N background. In total, 17 mice (males and females) were used in these studies. No animals were excluded from the analyses described here, and no exclusion criteria were pre-determined. Zebrafish embryos were obtained through natural matings, raised at 28.5°C, and staged according to morphological criteria and hours post fertilization (hpf) (Kimmel et al., 1995). Wild-type zebrafish were of the AB or NHGRI-1 strains. Sprague-Dawley female rats with early postnatal litters were obtained from Envigo/Harlan Laboratories. All animal studies were approved by the Institutional Animal Care and Use Committees at Virginia Commonwealth University (IACUC #AM10229 and #AM10189) and Akita University. Unless otherwise stated, $n$ = number of animals used when multiple animals were compared. This study was not preregistered, and no blinding or randomization was performed.

## 2.4 | Human tissue samples

Human white matter tissue samples from non-MS and MS donors were obtained from the Netherlands Brain Bank, Netherlands Institute for Neuroscience, Amsterdam (open access: www.brainbank.nl). All material has been collected from donors for or from whom a written informed consent for a brain autopsy and the use of the material and clinical information for research purposes had been obtained by the Netherlands Brain Bank. Based on medical history and autopsy evaluation, none of the MS individuals included in this study presented any neurodegenerative disorders other than MS. Brains were classified as MS or non-MS based on medical history and post-mortem pathological analyses. Details to the demographics of the donor patients are shown in Table 3.

## 2.5 | Cell culture

Primary OLG progenitors were isolated from postnatal day 2 (P2) rat brains by A2B5 immunopanning as described previously (Barres et al., 1992; Martinez-Lozada et al., 2014; Wheeler et al., 2015). For each individual experiment, brains from all animals (8–12; male and female pups) of an entire litter were pooled. For immunopanning, supernatants of A2B5 hybridoma cells (ATCC) cultured in Dulbecco's Modified Eagle's Medium (DMEM; Cat. No. 11995040,

**TABLE 3** Demographics of non-multiple sclerosis and multiple sclerosis patients

| | MS type | Age (yrs)/Sex | PMI (hrs) |
|---|---|---|---|
| Control 1 | Non-MS | 90/F | 7.25 |
| Control 2 | Non-MS | 84/M | - |
| Control 3 | Non-MS | 51/M | 7.5 |
| Control 4 | Non-MS | 87/F | 8 |
| Control 5 | Non-MS | 86/F | 13.3 |
| MS 1 | SPMS | 49/M | 8 |
| MS 2 | MS | 44/M | 10 |
| MS 3 | MS | 57/F | 8.75 |
| MS 4 | SPMS | 75/M | 7.5 |
| MS 5 | SPMS | 59/F | 4.75 |
| MS 6 | MS | 68/F | 8.25 |
| MS 7 | SPMS | 45/M | 7.75 |
| MS 8 | PPMS | 57/F | 5.75 |
| MS 9 | PPMS | 74/F | 5.5 |
| MS 10 | SPMS | 48/F | 11.75 |
| MS 11 | MS | 60/F | 10.5 |
| MS 12 | MS | 56/F | 8.25 |
| MS 13 | SPMS | 78/M | 8.75 |
| MS 14 | MS | 53/M | 10 |

Abbreviations: MS, multiple sclerosis; SPMS, secondary progressive multiple sclerosis; PPMS, primary progressive multiple sclerosis; PMI (hrs), postmortem interval in hours.

Gibco/Thermo Fisher Scientific) containing 10% fetal bovine serum (FBS; Cat. No. SH30071.03, HyClone, Cytvia) and 1% antibiotic-antimycotic (Cat. No. 15240062, Gibco/Thermo Fisher Scientific) were used directly or A2B5 antibodies were purified by ammonium sulfate precipitation (Andrew et al., 2009) and used at a concentration of 15μg/ml as determined by ELISA (Mouse IgM ELISA Kit, Cat. No. ab133047, Abcam). Isolated OLG progenitors were plated onto fibronectin(10 μg/ml; Cat. No 3416355MG or 341668500UG, MilliporeSigma)-coated tissue culture dishes, glass coverslips, or 96-well plates and cultured at 37°C and 5% $CO_2$ in serum-free proliferation medium [DMEM containing N2 supplement (Cat. No. 17502001, Thermo Fisher Scientific), 5 ng/ml human platelet-derived growth factor (PDGF, Cat No. 300-176P, Gemini Bio-Products) and 5 ng/ml basic fibroblast growth factor (bFGF, Cat. No. 300-113P, Gemini Bio-Products)] for 24 h, after which they were allowed to differentiate in serum-free differentiation medium [DMEM containing N2 supplement (Thermo Fisher Scientific) and 40 ng/ml tri-iodo-thyronine (T3; Cat. No. T2877, Sigma)] over the time periods indicated. Differentiating OLGs were collected for RNA isolation, and supernatants [phenol red-free DMEM, Cat. No. 31053036, Gibco/Thermo Fisher Scientific, with added L-glutamine (Cat. No 25030, Gibco/Thermo Fisher Scientific) and sodium pyruvate (Cat. No. 11360070 Gibco/Thermo Fisher Scientific)] were collected for determining cell viability using the Thermo Scientific Pierce LDH Cytotoxicity Assay Kit (Cat. No. 88954, Thermo Fisher Scientific) and a PHERAstar plate reader (BMG LABTECH Inc.). For all primary OLG cell culture studies, at least three independent experiments were performed, whereby an independent experiment refers to an experiment in which cells were isolated from a separate P2 rat litter at an independent time point (day) and treated separately from all other independent experiments.

For the determination of LPA receptor selectivity, the PRESTO-Tango assay was used (Kroeze et al., 2015). HTLA cells, (an HEK293 cell line stably expressing a tTA-dependent luciferase reporter and a β-arrestin2-TEV fusion gene) were kindly provided by Dr. Wesley Kroeze and maintained in DMEM supplemented with 10% FBS, 2μg/ml puromycin (Cat. No. A1113803, Gibco/Thermo Fisher Scientific) and 100μg/ml hygromycin B (Cat. No. 10687010, Thermo Fisher Scientific) in a humidified atmosphere at 37°C in 5% $CO_2$. This cell lines is not listed as commonly misidentified cell line by the International Cell Line Authentication Committee (ICLAC). TANGO-ized plasmid constructs for LPAR1, 2 and LPAR4-6 (Kroeze et al., 2015) were gifts from Dr. Bryan Roth and obtained through Addgene (LPAR1-Tango, RRID: Addgene_66418; LPAR2-Tango, RRID: Addgene_66419; LPAR4-Tango, RRID: Addgene_66420; LPAR5-Tango, RRID: Addgene_66421; LPAR6-Tango, RRID: Addgene_66422). The LPAR3-TANGO plasmid construct was designed analogous to all other TANGO-ized G protein-coupled receptor plasmid constructs and synthesized through Thermofisher Scientific's Synthetic Biology and Genome Engineering service. Plasmid constructs were confirmed by sequencing and purified using an EndoFree plasmid maxi prep kit (Cat. No. 12362, Quiagen Inc.). For transfection, HTLA cells were plated at a density of $1 \times 10^6$ cells per well into 12-well cell culture plates and transfected the following day (day 2) with 4 μg (LPA$_{1-5}$) or 8 μg (LPA$_6$) of 'TANGO-ized' LPA receptor plasmid construct per well using Lipofectamine 2000 (Cat. No. 11668019, Thermo Fisher Scientific) in serum-free Opti-MEM medium (Cat. No. 31985070, Gibco/Thermo Fisher Scientific) without antibiotics. On day 3, cells were re-plated at $1 \times 10^5$ cells per well into poly-L-lysine coated 96-well white, clear flat bottom microplates (Cat. No. CLS3610, Corning Life Sciences) in Opti-MEM medium containing 10% charcoal-stripped FBS (Cat. No. 12676029, Gibco/ThermoFisher Scientific). On day 4, 5× drug stimulation solutions were prepared in filter-sterilized assay buffer, which consisted of 20 mM HEPES in Hank's Balanced Salt Solution (HBSS, Cat. No. 14170112, Gibco/Thermo Fisher Scientific), pH 7.4, and 20μl were added to each well containing 80μl of medium. Constitutive activity controls received only the assay buffer. On day 5 (after about 18 h of incubation), luminescence, as a measure for receptor activation, was determined using the Bright-Glo Luciferase Assay System (Cat. No. E2610, Promega) and a PHERAstar plate reader (BMG LABTECH Inc.).

## 2.6 | Treatment with pharmacological compounds

Zebrafish embryos (at 24 hpf) and primary cultures of differentiating OLGs (at 24 h, i.e. at the time of switch to differentiation medium)

were treated with LPA, (2*S*)-OMPT or GL-8-28 at the concentrations indicated. LPA was dissolved in DMEM containing 0.1% fatty acid-free bovine serum albumin (BSA; Cat. No. A8806, Sigma), while (2*S*)-OMPT and GL-8-28 were dissolved in dimethyl sulfoxide (DMSO), resulting in a final experimental concentration of 0.1% DMSO. Vehicle treatments were used as controls.

## 2.7 | Immunocytochemistry, immunohistochemistry, RNAscope, and confocal microscopy

Differentiating OLGs, plated on fibronectin-coated coverslips, were immunostained live (O4 or A2B5 hybridoma supernatants, anti-LPA$_6$ antibodies) or after fixation in 4% paraformaldehyde/PBS (anti-MBP, anti-LPA$_6$ antibodies). In combined double staining procedures, live staining was performed first, followed by fixation. Fixed cells were permeabilized using 0.5% Triton X-100/PBS, and nonspecific binding sites were blocked by incubation in 10% FCS/DMEM (live cells) or 2% BSA/PBS (fixed cells) for 30 min at 20°C . Primary antibodies were diluted in 10% FCS/DMEM (live cells) or 1% BSA/PBS (fixed cells), and cells were incubated for 1 h at 20°C followed by incubation with secondary antibodies diluted in 1% BSA/PBS for 30 min or 1 h at 20°C. Nuclei were counterstained using Hoechst 33342 (Cat. No. 14533; MilliporeSigma), and sections were mounted using Vectashield (Cat. No. H-1000-10, Vector Laboratories).

Tissue sections for immunohistochemistry and RNAscope were prepared in principle as described previously (Benusa et al., 2017; Dupree et al., 1999). Briefly, mice were anesthetized by an intraperitoneal injection of 0.8 ml/20 g (of mouse body weight) 2-2-2 tribromoethanol (20 g/ml; Cat. No. T48402, Sigma-Aldrich) and then transcardially perfused with 4% paraformaldehyde in 0.1 M Millonig's phosphate buffer (Karlsson & Schultz, 1965); the brains were removed, post-fixed for 24 h in perfusion fixative, cryoprotected by immersion in 30% sucrose in PBS for 48 h, and then embedded and frozen in Tissue-Tek O.C.T. compound (Cat. No. 4583, Sakura Finetek USA). For immunohistochemistry, serial coronal sections (40-μm) were prepared using a Leica CM 1850 cryostat (Leica Biosystems) and stored at −80°C. Tissue sections were permeabilized for 10 minutes in ice-cold acetone and blocked for 1 h at 20°C using PBS containing 1% Triton X-100 and 5% cold fish gelatin (Cat. No. 50-259-35, Electron Microscopy Science). Primary antibodies were diluted in blocking solution, and sections were incubated for 48 h at 4°C followed by incubation with secondary antibodies for 90 min at 20°C . Nuclei were counterstained using Hoechst 33342 (Cat. No. 14533; MilliporeSigma), and sections were mounted using Vectashield (Cat. No. H-1000-10, Vector Laboratories). For RNAscope, coronal sections (15-μm) were prepared using a Leica CM 1850 cryostat (Leica Biosystems), sections were mounted on Leica Bond Plus slides (Cat. No. S21.2113.A, Leica Biosystems) and post-fixed as follows: 60°C for 30 min, 4% paraformaldehyde in PBS for 15 min at 4°C, 50% ethanol for 5 min at 20°C, 70% ethanol for 5 min at 20°C, 100% ethanol for 5 min at 20°C (twice), air

dried for 5 min, and stored at −80°C. RNAscope was performed using a Leica Biosystems Bond RX automated immunohistochemistry/in situ hybridization staining system (Leica Biosystems) located within VCU's Tissue and Data Acquisition and Analysis Core and the following RNAscope 2.5 LS Probe probes (all from Advanced Cell Diagnostics, Inc.): Mm-Lpar6 (Cat. No. 318358), Mm-Olig2-C2 (Cat. No. 447098-C2), Mm-Plp1-C4 (Cat. No. 428188-C4); for fluorescent detection, RNAscope LS Fluorescent Reagent and RNAscope LS 4-Plex Ancilliary kits (Cat Nos. 322 800 and 322 830, Advanced Cell Diagnostics, Inc.) were used in combination with the following Opal fluorophores (Akoya Biosciences): Opal 690 (Cat. No. PN FP1497001KT), Opal 620 (Cat. No. PN FP1495001KT), Opal 520 (Cat. No. PN FP1487001KT).

All confocal images were collected using a Zeiss LSM 710 or LSM 880 confocal laser scanning microscope (Carl Zeiss Microscopy, LLC) located within VCU's Microcopy Shared Resource. For immunostained cells, confocal z-stacks, each spanning the optical distance of the entire cell, were collected at 0.48 μm intervals using a 63× oil-immersion objective with a numerical aperture of 1.4 and the following settings: a pinhole size of one Airy unit, a dimension of 1912×1912 pixels, and 4 times line averaging. For immunostained sections, confocal z-stacks, each spanning an optical distance of 15 μm, were collected at 1 μm intervals using a 40× oil-immersion objective with a numerical aperture of 1.3 and the following settings: a pinhole size of one Airy unit, a dimension of 1248×1248 pixels, and 4 times line averaging. For sections labeled by RNAscope, confocal z-stacks, each spanning an optical distance of 15 μm, were collected at 0.5 μm intervals using a 63x oil-immersion objective with a numerical aperture of 1.4 and the following settings: a pinhole size of one Airy unit, a dimension of 1200×1200 pixels and 4 times line averaging. For image acquisition and the generation of maximum intensity projections ZEN imaging software (Carl Zeiss Microscopy, LLC; RRID:SCR_013672) was used.

## 2.8 | Western blot analysis

For western blot analysis, human tissue samples were homogenized in lysis buffer (10 μl per mg tissue; phosphate-buffered saline [PBS], 2 mM EDTA) containing 1x Halt protease and phosphatase inhibitor cocktail (Cat. No. 78430, Thermo Fisher Scientific). After centrifugation at 21 000 *g* for 15 min at 4°C, protein concentrations of the supernatants were determined using the BCA protein assay kit (Cat. No. 23225, Pierce/Thermo Fisher Scientific). Samples were heat-denatured (90°C for 5 min) in Laemmli sample buffer (Cat. No. S3401, MilliporeSigma), and equal amounts of denatured protein (60 μg) were separated by electrophoresis through 4–20% gradient sodium dodecyl sulfate (SDS)-polyacrylamide gels (Cat. No. 4561094, Bio-Rad Laboratories). Separated proteins were subsequently electroblotted onto Immobilon-P polyvinylidene difluoride (PVDF) membranes (Cat. No. IPVH00010, MilliporeSigma). Total protein levels were determined using Revert 700 Total Protein Stain (Cat. No. 926-11 011, LI-COR Biosciences) and membranes were

subsequently incubated in blocking buffer (Cat. No. 927-70001, LI-COR Biosciences) for 1 h at 20°C prior to incubation with primary antibodies diluted in blocking buffer (48 h at 4°C). Bound primary antibodies were detected using IRDye 680RD- or 800CW-conjugated secondary antibodies (LI-COR Biosciences) diluted in blocking buffer (3 h at 20°C). For quantification, membranes were imaged using an Odyssey infrared imaging system and analyzed using Image Studio and Empiria Studio software packages (LI-COR Biosciences).

## 2.9 | Flow cytometry

Differentiating OLGs were collected after 48 h culture in serum-free differentiation medium using Accutase cell detachment solution (Cat. No. A6964, MilliporeSigma). Cells were counted, and $10^6$ cells per sample were immunostained for analysis. Cells-only controls were placed immediately into flow cytometry buffer [0.5% bovine serum albumin (BSA) and 2 mM EDTA in phosphate-buffered saline (PBS)]. All immunostaining procedures were performed on ice in PBS containing 0.5% BSA and 2 mM EDTA. Fc receptors were blocked by incubation with anti-mouse CD16/32 for 15 min, and cells were incubated for 30 min first with anti-LPA receptor antibodies or their respective isotype controls and then with AlexaFluor 488-conjugated secondary antibodies. Cells were washed twice and resuspended in flow cytometry buffer. Immediately prior to flow analysis, 7-AAD viability stain (Cat. No. A1310, Invitrogen/eBioscience/Thermo Fisher Scientific) was added, and samples were run on a LSRFortessa-X20 flow cytometer (BD Biosciences) at 20°C using a 488 nm laser (>20 mW power, Coherent solid-state) and 530/30 nm and 647/20 nm bandpass filters. Settings were carefully determined empirically and exactly reproduced in each experiment. Gates were demarcated to count 488-positive (7-AAD-negative) cells up to 10 000 events. FACSDIVA software (BD Biosciences) was used for acquisition, and data were analyzed using FCS Express Flow Cytometry software (DeNovo Software).

## 2.10 | RNA Isolation and RT-qPCR

RNA was purified using RNeasy Mini (cultured OLGs) or Midi (zebrafish embryos) Kits (Cat Nos. 74104 and 75144, Qiagen LLC). For the isolation of RNA from cultured rodent OLGs, cells were plated on fibronectin-coated 12 well plates ($1 \times 10^6$ cells per well) and collected in RTL lysis buffer (Qiagen LLC) containing 1% 2-mercaptoethanol. For RNA isolation from zebrafish embryos at 48 hpf, embryos were anesthetized using 0.015% tricaine methanesulfonate (Syncaine, Syndel/Western Chemical), chorions were removed using 2 mg/ml Pronase (Cat. No. 11459643001, Sigma, St Louis, MO), and pools of about 20 embryos were homogenized in RTL lysis buffer (included in RNeasy kits, Qiagen LLC) containing 1% 2-mercaptoethanol. All RNA samples were treated with DNase (DNA-Free Kit; Cat. No. AM1906, Applied Biosystems/Thermo Fisher Scientific). RNA concentrations and purity were determined using a 2100 Bioanalyzer and RNA

6000 Pico kits (Cat. No. 5067–1513, Agilent); samples with an RNA integrity number above 7 were used for further analysis. Oligo-dT- and random hexamer-primed cDNAs were synthesized from 50 ng to 1 μg of RNA using Omniscript or Sensiscript Reverse Transcription Kits (Cat. Nos. 205113 and 205213, Qiagen LLC) according to the guidelines of the manufacturer. RNA samples were normalized to the same approximate concentration, and the same amount of RNA was used for all conditions of an individual independent RT-qPCR experiment.

For all RT-qPCR experiments the *Minimum Information for Publication of Quantitative Real-Time PCR Experiments* (MIQE) guidelines were followed (Bustin et al., 2009). Briefly, RT-qPCR primers (Table 3) were designed and in silico tested for specificity using the National Center for Biotechnology Information's basic local alignment search tool (Primer-BLAST) (Ye et al., 2012). All primers were designed to amplify all known splice variants, and for all primer pairs melting curves were used to ensure specificity. cDNA reactions without reverse transcriptase were performed for all samples to ensure no-reverse-transcriptase quantitation cycle ($C_q$) numbers of at least five cycles below the lowest $C_q$ for any of the experimental samples. RT-qPCR reactions with three technical replicates per sample were performed on a CFX96 real-time PCR detection system (Bio-Rad Laboratories) using the iTaq Universal SYBR Green Supermix (Cat. No. 1725121, Bio-Rad Laboratories). PCR conditions were as follows: 95°C for 3 min, followed by 40 cycles of 95°C for 15 s, 58°C for 30 s, and 95°C for 10 s. Expression levels were determined using the ΔΔCT method relative to the geometric mean of the three reference genes (Livak & Schmittgen, 2001).

## 2.11 | Homology modeling and molecular docking

The published zebrafish $LPA_6$ crystal structure was utilized as the template protein to build the 3D conformations of human $LPA_6$ (Taniguchi et al., 2017). The amino acid sequence for human $LPA_6$ was downloaded from UniProtKB (primary accession number P43657). The sequence alignment between target (human $LPA_6$) and template (zebrafish $LPA_6$) sequences were performed by the program ClustalX 2.1 (Larkin et al., 2007) with default parameters. Based on the sequence alignments, 100 3D models of $LPA_6$ were built by MODELER 9.19. The 3D models with the highest DOPE assessment score were selected as the optimal homology model for human $LPA_6$ (Shen & Sali, 2006).

GL-8-28 was sketched in Sybyl-X 2.0 and further energy minimized to a gradient of 0.05 with Gasteiger-Hückel charges assigned under the Tripos force field (TAFF) (Ballesteros & Weinstein, 1995). The molecular docking study was performed by GOLD 2020 (Cambridge Crystallographic Data Centre, CCDC, Cambridge, UK) to obtain the ligand-receptor complex. The putative docking sites of the human $LPA_6$ model were defined by 10 Å around the α-carbon atom of $V^{5.39}$ of $LPA_6$, which formed directly hydrophobic interaction with the LPA species in the crystal structure of the zebrafish $LPA_6$ (Taniguchi et al., 2017). Except for the above parameters,

molecular docking studies were conducted with standard default settings. Fifty docking solutions were generated in the respective optimal homology model of $LPA_6$. The docking solutions of GL-8-28 with the highest CHEM-PLP score within the fifty docking solutions were chosen as the optimal docking poses in the homology model of human $LPA_6$.

## 2.12 | Statistical analysis

GraphPad Prism (GraphPad Software Inc.; RRID:SCR_002798) was used for all statistical analyses. Prior sample calculations were not performed: sample size was estimated based on previous studies of a similar nature (Dennis et al., 2008; Lafrenaye & Fuss, 2011; Martinez-Lozada et al., 2014; Thomason et al., 2022; Waggener et al., 2013; Wheeler et al., 2015). Data were assessed for normality using the Shapiro–Wilk normality test prior to analysis. Data compared with a set control value lacking variability were analyzed using the one-sample t test (Dalgaard, 2008; Skokal & Rohlf, 1995) and presented in graphs showing individual data points plus means with SEM. For comparing multiple groups one-way ANOVA or in case of multiple data points per animal nested one-way ANOVA was used. PRESTO-Tango assays were analyzed using dose–response curves, and data are presented as means $\pm$ SEMs for each agonist concentration plus dose–response curves. $p \geq 0.05$ was used as threshold for significant for all statistical tests used. $EC_{50}$ values were calculated from the dose–response curves, and the percent maximum activity was calculated using the following formula: % maximum activity = (maximum response of GL-8-28—constitutive activity)/(maximum response of full agonist – constitutive activity) $\times 100$.

## 3 | RESULTS

### 3.1 | $LPA_6$ is expressed by OLG lineage cells and uniquely localized at the surface of earlier maturation stages

In order to gain a deeper understanding of the contribution of individual LPA receptors to the regulation of OLG maturation, we focused our studies here on the LPA receptor $LPA_6$, which has previously been shown to be expressed by OLG lineage cells (Suckau et al., 2019; Wheeler et al., 2015). To better define the expression and surface localization of $LPA_6$, enriched cultures of rat brain-derived differentiating OLGs were immunolabeled using anti- $LPA_6$ antibodies recognizing the second extracellular loop region of $LPA_6$ in combination with the following antibodies marking selective OLG maturation stages: A2B5 (OLG progenitor cells; (Duchala et al., 1995)), O4 (maturing OLGs (Duchala et al., 1995)), anti-MBP (mature OLGs (Dubois-Dalcq et al., 1986)). As shown in Figure 1a, upon fixation and permeabilization of cultured cells, $LPA_6$ protein could be detected at all stages of the OLG lineage. Similarly, in the
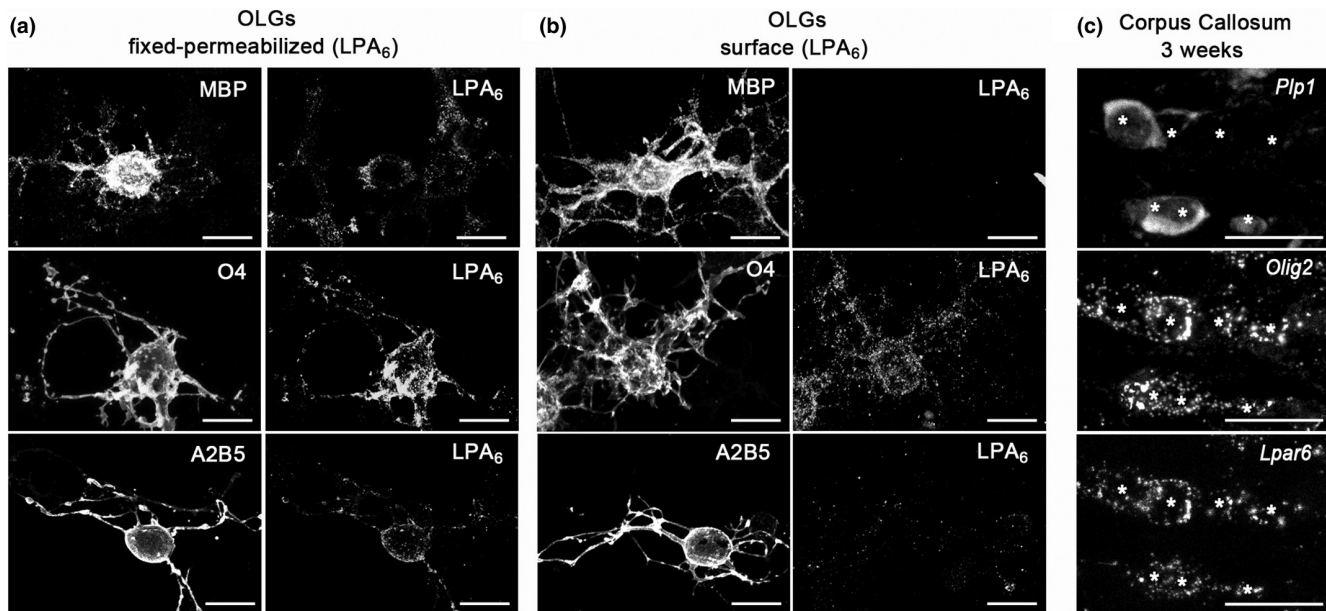


**FIGURE 1** $LPA_6$ is expressed throughout the OLG lineage but surface localization is restricted to earlier maturation stages of differentiating OLGs. (a, b) Representative confocal images of cultured rat brain-derived OLG lineage cells immunolabeled with antibodies detecting an extracellular surface epitope of $LPA_6$ in combination with the following antibodies marking selective maturation stages: A2B5 (OLG progenitor cells) (Duchala et al., 1995), O4 (maturing OLGs) (Duchala et al., 1995), and anti-MBP (mature OLGs) (Dubois-Dalcq et al., 1986). Cells were labeled after fixation and permeabilization (a) or live (b). Scale bar: 10 μm. (c) Representative confocal images of the 3-week-old mouse corpus callosum, triple labeled using RNAscope for mRNAs encoding *Lpar6*, *Olig2* to mark all OLG lineage cells (Lu et al., 2000; Wegner, 2001; Zhou et al., 2000) and *Plp1* to mark later OLG maturation stages (Dubois-Dalcq et al., 1986; Duchala et al., 1995). Stars indicate nuclei of *Olig2*-positive cells. Scale bar: 20 μm.

3-week-old mouse corpus callosum, *Lpar6* mRNA was detected in all cells expressing *Olig2*, a marker for all stages of the OLG lineage in rodents (Lu et al., 2000; Wegner, 2001; Zhou et al., 2000), including later stages of maturing OLGs as identified by the presence of *Plp1* mRNA (Dubois-Dalcq et al., 1986; Duchala et al., 1995) (Figure 1c). These findings are consistent with previously published mRNA profiling data (Marques et al., 2016; Suckau et al., 2019; Zhang et al., 2014). Interestingly, however, when using a live staining protocol, surface localization of $LPA_6$ was found to be restricted to earlier maturation stages of differentiating OLGs (Figure 1b). Taken together, these data indicate that while $LPA_6$ is expressed throughout the OLG lineage, its functional roles are likely restricted to earlier maturation stages of differentiating OLGs.

## 3.2 | During development, $LPA_6$ functions as a negative modulator of OLG maturation

After having established that $LPA_6$ is expressed by OLGs, we next assessed potential functional effects of a loss of $LPA_6$ on OLG maturation via the use of *Wt* and *Lpar6 KO* mice (Hata et al., 2016). More specifically, OLG maturation was analyzed in the corpus callosum and cortex at 2 and 3 weeks of age, a developmental time point that coincides with a rapid phase of myelination (Bergles & Richardson, 2015; Sturrock, 1980) associated with active proliferation of OLG lineage cells (Spitzer et al., 2019; Sturrock, 1983; Young et al., 2013). As shown in Figure 2b, based on immunostaining with anti-Olig2 antibodies, known to mark all OLG lineage cells in rodents (Lu et al., 2000; Wegner, 2001; Zhou et al., 2000), no changes in the total number of OLG lineage cells were noted. Co-immunostaining with CC1 antibodies, labeling maturing OLGs (Bin et al., 2016; Fuss et al., 2000), on the other hand, revealed an increased percentage of maturing OLG lineage cells at 3 but not 2 weeks of age (Figure 2c,d). Thus, there is a precocious appearance of maturing OLGs during the rapid phase of myelination in the corpus callosum and cortex of *Lpar6 KO* mice. This alteration appears largely due to an acceleration of OLG maturation rather than an overall increase in the number of OLG lineage cells, and it provides first evidence for a role of $LPA_6$ in modulating the timing of OLG maturation in a negative regulatory, or restraining, fashion.

## 3.3 | The small molecule GL-8-28 represents a dual $LPA_{4/6}$ ligand with preferential agonist activity at $LPA_6$

While the data thus far support a negative modulatory role of $LPA_6$ in the timing of OLG maturation, they do not directly address $LPA_6$ signaling in OLGs and the potential of pharmacological accessibility for $LPA_6$ initiated signaling. Hence, we turned our attention to a library of small molecules that had been designed and prepared by us as potential LPA receptor ligands. We first used the PRESTO-Tango GPCR assay system (Kroeze et al., 2015) to examine agonist activity at the six known LPA receptors ($LPA_{1-6}$). For $LPA_{1-5}$, the

well-established endogenous agonist LPA (18:1) served as positive control, while, due to the much lower affinity of LPA (18:1) for $LPA_6$, the LPA phosphorothioate analog (2*S*)-OMPT was used for assaying $LPA_6$ ligands (Inoue et al., 2011; Inoue et al., 2012; Jiang et al., 2013; Yanagida et al., 2009). As shown in Figure 4, one of the compounds from our library, designated here as GL-8-28 (Figure 3), was found to partially activate both $LPA_4$ and $LPA_6$. Notably, based on estimated $EC_{50}$ calculations, the potency of GL-8-28 appears to be approximately five times higher for $LPA_6$ compared to $LPA_4$. Neither of the remaining known LPA receptors were activated by GL-8-28 above a level of 20% of control (Figure 4b), thus defining GL-8-28 as a dual $LPA_{4/6}$ partial agonist with reasonable selectivity to $LPA_6$ over $LPA_4$ as well as other LPA receptors. This observation was further corroborated by molecular modeling and ligand-receptor docking using the published zebrafish $LPA_6$ crystal structure (Taniguchi et al., 2017) as a template to build the 3D conformations of human $LPA_6$ bound to the ligand GL-8-28. As shown in Figure 5, the polar head group of GL-8-28 interacts with the conserved positively charged residues $K^{1.31}$, $R^{2.60}$, $R^{6.62}$, and $R^{7.32}$, previously shown to be particularly important for ligand recognition and receptor activation (Taniguchi et al., 2017). Agonist binding to the $LPA_6$ receptor has been proposed to induce a conformational inward shift of the transmembrane helices 6 (TM6) and 7 (TM7) resulting in direct interaction with all of the above conserved positively charged residues with the ligand headgroup; this shift is not depicted in Figure 5. The long aliphatic chain of GL-8-28 is positioned within a hydrophobic environment formed at the TM4-TM5 interfaces; this hydrophobic cleft has been implicated in binding of the acyl chain of LPA (Taniguchi et al., 2017). Thus, GL-8-28 displays ligand-receptor interactions that involve binding pocket residues predicted to be crucial for binding of the endogenous agonist LPA and subsequent receptor activation.

## 3.4 | Pharmacological activation of $LPA_6$ signaling attenuates OLG maturation

In order to directly assess the effect of $LPA_6$ activation on OLG maturation, we treated primary cultures of differentiating rat brain-derived OLGs with the $LPA_6$ preferential agonist GL-8-28. In agreement with our live staining experiments (see Figure 1) surface localization was detected by flow cytometry on a subpopulation of OLG lineage cells (approximately 43%; see Figure 6a'). In contrast, only very few cells (approximately 6%) displayed detectable levels of surface localization for $LPA_4$ (Figure 6a'). Thus, any effects exerted by GL-8-28 are mediated primarily by its $LPA_6$ agonist activity and are directed at earlier maturation stages of differentiating OLGs (see Figure 1). As shown in Figure 6d, in the presence of the highest concentration tested, that is 10 μM, GL-8-28 treatment led to significantly reduced mRNA levels for OLG expressed genes associated with OLG maturation and CNS myelination, namely *2,′3′-cyclic nucleotide 3′-phosphodiesterase (Cnp)* (Gravel et al., 1998; Kurihara et al., 1992) and *UDP glycosyltransferase 8 (Ugt8)* (Bosio et al., 1996; Gard & Pfeiffer, 1990). This outcome was not found to be associated
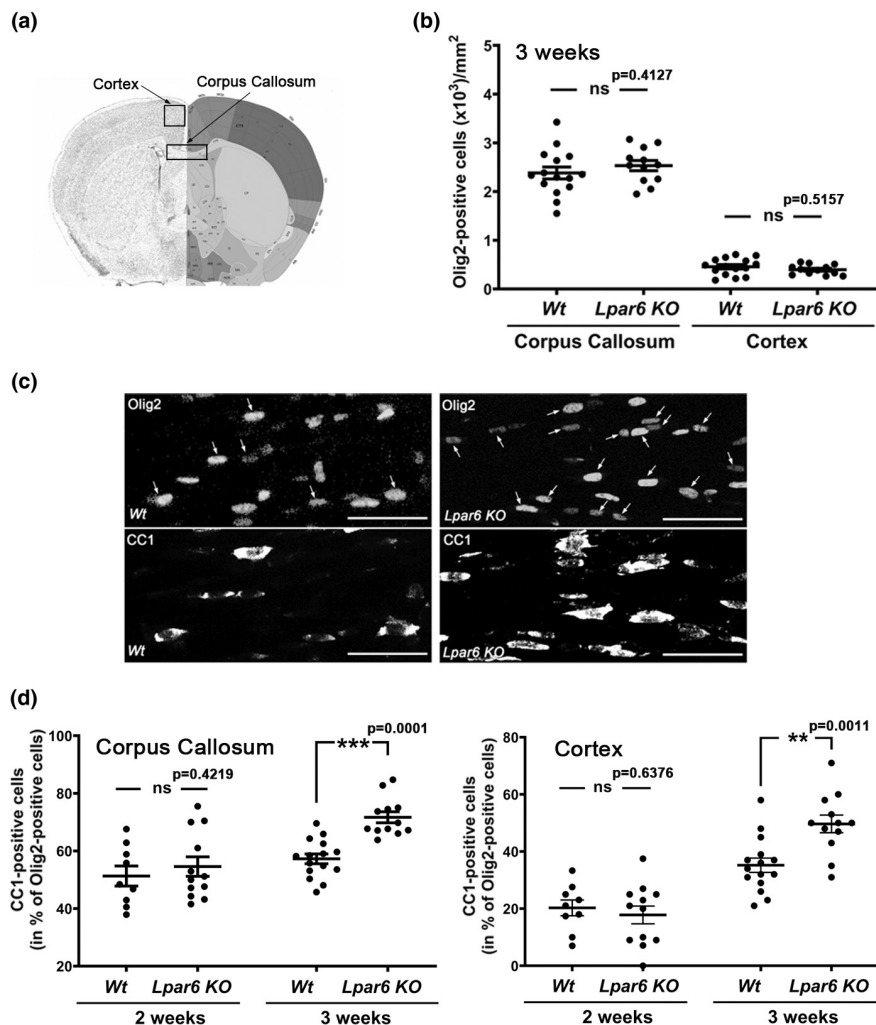
**FIGURE 2** Developmental maturation of OLGs is accelerated in *Lpar6 KO* mice. (a) Coronal brain section marking brain regions (Image credit: Allen Mouse Brain Atlas, Allen Institute). (b) Graph depicting the number of Olig2-positive OLG lineage cells per mm² in sections of 15 μm depth from 3-week-old *Wt* and *Lpar6 KO* mice as determined by immunostaining and subsequent image analysis. (c) Representative confocal images of the corpus callosum in 3-week-old *Wt* and *Lpar6 KO* mice double-immunostained with an anti-Olig2 antibody to mark all OLG lineage cells (Lu et al., 2000; Wegner, 2001; Zhou et al., 2000) and with the CC1 antibody to identify mature OLGs (Bin et al., 2016; Fuss et al., 2000); arrows mark CC1-Olig2 double-positive cells. Scale bar: 50 μm. (d) Graphs depicting the percentage of mature CC1-Olig2 double-positive OLGs in the midcaudal corpus callosum (left) and motor cortex (right) of *Wt* and *Lpar6 KO* mice at 2 weeks and 3 weeks of age as determined by immunostaining and subsequent image analysis. Dots in all graphs represent 3 fields of view (40× objective) from nonadjacent sections for each individual animal. ***$p \leq 0.001$, **$p \leq 0.01$ ns $p > 0.05$, 3 fields of view from 5 (3-week-old *Wt* mice) or 4 (2-week-old *Wt* and *Lpar6 KO* mice, 3 week *Lpar6 KO* mice) animals, nested two-tailed *t*-Test, $t = 0.8708$ and df = 7 (b, corpus callosum), $t = 0.6845$ and df = 7 (b, cortex), $t = 0.8294$ and df = 13 (d, two weeks), $t = 4.517$ and df = 25 (d, three weeks), $t = 0.5011$ and df = 5 (e, two weeks), $t = 3.680$ and df = 25 (three weeks).
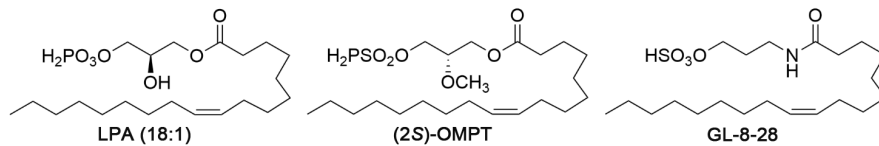


**FIGURE 3** Chemical structures of LPA (18:1; 1-oleyl-LPA), (2S)-OMPT (L-*sn*-1-*O*-oleoyl-2-*O*-methylglyceryl-3-phosphothionate), and GL-8-28. For the design of GL-8-28, a polar head was kept in place to ensure LPA receptor recognition, an amide bond was applied to replace the ester bond present in the natural ligand LPA to achieve higher stability in biological systems, and a long aliphatic tail was maintained.

with a cytotoxic effect (Figure 6b) or a change in the expression of *Olig2* (Figure 6c), a transcription factor expressed throughout the OLG lineage in rodents (Lu et al., 2000; Wegner, 2001; Zhou

et al., 2000). Additionally, at the 10 μM concentration, GL-8-28 significantly increased the expression of the transcriptional repressor *Egr1* (Sock et al., 1997; Swiss et al., 2011), a known inhibitor of the
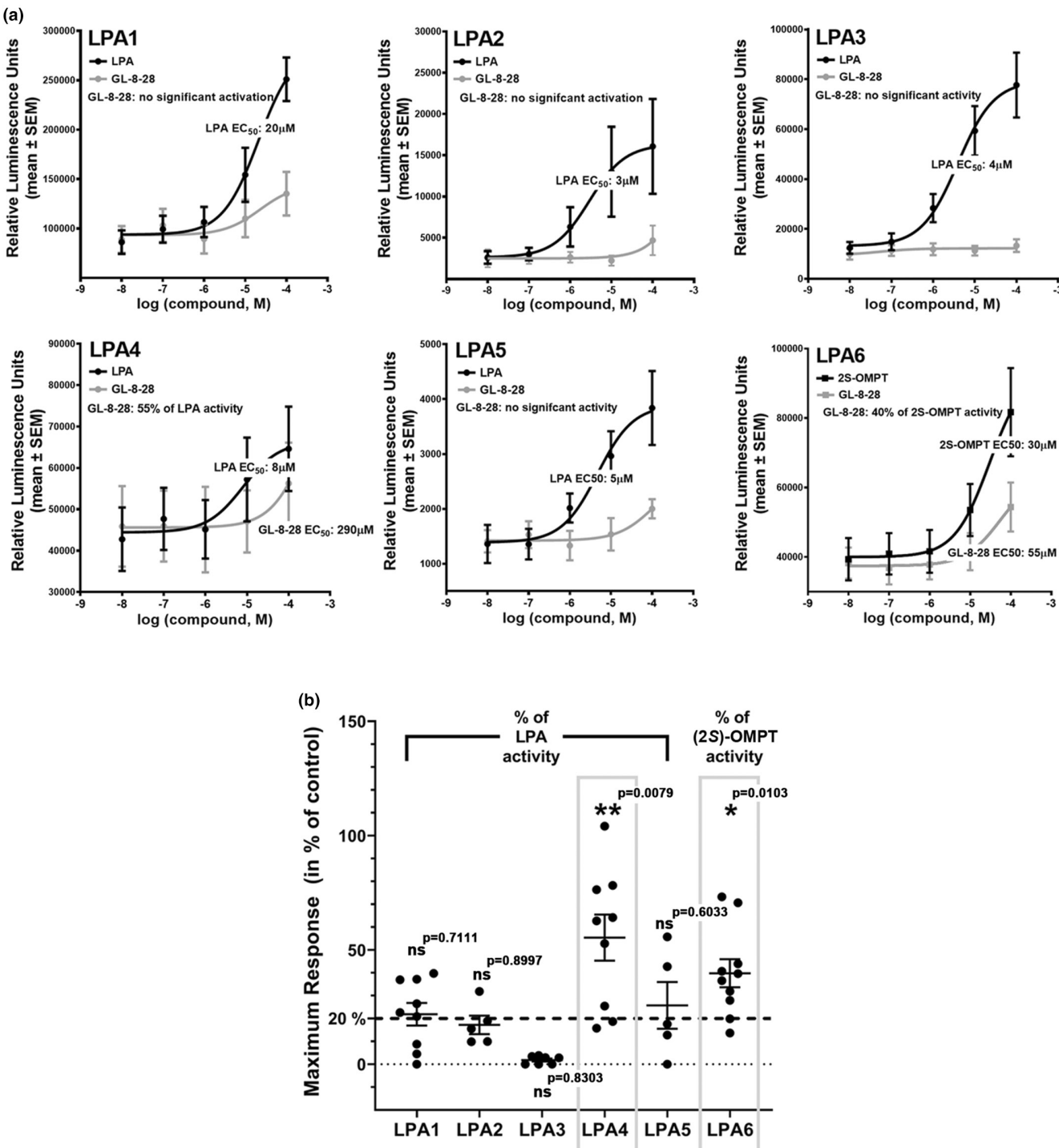
**FIGURE 4** GL-8-28 functions as an LPA$_{4/6}$ dual ligand with preferential LPA$_6$ agonist activity. (a) Graphs depicting dose response curves as determined by the PRESTO-Tango GPCR assay system (Kroeze et al., 2015). Note that LPA (18:1) was used as a previously established agonist for LPA$_{1-5}$, while (2S)-OMPT was used for LPA$_6$ (Jiang et al., 2013). Means ± SEM are shown for at least five independent experiments performed in triplicates. Significant agonist activity for GL-8-28 is defined as above 20% of control (see b). Note that the estimated potency for GL-8-28 is much higher for LPA$_6$ compared to LPA$_4$. (b) Graph depicting the percentage of GL-8-28 activity compared to control. Data points represent independent experiments ($n = 5$ (LPA$_5$), 6 (LPA$_2$), 7 (LPA$_3$), 9 (LPA$_{1,4}$), 10 (LPA$_6$)) performed in triplicates. *$p \leq 0.05$, **$p \leq 0.01$, one-sample two tailed $t$-test, theoretical mean set to 20% for LPA$_{1,2,4\ and\ 6}$; to 2% for LPA$_3$, $t = 0.3839$ and df = 8 (LPA$_1$), $t = 0.1326$ and df = 5 (LPA$_2$), $t = 0.2239$ and df = 6 (LPA$_3$), $t = 3.515$ and df = 8 (LPA$_4$), $t = 0.5633$ and df = 4 (LPA$_5$), $t = 3.230$ and df = 9 (LPA$_6$).

gene expression profile associated with OLG maturation and CNS myelination. In this context, it is important to note that downregulated *Egr1* expression concomitant with OLG differentiation was

previously shown to occur upon thyroid hormone application (Swiss et al., 2011), thus demonstrating that in differentiating OLGs upregulation of *Egr1* is not generally associated with a stimulus evoked
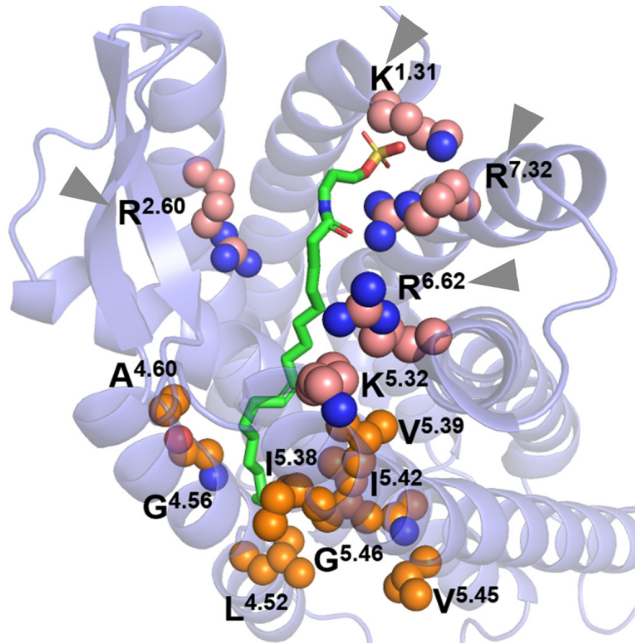
**FIGURE 5** GL-8-28 displays ligand-receptor interactions that involve binding pocket residues predicted to be crucial for binding of the endogenous agonist LPA and receptor activation. The binding pocket of LPA$_6$ is shown as cartoon model (lavender) and the ligand GL-8-28 is depicted as stick model (green carbon atoms). Key amino acid residues binding with GL-8-28 are shown as sphere model. Arrowheads (gray) point to conserved positively charged residues implicated in head group binding and receptor activation (Taniguchi et al., 2017); positively charged residues (pink), hydrophobic residues (orange), oxygen atoms (red), nitrogen atoms (blue), sulfonate atoms (yellow).

response as for example seen in the context of neuronal activity and plasticity (Duclot & Kabbaj, 2017).

In an attempt to extend these findings into an in vivo system and to gain initial insight into the in vivo use of GL-8-28, we took advantage of the following characteristics of the developing zebrafish. First, in this model, pharmacological agents can be taken up from the surrounding water source via passage through the skin (Rombough, 2002). Second, a lack of a functional blood–brain-barrier (BBB) prior to 3 days of age (Fleming et al., 2013; Li et al., 2017) allows diffusion into the developing CNS prior to completion of myelination (Brosamle & Halpern, 2002; Buckley et al., 2008; Jung et al., 2010; Yoshida & Macklin, 2005), for which key regulatory mechanisms are highly conserved during the development of mammals and zebrafish (Ackerman & Monk, 2016; Lyons & Talbot, 2014; Preston & Macklin, 2015). In this context, the expression of *proteolipid protein*, present in both maturing rodent (*Plp1*) and zebrafish (*plp1a/plp1b*) OLGs (Siems et al., 2021), as well as *myelin protein zero (mpz)* and *claudin K (cldnk)*, found more specifically in maturing zebrafish OLGs, has been reported to significantly increase between 24 and 48h post fertilization (hpf) in the CNS of the developing zebrafish embryo (Brosamle & Halpern, 2002; Munzel et al., 2012; Preston et al., 2019; Schweitzer et al., 2006; Takada & Appel, 2010; Wheeler et al., 2015; Yoshida & Macklin, 2005). In the presence of GL-8-28, mRNA levels

for all these three zebrafish genes known to be associated with OLG maturation were significantly reduced (Figure 7). At the same time, gross anatomical features remained unchanged up to a concentration of 1 µM (Figure 7b). Importantly, based on recently published gene expression profiling data (Marisca et al., 2020), LPA receptor expression in zebrafish OLGs appears to be limited to differentiating rather than progenitor stages of the lineage and restricted to the receptors *lpar1* and *lpar6a*. Furthermore, equivalents of several residues found to be important for ligand binding to human LPA$_6$ were also found to affect binding in models based on the crystallized structure of the zebrafish receptor, thus providing confidence of equivalent binding characteristics in all species analyzed here (Raza et al., 2014; Taniguchi et al., 2017). Thus, the OLG maturation attenuating effects of GL-8-28 in the developing zebrafish are likely to be mediated, at least in part, via activation of LPA$_6$ in differentiating OLGs. However, these effects of GL-8-28 were observed at much lower concentrations as seen in the rat primary cultures, possibly due to receptor desensitization in the culture system and/or cumulative effects in the in vivo system. Nevertheless, the above data demonstrate an important functional role of LPA$_6$ signaling in regulating the timely appearance of mature OLGs in both rodent cultures of differentiating OLG and the developing zebrafish.

## 3.5 | LPA$_6$ protein levels appear elevated in MS white matter lesions

In the context of development, the maturation attenuating functional role of LPA$_6$ likely serves to ensure timely coordination of circuit formation and myelination (Fletcher et al., 2021). Under pathological conditions, however, persistent LPA$_6$ expression and signaling could be seen as an inhibitor of efficient OLG maturation and myelin repair. In this regard, it is of particular interest that our analysis of human MS lesion samples (Figure 8) revealed, on average, elevated LPA$_6$ protein levels. Interestingly, the variance seen within the MS sample pool was significantly broader than the one for the control sample pool, an observation that is consistent with the increasingly recognized heterogeneity in MS pathology between patients (Lucchinetti et al., 2000; Patrikios et al., 2006; Smets et al., 2021). Curiously, in addition to a somewhat diffuse band with the expected apparent molecular weight of approximately 50 kDa, a sharp lower molecular weight band of approximately 40 kDa was observed in some of the MS samples, possibly reflecting differences in N-glycosylation (Suckau et al., 2019). Taken together, these data suggest that LPA$_6$ protein levels may be increased in at lest some types of MS white matter lesions, an observation that is consistent with recent transcriptome profiling data (Elkjaer et al., 2019; Falcão et al., 2018).

## 4 | DISCUSSION

In this study, we identified signaling via the LPA receptor LPA$_6$ as a novel modulator of the transcriptional regulation of OLG maturation.
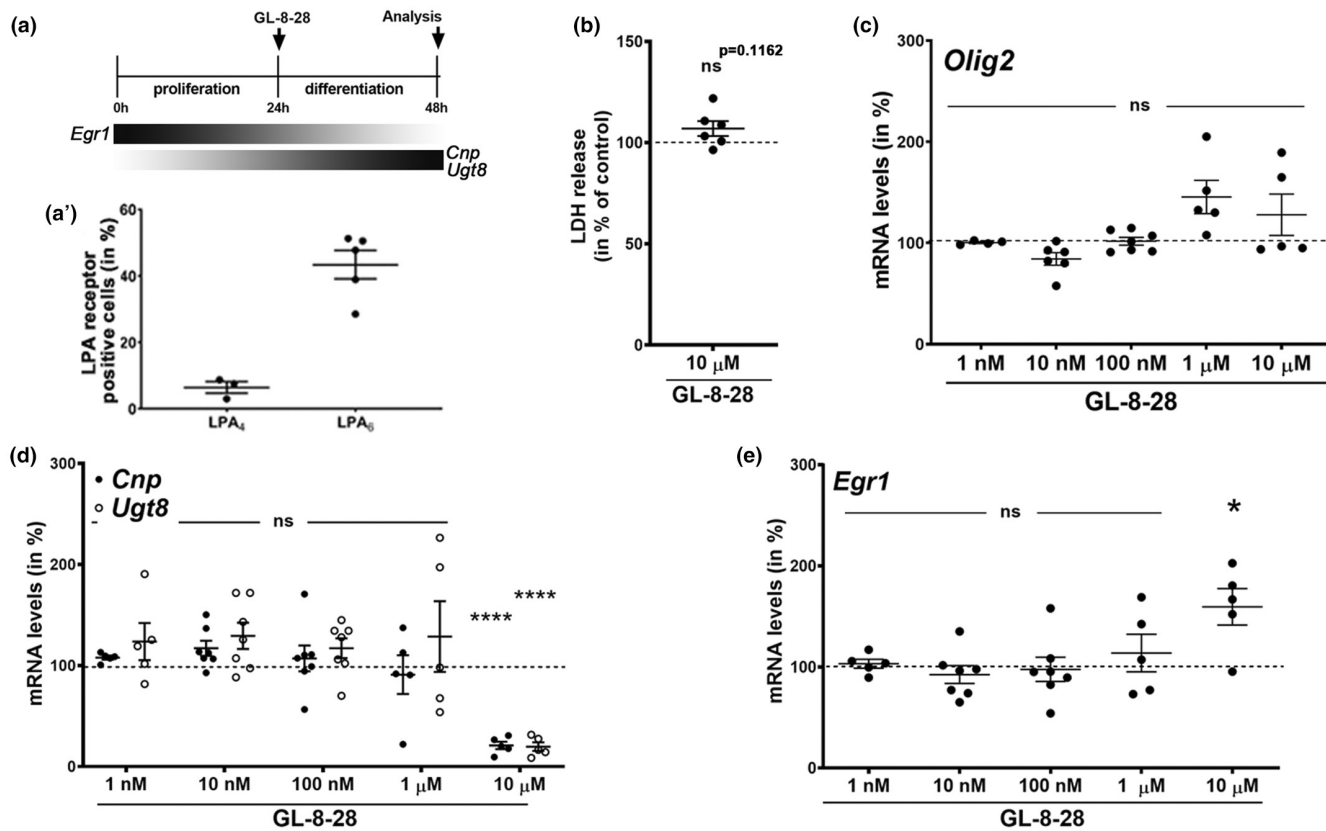
**FIGURE 6** The preferential LPA$_6$ agonist GL-8-28 attenuates maturation in primary cultures of rat OLGs. (a) Scheme depicting the experimental paradigm; the inset i in (a') represents the percent of LPA$_4$ (left) and LPA$_6$ (right) positive OLGs at 48 h, as determined by flow cytometry. (b–e) Graphs depicting the extracellular LDH levels (b) and mRNA levels as determined by RT-qPCR analysis (c–e). Levels for control (vehicle-treated) cells were set to 100% (horizontal dotted line) and relative levels were calculated accordingly. Individual data points represent independent experiments, means ± SEM are shown as horizontal lines with error bars. *$p \leq 0.05$ and ****$p \leq 0.0001$, one sample two-tailed $t$-test, B: $n = 6$, $t = 1.897$ and df = 5; C: 1 nM: $n = 4$, $p = 0.7220$, $t = 0.3909$, df = 3, 10 nM: $n = 6$, $p = 0.0523$, $t = 2.534$, df = 5, 100 nM: $n = 7$, $p = 0.6686$, $t = 0.4498$, df = 6, 1 µM: $n = 5$, $p = 0.0508$, $t = 2.760$, df = 4, 10 µM: $n = 5$, $p = 0.2441$, $t = 1.365$, df = 4; D: 1 nM: $n = 4$, $p = 0.0542$, $t = 3079$, df = 3 (CNP); $n = 5$, $p = 0.2653$, $t = 1.294$, df = 4 (Ugt8) 10 nM: $n = 7$, $p = 0.0606$, $t = 2.306$, df = 6 (CNP); $n = 6$, $p = 0.1412$, $t = 1.746$, df = 5 (Ugt8), 100 nM: $n = 7$, $p = 0.5995$, $t = 0.5543$, df = 6 (CNP); $n = 6$, $p = 0.2538$, $t = 1.289$, df = 5 (Ugt9), 1 µM: $n = 5$, $p = 0.6630$, $t = 0.4697$, df = 4 (CNP); $n = 5$, $p = 0.4583$, $t = 0.8188$, df = 4 (Ugt8), 10 µM: $n = 5$, $p < 0.0001$, 4$t = 21.56$, df = 4 (CNP), $n = 5$, $p < 0.0001$, $t = 18.93$, df = 4, E: 1 nM: $n = 5$, $p = 0.5163$, $t = 0.7111$, df = 4, 10 nM: $n = 7$, $p = 0.4297$, $t = 0.8465$, df = 6, 100 nM: $n = 7$, $p = 0.8491$, $t = 0.1986$, df = 6, 1 µM: $n = 5$, $p = 0.4981$, $t = 0.7442$, df = 4, 10 µM: $n = 5$, $p = 0.0300$, $t = 3.299$, df = 4.

More specifically, our data revealed a precocious developmental appearance of OLGs expressing a marker for more mature stages of the lineage in *Lpar6 KO* mice. Thus, initial evidence was obtained that activation of LPA$_6$ signaling in OLGs negatively modulates the transcriptional program associated with OLG maturation. This interpretation could be substantiated via the use of a novel LPA$_6$ selective ligand with agonist activity, here referred to as GL-8-28; both in vitro in cultures of differentiating OLGs and in vivo in the developing zebrafish, treatment with GL-8-28 was found to impede the expression of genes known to be associated with OLG maturation. During development, such a functional role for LPA$_6$ signaling is likely transient and serves to ensure timely coordination of circuit formation and myelination (Fletcher et al., 2021). This point of view may be supported by the apparent lack of an overt myelination phenotype in *Lpar6 KO* mice (Hata et al., 2016). However, future studies are needed to further substantiate such a proposed developmentally

transient functional role of LPA$_6$ signaling in maturing OLGs. Under pathological conditions accompanying white matter lesions in MS, LPA$_6$ signaling appears to be persistent, at least in some patients. Hence, our studies reveal a novel molecular mechanism modulating OLG maturation, and they uncover a novel and conceivably druggable signaling pathway with the potential for future developments toward innovative therapeutic interventions stimulating myelin repair.

## 4.1 | LPA signaling plays diverse roles in the regulation of OLG maturation and CNS myelination

A key step in the biosynthetic pathway(s) generating extracellular LPA is represented by the conversion from lysophosphatidylcholine (LPC) via the enzymatic activity of secreted autotaxin, also known as extracellular nucleotide pyrophosphatase-phosphodiesterase
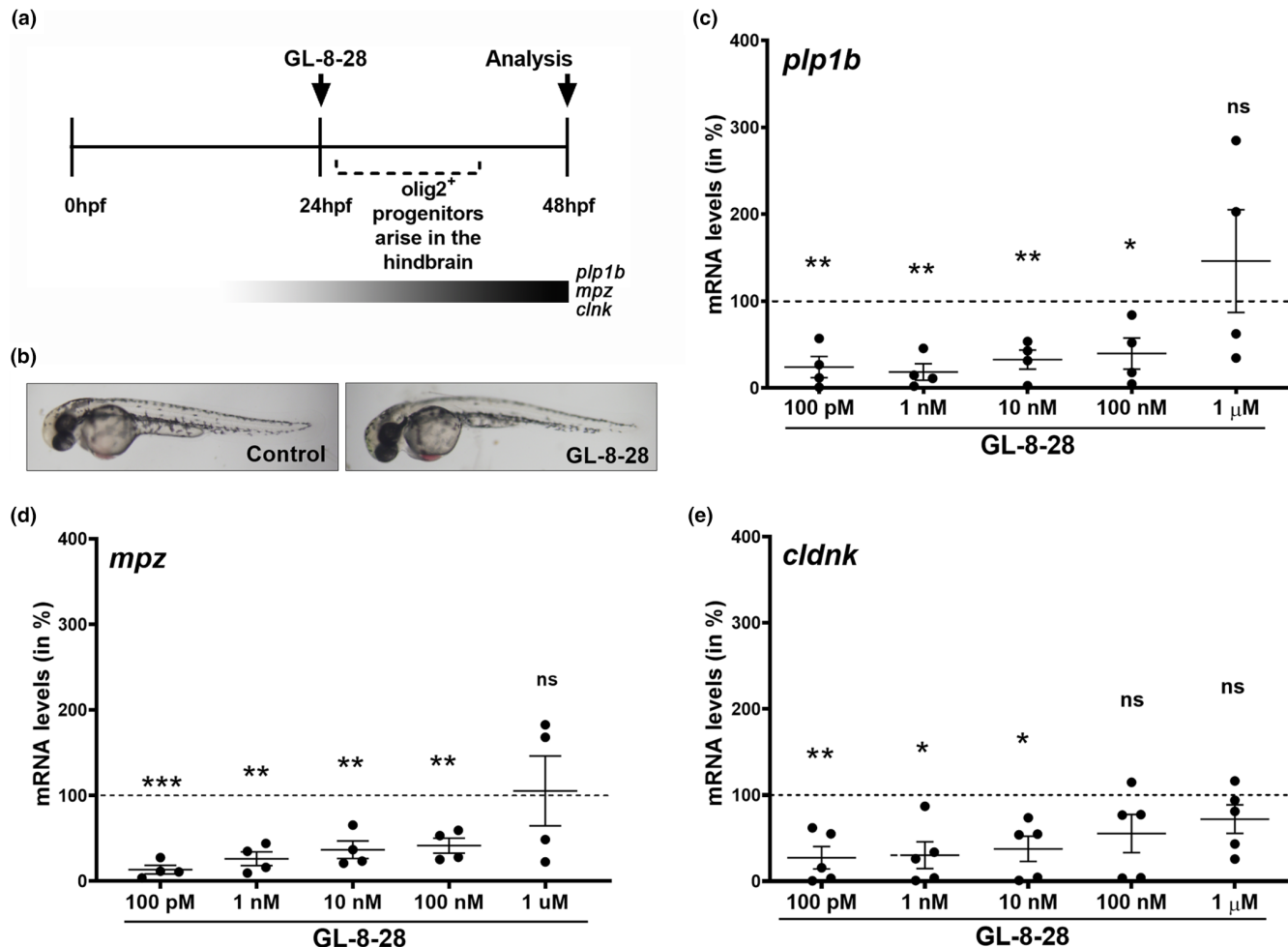
**FIGURE 7** The preferential LPA$_6$ agonist GL-8-28 attenuates OLG maturation in the developing zebrafish. (a) Scheme depicting the experimental paradigm. (b) Representative images of control and Gl-8-28 (1 μM)-treated zebrafish embryos at 48 hpf (hours post fertilization). (c–e) Graphs depicting mRNA levels as determined by RT-qPCR analysis. Levels for control (vehicle-treated) zebrafish embryos were set to 100% (horizontal dotted line) and relative levels were calculated accordingly. Individual data points represent independent experiments, means ± SEM are shown as horizontal lines with error bars. *plp1b*: *proteolipid protein*, *mpz*: *myelin protein zero*, *cldnk*: *claudin K*. *$p \leq 0.05$ and **$p \leq 0.001$, one sample two-tailed *t*-test; (c) 100pM: $n = 4$, $p = 0.0084$, $t = 6.226$, df = 3, 1nM: $n = 4$, $p = 0.0033$, $t = 8.621$, df = 3, 10nM: $n = 4$, $p = 0.0087$, $t = 6.142$, df = 3, 100nM: $n = 4$, $p = 0.0432$, $t = 3.377$, df = 3, 1μM: $n = 4$, $p = 0.4916$, $t = 0.7814$, df = 3; (d) $n = 4$, $p = 0.0004$, $t = 17.23$, df = 3, 1nM: $n = 4$, $t = 9.185$, df = 3, 10nM: $n = 4$, $p = 0.0085$, $t = 6.198$, df = 3, 100nM: $n = 4$, $p = 0.0067$, $t = 6.738$, df = 3, 1μM: $n = 4$, $p = 0.9009$, $t = 0.1353$, df = 3; (e) 100pM: $n = 5$, $p = 0.0051$, $t = 5.573$, df = 4, 1nM: $n = 5$, $p = 0.0109$, $t = 4.491$, df = 4, 10 nM: $n = 5$, $p = 0.0131$, $t = 4.258$, df = 4, 100nM: $n = 5$, $p = 0.1138$, $t = 0.1138$, $t = 2.017$, df = 4, 1μM: $n = 5$, $p = 0.1684$, $t = 1.679$, df = 4.

2 (ENPP2) or lysophospholipase D (lysoPLD) (Aoki et al., 2008; Gijsbers et al., 2003; Tanaka et al., 2006; Tokumura et al., 2002; Umezu-Goto et al., 2002; van Meeteren et al., 2006). In our previous studies, we had identified OLG expressed autotaxin as a positive regulator of OLG maturation (Dennis et al., 2008; Dennis et al., 2012; Fox et al., 2003; Fox et al., 2004; Nogaroli et al., 2009; Wheeler et al., 2015; Yuelling et al., 2012). Importantly, autotaxin was found to stimulate the transcriptional expression profile leading to OLG differentiation via its enzymatic activity generating LPA (Wheeler et al., 2015; Wheeler et al., 2016; Yuelling et al., 2012). In addition, autotaxin-dependent activation of specifically LPA$_6$ has recently been proposed to exert functional effects on cells other than OLGs (Masago et al., 2018; Matas-Rico et al., 2021; Okasato et al., 2021). Thus, a maturation attenuating role of LPA$_6$ signaling on OLGs, as described here, may appear puzzling. However, despite the simple basic structure of LPA, that is, a glycerol backbone connected to a phosphate head group at the *sn*-3 position and a fatty acid chain linked to the *sn*-1 or *sn*-2 position, variations in fatty acid side chain length, saturation, and backbone position generate diversity that impacts receptor selectivity and downstream signaling outcomes (Aikawa et al., 2015; Baker et al., 2001; Bandoh et al., 2000; Hayashi et al., 2001; Okudaira et al., 2010, 2014; Yoshida et al., 2003; Yung et al., 2014). Furthermore, structure–function analyses suggest a highly localized delivery of LPA to the respective receptor to be
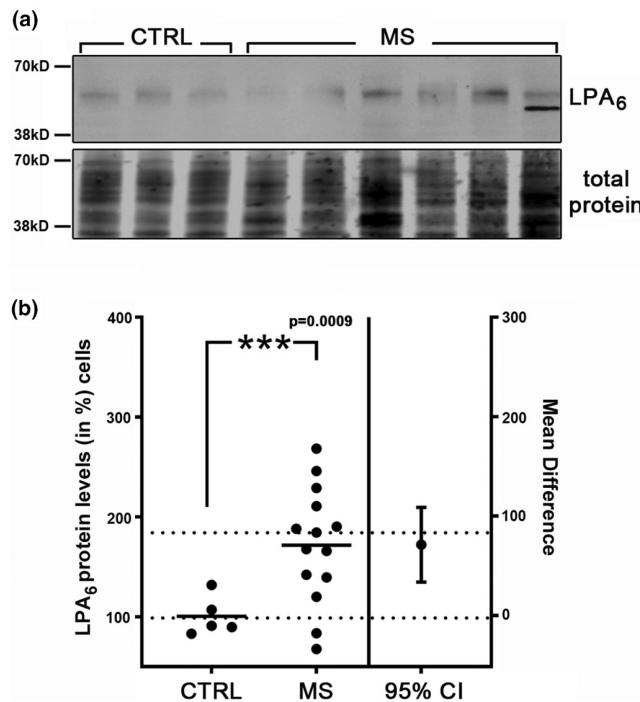
**FIGURE 8** LPA$_6$ protein levels are increased in multiple sclerosis (MS) white matter lesions. (a) Representative western blot depicting LPA$_6$ and total protein between molecular weight markers 70 kDa (top) and 38 kDa (bottom) in control (CTRL) white matter and multiple sclerosis (MS) white matter lesions; total protein per lane was used for normalization. (b). Graph depicting the percentage of LPA$_6$ protein levels in control (CTRL) white matter and MS white matter lesions (MS) (left y-axis) and the mean difference (right y-axis) as determined by Western blot analysis. Tissues were obtained from the Netherlands Brain Bank (for details, see Table 2). The mean control value, normalized to total protein, was set to 100% and all other values were adjusted accordingly (average values from two independent Western blots are shown). ***$p \leq 0.001$ Welch's two-tailed $t$-test ($^{Variance}p \leq 0.05$), Welch-corrected $t = 3.997$, df = 17.00. CI, confidence interval.

activated, thereby refining the selectivity for LPA receptor subtype activation (Fulkerson et al., 2011; Hausmann et al., 2011, 2013; Houben et al., 2013; Kanda et al., 2008; Moolenaar & Perrakis, 2011; Nishimasu et al., 2011; Taniguchi et al., 2017). Regarding LPA$_6$, preference for 2-acyl rather than 1-acyl LPA species confers somewhat unique characteristics within the LPA receptor family (Aikawa et al., 2015; Inoue et al., 2011, 2012; Morishige et al., 2007; Nishimasu et al., 2011; Tokumura et al., 2002; Yanagida et al., 2009). Thus, fine-tuned regulation of the LPA receptor profile present on OLG surfaces in combination with the availability and local delivery of specific LPA species may determine the balance between LPA-mediated maturation promoting and attenuating outcomes. Interestingly, a counter-regulatory function of LPA$_6$, compared to one or more of the remaining known LPA receptors, has also been described for cell types other than OLGs (Ishii et al., 2015; Matas-Rico et al., 2021; Takahashi et al., 2017).

## 4.2 | The small molecule GL-8-28 represents a novel chemical compound with preferential LPA$_6$ agonist activity

Small molecule modulators of the LPA family of G protein-coupled receptors are emerging as promising drugs for the treatment of a variety of diseases including those affecting the nervous system (Geraldo et al., 2021; Herr et al., 2020; Kihara et al., 2015; Liu et al., 2021; Stoddard & Chun, 2015; Yanagida & Valentine, 2020; Yung et al., 2015). Importantly, recent progress has been made in developing ligands with high selectivity for LPA receptor subtypes, in particular LPA$_{1-3}$ (Liu et al., 2021). In addition, despite the high sequence homology between LPA$_4$ and LPA$_6$ (Noguchi et al., 2003; Pasternack et al., 2008; Yanagida & Ishii, 2011), unique ligand preferences have been described (Kano et al., 2019; Yanagida et al., 2013), thereby supporting a long-term prospect of highly selective LPA$_6$ ligands. Intriguingly, a novel compound with selective LPA$_6$ antagonist activity has recently been reported (Gnocchi et al., 2020).

## 4.3 | The preferential LPA$_6$ agonist GL-8-28 attenuates OLG maturation in both the developing zebrafish and primary cultures of differentiating OLGs

In both the in vitro cell culture and the in vivo zebrafish model, GL-8-28 was found to attenuate the gene expression profile associated with OLG maturation. However, much higher ligand concentrations were needed in the in vitro studies. In this context, it has been well-established that LPA receptors, similar to other G protein-coupled receptors, can be subject to receptor desensitization (Alcántara-Hernández et al., 2015; Avendaño-Vázquez et al., 2005; Solís et al., 2021; Urs et al., 2005; Zhao et al., 2021). Interestingly, next to homologous desensitization by the agonist, there is evidence for agonist-independent heterologous desensitization (Alcántara-Hernández et al., 2015; Castillo-Badillo et al., 2015). Thus, it is conceivable that the culture conditions used in the in vitro experiments regulate extracellular LPA levels differently than seen in vivo and/or more significantly contribute to heterologous LPA$_6$ desensitization, thereby requiring higher GL-8-28 concentrations to trigger measurable functional outcomes. In addition, in the in vivo studies using the developing zebrafish, functional consequences of GL-8-28 on cell types other than OLGs could contribute to the observed attenuation of OLG maturation. In particular, LPA$_6$ signaling has been implicated in the regulation of vascular development (Kano et al., 2019; Okasato et al., 2021; Yasuda et al., 2019), and OLG-vascular crosstalk has been associated with a modulation of developmental OLG differentiation (De La Fuente et al., 2017; Tsai et al., 2016; Yuen et al., 2014). Further studies will be necessary to dissect the contributions of receptor desensitization and LPA$_6$-mediated non-OLG target effects to the differences in GL-8-28 sensitivity observed in the in vitro versus in vivo systems used here. Nevertheless, both the in vivo and in vitro data provide compelling support for a negative modulatory role of LPA$_6$ signaling on the expression of genes associated with OLG maturation.

## 4.4 | LPA$_6$ signaling emerges as a novel and conceivably druggable signaling pathway with the potential toward promoting myelin repair

Changes in transcriptional regulation are thought to be linked to modifications in OLG heterogeneity (Falcão et al., 2018; Jäkel et al., 2019) and inefficiencies in OLG maturation and myelin repair (Chang et al., 2002; Duncan et al., 2017; Kuhlmann et al., 2008). As cause for such dysregulated gene expression in OLGs, recent evidence points to the actions of extrinsic factors rather than intrinsic OLG defects (Golan et al., 2021; Kirby et al., 2019; Mozafari et al., 2020; Saraswat et al., 2021; Starost et al., 2020). Thus, targeting druggable signaling pathways with the capacity to modulate gene expression profiles associated with OLG maturation has emerged as a promising approach toward promoting repair of the myelin sheath in MS (Angelini et al., 2021; Gaesser & Fyffe-Maricich, 2016; Göttle et al., 2019; Green et al., 2017; Jeffries et al., 2016, 2021; Lecca et al., 2020; Mausner-Fainberg et al., 2021; Mierzwa et al., 2013; Petersen et al., 2021; Rajendran et al., 2021; Roggeri et al., 2020; Skinner & Lane, 2020; Thümmler et al., 2019; Wang et al., 2020; Welliver et al., 2018). Despite an increasing number of potential pathways with promyelinating characteristics, however, clinical translation has, up until now, been below expectation (Abu-Rub & Miller, 2018; Lubetzki et al., 2020). In light of the evidence for increased levels of LPA$_6$ in MS white matter lesions, targeting LPA$_6$ signaling may, therefore, represent a promising novel approach for stimulating OLG maturation in the context of myelin repair.

### AUTHOR CONTRIBUTIONS

SAS, ESP, JSV, YZ, and BF were directly involved in the design of the study, the analysis of data and the preparation of the manuscript. SAS, ESP, JSV, HW, FSA, GL, and SM performed experiments, acquired data, and contributed to method optimization. DY and SI provided study materials. AO and JAL provided technical training and contributed critical revisions of the manuscript. All authors gave consent for publication.

### CONFLICT OF INTEREST

BF is a consultant for Gryphon Bio, Inc. Arturo Ortega is a current handling editor for Journal of Neurochemistry. The remaining authors declare that the research was conducted in the absence of any commercial or financial relationships that could be construed as a potential conflict of interest.

### DATA AVAILABILITY STATEMENT

The data that support the findings of this study are available from the corresponding author upon reasonable request.

### ORCID

*Samantha A. Spencer* https://orcid.org/0000-0001-5048-1736
*Edna Suárez-Pozos* https://orcid.org/0000-0002-3115-063X
*Jazmín Soto-Verdugo* https://orcid.org/0000-0002-7050-4015
*Arturo Ortega* https://orcid.org/0000-0002-9594-8114
*Babette Fuss* https://orcid.org/0000-0002-0356-2135

### REFERENCES

Abu-Rub, M., & Miller, R. H. (2018). Emerging cellular and molecular strategies for enhancing central nervous system (CNS) remyelination. *Brain Sciences*, 8, 111.

Ackerman, S. D., & Monk, K. R. (2016). The scales and tales of myelination: Using zebrafish and mouse to study myelinating glia. *Brain Research*, 1641, 79–91.

Adams, K. L., Dahl, K. D., Gallo, V., & Macklin, W. B. (2021). Intrinsic and extrinsic regulators of oligodendrocyte progenitor proliferation and differentiation. *Seminars in Cell & Developmental Biology*, 116, 16–24.

Aikawa, S., Hashimoto, T., Kano, K., & Aoki, J. (2015). Lysophosphatidic acid as a lipid mediator with multiple biological actions. *Journal of Biochemistry*, 157, 81–89.

Alcántara-Hernández, R., Hernández-Méndez, A., Campos-Martínez, G. A., Meizoso-Huesca, A., & García-Sáinz, J. A. (2015). Phosphorylation and internalization of lysophosphatidic acid receptors LPA1, LPA2, and LPA3. *PLoS One*, 10, e0140583.

Andrew, S. M., Titus, J. A., Amin, A. and Coico, R. (2009) Isolation of murine and human immunoglobulin m and murine immunoglobulin D. *Current Protocols in Immunology* Chapter 2, Unit 2 9.

Angelini, J., Marangon, D., Raffaele, S., Lecca, D., & Abbracchio, M. P. (2021). The distribution of GPR17-expressing cells correlates with white matter inflammation status in brain tissues of multiple sclerosis patients. *International Journal of Molecular Sciences*, 22, 4574.

Anliker, B., Choi, J. W., Lin, M. E., Gardell, S. E., Rivera, R. R., Kennedy, G., & Chun, J. (2013). Lysophosphatidic acid (LPA) and its receptor, LPA1, influence embryonic schwann cell migration, myelination, and cell-to-axon segregation. *Glia*, 61, 2009–2022.

Aoki, J., Inoue, A., & Okudaira, S. (2008). Two pathways for lysophosphatidic acid production. *Biochimica et Biophysica Acta*, 1781, 513–518.

Avendaño-Vázquez, S. E., García-Caballero, A., & García-Sáinz, J. A. (2005). Phosphorylation and desensitization of the lysophosphatidic acid receptor LPA1. *The Biochemical Journal*, 385, 677–684.

Baker, D. L., Desiderio, D. M., Miller, D. D., Tolley, B., & Tigyi, G. J. (2001). Direct quantitative analysis of lysophosphatidic acid molecular species by stable isotope dilution electrospray ionization liquid chromatography-mass spectrometry. *Analytical Biochemistry*, 292, 287–295.

Ballesteros, J. A., & Weinstein, H. (1995). Integrated methods for the construction of three-dimensional models and computational probing of structure-function relations in G protein-coupled receptors. *Methods in Neurosciences*, 25, 366–428.

Bandoh, K., Aoki, J., Taira, A., Tsujimoto, M., Arai, H., & Inoue, K. (2000). Lysophosphatidic acid (LPA) receptors of the EDG family are

differentially activated by LPA species. Structure-activity relationship of cloned LPA receptors. *FEBS Letters*, 478, 159–165.

Barres, B. A., Hart, I. K., Coles, H. S., Burne, J. F., Voyvodic, J. T., Richardson, W. D., & Raff, M. C. (1992). Cell death and control of cell survival in the oligodendrocyte lineage. *Cell*, 70, 31–46.

Baydyuk, M., Morrison, V. E., Gross, P. S., & Huang, J. K. (2020). Extrinsic factors driving oligodendrocyte lineage cell progression in CNS development and injury. *Neurochemical Research*, 45, 630–642.

Benusa, S. D., George, N. M., Sword, B. A., DeVries, G. H., & Dupree, J. L. (2017). Acute neuroinflammation induces AIS structural plasticity in a NOX2-dependent manner. *Journal of Neuroinflammation*, 14, 116.

Bergles, D. E., & Richardson, W. D. (2015). Oligodendrocyte development and plasticity. *Cold Spring Harbor Perspectives in Biology*, 8, a020453.

Bin, J. M., Harris, S. N., & Kennedy, T. E. (2016). The oligodendrocyte-specific antibody 'CC1' binds Quaking 7. *Journal of Neurochemistry*, 139, 181–186.

Bosio, A., Binczek, E., & Stoffel, W. (1996). Molecular cloning and characterization of the mouse CGT gene encoding UDP-galactose ceramide-galactosyltransferase (cerebroside synthetase). *Genomics*, 35, 223–226.

Brosamle, C., & Halpern, M. E. (2002). Characterization of myelination in the developing zebrafish. *Glia*, 39, 47–57.

Buckley, C. E., Goldsmith, P., & Franklin, R. J. (2008). Zebrafish myelination: A transparent model for remyelination? *Disease Models & Mechanisms*, 1, 221–228.

Bustin, S. A., Benes, V., Garson, J. A., Hellemans, J., Huggett, J., Kubista, M., Mueller, R., Nolan, T., Pfaffl, M. W., Shipley, G. L., Vandesompele, J., & Wittwer, C. T. (2009). The MIQE guidelines: Minimum information for publication of quantitative real-time PCR experiments. *Clinical Chemistry*, 55, 611–622.

Cahoy, J. D., Emery, B., Kaushal, A., Foo, L. C., Zamanian, J. L., Christopherson, K. S., Xing, Y., Lubischer, J. L., Krieg, P. A., Krupenko, S. A., Thompson, W. J., & Barres, B. A. (2008). A transcriptome database for astrocytes, neurons, and oligodendrocytes: A new resource for understanding brain development and function. *The Journal of Neuroscience: The Official Journal of the Society for Neuroscience*, 28, 264–278.

Castillo-Badillo, J. A., Sánchez-Reyes, O. B., Alfonzo-Méndez, M. A., Romero-Ávila, M. T., Reyes-Cruz, G., & García-Sáinz, J. A. (2015). α1B-adrenergic receptors differentially associate with Rab proteins during homologous and heterologous desensitization. *PLoS One*, 10, e0121165.

Chang, A., Tourtellotte, W. W., Rudick, R., & Trapp, B. D. (2002). Premyelinating oligodendrocytes in chronic lesions of multiple sclerosis. *The New England Journal of Medicine*, 346, 165–173.

Dalgaard, P. (2008). *Introductory Statistics with R*. Springer.

De La Fuente, A. G., Lange, S., Silva, M. E., et al. (2017). Pericytes stimulate oligodendrocyte progenitor cell differentiation during CNS remyelination. *Cell Reports*, 20, 1755–1764.

Dennis, J., Morgan, M. K., Graf, M. R., & Fuss, B. (2012). P2Y(12) receptor expression is a critical determinant of functional responsiveness to ATX's MORFO domain. *Purinergic Signal*, 8, 181–190.

Dennis, J., White, M. A., Forrest, A. D., Yuelling, L. M., Nogaroli, L., Afshari, F. S., Fox, M. A., & Fuss, B. (2008). Phosphodiesterase-Ialpha/autotaxin's MORFO domain regulates oligodendroglial process network formation and focal adhesion organization. *Molecular and Cellular Neurosciences*, 37, 412–424.

Dubois-Dalcq, M., Behar, T., Hudson, L., & Lazzarini, R. A. (1986). Emergence of three myelin proteins in oligodendrocytes cultured without neurons. *The Journal of Cell Biology*, 102, 384–392.

Duchala, C. S., Asotra, K., & Macklin, W. B. (1995). Expression of cell surface markers and myelin proteins in cultured oligodendrocytes from neonatal brain of rat and mouse: A comparative study. *Developmental Neuroscience*, 17, 70–80.

Duclot, F., & Kabbaj, M. (2017). The role of early growth response 1 (EGR1) in brain plasticity and neuropsychiatric disorders. *Frontiers in Behavioral Neuroscience*, 11, 35.

Duncan, G. J., Plemel, J. R., Assinck, P., Manesh, S. B., Muir, F. G. W., Hirata, R., Berson, M., Liu, J., Wegner, M., Emery, B., Moore, G. R. W., & Tetzlaff, W. (2017). Myelin regulatory factor drives remyelination in multiple sclerosis. *Acta Neuropathologica*, 134, 403–422.

Dupree, J. L., Girault, J. A., & Popko, B. (1999). Axo-glial interactions regulate the localization of axonal paranodal proteins. *The Journal of Cell Biology*, 147, 1145–1152.

Elbaz, B., & Popko, B. (2019). Molecular control of oligodendrocyte development. *Trends in Neurosciences*, 42, 263–277.

Elkjaer, M. L., Frisch, T., Reynolds, R., Kacprowski, T., Burton, M., Kruse, T. A., Thomassen, M., Baumbach, J., & Illes, Z. (2019). Molecular signature of different lesion types in the brain white matter of patients with progressive multiple sclerosis. *Acta Neuropathologica Communications*, 7, 205.

Emery, B., & Lu, Q. R. (2015). Transcriptional and epigenetic regulation of oligodendrocyte development and myelination in the central nervous system. *Cold Spring Harbor Perspectives in Biology*, 7, a020461.

Estivill-Torrus, G., Llebrez-Zayas, P., Matas-Rico, E., et al. (2008). Absence of LPA1 signaling results in defective cortical development. *Cerebral cortex (New York, N.Y.: 1991)*, 18, 938–950.

Falcão, A. M., van Bruggen, D., Marques, S., Meijer, M., Jäkel, S., Agirre, E., Samudyata, Floriddia, E. M., Vanichkina, D. P., ffrench-Constant, C., Williams, A., Guerreiro-Cacais, A. O., & Castelo-Branco, G. (2018). Disease-specific oligodendrocyte lineage cells arise in multiple sclerosis. *Nature Medicine*, 24, 1837–1844.

Fleming, A., Diekmann, H., & Goldsmith, P. (2013). Functional characterisation of the maturation of the blood-brain barrier in larval zebrafish. *PLoS One*, 8, e77548.

Fletcher, J. L., Makowiecki, K., Cullen, C. L., & Young, K. M. (2021). Oligodendrogenesis and myelination regulate cortical development, plasticity and circuit function. *Seminars in Cell & Developmental Biology*, 118, 14–23.

Fox, M. A., Alexander, J. K., Afshari, F. S., Colello, R. J., & Fuss, B. (2004). Phosphodiesterase-I alpha/autotaxin controls cytoskeletal organization and FAK phosphorylation during myelination. *Molecular and Cellular Neurosciences*, 27, 140–150.

Fox, M. A., Colello, R. J., Macklin, W. B., & Fuss, B. (2003). Phosphodiesterase-Ialpha/autotaxin: A counteradhesive protein expressed by oligodendrocytes during onset of myelination. *Molecular and Cellular Neurosciences*, 23, 507–519.

Fulkerson, Z., Wu, T., Sunkara, M., Kooi, C. V., Morris, A. J., & Smyth, S. S. (2011). Binding of autotaxin to integrins localizes lysophosphatidic acid production to platelets and mammalian cells. *The Journal of Biological Chemistry*, 286, 34654–34663.

Fuss, B., Mallon, B., Phan, T., Ohlemeyer, C., Kirchhoff, F., Nishiyama, A., & Macklin, W. B. (2000). Purification and analysis of in vivo-differentiated oligodendrocytes expressing the green fluorescent protein. *Developmental Biology*, 218, 259–274.

Gaesser, J. M., & Fyffe-Maricich, S. L. (2016). Intracellular signaling pathway regulation of myelination and remyelination in the CNS. *Experimental Neurology*, 283, 501–511.

Garcia-Diaz, B., Riquelme, R., Varela-Nieto, I., Jimenez, A. J., de Diego, I., Gomez-Conde, A. I., Matas-Rico, E., Aguirre, J. A., Chun, J., Pedraza, C., Santin, L. J., Fernandez, O., Rodriguez de Fonseca, F., & Estivill-Torrus, G. (2015). Loss of lysophosphatidic acid receptor LPA1 alters oligodendrocyte differentiation and myelination in the mouse cerebral cortex. *Brain Struct Funct*, 220, 3701–3720.

Gard, A. L., & Pfeiffer, S. E. (1990). Two proliferative stages of the oligodendrocyte lineage (A2B5+O4- and O4+GalC-) under different mitogenic control. *Neuron*, 5, 615–625.

Gennero, I., Laurencin-Dalicieux, S., Conte-Auriol, F., Briand-Mésange, F., Laurencin, D., Rue, J., Beton, N., Malet, N., Mus, M., Tokumura, A., Bourin, P., Vico, L., Brunel, G., Oreffo, R. O. C., Chun, J., & Salles,

J. P. (2011). Absence of the lysophosphatidic acid receptor LPA1 results in abnormal bone development and decreased bone mass. *Bone*, 49, 395–403.

Geraldo, L. H. M., Spohr, T., Amaral, R. F. D., Fonseca, A., Garcia, C., Mendes, F. A., Freitas, C., dosSantos, M. F., & Lima, F. R. S. (2021). Role of lysophosphatidic acid and its receptors in health and disease: Novel therapeutic strategies. *Signal Transduction and Targeted Therapy*, 6, 45.

Gijsbers, R., Aoki, J., Arai, H., & Bollen, M. (2003). The hydrolysis of lysophospholipids and nucleotides by autotaxin (NPP2) involves a single catalytic site. *FEBS Letters*, 538, 60–64.

Gnocchi, D., Kapoor, S., Nitti, P., Cavalluzzi, M. M., Lentini, G., Denora, N., Sabbà, C., & Mazzocca, A. (2020). Novel lysophosphatidic acid receptor 6 antagonists inhibit hepatocellular carcinoma growth through affecting mitochondrial function. *Journal of Molecular Medicine (Berlin, Germany)*, 98, 179–191.

Golan, M., Krivitsky, A., Mausner-Fainberg, K., Benhamou, M., Vigiser, I., Regev, K., Kolb, H., & Karni, A. (2021). Increased expression of Ephrins on immune cells of patients with relapsing remitting multiple sclerosis affects oligodendrocyte differentiation. *International Journal of Molecular Sciences*, 22, 2182.

Göttle, P., Förster, M., Weyers, V., Küry, P., Rejdak, K., Hartung, H. P., & Kremer, D. (2019). An unmet clinical need: Roads to remyelination in MS. *Neurological Research and Practice*, 1, 21.

Gravel, M., Di Polo, A., Valera, P. B., & Braun, P. E. (1998). Four-kilobase sequence of the mouse CNP gene directs spatial and temporal expression of lacZ in transgenic mice. *Journal of Neuroscience Research*, 53, 393–404.

Green, A. J., Gelfand, J. M., Cree, B. A., Bevan, C., Boscardin, W. J., Mei, F., Inman, J., Arnow, S., Devereux, M., Abounasr, A., Nobuta, H., Zhu, A., Friessen, M., Gerona, R., von Büdingen, H. C., Henry, R. G., Hauser, S. L., & Chan, J. R. (2017). Clemastine fumarate as a remyelinating therapy for multiple sclerosis (ReBUILD): A randomised, controlled, double-blind, crossover trial. *Lancet (London, England)*, 390, 2481–2489.

Hata, E., Sasaki, N., Takeda, A., Tohya, K., Umemoto, E., Akahoshi, N., Ishii, S., Bando, K., Abe, T., Kano, K., Aoki, J., Hayasaka, H., & Miyasaka, M. (2016). Lysophosphatidic acid receptors LPA4 and LPA6 differentially promote lymphocyte transmigration across high endothelial venules in lymph nodes. *International Immunology*, 28, 283–292.

Hausmann, J., Kamtekar, S., Christodoulou, E., Day, J. E., Wu, T., Fulkerson, Z., Albers, H. M. H. G., van Meeteren, L. A., Houben, A. J. S., van Zeijl, L., Jansen, S., Andries, M., Hall, T., Pegg, L. E., Benson, T. E., Kasiem, M., Harlos, K., Kooi, C. W. V., Smyth, S. S., ... Perrakis, A. (2011). Structural basis of substrate discrimination and integrin binding by autotaxin. *Nature Structural & Molecular Biology*, 18, 198–204.

Hausmann, J., Perrakis, A., & Moolenaar, W. H. (2013). Structure-function relationships of autotaxin, a secreted lysophospholipase D. *Advances in Biological Regulation*, 53, 112–117.

Hayashi, K., Takahashi, M., Nishida, W., Yoshida, K., Ohkawa, Y., Kitabatake, A., Aoki, J., Arai, H., & Sobue, K. (2001). Phenotypic modulation of vascular smooth muscle cells induced by unsaturated lysophosphatidic acids. *Circulation Research*, 89, 251–258.

Hecht, J. H., Weiner, J. A., Post, S. R., & Chun, J. (1996). Ventricular zone gene-1 (vzg-1) encodes a lysophosphatidic acid receptor expressed in neurogenic regions of the developing cerebral cortex. *The Journal of Cell Biology*, 135, 1071–1083.

Herr, D. R., Chew, W. S., Satish, R. L., & Ong, W. Y. (2020). Pleotropic roles of autotaxin in the nervous system present opportunities for the development of novel therapeutics for neurological diseases. *Molecular Neurobiology*, 57, 372–392.

Houben, A. J., van Wijk, X. M., van Meeteren, L. A., et al. (2013). The polybasic insertion in autotaxin alpha confers specific binding to heparin and cell surface heparan sulfate proteoglycans. *The Journal of Biological Chemistry*, 288, 510–519.

Inoue, A., Arima, N., Ishiguro, J., Prestwich, G. D., Arai, H., & Aoki, J. (2011). LPA-producing enzyme PA-PLA(1)alpha regulates hair follicle development by modulating EGFR signalling. *The EMBO Journal*, 30, 4248–4260.

Inoue, A., Ishiguro, J., Kitamura, H., Arima, N., Okutani, M., Shuto, A., Higashiyama, S., Ohwada, T., Arai, H., Makide, K., & Aoki, J. (2012). TGFα shedding assay: An accurate and versatile method for detecting GPCR activation. *Nature Methods*, 9, 1021–1029.

Ishii, S., Hirane, M., Fukushima, K., Tomimatsu, A., Fukushima, N., & Tsujiuchi, T. (2015). Diverse effects of LPA4, LPA5 and LPA6 on the activation of tumor progression in pancreatic cancer cells. *Biochemical and Biophysical Research Communications*, 461, 59–64.

Jäkel, S., Agirre, E., Mendanha Falcão, A., van Bruggen, D., Lee, K. W., Knuesel, I., Malhotra, D., ffrench-Constant, C., Williams, A., & Castelo-Branco, G. (2019). Altered human oligodendrocyte heterogeneity in multiple sclerosis. *Nature*, 566, 543–547.

Jeffries, M. A., McLane, L. E., Khandker, L., Mather, M. L., Evangelou, A. V., Kantak, D., Bourne, J. N., Macklin, W. B., & Wood, T. L. (2021). mTOR signaling regulates metabolic function in oligodendrocyte precursor cells and promotes efficient brain remyelination in the cuprizone model. *The Journal of Neuroscience: The Official Journal of the Society for Neuroscience*, 41, 8321–8337.

Jeffries, M. A., Urbanek, K., Torres, L., Wendell, S. G., Rubio, M. E., & Fyffe-Maricich, S. L. (2016). ERK1/2 activation in preexisting oligodendrocytes of adult mice drives new myelin synthesis and enhanced CNS function. *The Journal of Neuroscience: The Official Journal of the Society for Neuroscience*, 36, 9186–9200.

Jiang, G., Inoue, A., Aoki, J., & Prestwich, G. D. (2013). Phosphorothioate analogs of sn-2 radyl lysophosphatidic acid (LPA): Metabolically stabilized LPA receptor agonists. *Bioorganic & Medicinal Chemistry Letters*, 23, 1865–1869.

Jung, S. H., Kim, S., Chung, A. Y., Kim, H. T., So, J. H., Ryu, J., Park, H. C., & Kim, C. H. (2010). Visualization of myelination in GFP-transgenic zebrafish. *Developmental Dynamics: An Official Publication of the American Association of Anatomists*, 239, 592–597.

Kanda, H., Newton, R., Klein, R., Morita, Y., Gunn, M. D., & Rosen, S. D. (2008). Autotaxin, an ectoenzyme that produces lysophosphatidic acid, promotes the entry of lymphocytes into secondary lymphoid organs. *Nature Immunology*, 9, 415–423.

Kano, K., Aoki, J., & Hla, T. (2021). Lysophospholipid mediators in health and disease. *Annual Review of Pathology*, 17, 459–483.

Kano, K., Matsumoto, H., Inoue, A., Yukiura, H., Kanai, M., Chun, J., Ishii, S., Shimizu, T., & Aoki, J. (2019). Molecular mechanism of lysophosphatidic acid-induced hypertensive response. *Scientific Reports*, 9, 2662.

Karlsson, U., & Schultz, R. L. (1965). Fixation of the central nervous system from electron microscopy by aldehyde perfusion. I. Preservation with aldehyde perfusates versus direct perfusion with osmium tetroxide with special reference to membranes and the extracellular space. *Journal of Ultrastructure Research*, 12, 160–186.

Kihara, Y., Maceyka, M., Spiegel, S., & Chun, J. (2014). Lysophospholipid receptor nomenclature review: IUPHAR review 8. *British Journal of Pharmacology*, 171, 3575–3594.

Kihara, Y., Mizuno, H., & Chun, J. (2015). Lysophospholipid receptors in drug discovery. *Experimental Cell Research*, 333, 171–177.

Kimmel, C. B., Ballard, W. W., Kimmel, S. R., Ullmann, B., & Schilling, T. F. (1995). Stages of embryonic development of the zebrafish. *Developmental Dynamics: An Official Publication of the American Association of Anatomists*, 203, 253–310.

Kirby, L., Jin, J., Cardona, J. G., Smith, M. D., Martin, K. A., Wang, J., Strasburger, H., Herbst, L., Alexis, M., Karnell, J., Davidson, T., Dutta, R., Goverman, J., Bergles, D., & Calabresi, P. A. (2019). Oligodendrocyte precursor cells present antigen and are cytotoxic targets in inflammatory demyelination. *Nature Communications*, 10, 3887.

Kroeze, W. K., Sassano, M. F., Huang, X. P., Lansu, K., McCorvy, J. D., Giguere, P. M., Sciaky, N., & Roth, B. L. (2015). PRESTO-Tango as an open-source resource for interrogation of the druggable human GPCRome. *Nature Structural & Molecular Biology*, *22*, 362–369.

Kuhlmann, T., Miron, V., Cui, Q., Wegner, C., Antel, J., & Bruck, W. (2008). Differentiation block of oligodendroglial progenitor cells as a cause for remyelination failure in chronic multiple sclerosis. *Brain: A Journal of Neurology*, *131*, 1749–1758.

Kurihara, T., Monoh, K., Takahashi, Y., Goto, K., & Kondo, H. (1992). 2′,3'-Cyclic-nucleotide 3′-phosphodiesterase. Complementary DNA and gene cloning for mouse enzyme and in situ hybridization of the messenger RNA in mouse brain. *Advances in Second Messenger and Phosphoprotein Research*, *25*, 101–110.

Lafrenaye, A. D., & Fuss, B. (2011). Focal adhesion kinase can play unique and opposing roles in regulating the morphology of differentiating oligodendrocytes. *Journal of Neurochemistry*, *115*, 269–282.

Larkin, M. A., Blackshields, G., Brown, N. P., Chenna, R., McGettigan, P. A., McWilliam, H., Valentin, F., Wallace, I. M., Wilm, A., Lopez, R., Thompson, J. D., Gibson, T. J., & Higgins, D. G. (2007). Clustal W and Clustal X version 2.0. *Bioinformatics (Oxford, England)*, *23*, 2947–2948.

Lecca, D., Raffaele, S., Abbracchio, M. P., & Fumagalli, M. (2020). Regulation and signaling of the GPR17 receptor in oligodendroglial cells. *Glia*, *68*, 1957–1967.

Li, Y., Chen, T., Miao, X., Yi, X., Wang, X., Zhao, H., Lee, S. M., & Zheng, Y. (2017). Zebrafish: A promising in vivo model for assessing the delivery of natural products, fluorescence dyes and drugs across the blood-brain barrier. *Pharmacological Research*, *125*, 246–257.

Liu, J., Moyon, S., Hernandez, M., & Casaccia, P. (2016). Epigenetic control of oligodendrocyte development: Adding new players to old keepers. *Current Opinion in Neurobiology*, *39*, 133–138.

Liu, W., Hopkins, A. M., & Hou, J. (2021). The development of modulators for lysophosphatidic acid receptors: A comprehensive review. *Bioorganic Chemistry*, *117*, 105386.

Livak, K. J., & Schmittgen, T. D. (2001). Analysis of relative gene expression data using real-time quantitative PCR and the 2(-Delta Delta C[T]) Method. *Methods (San Diego, Calif.)*, *25*, 402–408.

Lu, Q. R., Yuk, D., Alberta, J. A., Zhu, Z., Pawlitzky, I., Chan, J., McMahon, A. P., Stiles, C. D., & Rowitch, D. H. (2000). Sonic hedgehog–regulated oligodendrocyte lineage genes encoding bHLH proteins in the mammalian central nervous system. *Neuron*, *25*, 317–329.

Lubetzki, C., Zalc, B., Williams, A., Stadelmann, C., & Stankoff, B. (2020). Remyelination in multiple sclerosis: From basic science to clinical translation. *The Lancet Neurology*, *19*, 678–688.

Lucchinetti, C., Bruck, W., Parisi, J., Scheithauer, B., Rodriguez, M., & Lassmann, H. (2000). Heterogeneity of multiple sclerosis lesions: implications for the pathogenesis of demyelination. *Annals of Neurology*, *47*, 707–717.

Lyons, D. A., & Talbot, W. S. (2014). Glial cell development and function in zebrafish. *Cold Spring Harbor Perspectives in Biology*, *7*, a020586.

Marisca, R., Hoche, T., Agirre, E., Hoodless, L. J., Barkey, W., Auer, F., Castelo-Branco, G., & Czopka, T. (2020). Functionally distinct subgroups of oligodendrocyte precursor cells integrate neural activity and execute myelin formation. *Nature Neuroscience*, *23*, 363–374.

Marques, S., Zeisel, A., Codeluppi, S., et al. (2016). Oligodendrocyte heterogeneity in the mouse juvenile and adult central nervous system. *Science (New York N.Y.)*, *352*, 1326–1329.

Martinez-Lozada, Z., Waggener, C. T., Kim, K., Zou, S., Knapp, P. E., Hayashi, Y., Ortega, A., & Fuss, B. (2014). Activation of sodium-dependent glutamate transporters regulates the morphological aspects of oligodendrocyte maturation via signaling through calcium/calmodulin-dependent kinase IIbeta's actin-binding/−stabilizing domain. *Glia*, *62*, 1543–1558.

Masago, K., Kihara, Y., Yanagida, K., Hamano, F., Nakagawa, S., Niwa, M., & Shimizu, T. (2018). Lysophosphatidic acid receptor, LPA6, regulates endothelial blood-brain barrier function: Implication for hepatic encephalopathy. *Biochemical and Biophysical Research Communications*, *501*, 1048–1054.

Matas-Rico, E., Frijlink, E., van der Haar Àvila, I., Menegakis, A., van Zon, M., Morris, A. J., Koster, J., Salgado-Polo, F., de Kivit, S., Lança, T., Mazzocca, A., Johnson, Z., Haanen, J., Schumacher, T. N., Perrakis, A., Verbrugge, I., van den Berg, J. H., Borst, J., & Moolenaar, W. H. (2021). Autotaxin impedes anti-tumor immunity by suppressing chemotaxis and tumor infiltration of CD8(+) T cells. *Cell Reports*, *37*, 110013.

Mausner-Fainberg, K., Benhamou, M., Golan, M., Kimelman, N. B., Danon, U., Marom, E., & Karni, A. (2021). Specific blockade of bone morphogenetic protein-2/4 induces oligodendrogenesis and remyelination in demyelinating disorders. *Neurotherapeutics: The Journal of the American Society for Experimental NeuroTherapeutics*, *18*, 1798–1814.

Mierzwa, A. J., Zhou, Y. X., Hibbits, N., Vana, A. C., & Armstrong, R. C. (2013). FGF2 and FGFR1 signaling regulate functional recovery following cuprizone demyelination. *Neuroscience Letters*, *548*, 280–285.

Mitew, S., Hay, C. M., Peckham, H., Xiao, J., Koenning, M., & Emery, B. (2014). Mechanisms regulating the development of oligodendrocytes and central nervous system myelin. *Neuroscience*, *276*, 29–47.

Moolenaar, W. H., & Perrakis, A. (2011). Insights into autotaxin: how to produce and present a lipid mediator. *Nature Reviews. Molecular Cell Biology*, *12*, 674–679.

Morishige, J., Touchika, K., Tanaka, T., Satouchi, K., Fukuzawa, K., & Tokumura, A. (2007). Production of bioactive lysophosphatidic acid by lysophospholipase D in hen egg white. *Biochimica et Biophysica Acta*, *1771*, 491–499.

Mormann, W., & Leukel, G. (1988). A simple and versatile synthesis of trimethylsiloxy-substituted isocyanates. *Synthesis*, *12*, 990–992.

Mozafari, S., Starost, L., Manot-Saillet, B., Garcia-Diaz, B., Xu, Y. K. T., Roussel, D., Levy, M. J. F., Ottoboni, L., Kim, K. P., Schöler, H. R., Kennedy, T. E., Antel, J. P., Martino, G., Angulo, M. C., Kuhlmann, T., & Baron-van Evercooren, A. (2020). Multiple sclerosis iPS-derived oligodendroglia conserve their properties to functionally interact with axons and glia in vivo. *Science Advances*, *6*, eabc6983.

Munzel, E. J., Schaefer, K., Obirei, B., et al. (2012). Claudin k is specifically expressed in cells that form myelin during development of the nervous system and regeneration of the optic nerve in adult zebrafish. *Glia*, *60*, 253–270.

Nishimasu, H., Okudaira, S., Hama, K., Mihara, E., Dohmae, N., Inoue, A., Ishitani, R., Takagi, J., Aoki, J., & Nureki, O. (2011). Crystal structure of autotaxin and insight into GPCR activation by lipid mediators. *Nature Structural & Molecular Biology*, *18*, 205–212.

Nogaroli, L., Yuelling, L. M., Dennis, J., Gorse, K., Payne, S. G., & Fuss, B. (2009). Lysophosphatidic acid can support the formation of membranous structures and an increase in MBP mRNA levels in differentiating oligodendrocytes. *Neurochemical Research*, *34*, 182–193.

Noguchi, K., Ishii, S., & Shimizu, T. (2003). Identification of p2y9/GPR23 as a novel G protein-coupled receptor for lysophosphatidic acid, structurally distant from the Edg family. *The Journal of Biological Chemistry*, *278*, 25600–25606.

Okasato, R., Kano, K., Kise, R., Inoue, A., Fukuhara, S., & Aoki, J. (2021). An ATX-LPA(6)-Gα(13)-ROCK axis shapes and maintains caudal vein plexus in zebrafish. *iScience*, *24*, 103254.

Okudaira, M., Inoue, A., Shuto, A., Nakanaga, K., Kano, K., Makide, K., Saigusa, D., Tomioka, Y., & Aoki, J. (2014). Separation and quantification of 2-acyl-1-lysophospholipids and 1-acyl-2-lysophospholipids in biological samples by LC-MS/MS. *Journal of Lipid Research*, *55*, 2178–2192.

Okudaira, S., Yukiura, H., & Aoki, J. (2010). Biological roles of lyso-phosphatidic acid signaling through its production by autotaxin. *Biochimie*, 92, 698–706.

Pasternack, S. M., von Kugelgen, I., Al Aboud, K., et al. (2008). G protein-coupled receptor P2Y5 and its ligand LPA are involved in mainte-nance of human hair growth. *Nature Genetics*, 40, 329–334.

Patrikios, P., Stadelmann, C., Kutzelnigg, A., Rauschka, H., Schmidbauer, M., Laursen, H., Sorensen, P. S., Bruck, W., Lucchinetti, C., & Lassmann, H. (2006). Remyelination is extensive in a subset of multiple sclerosis patients. *Brain: A Journal of Neurology*, 129, 3165–3172.

Petersen, M. A., Tognatta, R., Meyer-Franke, A., Bushong, E. A., Mendiola, A. S., Yan, Z., Muthusamy, A., Merlini, M., Meza-Acevedo, R., Cabriga, B., Zhou, Y., Thomas, R., Ryu, J. K., Lassmann, H., Ellisman, M. H., & Akassoglou, K. (2021). BMP receptor blockade overcomes extrinsic inhibition of remyelin-ation and restores neurovascular homeostasis. *Brain: A Journal of Neurology*, 144, 2291–2301.

Pogorevc, M., & Faber, K. (2002). Enantioselective stereoinversion of sec-alkyl sulfates by an alkylsulfatase from Rhodococcus ruber DSM 44541. *Tetrahedron: Asymmetry*, 13, 1435–1441.

Preston, M. A., Finseth, L. T., Bourne, J. N., & Macklin, W. B. (2019). A novel myelin protein zero transgenic zebrafish designed for rapid readout of in vivo myelination. *Glia*, 67, 650–667.

Preston, M. A., & Macklin, W. B. (2015). Zebrafish as a model to investi-gate CNS myelination. *Glia*, 63, 177–193.

Rajendran, R., Böttiger, G., Stadelmann, C., Karnati, S., & Berghoff, M. (2021). FGF/FGFR pathways in multiple sclerosis and in its disease models. *Cell*, 10, 884.

Raza, S. I., Muhammad, D., Jan, A., Ali, R. H., Hassan, M., Ahmad, W., & Rashid, S. (2014). In silico analysis of missense mutations in LPAR6 reveals abnormal phospholipid signaling pathway leading to hypo-trichosis. *PLoS One*, 9, e104756.

Roggeri, A., Schepers, M., Tiane, A., Rombaut, B., van Veggel, L., Hellings, N., Prickaerts, J., Pittaluga, A., & Vanmierlo, T. (2020). Sphingosine-1-phosphate receptor modulators and oligodendroglial cells: Beyond immunomodulation. *International Journal of Molecular Sciences*, 21, 7537.

Rombough, P. (2002). Gills are needed for ionoregulation before they are needed for O(2) uptake in developing zebrafish, Danio rerio. *The Journal of Experimental Biology*, 205, 1787–1794.

Saraswat, D., Shayya, H. J., Polanco, J. J., Tripathi, A., Welliver, R. R., Pol, S. U., Seidman, R. A., Broome, J. E., O'Bara, M. A., van Kuppervelt, T. H., Phillips, J. J., Dutta, R., & Sim, F. J. (2021). Overcoming the inhibitory microenvironment surrounding oligodendrocyte progenitor cells following experimental demyelination. *Nature Communications*, 12, 1923.

Schirmer, L., Velmeshev, D., Holmqvist, S., Kaufmann, M., Werneburg, S., Jung, D., Vistnes, S., Stockley, J. H., Young, A., Steindel, M., Tung, B., Goyal, N., Bhaduri, A., Mayer, S., Engler, J. B., Bayraktar, O. A., Franklin, R. J. M., Haeussler, M., Reynolds, R., ... Rowitch, D. H. (2019). Neuronal vulnerability and multilineage diversity in multiple sclerosis. *Nature*, 573, 75–82.

Schweitzer, J., Becker, T., Schachner, M., Nave, K. A., & Werner, H. (2006). Evolution of myelin proteolipid proteins: Gene duplica-tion in teleosts and expression pattern divergence. *Molecular and Cellular Neurosciences*, 31, 161–177.

Shen, M. Y., & Sali, A. (2006). Statistical potential for assessment and prediction of protein structures. *Protein Science: A Publication of the Protein Society*, 15, 2507–2524.

Shimomura, Y., Wajid, M., Ishii, Y., Shapiro, L., Petukhova, L., Gordon, D., & Christiano, A. M. (2008). Disruption of P2RY5, an orphan G protein-coupled receptor, underlies autosomal recessive woolly hair. *Nature Genetics*, 40, 335–339.

Siems, S. B., Jahn, O., Hoodless, L. J., Jung, R. B., Hesse, D., Möbius, W., Czopka, T., & Werner, H. B. (2021). Proteome Profile of Myelin in the Zebrafish Brain. *Frontiers in Cell and Developmental Biology*, 9, 640169.

Skinner, D. D., & Lane, T. E. (2020). CXCR2 Signaling and Remyelination in Preclinical Models of Demyelination. *DNA and Cell Biology*, 39, 3–7.

Skokal, R. R., & Rohlf, F. J. (1995). *Biometry: The principle and practice in biological research*. W. H. Freeman and Company.

Smets, I., Goris, A., Vandebergh, M., Demeestere, J., Sunaert, S., Dupont, P., & Dubois, B. (2021). Quantitative MRI phenotypes capture bi-ological heterogeneity in multiple sclerosis patients. *Scientific Reports*, 11, 1573.

Sock, E., Leger, H., Kuhlbrodt, K., Schreiber, J., Enderich, J., Richter-Landsberg, C., & Wegner, M. (1997). Expression of Krox proteins during differentiation of the O-2A progenitor cell line CG-4. *Journal of Neurochemistry*, 68, 1911–1919.

Sock, E., & Wegner, M. (2021). Using the lineage determinants Olig2 and Sox10 to explore transcriptional regulation of oligodendrocyte de-velopment. *Developmental Neurobiology*, 81, 892–901.

Solís, K. H., Romero-Ávila, M. T., Guzmán-Silva, A., & García-Sáinz, J. A. (2021). The LPA(3) receptor: Regulation and activation of signaling pathways. *International Journal of Molecular Sciences*, 22, 6704.

Spitzer, S. O., Sitnikov, S., Kamen, Y., Evans, K. A., Kronenberg-Versteeg, D., Dietmann, S., de Faria, O. Jr., Agathou, S. and Karadottir, R. T. (2019) Oligodendrocyte progenitor cells become regionally di-verse and heterogeneous with age. *Neuron* 101, 459–471 e455, 459, 471.e5.

Stankoff, B., Barron, S., Allard, J., Barbin, G., Noël, F., Aigrot, M. S., Premont, J., Sokoloff, P., Zalc, B., & Lubetzki, C. (2002). Oligodendroglial expression of Edg-2 receptor: developmental analysis and pharmacological responses to lysophosphatidic acid. *Molecular and Cellular Neurosciences*, 20, 415–428.

Starost, L., Lindner, M., Herold, M., Xu, Y. K. T., Drexler, H. C. A., Heß, K., Ehrlich, M., Ottoboni, L., Ruffini, F., Stehling, M., Röpke, A., Thomas, C., Schöler, H. R., Antel, J., Winkler, J., Martino, G., Klotz, L., & Kuhlmann, T. (2020). Extrinsic immune cell-derived, but not intrinsic oligodendroglial factors contribute to oligodendroglial dif-ferentiation block in multiple sclerosis. *Acta Neuropathologica*, 140, 715–736.

Stoddard, N. C., & Chun, J. (2015). Promising pharmacological directions in the world of lysophosphatidic Acid signaling. *Biomol Ther (Seoul)*, 23, 1–11.

Sturrock, R. R. (1980). Myelination of the mouse corpus callosum. *Neuropathology and Applied Neurobiology*, 6, 415–420.

Sturrock, R. R. (1983). Identification of mitotic oligodendrocytes in semithin sections of the developing mouse corpus callosum and hippocampal commissure. *Journal of Anatomy*, 137(Pt 1), 47–55.

Suckau, O., Gross, I., Schrotter, S., et al. (2019). LPA1, LPA2, LPA4, and LPA6 receptor expression during mouse brain development. *Developmental dynamics: an official publication of the American Association of Anatomists*, 248, 375–395.

Swiss, V. A., Nguyen, T., Dugas, J., Ibrahim, A., Barres, B., Androulakis, I. P., & Casaccia, P. (2011). Identification of a gene regulatory network necessary for the initiation of oligodendrocyte differentiation. *PLoS One*, 6, e18088.

Takada, N., & Appel, B. (2010). Identification of genes expressed by ze-brafish oligodendrocytes using a differential microarray screen. *Developmental dynamics: an official publication of the American Association of Anatomists*, 239, 2041–2047.

Takahashi, K., Fukushima, K., Onishi, Y., Inui, K., Node, Y., Fukushima, N., Honoki, K., & Tsujiuchi, T. (2017). Lysophosphatidic acid (LPA) signaling via LPA4 and LPA6 negatively regulates cell motile ac-tivities of colon cancer cells. *Biochemical and Biophysical Research Communications*, 483, 652–657.

Tanaka, M., Okudaira, S., Kishi, Y., Ohkawa, R., Iseki, S., Ota, M., Noji, S., Yatomi, Y., Aoki, J., & Arai, H. (2006). Autotaxin stabilizes blood vessels and is required for embryonic vasculature by producing

lysophosphatidic acid. *The Journal of Biological Chemistry, 281*, 25822–25830.

Taniguchi, R., Inoue, A., Sayama, M., Uwamizu, A., Yamashita, K., Hirata, K., Yoshida, M., Tanaka, Y., Kato, H. E., Nakada-Nakura, Y., Otani, Y., Nishizawa, T., Doi, T., Ohwada, T., Ishitani, R., Aoki, J., & Nureki, O. (2017). Structural insights into ligand recognition by the lysophosphatidic acid receptor LPA(6). *Nature, 548*, 356–360.

Thomason, E. J., Suárez-Pozos, E., Afshari, F. S., Rosenberg, P. A., Dupree, J. L., & Fuss, B. (2022). Deletion of the sodium-dependent glutamate transporter GLT-1 in maturing oligodendrocytes attenuates myelination of callosal axons during a postnatal phase of central nervous system development. *Frontiers in Cellular Neuroscience, 16*, 905299.

Thümmler, K., Rom, E., Zeis, T., Lindner, M., Brunner, S., Cole, J. J., Arseni, D., Mücklisch, S., Edgar, J. M., Schaeren-Wiemers, N., Yayon, A., & Linington, C. (2019). Polarizing receptor activation dissociates fibroblast growth factor 2 mediated inhibition of myelination from its neuroprotective potential. *Acta Neuropathologica Communications, 7*, 212.

Tokumura, A., Majima, E., Kariya, Y., Tominaga, K., Kogure, K., Yasuda, K., & Fukuzawa, K. (2002). Identification of human plasma lysophospholipase D, a lysophosphatidic acid-producing enzyme, as autotaxin, a multifunctional phosphodiesterase. *The Journal of Biological Chemistry, 277*, 39436–39442.

Tsai, H. H., Niu, J., Munji, R., et al. (2016). Oligodendrocyte precursors migrate along vasculature in the developing nervous system. *Science (New York N.Y.), 351*, 379–384.

Umezu-Goto, M., Kishi, Y., Taira, A., Hama, K., Dohmae, N., Takio, K., Yamori, T., Mills, G. B., Inoue, K., Aoki, J., & Arai, H. (2002). Autotaxin has lysophospholipase D activity leading to tumor cell growth and motility by lysophosphatidic acid production. *The Journal of Cell Biology, 158*, 227–233.

Urs, N. M., Jones, K. T., Salo, P. D., Severin, J. E., Trejo, J., & Radhakrishna, H. (2005). A requirement for membrane cholesterol in the beta-arrestin- and clathrin-dependent endocytosis of LPA1 lysophosphatidic acid receptors. *Journal of Cell Science, 118*, 5291–5304.

van Meeteren, L. A., Ruurs, P., Stortelers, C., Bouwman, P., van Rooijen, M. A., Pradère, J. P., Pettit, T. R., Wakelam, M. J. O., Saulnier-Blache, J. S., Mummery, C. L., Moolenaar, W. H., & Jonkers, J. (2006). Autotaxin, a secreted lysophospholipase D, is essential for blood vessel formation during development. *Molecular and Cellular Biology, 26*, 5015–5022.

Waggener, C. T., Dupree, J. L., Elgersma, Y., & Fuss, B. (2013). CaMKIIbeta regulates oligodendrocyte maturation and CNS myelination. *The Journal of Neuroscience: The Official Journal of the Society for Neuroscience, 33*, 10453–10458.

Wang, J., He, X., Meng, H., Li, Y., Dmitriev, P., Tian, F., Page, J. C., Lu, Q. R., & He, Z. (2020). Robust myelination of regenerated axons induced by combined manipulations of GPR17 and microglia. *Neuron, 108*, 876–886.e874.

Wegner, M. (2001). Expression of transcription factors during oligodendroglial development. *Microscopy Research and Technique, 52*, 746–752.

Weiner, J. A., Hecht, J. H., & Chun, J. (1998). Lysophosphatidic acid receptor gene vzg-1/lpA1/edg-2 is expressed by mature oligodendrocytes during myelination in the postnatal murine brain. *The Journal of Comparative Neurology, 398*, 587–598.

Welliver, R. R., Polanco, J. J., Seidman, R. A., Sinha, A. K., O'Bara, M. A., Khaku, Z. M., Santiago González, D. A., Nishiyama, A., Wess, J., Feltri, M. L., Paez, P. M., & Sim, F. J. (2018). Muscarinic receptor M(3)R signaling prevents efficient remyelination by human and mouse oligodendrocyte progenitor cells. *The Journal of Neuroscience: The Official Journal of the Society for Neuroscience, 38*, 6921–6932.

Wheeler, N. A., & Fuss, B. (2016). Extracellular cues influencing oligodendrocyte differentiation and (re)myelination. *Experimental Neurology, 283*, 512–530.

Wheeler, N. A., Fuss, B., Knapp, P. E., & Zou, S. (2016). HIV-1 tat inhibits autotaxin lysophospholipase D activity and modulates oligodendrocyte differentiation. *ASN Neuro, 8*, 175909141666961.

Wheeler, N. A., Lister, J. A., & Fuss, B. (2015). The autotaxin-lysophosphatidic acid axis modulates histone acetylation and gene expression during oligodendrocyte differentiation. *The Journal of Neuroscience: The Official Journal of the Society for Neuroscience, 35*, 11399–11414.

Yanagida, K., & Ishii, S. (2011). Non-Edg family LPA receptors: The cutting edge of LPA research. *Journal of Biochemistry, 150*, 223–232.

Yanagida, K., Kurikawa, Y., Shimizu, T., & Ishii, S. (2013). Current progress in non-Edg family LPA receptor research. *Biochimica et Biophysica Acta, 1831*, 33–41.

Yanagida, K., Masago, K., Nakanishi, H., Kihara, Y., Hamano, F., Tajima, Y., Taguchi, R., Shimizu, T., & Ishii, S. (2009). Identification and characterization of a novel lysophosphatidic acid receptor, p2y5/LPA6. *The Journal of Biological Chemistry, 284*, 17731–17741.

Yanagida, K., & Valentine, W. J. (2020). Druggable lysophospholipid signaling pathways. *Advances in Experimental Medicine and Biology, 1274*, 137–176.

Yasuda, D., Kobayashi, D., Akahoshi, N., Ohto-Nakanishi, T., Yoshioka, K., Takuwa, Y., Mizuno, S., Takahashi, S., & Ishii, S. (2019). Lysophosphatidic acid-induced YAP/TAZ activation promotes developmental angiogenesis by repressing Notch ligand Dll4. *The Journal of Clinical Investigation, 129*, 4332–4349.

Ye, J., Coulouris, G., Zaretskaya, I., Cutcutache, I., Rozen, S., & Madden, T. L. (2012). Primer-BLAST: A tool to design target-specific primers for polymerase chain reaction. *BMC Bioinformatics, 13*, 134.

Yoshida, K., Nishida, W., Hayashi, K., Ohkawa, Y., Ogawa, A., Aoki, J., Arai, H., & Sobue, K. (2003). Vascular remodeling induced by naturally occurring unsaturated lysophosphatidic acid in vivo. *Circulation, 108*, 1746–1752.

Yoshida, M., & Macklin, W. B. (2005). Oligodendrocyte development and myelination in GFP-transgenic zebrafish. *Journal of Neuroscience Research, 81*, 1–8.

Young, K. M., Psachoulia, K., Tripathi, R. B., Dunn, S. J., Cossell, L., Attwell, D., Tohyama, K., & Richardson, W. D. (2013). Oligodendrocyte dynamics in the healthy adult CNS: Evidence for myelin remodeling. *Neuron, 77*, 873–885.

Yu, N., Lariosa-Willingham, K. D., Lin, F. F., Webb, M., & Rao, T. S. (2004). Characterization of lysophosphatidic acid and sphingosine-1-phosphate-mediated signal transduction in rat cortical oligodendrocytes. *Glia, 45*, 17–27.

Yuelling, L. W., Waggener, C. T., Afshari, F. S., Lister, J. A., & Fuss, B. (2012). Autotaxin/ENPP2 regulates oligodendrocyte differentiation in vivo in the developing zebrafish hindbrain. *Glia, 60*, 1605–1618.

Yuen, T. J., Silbereis, J. C., Griveau, A., Chang, S. M., Daneman, R., Fancy, S. P. J., Zahed, H., Maltepe, E., & Rowitch, D. H. (2014). Oligodendrocyte-encoded HIF function couples postnatal myelination and white matter angiogenesis. *Cell, 158*, 383–396.

Yung, Y. C., Stoddard, N. C., & Chun, J. (2014). LPA receptor signaling: Pharmacology, physiology, and pathophysiology. *Journal of Lipid Research, 55*, 1192–1214.

Yung, Y. C., Stoddard, N. C., Mirendil, H., & Chun, J. (2015). Lysophosphatidic Acid signaling in the nervous system. *Neuron, 85*, 669–682.

Zalc, B. (2016). The acquisition of myelin: An evolutionary perspective. *Brain Research, 1641*, 4–10.

Zalc, B., Goujet, D., & Colman, D. (2008). The origin of the myelination program in vertebrates. *Current Biology: CB, 18*, R511–R512.

Zhang, Y., Chen, K., Sloan, S. A., Bennett, M. L., Scholze, A. R., O'Keeffe, S., Phatnani, H. P., Guarnieri, P., Caneda, C., Ruderisch, N., Deng, S.,

Liddelow, S. A., Zhang, C., Daneman, R., Maniatis, T., Barres, B. A., & Wu, J. Q. (2014). An RNA-sequencing transcriptome and splicing database of glia, neurons, and vascular cells of the cerebral cortex. *The Journal of Neuroscience: The Official Journal of the Society for Neuroscience*, *34*, 11929–11947.

Zhao, J., Stephens, T., & Zhao, Y. (2021). Molecular regulation of lysophosphatidic acid receptor 1 maturation and desensitization. *Cell Biochemistry and Biophysics*, *79*, 477–483.

Zhou, Q., Wang, S., & Anderson, D. J. (2000). Identification of a novel family of oligodendrocyte lineage-specific basic helix-loop-helix transcription factors. *Neuron*, *25*, 331–343.

**ORIGINAL PAPER**

# GLAST Activity is Modified by Acute Manganese Exposure in Bergmann Glial Cells

Miguel Escalante[1] · Jazmín Soto-Verdugo[1] · Luisa C. Hernández-Kelly[1] · Dinorah Hernández-Melchor[1] ·
Esther López-Bayghen[1] · Tatiana N. Olivares-Bañuelos[2] · Arturo Ortega[1]

## Abstract

Glutamate is the major excitatory amino acid neurotransmitter in the vertebrate brain. It exerts its actions through the activation of specific plasma membrane receptors expressed in neurons and glial cells. Overactivation of glutamate receptors results in neuronal death, known as excitotoxicity. A family of sodium-dependent glutamate transporters enriched in glial cells are responsible of the vast majority of the removal of this amino acid form the synaptic cleft. Therefore, a precise and exquisite regulation of these proteins is required not only for a proper glutamatergic transmission but also for the prevention of an excitotoxic insult. Manganese is a trace element essential as a cofactor for several enzymatic systems, although in high concentrations is involved in the disruption of brain glutamate homeostasis. The molecular mechanisms associated to manganese neurotoxicity have been focused on mitochondrial function, although energy depletion severely compromises the glutamate uptake process. In this context, in this contribution we analyze the effect of manganese exposure in glial glutamate transporters function. To this end, we used the well-established model of chick cerebellar Bergmann glia cultures. A time and dose dependent modulation of [$^3$H]-D-aspartate uptake was found. An increase in the transporter catalytic efficiency, most probably linked to a discrete increase in the affinity of the transporter was detected upon manganese exposure. Interestingly, glucose uptake was reduced by this metal. These results favor the notion of a direct effect of manganese on glial cells, this in turn alters their coupling with neurons and might lead to changes in glutamatergic transmission.

**Keywords** GLAST · Bergmann glia · Glutamate · Manganese · Neurotoxicity

## Introduction

Glutamate is the major excitatory amino acid transmitter in the vertebrate brain. It exerts its actions through the activation of specific membrane receptors that have been subdivided in terms of their molecular structure and signaling properties in ionotropic (iGluRs) and metabotropic (mGluRs) glutamate receptors [1, 2]. Neurons and glial

cells express both subtypes of receptors, several membrane to nucleus signaling cascades have been described to be activated by glutamate in both cell types [3].

Overstimulation of glutamate receptors is linked to neuronal death, and most of the time it is related to a deficient removal of this amino acid transmitter from the synaptic cleft [4]. A family of sodium-dependent plasma membrane glutamate transporters, known as excitatory amino acid transporters (EAATs), are responsible for the glutamate uptake mainly into glial cells, albeit these proteins are also present in neurons. Of the five EAATs subtypes described thus far, EAAT1 also known as glutamate/aspartate transporter (GLAST) and EAAT2 first named as glutamate transporter 1 (Glt-1) are regarded as glial glutamate transporters, although Glt-1 has been also found in neurons [5]. In any event, the density of glial glutamate transporters exceeds that of their neuronal counterparts and therefore the vast majority of the brain glutamate uptake activity takes place in glial cells [6].

---

✉ Arturo Ortega
  arortega@cinvestav.mx

1   Departamento de Toxicología, Centro de Investigación Y de Estudios Avanzados del IPN, Apartado Postal 14-740, 07360 Ciudad de Mexico, Mexico

2   Instituto de Investigaciones Oceanológicas, Universidad Autónoma de Baja California, 22860 Ensenada, Baja California, Mexico

🙋 Springer

Once internalized into the glial compartment, a fraction of glutamate is metabolized to glutamine via the glia-enriched enzyme glutamine synthetase. The associated $Na^+$ influx reverses the direction of the neutral amino acid transporter (SNAT3/5) resulting in the astrocytic release of glutamine in the vicinity of the presynaptic terminal, which takes it up presumably by means of SNAT2 [7, 8]. Glutamine is then converted back to glutamate by the enzyme glutaminase and packed into synaptic vesicles completing the recycling of this neurotransmitter in what has been known as the *Glutamate/Glutamine* shuttle [9]. An exquisite and precise coupling between glutamate uptake and glutamine release is achieved through an activity-dependent interaction of glial glutamate and glutamine transporters [10, 11].

Manganese (Mn) is a trace element widely found in the environment and for which defined roles as enzyme cofactor have been acknowledged [12]. Nevertheless, occupational exposure as the one present in workers of the mining industry has been linked to symptoms that resemble Parkinson's disease: tremors, bradykinesia, facial spasms [13]. An accumulation of this metal in the *globus pallidus* has been reported in post-mortem samples of exposed population [14]. In fact, the dopaminergic neurons of the *substantia nigra pars compacta* have been identified as a target of manganese accumulation [15].

A significant amount of work has been reported in recent years regarding the biological basis of Mn neurotoxicity and its parallelism to Parkinson's disease. Upon sustained Mn exposure, a disruption of $Ca^{2+}$ homeostasis is present resulting in the activation of proteases such as calpains, that damages the soluble NSF attachment protein receptor (SNARE) complex halting neurotransmitter release [16]. Concomitantly, an increase in α-synuclein expression that leads to endoplasmic reticulum (ER) stress is also present after exposure to this metal both in neurons and astrocytes [17].

All of the cellular responses described above, lead to an energy deficit that most probably distort the highly ATP-consuming glutamate uptake. Pioneer work from the groups of Aschner and Lee have described that long term Mn exposure affects glutamate turnover using cortical astrocytes [18, 19]. In this contribution, we decided to evaluate the effect of short term Mn exposure in the well-established model of chick cerebellar cultured Bergmann glial cells (BGC), as a proven model system of radial glia that totally enwrap glutamatergic synapses: the ones established between the parallel fibers and the Purkinje cells in the molecular layer of the cerebellum [20]. Moreover, we also decided to explore a plausible interaction of Mn with the glutamate transporter expressed in these cells: GLAST/EAAT1. Our results strongly suggest that Mn modulates the transporter function by slightly increasing its catalytic efficiency to uptake

glutamate. Surprisingly, also a robust decrease in glucose uptake was found.

## Methods

### Animals

Chicken embryos (Avimex, Mexico City, Mexico) were kept at 37 °C until usage. All experiments were performed according to the International Guidelines on the Ethical Use of Animals in Research and approved by the Cinvestav Animal Ethics Committee. Every effort was made to reduce the number of embryos used and their suffering.

### Bergmann Glia Cells Cultures

Bergmann glia primary cultures were prepared according to a previously established protocol [21]. BGC were isolated from chicken embryos (14-day-old). Cerebella were dissected out, cut into small pieces and incubated for 15 min at 37 °C in Puck's medium containing trypsin (0.25 mg/mL) and DNase (0.08 mg/mL) to dissociate the tissue. The media was removed and substituted with Opti-MEM containing 2.5% fetal bovine serum (FBS), 2 mM glutamine, and gentamicin (50 µg/mL) for mechanical dissociation. BGC were then recovered by the repeated removal of dissociated cells and diluted to $1 \times 10^6$ cells/mL. The cultures were maintained at 37ºC and 95% air/5% $CO_2$ in a humidified incubator. All experiments were performed 4–7 days post-isolation.

### Cell Viability Assay

Cell viability was measured by the 3-(4,5-dimethylthiazol-2-yl)-2,5-diphenyltetrazolium bromide (MTT) assay. BGC were seeded in 96-well plates ($1 \times 10^5$ cells/well) and maintained as mentioned above. Subsequently, the cultures were treated with $MnCl_2$ or vehicle in DMEM reduced serum medium (0.5% FBS) for the indicated time. After treatment, 20 µL of MTT solution (5 mg/mL) were added to each well and plates were incubated for 3 h at 37 °C. Next, media were discarded and 50 µL of dimethyl sulfoxide (DMSO) (Sigma-Aldrich, MO, USA) were added to each well to dissolve the crystals formed by MTT reagent (Sigma-Aldrich, MO, USA). Absorbance was measured with a microplate reader (BioTek Instruments, VT, USA) at 570 nm. Experiments were performed in quadruplicates in three independent cultures.

### [³H]-ᴅ-Aspartate Uptake

ᴅ-Aspartate uptake studies were carried out as previously described [22]. BGC were seeded in 24-well plates

(5 × 10^5 cells/well) and maintained as described above. On the day of the experiment, culture media were washed and replaced with uptake buffer (pre-warmed HEPES-buffered solution containing 25 mM HEPES, 130 mM NaCl, 5.4 mM KCl, 1.8 mM CaCl$_2$, 0.8 mM MgCl$_2$, 33.3 mM glucose, and 1 mM NaH$_2$PO$_4$, pH 7.4). Next, cultures were treated with MnCl$_2$ (indicated concentrations) or vehicle for the indicated time periods. After treatment, cultures were incubated with pre-warmed uptake buffer containing 0.4 μCi/mL [^3H]-D-aspartate ([^3H]-D-Asp) (specific activity: 16.5 Ci/mmol, Perkin Elmer, MA, USA). D-Asp (glutamate analogue) was used as it has the advantage of being nonmetabolizable while still using the same transporter system as glutamate. Uptake was terminated after 12 min of incubation with ice-cold uptake buffer, and cells were lysed by incubation with 0.1 N NaOH for 2 h at room temperature. An aliquot of the lysate was transferred to a scintillation vial, liquid scintillation cocktail and 50 μL of glacial acetic acid (to quench chemiluminescence) were added, and radioactivity was measured in a scintillation analyzer (PerkinElmer, MA, USA). The remainder of the lysate was used for protein determination by the Bradford protein assay (Bio-Rad, CA, USA). Radioactivity counts were corrected for protein levels and calculated as [^3H]-D-Asp pmol/(mg protein min$^{-1}$). Experiments were performed in quadruplicates in three–four independent cultures.

For the determination of the kinetic constants $K_m$ and $V_{max}$, cultures were treated with 200 μM MnCl$_2$ or vehicle for 30 min. After treatment, cultures were incubated with pre-warmed uptake buffer containing 0.4 μCi/mL [^3H]-D-Asp (24.2 nM) + D-Asp (unlabeled D-aspartate concentrations of 0–250 μM) (Sigma-Aldrich, MO, USA). Uptake was terminated after 12 min of incubation by three washes with ice-cold uptake buffer, and cells were lysed by incubation with 0.1 N NaOH for 2 h at room temperature. Sample aliquots were then measured for incorporated radioactivity and protein content as described above. A robust nonlinear regression was used to fit a model to the experimental data and estimate the parameters of Michaelis–Menten equation (GraphPad Prism Software, La Jolla California USA). Experiments were performed in quadruplicates in three independent cultures.

Some experiments were performed just by adding MnCl$_2$ (final concentration of 200 μM) or vehicle to the uptake buffer (containing 0.4 μCi/mL [^3H]-D-Asp), and the incorporated radioactivity as a function of time was evaluated. These experiments were terminated after the indicated incubation time points by three washes with ice-cold uptake buffer. Next, cells were lysed and measured for incorporated radioactivity and protein content as previously described. A robust nonlinear regression was used to fit a model to the

experimental data (GraphPad Prism Software, La Jolla California USA). Experiments were performed in quadruplicates in three independent cultures.

## [^3H]-2-Deoxy-D-Glucose Uptake

Glucose uptake studies were carried out as previously described [23]. BGC were seeded in 24-well plates (5 × 10^5 cells/well) and maintained as above mention. On the day of the experiment, culture media were washed and replaced with uptake buffer (pre-warmed HEPES-buffered solution containing 25 mM HEPES, 130 mM NaCl, 5.4 mM KCl, 1.8 mM CaCl$_2$, 0.8 mM MgCl$_2$, 5 mM glucose, and 1 mM NaH$_2$PO$_4$, pH 7.4). Next, cultures were treated with 200 μM MnCl$_2$ or vehicle for 30 min. After treatment, cultures were incubated with pre-warmed uptake buffer (without glucose) containing 0.8 μCi/mL [^3H]-2-deoxy-D-glucose ([^3H]-2DOG) (specific activity: 32.5 Ci/mmol, Perkin Elmer, MA, USA) + 2DOG (unlabeled 2-deoxy-D-glucose concentrations of 0–5 mM) (Sigma-Aldrich, MO, USA). Uptake was terminated after 30 min of incubation by three washes with ice-cold uptake buffer (without glucose), and cells were lysed by incubation with 0.1 N NaOH for 2 h at room temperature. An aliquot of the lysate was transferred to a scintillation vial, liquid scintillation cocktail and 50 μL of glacial acetic acid (to quench chemiluminescence) were added, and radioactivity was measured in a scintillation analyzer (PerkinElmer, MA, USA). The remainder of the lysate was used for protein determination by the Bradford protein assay (Bio-Rad, CA, USA). Radioactivity counts were corrected for protein levels and calculated as [^3H]-2DOG pmol/(mg protein min$^{-1}$). A robust nonlinear regression was used to fit a model to the experimental data and estimate the parameters of Michaelis–Menten equation. Experiments were performed in quadruplicates in three independent cultures.

## Real-Time PCR

Confluent monolayers were treated with 150 μM D-Asp in DMEM reduced serum medium (0.5% FBS) for the indicated time periods. After treatment, cells were harvested with TRIzol Reagent (Sigma-Aldrich, MO, USA) and total RNA was isolated using the Direct-zol RNA MiniPrep kit (Zymo Research, CA USA). Real-time PCR was performed for the amplification of glutamate/aspartate transporter (GLAST) with a cycler real-time PCR detection system (Applied Biosystem, CA, USA). The real-time PCR reactions were carried out in a total volume of 10 μL, containing a 20 ng RNA template of each sample, 200 nM of the appropriate primers (Table 1) and the KAPA SYBR FAST One-Step qRT-PCR Master Mix (1X KAPA SYBR FAST qPCR Master Mix Universal, 10 nM dNTP, 1X KAPA RT

**Table 1** Sequences of primers for RT-PCR reactions

| cDNA | Primers |
| --- | --- |
| GLAST | Forward: GGCTGCGGGCATTCCTC |
|  | Reverse: CGGAGACGATCCAAGAACCA |
| S17 | Forward: CCGCTGGATGCGCTTCATCAG |
|  | Reverse: TACACCCGTCTGGGCAAC |

*GLAST* glutamate/aspartate transporter, *S17* ribosomal protein S17

Mix and/or 1X ROX dye) (Kapa Biosystems, MA, USA). The PCR protocol was carried out as follows: 5 min at 42 °C for cDNA synthesis followed by 5 min at 95 °C for inactivation. Next, 3 s denaturation at 95 °C and 30 s at the specific annealing temperature (Ta) for 40 cycles. Fluorescence was detected at the end of each elongation step. Each sample was normalized with the relative amplification of the ribosomal protein S17. Relative quantification of mRNA in the samples was calculated by the $2^{-\Delta\Delta C_T}$ method. Experiments were performed in duplicates in four independent cultures.

## Statistical Analysis

Results are expressed as the mean ± SEM from a minimum of three independent cultures. Statistical analysis was carried out with one-way analysis of variance (ANOVA) followed by Dunnett's multiple comparison test. Multiple t tests (one unpaired t test per condition) were used for statistical analysis of transport kinetic experiments. A probability of 0.05 or less was considered statistically significant. All analyses were performed with GraphPad Prism Software (La Jolla California USA).

## Results

### Effect of Mn on Bergmann Glia Viability

Several studies had established the susceptibility of various cell types to Mn-induced neurotoxicity, astrocytes being more resistant compared to neurons [24–27]. The basal ganglia represent the main target for Mn neurotoxicity, but Mn is also well known to accumulate in other brain regions including the cerebellum [28, 29], thus providing a rationale for examining cells derived from this region. Cell viability of BGC was assessed by the MTT assay. As shown in Fig. 1, there was no apparent cell death in cultured Bergmann glia exposed to different time periods (0.5, 12 and 24 h, panel A, B, and C respectively), and Mn concentrations (100, 200, 300, 500 and 1000 μM). These results allowed us to move forward and evaluate the activity of the glutamate/aspartate transporter (GLAST) upon exposure to Mn in the absence of direct cell death.
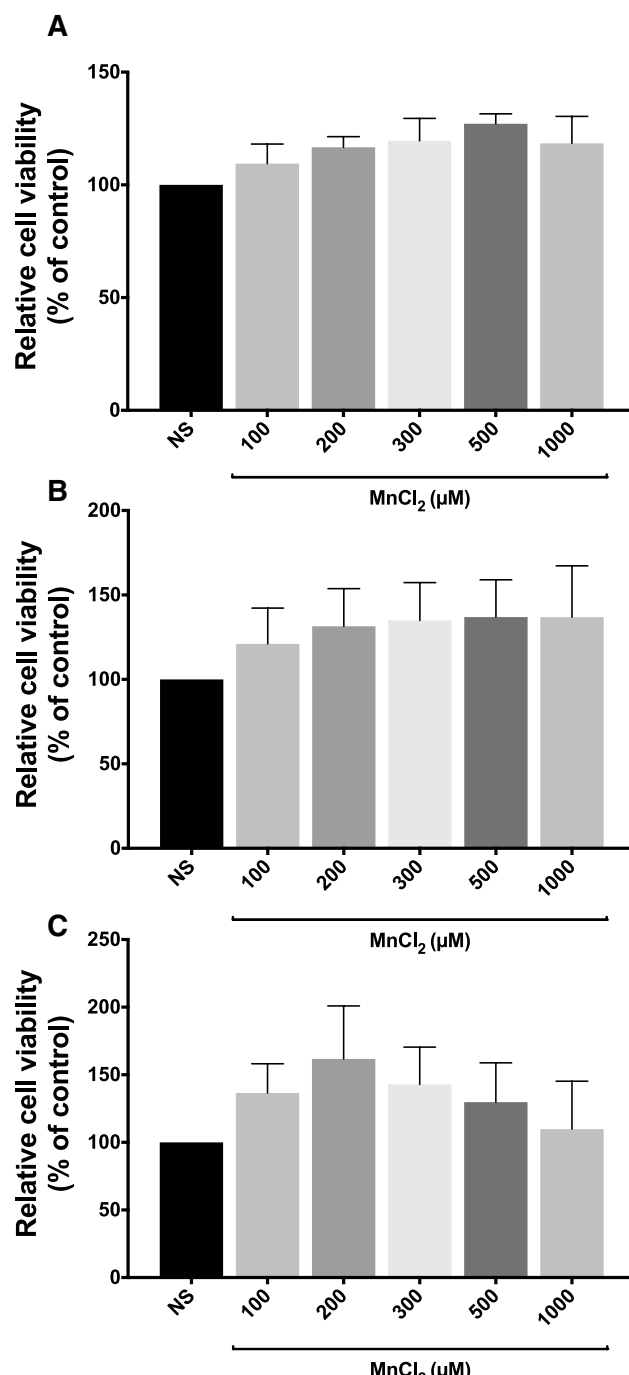


**Fig. 1** Mn does not affect cell viability of Bergmann glial cells. Total formazan was measured in control (*NS,* non-stimulated) and MnCl$_2$ (100, 200, 300, 500 or 1000 μM) treated primary cultures of BGC for 0.5 h (**a**), 12 h (**b**) or 24 h (**c**). Data represent the mean ± SEM from three independent sets of cultures, each performed in quadruplicate (one-way ANOVA followed by Dunnett's multiple comparison test)

### Mn Exposure Modifies [$^3$H] D-Aspartate Uptake

An increasing body of evidence have showed that Mn decreases GLAST/GLT-1 expression and function in

astrocyte cultures, possibly leading to excitotoxic neuronal injury [30, 31]. Although these studies have advanced our understanding on the mechanisms by which Mn represses these transporters, little is known about Mn-acute exposure consequences over their function. In order to gain insight into a plausible effect of Mn on GLAST activity we performed [3H]-D-Asp uptake assays with a fixed radioligand concentration (24.2 nM). BGC exposed to Mn (30 min), either to 200 or 300 µM, results in a significant increase in the amount of [3H]-D-Asp incorporated into the cells. As shown in Fig. 2, this effect is the same whether or not Mn is present in the uptake buffer. Although, when Mn is present in the uptake buffer a marginally reduction on GLAST activity increase is observed. Previous work from our lab has demonstrated that exposure to D-Asp (1 mM) reduces BGC uptake activity and leads to the activation of many signal transduction pathways [32, 33]. The fact that the Mn-induced GLAST activity increment is overturned by co-treatment with 1 mM D-Asp suggest that D-Asp and Mn trigger different mechanisms that affects GLAST function.

Next, we performed time and dose course studies to try to establish a direct correlation between the previously observed effect and Mn exposure. As depicted in Fig. 3, Mn-induced GLAST activity increase is dose (A) and time-dependent (B). Moreover, we can also observe that this effect reaches its maximum after 5 min of incubation.

From our perspective, two possible hypotheses were worth in-deep investigation. Either exposure to Mn increases plasma membrane glutamate transporters, or it affect the transporter's kinetic parameters. Our first approach was to perform [3H]-D-Asp uptake assays after a 24 h pre-incubation with 150 µM D-Asp. We know from unpublish work of our lab that a long-term incubation with D-Asp, at a concentration where $V_0$ tends to equal $V_{max}$ (150 µM D-Asp), significative lessens the total amount of GLAST mRNA (Fig. 4, box). Under these circumstances, the effect of Mn
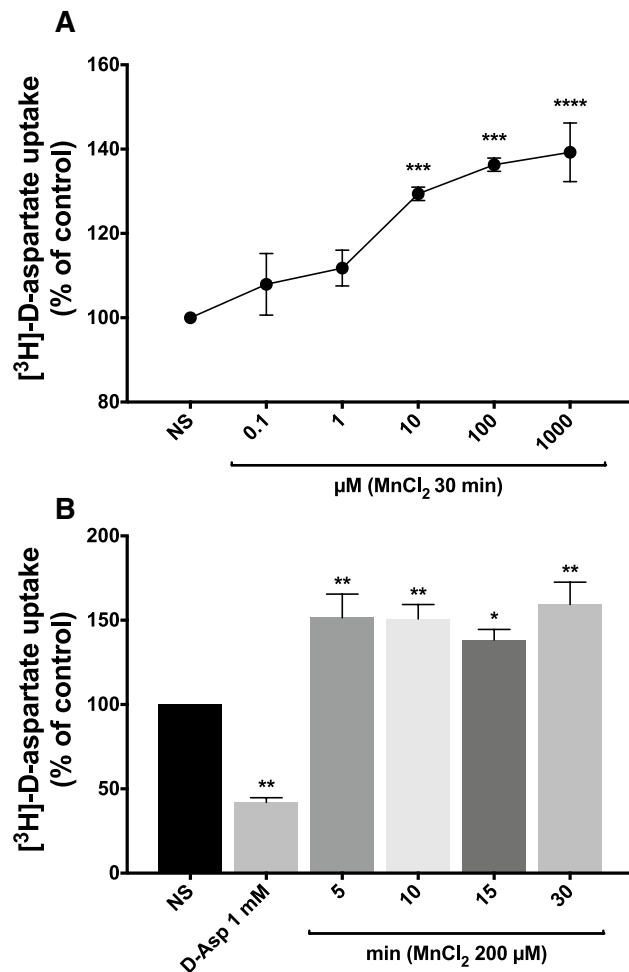
**Fig. 3** Mn-induced GLAST activity increase is dose- and time-dependent. **a** Total [3H]-D-Asp (0.4 µCi/mL, specific activity: 16.5 Ci/mmol) uptake was measured in control (NS, non-stimulated) and MnCl$_2$ (0.1, 1, 10, 100, or 1000 µM) treated primary cultures of BGC for 0.5 h. **b** Total [3H]-D-Asp (0.4 µCi/mL, specific activity: 16.5 Ci/mmol) uptake was measured in control (NS, non-stimulated) and MnCl$_2$ (200 µM) treated primary cultures of BGC for 5, 10, 15 or 30 min. Statistically significant differences between the controls and experimental groups are indicated by *p < 0.05, **p < 0.01, ***p < 0.001, ****p < 0.0001 versus NS. Data represent the mean ± SEM from three independent sets of cultures, each performed in quadruplicate (one-way ANOVA followed by Dunnett's multiple comparison test)

**Fig. 2** Mn exposure augments GLAST activity. Total [3H]-D-Asp (0.4 µCi/mL, specific activity: 16.5 Ci/mmol) uptake was measured in control (NS, non-stimulated) and MnCl$_2$ (200 or 300 µM) treated primary cultures of BGC for 0.5 h. MnCl$_2$ (300 µM) was added to the uptake buffer when indicated. Statistically significant differences between the controls and experimental groups are indicated by **p < 0.01, ***p < 0.001, ****p < 0.0001 versus NS. Data represent the mean ± SEM from four independent sets of cultures, each performed in quadruplicate (one-way ANOVA followed by Dunnett's multiple comparison test)

over GLAST activity remains as a discrete but significative augmentation that is also overturned by co-treatment with D-Asp (Fig. 4). This result suggests that the total amount of transporters at the plasma membrane may not be affected by Mn exposure.

In order to gain an insight of the mechanism by which Mn exposure increases GLAST activity, we decided to determine the kinetic parameters of the transporter in treated (200 μM for 30 min) and non-treated cells. As shown in panel A from Fig. 5, no apparent change in $V_{max}$ was detected. Furthermore, even there was a slightly reduction in the $K_m$, more importantly there was a considerable change in the catalytic efficiency ($V_{max}/K_m$) of the transporter in Mn-treated cells. $V_{max}/K_m$ is the rate constant for the coming together of substrate and product into a productive complex, which at concentrations much smaller than $K_m$ becomes the

limiting factor of the catalyzed reaction [34]. This change in the catalytic efficiency of GLAST could account for the increased amount of [³H]-D-Asp incorporated without altering the Michaelis–Menten parameters. In addition, we



**A**

| Saturable Transport | | |
|---|---|---|
| $V_{max}$ (pmol/mg·min) | $K_m$ (μmol/L) | $V_{max}/K_m$ (pmol/mg·min/(μmol/L)) |
| **NS** 469.0 | 21.21 | 22.112 |
| **MnCl₂** 437.0 | 16.46 | 26.549 |
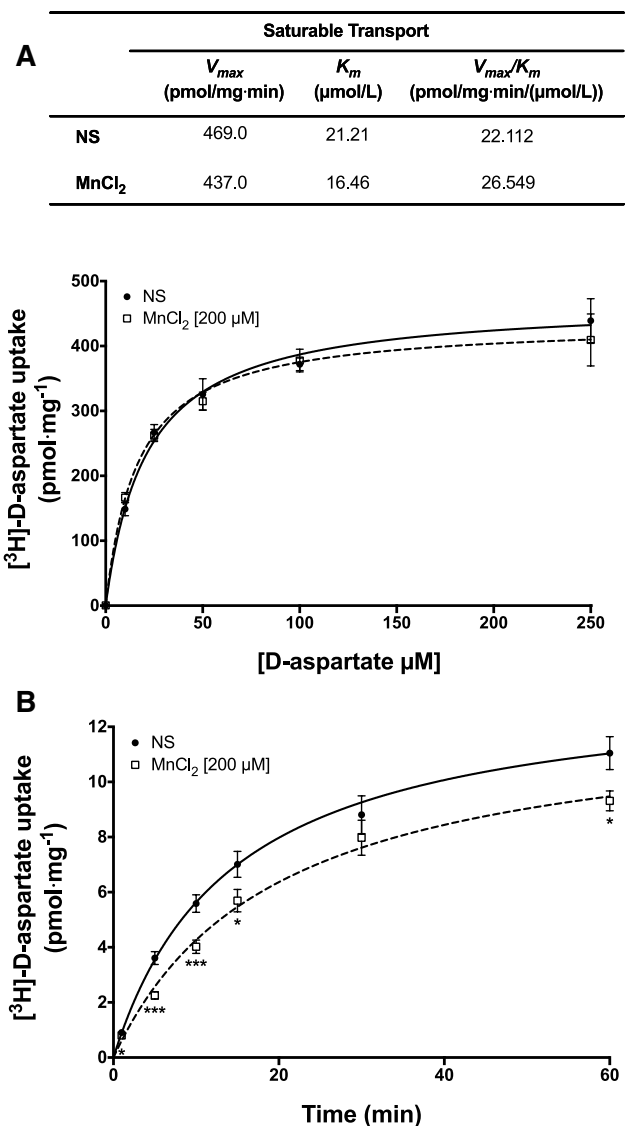
**Fig. 5** Impact of Mn exposure on GLAST kinetic parameters. **a** Total [³H]-D-Asp (0.4 μCi/mL, specific activity: 16.5 Ci/mmol) uptake was measured in control (NS, non-stimulated) and MnCl₂ (200 μM) treated primary cultures of BGC for 0.5 h. Varying concentrations of D-Asp (ranging from 0 to 250 μM) + [³H]-D-Asp (24.2 nM) were added to the uptake buffer and uptake was measured over a 12 min period of time in order to determine the kinetic parameters of the transporter. **b** Total [³H]-D-Asp (0.4 μCi/mL, specific activity: 16.5 Ci/mmol) uptake was measured in the presence (200 μM MnCl₂) or absence (NS) of Mn in the uptake buffer for 1, 5, 10, 15, 30 or 60 min. Statistically significant differences between the controls and experimental groups are indicated by *p < 0.05, ***p < 0.001 versus NS. Data represent the mean ± SEM from three independent sets of cultures, each performed in quadruplicate (Multiple t tests). A robust nonlinear regression was used to fit a model to our data and estimate the kinetic parameters



**Fig. 4** Mn effect on GLAST activity after a decrease in GLAST expression. Total [³H]-D-Asp (0.4 μCi/mL, specific activity: 16.5 Ci/ mmol) uptake was measured in control (NS, non-stimulated) and MnCl₂ (200 μM) treated primary cultures of BGC for 0.5 h after a pre-incubation with 150 μM D-Asp for 24 h. An incubation with 150 μM D-Asp for 24 h reduces the relative amount of GLAST mRNA in BGC (Box: Relative GLAST mRNA was quantify in control (NS) and D-Asp (150 μM) treated primary cultures of BGC for 3, 6, 12 or 24 h). Statistically significant differences between the controls and experimental groups are indicated by *p < 0.05, ****p < 0.0001 versus NS. Data represent the mean ± SEM from three independent sets of cultures, each performed in quadruplicate (one-way ANOVA followed by Dunnett's multiple comparison test)

decided to examine if the merely presence of Mn (200 μM) in the uptake buffer could have an effect on the function of the transporter. Panel B from Fig. 5 shows that there is a significant reduction on the incorporation of [³H]-D-Asp as a function of time when Mn is added to the uptake buffer. These results support the notion of a direct interaction of Mn with GLAST.

## Mn Affects Glucose Transport Activity

An increase in glutamate uptake in glial cells has been regarded as a signal to an augmented glucose uptake, in a metabolic coupling known as the *astrocyte/neuronal lactate shuttle* [35]. Glial metabolism is mainly glycolytic, and the accumulation of lactate leads to its release to the extracellular space via the monocarboxylate transporter 1 (MCT-1) [36]. Neurons take up this lactate via MCT-4 and metabolize it through the tricarboxylic acid cycle. In BGC cultures, we have previously reported an aspartate-dependent increase in [³H]-2-DOG influx [23]. To our surprise, a clear reduction in glucose uptake was found in Mn-treated cells (Fig. 6). This diminished transport is related to a significant decrease in $V_{max}$, suggesting a reduced amount of glucose transporters in the plasma membrane. Further experiments, beyond the scope of this communication, will address this non-expected finding.

## Discussion

The molecular mechanisms associated to Mn toxicity in the central nervous system have been focused on the deleterious action of this metal to the mitochondria of dopaminergic neurons and related model systems such as pheochromocytoma cells (PC-12) or induced pluripotent stem cells (iPSC)-derived human dopaminergic neurons [18, 37]. Nevertheless, the clear association between peripheral manganese levels and attention-deficit/hyperactivity disorder, calls for glutamatergic synapses as targets of this metal [38]. In fact, pioneer work from Aschner and his colleagues has demonstrated that one of the mechanisms of Mn neurotoxicity is associated with the disruption of the glutamate and glutamine transport systems in cortical glial cells [39, 40]. Despite of these well-documented reports, a closer look into the effects of acute Mn exposure of radial glial cells, that in the one hand completely enwrap glutamatergic synapses [41], and in the other hand do not undergo the so-called astrocytic conversion [42] is lacking. One could argue that this is not a major issue, but it is clear that GLAST regulation is different in radial glia such as Bergmann and Müller cells compared to cortical astrocytes [43–45]. While in radial glia glutamate down-regulates GLAST expression and function, the opposite effect takes place in cortical

| | Saturable Transport | | |
|---|---|---|---|
| | $V_{max}$ (pmol/mg·min) | $K_m$ (mmol/L) | $V_{max}/K_m$ (pmol/mg·min/(mmol/L)) |
| **NS** | 2317 | 3.360 | 689.583 |
| **MnCl₂** | 1908 | 4.018 | 474.863 |
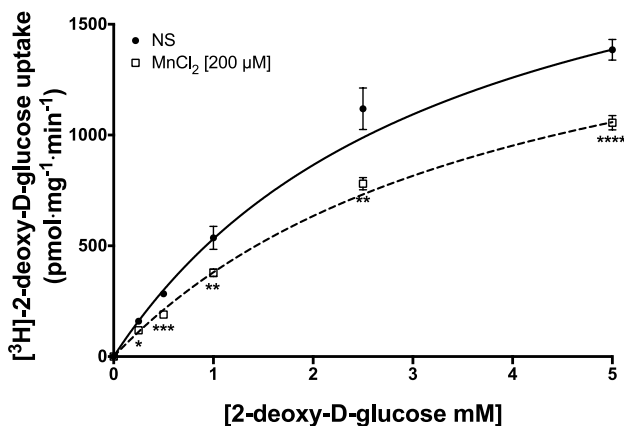


**Fig. 6** Mn decreases BGC glucose transport capacity. Total [³H]-2DOG (0.8 μCi/mL, specific activity: 32.5 Ci/mmol) uptake was measured in control (NS, non-stimulated) and MnCl₂ (200 μM) treated primary cultures of BGC for 0.5 h. Varying concentrations of 2DOG (ranging from 0 to 5 mM) + [³H]-2DOG (24.6 nM) were added to the uptake buffer and uptake was measured over a 30 min period of time in order to determine the kinetic parameters of the transporter. Statistically significant differences between the controls and experimental groups are indicated by *p < 0.05, **p < 0.01, ***p < 0.001, ****p < 0.0001 versus NS. Data represent the mean ± SEM from three independent sets of cultures, each performed in quadruplicate (Multiple t tests). A robust nonlinear regression was used to fit a model to our data and estimate the kinetic parameters

astrocytes. Therefore, in this contribution, we addressed the effect of short-term (min) manganese exposure of chick cerebellar BGC cultures, a model system that has proven useful in the characterization of the involvement of glial cells in glutamatergic glia/neuron coupling (reviewed in [46]).

After the corroboration that Mn at micromolar concentrations does not compromise cell viability, we explored the effect of the treatment of confluent BGC monolayers with this metal on GLAST activity. The high abundance of this protein allows us to measure the uptake activity at a low concentration of the radioactive tracer ([³H]-D-Asp). We were able to reproduce a 1.5-fold increase in GLAST activity due to the treatment of the cells with different Mn concentrations (Fig. 3, panel a). The effect is dose-dependent and reaches its maximal effect after 5 min. In order to gain an insight into the kinetic parameters affected by this metal, we performed Michaelis–Menten saturation curves. Although at first sight we expected an increase in $V_{max}$ that could be related to an augmentation of GLAST molecules

**Fig. 7** Proposed model for the effects of acute Mn exposure on GLAST activity in BGC. See text for details
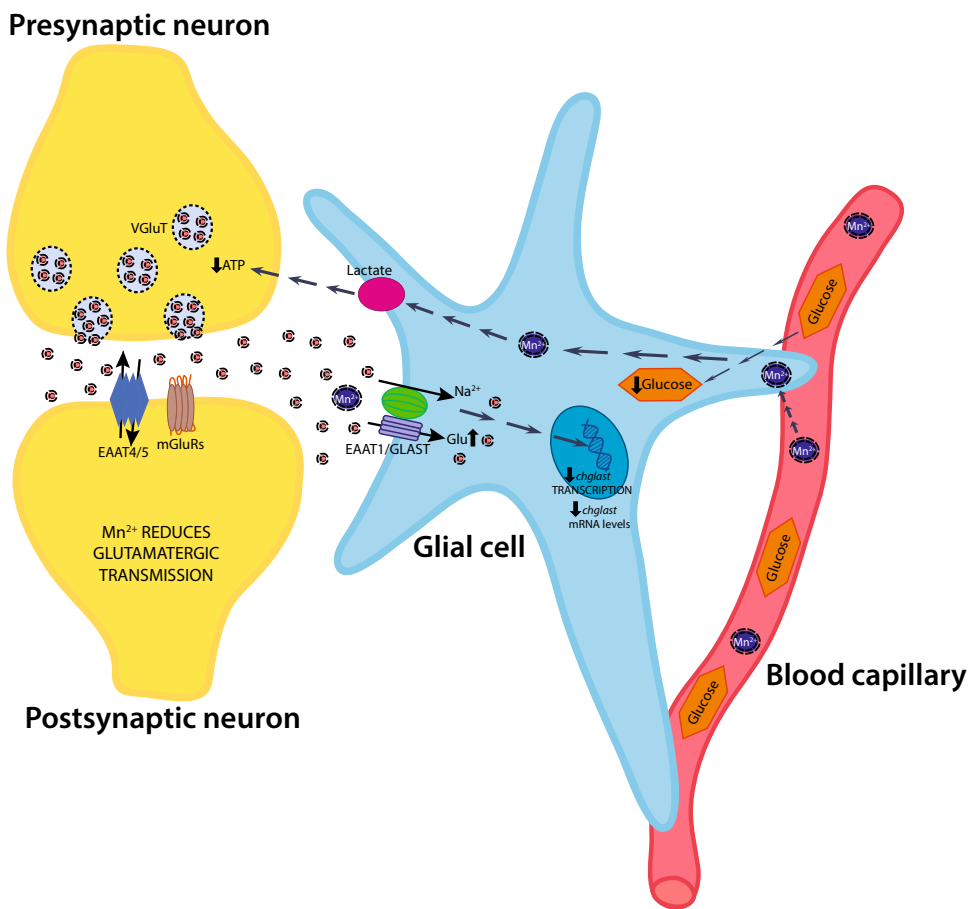
in the plasma membrane, we could only detect a discrete augmentation of the affinity of the transporter triggered by Mn. Interestingly, the ratio between $V_{max}$ and $K_m$, a parameter known as the catalytic efficiency [47], presented an increase after incubation with Mn. It is tempting to speculate that this metal interacts with the glutamate transporters present at the plasma membrane leading to a change in their conformation that is reflected in an increased uptake efficiency. To better understand this direct possible interaction, we performed a time course of [$^3$H] D-Asp uptake in the presence of 200 μM MnCl$_2$. A discrete reduction in the uptake was obtained and although the identity of the metal molecular target(s) is unknown, a direct interaction of Mn with the transporter cannot be ruled out. Still, we are unable to explain the increase in the uptake at low aspartate concentrations when the cells are preincubated with Mn. We expected either an increase in $V_{max}$ or a clear-cut change in the affinity of the transporter. This is not the case; we only detected an augmentation in the transporter catalytic efficiency that in fact reflects the increase in GLAST activity upon MnCl$_2$ exposure.

What could be the relevance of this small change in glutamate transport in the context of Bergmann glia function? To shed some light into this issue, we decided to evaluate the

uptake of [$^3$H]-2-DOG. Glutamate uptake has been linked to glucose entrance in various glial systems, including cultured Bergmann glia. Again, an unexpected result was detected. A clear reduction in glucose uptake is present after a 30 min incubation with 200 μM MnCl$_2$. It is an unexpected finding taking into consideration that upon Mn exposure only a small increase in aspartate transport is present, one would expect either no effect in glucose uptake or a small increase. At this stage, it is clear that the exposure to environmental relevant concentrations of Mn has a complex action in cultured Bergmann glia that it is quite possible to interfere with glutamatergic transmission in the cerebellar cortex in vivo [48]. A graphical summary of our findings and their plausible impact in glutamatergic neurons is presented in Fig. 7. It is tempting to speculate that Mn neurotoxicity is at least in part, glia-mediated: the recorded decrease in D-Asp incorporation as a function of time when Mn is present could lead to a sustained increase in extra synaptic glutamate, that in turn could over-stimulate neuronal glutamate receptors resulting in an excitotoxic insult. Moreover, the decrease in glucose uptake after Mn exposure could interrupt the astrocyte/neuronal/lactate shuttle reducing the lactate supplied to neurons, with a consequent decrease in the repolarization process and thus hampering glutamatergic transmission. Work actually

in progress in our group is aimed to characterize the effect Mn exposure in glia metabolism.

# References

1. Maj C, Minelli A, Giacopuzzi E et al (2016) The role of metabotropic glutamate receptor genes in schizophrenia. Curr Neuropharmacol 14:540–550

2. Mayer ML (2011) Structure and mechanism of glutamate receptor ion channel assembly, activation and modulation. Curr Opin Neurobiol 21:283–290. https://doi.org/10.1016/j.conb.2011.02.001

3. Borroto-Escuela DO, Tarakanov AO, Brito I, Fuxe K (2018) Glutamate heteroreceptor complexes in the brain. Pharmacol Rep 70:936–950. https://doi.org/10.1016/j.pharep.2018.04.002

4. Ambrogini P, Torquato P, Bartolini D et al (2019) Excitotoxicity, neuroinflammation and oxidant stress as molecular bases of epileptogenesis and epilepsy-derived neurodegeneration: the role of vitamin E. Biochim Biophys Acta Mol Basis Dis. https://doi.org/10.1016/j.bbadis.2019.01.026

5. Danbolt NC, Furness DN, Zhou Y (2016) Neuronal vs glial glutamate uptake: resolving the conundrum. Neurochem Int 98:29–45. https://doi.org/10.1016/j.neuint.2016.05.009

6. Danbolt NC (2001) Glutamate uptake. Prog Neurobiol 65:1–105

7. Chaudhry FA, Schmitz D, Reimer RJ et al (2002) Glutamine uptake by neurons: interaction of protons with system a transporters. J Neurosci 22:62–72

8. Billups D, Marx M-C, Mela I, Billups B (2013) Inducible presynaptic glutamine transport supports glutamatergic transmission at the calyx of Held synapse. J Neurosci 33:17429–17434. https://doi.org/10.1523/JNEUROSCI.1466-13.2013

9. Shank RP, Campbell GL (1984) Glutamine, glutamate, and other possible regulators of alpha-ketoglutarate and malate uptake by synaptic terminals. J Neurochem 42:1162–1169

10. Martínez-Lozada Z, Guillem AM, Flores-Méndez M et al (2013) GLAST/EAAT1-induced Glutamine release via SNAT3 in Bergmann glial cells: evidence of a functional and physical coupling. J Neurochem 125:545–554. https://doi.org/10.1111/jnc.12211

11. Marx M-C, Billups D, Billups B (2015) Maintaining the presynaptic glutamate supply for excitatory neurotransmission. J Neurosci Res 93:1031–1044. https://doi.org/10.1002/jnr.23561

12. Takeda A (2003) Manganese action in brain function. Brain Res Brain Res Rev 41:79–87

13. Kwakye G, Paoliello M, Mukhopadhyay S et al (2015) Manganese-induced parkinsonism and Parkinson's disease: shared and distinguishable features. Int J Environ Res Public Health 12:7519–7540. https://doi.org/10.3390/ijerph120707519

14. Reaney SH, Bench G, Smith DR (2006) Brain accumulation and toxicity of Mn(II) and Mn(III) exposures. Toxicol Sci 93:114–124. https://doi.org/10.1093/toxsci/kfl028

15. Robison G, Sullivan B, Cannon JR, Pushkar Y (2015) Identification of dopaminergic neurons of the substantia nigra pars compacta as a target of manganese accumulation. Metallomics 7:748–755. https://doi.org/10.1039/c5mt00023h

16. Wang C, Ma Z, Yan D-Y et al (2018) Alpha-synuclein and calpains disrupt SNARE-mediated synaptic vesicle fusion during manganese exposure in SH-SY5Y cells. Cells 7:258. https://doi.org/10.3390/cells7120258

17. Liu C, Yan D-Y, Tan X et al (2018) Effect of the cross-talk between autophagy and endoplasmic reticulum stress on Mn-induced alpha-synuclein oligomerization. Environ Toxicol 33:315–324. https://doi.org/10.1002/tox.22518

18. Chen P, Bornhorst J, Aschner M (2018) Manganese metabolism in humans. Front Biosci (Landmark Ed 23:1655–1679.

19. Lee E, Karki P, Johnson JJ et al (2017) Manganese control of glutamate transporters' gene expression. Adv Neurobiol 16:1–12. https://doi.org/10.1007/978-3-319-55769-4_1

20. Somogyi P, Takagi H, Richards JG, Mohler H (1989) Subcellular localization of benzodiazepine/GABAA receptors in the cerebellum of rat, cat, and monkey using monoclonal antibodies. J Neurosci 9:2197–2209

21. Ortega A, Eshhar N, Teichberg VI (1991) Properties of kainate receptor/channels on cultured Bergmann glia. Neuroscience 41:335–349

22. Ruiz M, Ortega A (1995) Characterization of an Na(+)-dependent glutamate/aspartate transporter from cultured Bergmann glia. NeuroReport 6:2041–2044

23. Mendez-Flores OG, Hernández-Kelly LC, Suárez-Pozos E et al (2016) Coupling of glutamate and glucose uptake in cultured Bergmann glial cells. Neurochem Int 98:72–81. https://doi.org/10.1016/j.neuint.2016.05.001

24. Lee E-SY, Yin Z, Milatovic D et al (2009) Estrogen and tamoxifen protect against Mn-induced toxicity in rat cortical primary cultures of neurons and astrocytes. Toxicol Sci 110:156–167. https://doi.org/10.1093/toxsci/kfp081

25. Malthankar GV, White BK, Bhushan A et al (2004) Differential lowering by manganese treatment of activities of glycolytic and tricarboxylic acid (TCA) cycle enzymes investigated in neuroblastoma and astrocytoma cells is associated with manganese-induced cell death. Neurochem Res 29:709–717

26. Kim J, Pajarillo E, Rizor A et al (2019) LRRK2 kinase plays a critical role in manganese-induced inflammation and apoptosis in microglia. PLoS ONE 14:e0210248. https://doi.org/10.1371/journal.pone.0210248

27. Gandhi D, Sivanesan S, Kannan K (2018) Manganese-induced neurotoxicity and alterations in gene expression in human neuroblastoma SH-SY5Y cells. Biol Trace Elem Res 183:245–253. https://doi.org/10.1007/s12011-017-1153-5

28. Sepúlveda MR, Dresselaers T, Vangheluwe P, Everaerts W (2012) Evaluation of manganese uptake and toxicity in mouse brain during continuous MnCl2 administration using osmotic pumps. Contrast Media Mol Imaging 7(4):426–434. https://doi.org/10.1002/cmmi.1469

29. Ye Q, Kim J (2015) Effect of olfactory manganese exposure on anxiety-related behavior in a mouse model of iron overload hemochromatosis. Environ Toxicol Pharmacol 40:333–341. https://doi.org/10.1016/j.etap.2015.06.016

30. Karki P, Smith K, Johnson J et al (2014) Role of transcription factor yin yang 1 in manganese-induced reduction of astrocytic glutamate transporters: putative mechanism for manganese-induced neurotoxicity. Neurochem Int 88:53–59. https://doi.org/10.1016/j.neuint.2014.08.002

31. Karki P, Webb A, Smith K et al (2014) Yin Yang 1 is a repressor of glutamate transporter EAAT2, and it mediates manganese-induced decrease of EAAT2 expression in astrocytes. Mol Cell Biol 34:1280–1289. https://doi.org/10.1128/MCB.01176-13

32. Martínez-Lozada Z, Hernández-Kelly LC, Aguilera J et al (2011) Signaling through EAAT-1/GLAST in cultured Bergmann glia cells. Neurochem Int 59:871–879. https://doi.org/10.1016/j.neuint.2011.07.015

33. Martinez D, Garcia L, Aguilera J, Ortega A (2014) An acute glutamate exposure induces long-term down regulation of GLAST/EAAT1 uptake activity in cultured Bergmann glia cells. Neurochem Res 39:142–149. https://doi.org/10.1007/s11064-013-1198-6

34. Northrop DB (1998) On the Meaning of Km and V/K in Enzyme Kinetics. J Chem Educ 75:1153. https://doi.org/10.1021/ed075p1153

35. Pellerin L, Magistretti PJ (2012) Sweet sixteen for ANLS. J Cereb Blood Flow Metab 32:1152–1166. https://doi.org/10.1038/jcbfm.2011.149

36. Broer S, Rahman B, Pellegri G et al (1997) Comparison of lactate transport in astroglial cells and monocarboxylate transporter 1 (MCT 1) expressing Xenopus laevis oocytes. Expression of two different monocarboxylate transporters in astroglial cells and neurons. J Biol Chem 272:30096–30102

37. Neely MD, Davison CA, Aschner M, Bowman AB (2017) Manganese and rotenone-induced oxidative stress signatures differ in iPSC-derived human dopamine neurons. Toxicol Sci 159:366–379. https://doi.org/10.1093/toxsci/kfx145

38. Shih J-H, Zeng B-Y, Lin P-Y et al (2018) Association between peripheral manganese levels and attention-deficit/hyperactivity disorder: a preliminary meta-analysis. Neuropsychiatr Dis Treat 14:1831–1842. https://doi.org/10.2147/NDT.S165378

39. Sidoryk-Wegrzynowicz M, Aschner M (2013) Manganese toxicity in the central nervous system: the glutamine/glutamate-gamma-aminobutyric acid cycle. J Intern Med 273:466–477. https://doi.org/10.1111/joim.12040

40. Johnson J, Pajarillo EAB, Taka E et al (2018) Valproate and sodium butyrate attenuate manganese-decreased locomotor activity and astrocytic glutamate transporters expression in mice. Neurotoxicology 64:230–239. https://doi.org/10.1016/j.neuro.2017.06.007

41. Somogyi P, Tamás G, Lujan R, Buhl EH (1998) Salient features of synaptic organisation in the cerebral cortex. Brain Res Brain Res Rev 26:113–135

42. Buffo A, Rossi F (2013) Origin, lineage and function of cerebellar glia. Prog Neurobiol 109:42–63. https://doi.org/10.1016/j.pneurobio.2013.08.001

43. Gegelashvili G, Civenni G, Racagni G et al (1996) Glutamate receptor agonists up-regulate glutamate transporter GLAST in astrocytes. NeuroReport 8:261–265

44. Bernabe A, Mendez JA, Hernandez-Kelly LCR, Ortega A (2003) Regulation of the Na$^+$-dependent glutamate/aspartate transporter in rodent cerebellar astrocytes. Neurochem Res 28:1843–1849

45. Ramirez-Sotelo G, Lopez-Bayghen E, Hernandez-Kelly LCR et al (2007) Regulation of the mouse Na$^+$-dependent glutamate/aspartate transporter GLAST: putative role of an AP-1 DNA binding site. Neurochem Res 32:73–80. https://doi.org/10.1007/s11064-006-9227-3

46. Martinez-Lozada Z, Ortega A (2015) Glutamatergic transmission: a matter of three. Neural Plast 2015:787396. https://doi.org/10.1155/2015/787396

47. Koshland DE (2002) The application and usefulness of the ratio kcat/KM. Bioorg Chem 30:211–213. https://doi.org/10.1006/BIOO.2002.1246

48. Miyazaki T, Yamasaki M, Hashimoto K et al (2017) Glutamate transporter GLAST controls synaptic wrapping by Bergmann glia and ensures proper wiring of Purkinje cells. Proc Natl Acad Sci USA 114:7438–7443. https://doi.org/10.1073/pnas.1617330114

*Review Article*

# Critical Involvement of Glial Cells in Manganese Neurotoxicity

**Jazmín Soto-Verdugo** [iD] **and Arturo Ortega** [iD]

*Departamento de Toxicología, Centro de Investigación y de Estudios Avanzados del Instituto Politécnico Nacional,*
*07360 Ciudad de México, Mexico*

Correspondence should be addressed to Arturo Ortega; arortega@cinvestav.mx

Over the years, most of the research concerning manganese exposure was restricted to the toxicity of neuronal cells. Manganese is an essential trace element that in high doses exerts neurotoxic effects. However, in the last two decades, efforts have shifted toward a more comprehensive approach that takes into account the involvement of glial cells in the development of neurotoxicity as a brain insult. Glial cells provide structural, trophic, and metabolic support to neurons. Nevertheless, these cells play an active role in adult neurogenesis, regulation of synaptogenesis, and synaptic plasticity. Disturbances in glial cell function can lead to neurological disorders, including neurodegenerative diseases. This review highlights the pivotal role that glial cells have in manganese-induced neurotoxicity as well as the most sounding mechanisms involved in the development of this phenomenon.

## 1. Introduction

The central nervous system (CNS) is comprised mainly of two types of cells: neurons and glia. From a neurocentric point of view, neurons are the cells that process and transfer information in the brain by triggering action potentials and propagating these electrical signals [1]. On the other hand, glial cells, which are as numerous as neurons across the whole brain [2], were first described as the connective structure that holds nerve cells in place. However, in the last decades, these cells are starting to be recognized as master regulators of synaptic plasticity [3]. Glial cells can be classified into two main categories: macroglia and microglia. Oligodendrocytes and astrocytes (members of the former category) are originated in the embryonic neural tube and forebrain from neural progenitor cells (NPC), then NPCs are transformed into radial glia, which are precursors of neurons and glia [4]. Following the production of neurons, a "gliogenic switch" allows radial glia to give rise to astrocytes and oligodendrocytes. Oligodendrocytes, the myelinating glia of the CNS, are produced *via* the generation of intermediate precursor cells known as NG2 glia or oligodendrocyte precursor cells (OPC). Astrocytes are also produced from radial glia but in response to distinct external signals in specific regions of the brain. Interestingly, microglia are generated from primitive macrophages in the embryonic yolk sac that migrates to the CNS and becomes microglia [4, 5]. Each of these types of glial cells has essential roles in CNS development and is a fundamental piece for the correct functioning of the brain.

Manganese (Mn) is the $5^{th}$ and $12^{th}$ more abundant metal and element, respectively; it is ubiquitously found across the earth's crust. Moreover, Mn is an essential trace element required for proper physiological development and tight regulation of cellular and biochemical reactions [6, 7]. This element is mainly found in its $Mn^{2+}$ and $Mn^{3+}$ species within mammalian tissues, although it can be found in a great variety of oxidation states [6]. Due to their essentiality, Mn is an important cofactor of enzymes like glutamine synthetase (GS), superoxide dehydrogenase (SOD), arginase, and pyruvate carboxylase. Some of the main functions in which Mn has been implicated are protein, lipid, and carbohydrate metabolism, detoxification of reactive oxide species (ROS), immune response, energy metabolism, and glucose regulation, among others [8, 9]. Nevertheless, chronic overexposure to this transition metal may result in a neurological

disorder known as "manganism," which resembles some of the symptoms of Parkinson's disease (PD) [10]. The toxic effects of Mn in the brain respond to an increase in the levels of this metal by around three times the concentration found in "normal" conditions. The "normal" concentrations are ranging from 1.1-2.9 ppm in the whole human brain [11]. Hence, Mn is necessary for proper brain function, yet alterations in its physiological levels can cause neurotoxic effects, either overexposure or insufficiency, although the last one is less common [12], which points out the hormetic nature of Mn and its nonmonotonic dose-response patterns for the development of neurotoxicity. The main routes of exposure are inhalation due to exposure to Mn enriched dust, fumes, or particulate matter and by ingestion of food or water rich in Mn. Upon Mn absorption, this metal widely distributes to a variety of body compartments [13]. The capability of Mn to cross several blood-tissue barriers resides in its potential to be transported by several membrane carriers. The divalent metal transporter 1 (DMT1), transferrin receptor (TfR), zinc transporters ZIP8 and ZIP14, citrate transporter, choline transporter, dopamine transporter (DAT), and calcium ($Ca^{2+}$) channels had been described for import of this metal, whereas ferroportin (Fpn), SLC30A10, ATPase 13A2 (ATP13A2), and secretory pathway $Ca^{2+}$-ATPase 1 (SPCA1) for the export [14]. Mn is eliminated mainly via the hepatobiliary system; meanwhile, other excretion pathways like the urinary and pancreatic are minimally engaged in Mn clearance [15]. In humans, the whole-body half-life of Mn has been described after oral administration and intravenous injection, with values ranging from 6-43 days and 24-74 days, respectively [16]. However, loss of function in Mn transporters promotes its accumulation in the CNS. Hepatic dysfunction, such as cirrhosis and hepatic encephalopathy, increases the risk of excessive build-up of Mn concentrations in the brain [17].

This contribution is aimed at emphasizing the pivotal role that glial cells have in the neurotoxicity induced by Mn exposure and the most supported mechanisms involved in the development of this phenomenon.

## 2. The Importance of Glial Cells in Neurotoxicity Development

The days when glial cells were considered the "glue" of synapses are fortunately long past gone. Nowadays, increasing evidence has emphasized their crucial role in proper brain functioning and CNS development [18]. Indeed, these cells provide structural, trophic, and metabolic support to neurons [19] and play an active role in important brain functions such as the uptake and synthesis of neurotransmitters, buffering of ion strength, immunomodulation, and adult neurogenesis, acting as a part of the blood-brain barrier controlling the in and out of substances from the bloodstream to the brain, intercellular communication through the formation of a glial syncytium, regulation of synaptogenesis, and synaptic plasticity while associated to synapses [4, 20]. Even though glial cells are incapable of firing action potentials, these cells can communicate with other cells through chemical signals, such as neurotransmitters, ions,

neurotrophic, and neurotoxic factors; since these cells express a broad repertoire of membrane transporters, neurotransmitters as well as neurotrophic receptors, voltage-gated ion channels, and ion exchangers that allow them to receive and send signals to the neurons and other glia [21, 22]. Within the glial network, calcium activity (spatial and temporally coordinated) influences different states of the neuronal network leading to repercussions in high-order cognitive functions [23]. Over the last years, it has been well documented that disturbances in glia physiology can lead to neurological disorders, including neurodegenerative diseases such as PD, Alzheimer's, and Huntington's diseases (AD and HD), as well as epilepsy, ischemic stroke, depression, autism, or glioma [1]. This shifting from the neurocentric approach has spotlighted the fact that there is more nuance in glial cells' crosstalk with neurons than previously thought. Moreover, whether glia dysfunction is the cause or a consequence of neurotoxicology development is a question that remains to be determined but is undoubtedly glia is a key player that should not be neglected.

*2.1. Glia Involvement in Mn Neurotoxicity.* Several studies have focused on the effects of Mn toxicity in the CNS since James Couper first described "manganism" as a neurological disorder caused by overexposure to Mn dioxide in the midnineteenth century [24]. Over the years, most of the research concerning Mn exposure was centered on the disruption of neurons, given that these cells are more sensitive to the toxic effects of Mn. However, in the last two decades, it has shifted to a more comprehensive approach that considers the involvement of glia in the development of neurotoxicity [25, 26]. Some of the major effects of Mn toxicity in glia are listed below.

*2.1.1. Astrocytes.* The most abundant type of glial cells in the CNS is astrocytes. A single human astrocyte is capable of ensheathing more than 100,000 synapses [5]. The best-characterized functions of these cells are the turnover of neurotransmitters, ion homeostasis, as a constituent of the neurovascular unit, synaptogenesis, neuronal remodeling, and so on [18]. Astrocytes can be classified at least into two main categories regarding their localization and morphology: fibrous in the white matter with a clear star shape, and protoplasmic in the grey matter with a more plain appearance [27]. Furthermore, astrocytes oversee and protect neurons from neurotoxic insults elicited by heavy metals, which makes them the primary target of heavy metal toxicity [28]. Mn accumulates 50-200 times more in astrocytes than in neurons [29, 30]. Besides, astrocytes are more resilient to the cytotoxic effects of Mn exposure [31, 32], but even at concentrations below the cytotoxic threshold, there are several adverse effects in glial cells that could affect glia-neuron homeostasis. The first study that put in the limelight the repercussions of Mn overexposure on astrocytes observed that Mn increases nitric oxide (NO) synthesis in astrocytes [33]. NO is a free radical and a known signaling messenger that may cause detrimental consequences to neighboring neurons when it is produced persistently [34]. Several studies have demonstrated that Mn exposure

disrupts the glutamate/glutamine cycle (GGC) [35], rendering a myriad of adverse consequences that are going to be discussed in further detail below.

*2.1.2. Radial Glia.* As mentioned before, radial glia is a specialized type of astrocyte that has been identified as a primary progenitor cell for both astrocytes and neurons. Radial glia serves as a scaffold for the migration of nascent cortical and cerebellar neurons, underlining their pivotal role in CNS development [21]. Moreover, these cells have an active role in adult neurogenesis due to their proven capacity to divide and give rise to new neurons, in response to brain injury, acting as neural stem cells in the adult CNS [5]. There is a great diversity of radial glia in the CNS; Müller radial glia can be found across the retina, in the cerebellum: Bergmann glia, tanycytes are located in the third ventricle of the brain, to mention few examples [36]. An increase in the catalytic efficiency of glutamate transporters, as well as a decrease in glucose transport of Bergmann glia, was found after short-term exposure to Mn, with an absence of cell death [37]. This is not a minor finding since glial metabolism is predominantly glycolytic and metabolic coupling of glutamate and glucose transport has been described [38]. Considering that Bergmann glia outnumbers neurons in the cerebellar cortex and that the neurotoxic effects of Mn over cerebellar granular neurons are more pronounced than in neocortical neurons [39], the potential role of the local radial glia in the neurotoxic effects of Mn should not be taken lightly.

*2.1.3. Microglia.* Widely known as the resident immune cell of the CNS, microglia makes up about 10% of the CNS glia [22]. The leading roles of microglia are immune surveillance, extracellular matrix remodeling, clearance of cellular debris and synaptic pruning, neurogenesis regulation, among other functions [18, 22]. Under basal conditions, microglia have a distinct ramified morphology with extended processes for CNS surveillance. Meanwhile, upon a pathologic scenario, these cells present enlarged somas and sprouts and an ameboid or hypertrophic phenotype [40]. In an activated mode, microglia triggers and maintains an inflammatory response, deluging neurons to inflammatory mediators leading to neuronal cell death, making them an essential mediator of neurotoxicity phenomena. Mn exposure upregulates inducible nitric oxide synthase (iNOS) and tumor necrosis factor-$\alpha$ (TNF-$\alpha$), and interleukin-1$\beta$ (IL-1$\beta$) with dopaminergic dysfunction after microglial activation [41, 42]. Moreover, microglial TNF-$\alpha$ and IL-1$\beta$ release induced by Mn is presumably triggered by the activation of the Janus kinase 2/signal transducer and activator of transcription 3 (JAK2-STAT3) signaling pathway [43]. Sodium *para*-aminosalicylic acid (PAS-Na) prevents Mn effects [44, 45]. Moreover, Mn treatment induces microglial cell death by regulating necrosis due to lysosomal membrane permeabilization and cathepsin activation [46].

# 3. Mechanisms of Toxicity Elicited by Mn in Glial Cells

*3.1. Glu/Gln Cycle.* Glutamate (Glu) is the main excitatory amino acid neurotransmitter in vertebrates. Once released

in the synaptic cleft exerts its actions through the activation of specific receptors expressed in the plasma membrane of neurons and glial cells. Glu receptors have been categorized into two main groups: ionotropic Glu receptors, which are ligand-gated ion channels rendering excitatory Glu-evoked currents, and metabotropic Glu receptors, which are G-protein coupled receptors managing cellular processes *via* second messenger signaling [47]. Overactivation of Glu receptors may end in neuronal death, a phenomenon coined as "*excitotoxicity*" [48]. Since no known enzyme degrades Glu in the extracellular space, the removal of Glu from the synaptic cleft is needed to maintain the levels necessary for appropriate synaptic transmission. Such work is carried out by high-affinity $Na^+$-dependent transporters mainly found in astrocytes. Once inside the glial cell, the enzyme glutamine synthetase (GS) converts Glu to glutamine (Gln) or is taken up into the Krebs cycle after being transformed into $\alpha$-ketoglutarate [49]. The transformed Gln is imported into the astrocyte by a series of Gln transporters allowing the recycling of neurotransmitters and reducing the energy expenditure of the neurons [50]. This process is termed GGC or Glu/Gln shuttle (Figure 1(a)), and the impairment of this cycle is a common mechanism of neurodegenerative diseases and other disorders [51].

*3.1.1. Glutamate Transport.* The levels of Glu in the synaptic cleft are tightly regulated by a family of sodium-dependent plasma membrane transporters, known as excitatory amino acid transporters (EAATs) [51, 52]. There are five members in this family of transporters, glutamate/aspartate transporter (GLAST)/EAAT1, Glu transporter 1 (Glt-1)/EAAT2, excitatory amino acid carrier 1 (EAAC1)/EAAT3, EAAT4, and EAAT5. Glt-1 and GLAST are mainly expressed in astrocytes, although Glt-1 can be expressed in hippocampal neurons. EAAC1 and EAAT4 can be found mostly in neurons, whereas EAAT5 is expressed in bipolar cells and photoreceptors in the retina [53]. EAATs transport a single molecule of Glu paired with three $Na^+$ ions and a proton, with the antiport of a $K^+$ ion. The timely removal of Glu from the synaptic cleft and its consequent recycling is fundamental for proper glutamatergic neurotransmission and to avoid excitotoxicity (Figure 1(a)) [53]. The disruption of the Glu transport has been a focal point in the study of the critical role of glial cells in Mn neurotoxicity (Figure 1(b)). As shown in Table 1, Mn exposure disrupts glutamate transport in different models *in vivo* and *in vitro*. Glu uptake decreased in primary cortical astrocytes exposed to Mn [54] and in Chinese hamster ovarian cells transfected with GLAST and Glt-1 [55]. Nonhuman primates presented a decrease in the protein and mRNA levels of GLAST and Glt-1 in different brain regions after Mn exposure [52, 56]. Contrastingly, short-term exposure to Mn in Bergmann glia showed an increase in the uptake and catalytic efficiency of GLAST [37]. While several studies have demonstrated that Mn affects Glu transporters (Table 1), current research has been directed to dissect the mechanisms by which Mn downregulates GLAST and Glt-1. Previous reports revealed that astrocytes treated with Mn had increased activity of the protein kinase C (PKC) [57]. Besides, activation of
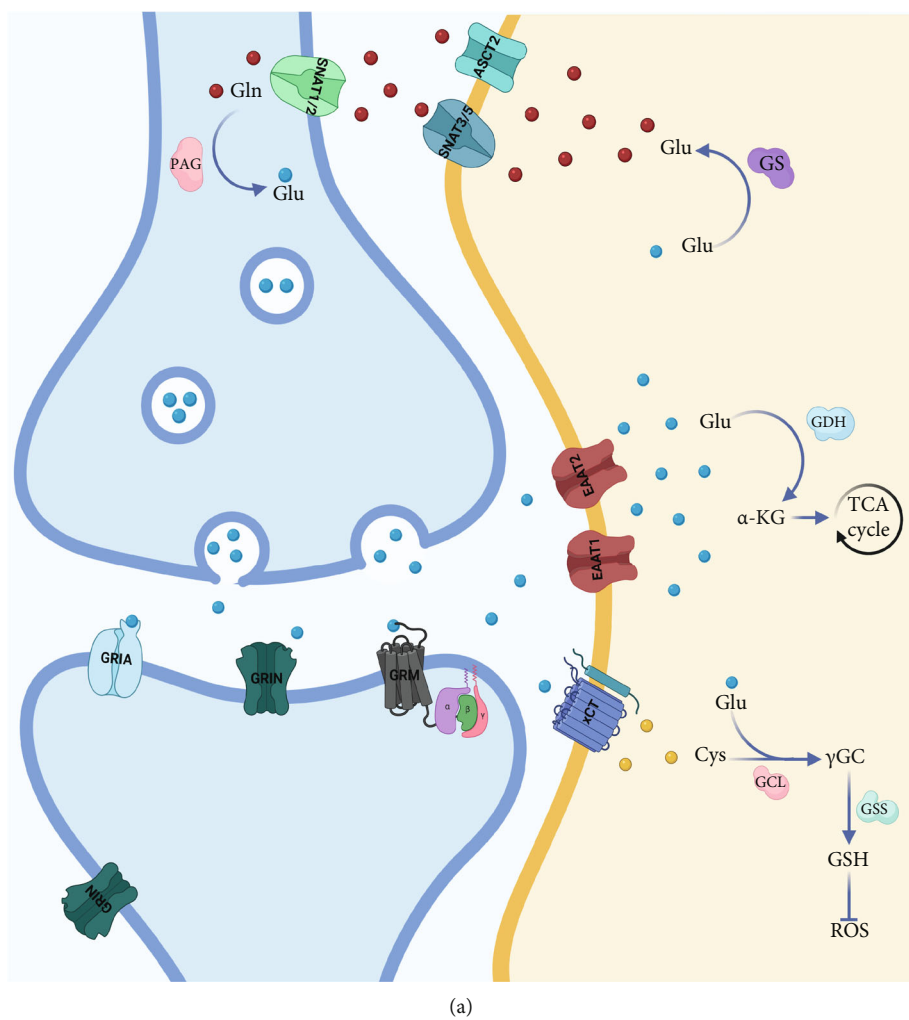
(a)

FIGURE 1: Continued.

(b)
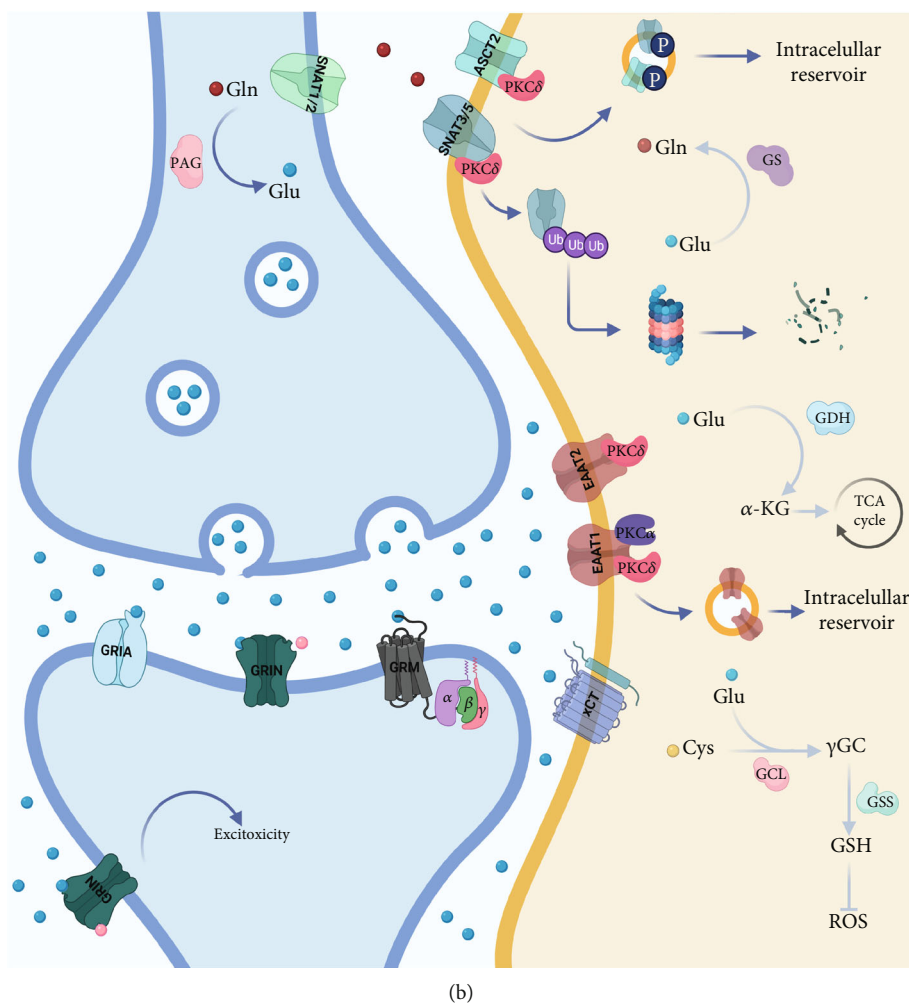
Figure 1: Effect of Mn exposure over the glutamatergic tripartite synapse. (a) Glu/Glu shuttle in normal conditions; Glu levels at the synaptic cleft are tightly regulated by EAATs in glial cells, once inside Glu can be transformed to Gln by GS and then Gln transported by SNATs to the neurons to replenish the Glu stores since Gln can be transformed to Glu by glutaminase. (b) Mn exposure affects the main effector proteins of the Glu/Gln shuttle, when Mn has surpassed the physiological threshold, and Glu tends to accumulate in the synaptic cleft due to the downregulation of EAAT1/2, mostly due to PKC activation. This promotes the overactivation of Glu receptors, even the ones in the extra-synaptic space, triggering the activation of death signaling pathways, a phenomenon known as excitotoxic death. Moreover, GS activity is also diminished along with the downregulation of Gln transporters, distressing all levels of the Glu/Gln cycle rendering defective glutamatergic neurotransmission.

PKC by Mn decreases Glu uptake and expression of GLAST and Glt-1. PKCδ isoform interacts specifically with Glt-1 while PKCα with GLAST (Figure 1(b)). Additionally, the lysosomal pathway appears to be responsible for the downregulation of Glu transporters [58]. Mn treatment decreases the expression of transforming growth factor-alpha and beta (TGF-$\alpha/\beta$) [31, 59].

Recent studies demonstrate that Mn induces tumor necrosis factor-alpha (TNF-$\alpha$) release, promoting NF-$\kappa$B signaling that activates the transcription factor ying-yang 1 (YY1), which along with histone deacetylases (HDACs) forms a repressor complex that decreases the levels of GLAST and Glt-1. The deletion of astrocytic YY1 attenuates the Mn-induced effect over the Glu transporter. In contrast, the interaction of YY1/HDAC with p65 overrides the stimulatory effects of NF-$\kappa$B over GLAST and Glt-1 promoters downregulating their expression in the plasma membrane

of astrocytes [60–63]. Deletion of astrocytic YY1 attenuated the Mn-induced decrease of GLAST and Glt-1 [62]. Ephrin-A3 is known to downregulate Glu transporters; the involvement of this protein in Mn-induced downregulation of GLAST and Glt-1 seems like a plausible mechanism for Mn-elicited neurotoxicity [64]. Moreover, a special effort has been put into ameliorating the effects of Mn on Glu transporters; treatments such as raloxifene [65], arundic acid [60], valproate [66, 67], riluzole [64, 68, 69], sodium butyrate [66], 17$\beta$-estradiol [70], tamoxifen, fluoxetine [64], and PAS-Na [71] have proved to prevent the effects of Mn over Glu transporters.

*3.1.2. Glutamine Synthetase.* In the brain, GS is an astrocyte-enriched protein that catalyzes the conversion of glutamate and ammonium ions into Gln, the only known source of endogenous Gln in mammals [72]. Moreover, GS is a Mn-

TABLE 1: Effect of Mn exposure on glutamate transporter expression and activity *in vitro* and *in vivo*.

| Model | Treatments [Mn] | T | EAAT1/GLAST mRNA | EAAT1/GLAST Protein | EAAT1/GLAST Activity | EAAT2/GLT-1 mRNA | EAAT2/GLT-1 Protein | EAAT2/GLT-1 Activity | Ref. |
|---|---|---|---|---|---|---|---|---|---|
| Rat cortical astrocytes | MnCl$_2$ 100 $\mu$M | 2 d | ↓ | – | ↓ activity in Glu uptake in general | – | ↓ activity in Glu uptake in general | – | [54] |
| Rat cortical astrocytes | MnCl$_2$ 250-500 $\mu$M | ≈18 h | ↓ | – | → | – | – | – | [134] |
| Rat cortical astrocytes | MnCl$_2$, MnPO$_4$, and MnSO$_4$ 100-300 $\mu$M | 6 h | ↓ | – | – | – | – | – | [135] |
| DbB7 cell line | MnCl$_2$ 0.5-1 mM | 6 h | – | – | → | – | – | → | [55] |
| Rhesus monkey | 0.18, 0.92, and 4.62 mg MnSO$_4$/m$^3$ | 65 d | ↑ (GP,Cb) | ↓ (GP,Cb,OC, FC) | – | ↓ (C,GP,OC) | ↓ (C,GP,Cb,OC) | – | [52] |
| Rhesus monkey | 1.5 mg MnSO$_4$/m$^3$ | 15-65 d | ↓ (Cb) ↑ (GP,OC) | ↓ (GP) | – | ↑ (C, Cb,FC) | ↓ (GP,OC) | – | [56] |
| Rat cortical astrocytes | MnCl$_2$ 250-500 $\mu$M | 6 h | → | → | → | → | → | → | [27, 40, 41, 51, 53, 56] |
| Rat striatum | 8, 40, and 200 $\mu$M/kg MnCl$_2$ | 4 w | → | → | – | → | → | – | [68] |
| Rat cortical astrocytes | MnCl$_2$ 250-500 $\mu$M | 24 h | → | → | → | → | → | → | [69] |
| Rat cortical astrocytes | MnCl$_2$ 100 and 500 $\mu$M | 0.5-24 h | – | → | → | – | → | → | [58] |
| Mouse cortex and Cb | 30 mg/kg MnCl$_2$ | 21 d | → | → | – | → | → | – | [66] |
| H4 cell line and mouse brain | 250 $\mu$M; 30 mg/kg MnCl$_2$ | 6h; 21 d | → | → | – | → | → | – | [67] |
| Mouse St and Cb | 1 $\mu$mol/$\mu$l of MnCl$_2$ | 1 w | → | → | – | → | → | – | [70] |
| Mouse St astrocytes and St | 500 $\mu$M; 50 mg/kg MnCl$_2$ | 24h; 2 w | → | – | – | → | → | – | [64] |
| Chick Bergmann glia | MnCl$_2$ 200 $\mu$M | 30' | ↓ (24 h) | – | ↑ | – | – | – | [37] |
| Rat brain (St, GP, Hp, and Th) | 15 mg/kg MnCl$_2$ | 4 w | → | → | – | → | – | – | [71] |
| Mouse midbrain | 30 mg/kg MnCl$_2$ | 21 d | → | → | – | → | → | → | [62] |

↑: increase; ↓: decrease; –: not analyzed; Cb: cerebellum; St: striatum; GP: globus pallidus; C: caudate; P: putamen; FC: frontal cortex; OC: olfactory cortex; Hp: hippocampus; Th: thalamus.

TABLE 2: Effect of Mn exposure on glutamine synthetase expression and enzymatic activity *in vivo* and *in vitro*.

| Model | Treatments [Mn] | Time | mRNA | Protein | Activity | Ref. |
|---|---|---|---|---|---|---|
| Sprague-Dawley rats | 6 mg/kg $MnCl_2$ | 30 d | ↑ | – | – | [136] |
| Sprague-Dawley rats | 25 and 50 mg/kg $MnCl_2$ | PN: 21 d | – | n.s. | n.s. | [137] |
| Rat cortical astrocytes | $MnCl_2$ 100 and 200 $\mu$M | 24 h | – | ↑ | – | [80] |
| Sprague-Dawley rats | 0.03, 0.3, and 3 mg $MnSO_4/m^3$ | 14 d | ↑ (Cb) | ↑ (OB,Ht) ↓ (Cb) | – | [138] |
| Sprague-Dawley rats | 0.05, 0.5, or 1 mg $MnSO_4/m^3$ | 13 w | ↑ (Ht$^F$) ↓ (Cb$^M$,OB$^M$,Hp$^M$) | ↑ (OB$^F$,Hp$^M$) ↓ (Hp$^F$,Ht$^M$) | – | [139] |
| Sprague-Dawley rats | 0.05, 0.5, or 1 mg $MnSO_4/m^3$ | IU: 19 d PN:18 d | ↓ | ↓ | – | [78, 79] |
| Rhesus monkey | 0.18, 0.92, and 4.62 mg $MnSO_4/m^3$ | 65 d | ↓ (FC,OC,C) | ↓ (GP,Cb,FC,P) | – | [52] |
| Wistar rats (St, GP) | 100 mM $MnCl_2$ | 13 d | – | ↓ | ↓ | [140] |
| Rhesus monkeys | 1.5 mg $MnSO_4/m^3$ | 15-65 d | ↓ (C) | ↓ (Cb,GP,P) | – | [56] |
| Sprague-Dawley rats (St) | 8-200 $\mu$M/kg $MnCl_2$ | 4 w | ↓ | ↓ | ↓ | [68] |
| *Cynomolgus macaques* | 3-10 mg/kg $MnCl_2$ | 7-59 w | – | ↓(GP) | – | [77] |
| Wistar rats | 200 $\mu$M/kg $MnCl_2$ | 4 w | – | – | ↓ | [141] |
| Rat cortical astrocytes | $MnCl_2$ 125-500 $\mu$M | 24 h | ↓ | ↓ | ↓ | [69] |
| Sprague-Dawley rats (St,GP,Th) | 15 mg/kg $MnCl_2$ | 4 w | – | – | ↓ | [71] |

↑: increase; ↓: decrease; –: not analyzed; n.s.: no significative; Cb: cerebellum; St: striatum; GP: globus pallidus; C: caudate; P: putamen; FC: frontal cortex; OC: olfactory cortex; Hp: hippocampus; Th: thalamus; Ht: hypothalamus; IU: *in utero*; PN: postnatal; $^F$: female; $^M$: male.

activated enzyme that forms an octamer with four $Mn^{+2}$ ions [73], accounting for about 80% of Mn concentration in the brain [74]. GS is essential in the recycling of neurotransmitters such as Glu and gamma-aminobutyric acid (GABA) and is crucial in ammonia detoxification and as a marker of ROS production due to its susceptibility to oxidative degradation (Figure 1(a)) [75]. Furthermore, this enzyme plays a major role in CNS function, and its disruption is linked to Alzheimer's disease incidence, temporal lobe epilepsy, schizophrenia, and other neurological disorders [76]. Chronic Mn overload has been shown to downregulate the expression and activity of GS in different *in vivo* and *in vitro* models (Figure 1(b)), such as nonhuman primates [52, 56, 77] and rodents, even at *in utero* exposure [78, 79]. Mn-induced alterations in the mRNA and protein levels of GS were also observed in primary cortical astrocytes, as well as decreased enzymatic activity (Table 2) [69, 80].

*3.1.3. Glutamine Transport.* Gln, the most abundant amino acid in the CNS, has a pivotal role in brain metabolism and as a precursor of neurotransmitters. The transport of Gln involves the efflux from astrocytes and the consequent influx into neurons (Figure 1(a)); such a process requires a variety of transport systems [81]. Briefly, the release of Gln is mainly done by system N: sodium-coupled neutral amino acid transporter (SNAT) 3/5, although the system ASC: Alanine-Serine-Cysteine transporter (ASCT) 1/2 can also take on this duty to a lesser extent. On the other hand, the uptake can also be achieved by the systems mentioned above in addition to system A: SNAT1/2 and L: L-type amino acid transporter (LAT) 1/2; the latter pair is mostly expressed in neurons, although all transporters are expressed in glia [82]. Exposure to high Mn concentrations inhibited the

uptake of Gln by cortical astrocytes in a concentration-dependent fashion and decreased the mRNA levels of SNAT1 and SNAT3 [83]. Moreover, the involvement of systems N, ASC, and L in the diminished uptake of Gln after Mn overexposure was suggested, concomitant with a drop in the mRNA and protein levels of Gln transport systems (Table 3). The decline in SNAT3 levels was associated with the transporter's degradation *via* the ubiquitin-mediated proteolytic system through the interaction of SNAT3 with the ubiquitin ligase Nedd4-2 (neural precursor cells expressed developmentally downregulated 4-2) [84]. In the same vein, Mn-induced PKC signaling has been involved in the downregulation of Gln transport (Figure 1(b)). The inhibition of PKC activation reverses the Mn-induced decrease in SNAT3-dependent Gln transport [57]. PKCδ isoforms bind to SNAT3 or ASCT2, possibly inducing their phosphorylation and internalization (Figure 1(b)), as previously suggested [85].

*3.2. Mitochondrial Impairment and Energy Metabolism.* Mn accumulates preferentially in the mitochondria through the mitochondrial $Ca^{2+}$ uniport (MCU) [86]. Once inside, Mn exerts its toxic traits by inhibiting the oxidative phosphorylation process, sequestering $Ca^{2+}$ in the matrix, and promoting ROS production [86, 87]. Mn treatment disrupts the energy metabolism in glial cells [29]. The treatment of cortical astrocytes with Mn induces the mitochondrial permeability transition pore (PTP), a $Ca^{2+}$ dependant process that promotes membrane permeability (Figure 2). This leads to the disruption of the inner membrane potential, resulting in mitochondrial failure [88]. Besides, the activation of the mitogen-activated kinase (MAPK) an extracellular signal-regulated kinase (ERK) pathway induced by Mn exposure

TABLE 3: Effect of Mn exposure on glutamine transporter expression and activity *in vitro*.

| Model | Treatments [Mn] | Time | Transporters | mRNA | Protein | Activity | Ref. |
|---|---|---|---|---|---|---|---|
| Rat cortical astrocytes | MnCl$_2$ 100 and 500 $\mu$M | 30' and 24 h | *System A* | | – | ↓* | [83] |
| | | | SNAT1 | ↓ | | | |
| | | | *System N* | | | | |
| | | | SNAT3 | ↓ | | | |
| | | | *System ASC* | | | | |
| | | | ASCT2 | n.s. | | | |
| Rat cortical astrocytes | MnCl$_2$ 0.1, 0.5, and 1 mM | 1-24 h | *System A* | | | | [142] |
| | | | SNAT2 | ↓ | ↓ | n.s. | |
| | | | *System N* | | | | |
| | | | SNAT3 | ↓ | ↓ | ↓ | |
| | | | *System L* | | | | |
| | | | LAT2 | ↓ | ↓ | ↓ | |
| | | | *System ASC* | | | | |
| | | | ASCT2 | – | ↓ | ↓ | |
| Rat cortical astrocytes | MnCl$_2$ 0.1, 0.5, and 1 mM | 4 h | *System N* | – | ↓ | – | [84] |
| | | | SNAT3 | | | | |
| | | | *System A* | – | | | |
| | | | SNAT2 | | n.s. | n.s. | |
| Rat cortical astrocytes | MnCl$_2$ 0.5 and 1 mM | 4-24 h | *System N* | | | | [57] |
| | | | SNAT3 | | ↓ | ↓ | |
| | | | *System L* | | | | |
| | | | LAT2 | | n.s. | n.s. | |
| | | | *System ASC* | | | | |
| | | | ASCT2 | | ↓ | ↓ | |

↑: increase; ↓: decrease; −: not analyzed; n.s.: no significative; ∗: all systems Gln uptake.

in astrocytes and the collapse of the mitochondrial membrane potential triggers apoptosis through caspase-3 activation [89]. Mn-induced apoptosis in astrocytes activates in response to depolarization of the mitochondrial membrane, which releases cytochrome C, induces caspases 3/7, and modulates the expression of B-cell lymphome 2 (Bcl-2) proteins [90]. Complex II of the respiratory chain is altered by Mn exposure, producing ROS in microglia (Figure 2) [91]. *Noteworthy, mitochondria dysfunction has been associated with inhibition of alternative activation of microglia, consequently exacerbating neuroinflammation [93].* Mn exposure produces lysosomal membrane permeabilization and cathepsin release, which activates BH3-interacting domain death agonist (Bid) promoting mitochondrial damage in glial cells [93]; similar outcomes were found in microglia [46]. Human astrocytes treated with Mn presented activation of the caspase-dependent mitochondrial apoptotic pathway coupled with dysregulation of the expression levels of mitochondria-shaped proteins like mitochondrial dynamin-like GTPase (Opa-1), mitofusin 2 (Mfn-2), and dynamin-related protein 1 (Drp-1) [94].

3.3. *Oxidative Stress.* The main production site of ROS in the cell is the electron transport chain in the mitochondria, and as was briefly discussed before, mitochondria are a primary target of Mn toxicity, promoting ROS production [95]. In comparison to neurons, glial cells are more equipped to endure oxidative damage [96]. Once inside the cell, divalent Mn can be oxidized by ceruloplasmin to its trivalent state, known to be more toxic [97]. Proof of this is that trivalent Mn oxidizes catecholamines *via* oxidative stress [98]. Moreover, in primary cultures of astrocytes, Mn exposure increases the levels of ROS [80]. Mn-induced ROS production in the mitochondria augments nitric oxide synthase expression and activation of NF-$\kappa$B [99]. In addition, the nuclear factor erythroid 2-related factor (Nrf2), a known regulator of the antioxidant response (Figure 3(a)), is significantly increased in astrocytes after Mn exposure. However, at the same time, Mn reduces protein deglycase 1 (DJ-1)/PARK7 expression, a multifunctional protein that acts as a redox sensor (Figure 3(b)) [100]. This protein impairs the binding of Kelch-like ECH-associated protein 1 (Keap1) to Nrf2, avoiding its degradation by the ubiquitin proteosome and promoting Nrf2 activation allowing the transcription of several antioxidant genes (Figure 3(a)). DJ-1/PARK7 downregulation, as with Mn exposure, makes astrocytes more susceptible to oxidative stress (Figure 3(b)) [101, 102]. Another protein involved in the regulation of antioxidant genes and that also has been tied to Mn toxicity in glial cells is the forkhead box transcription factor class O (FoxO)
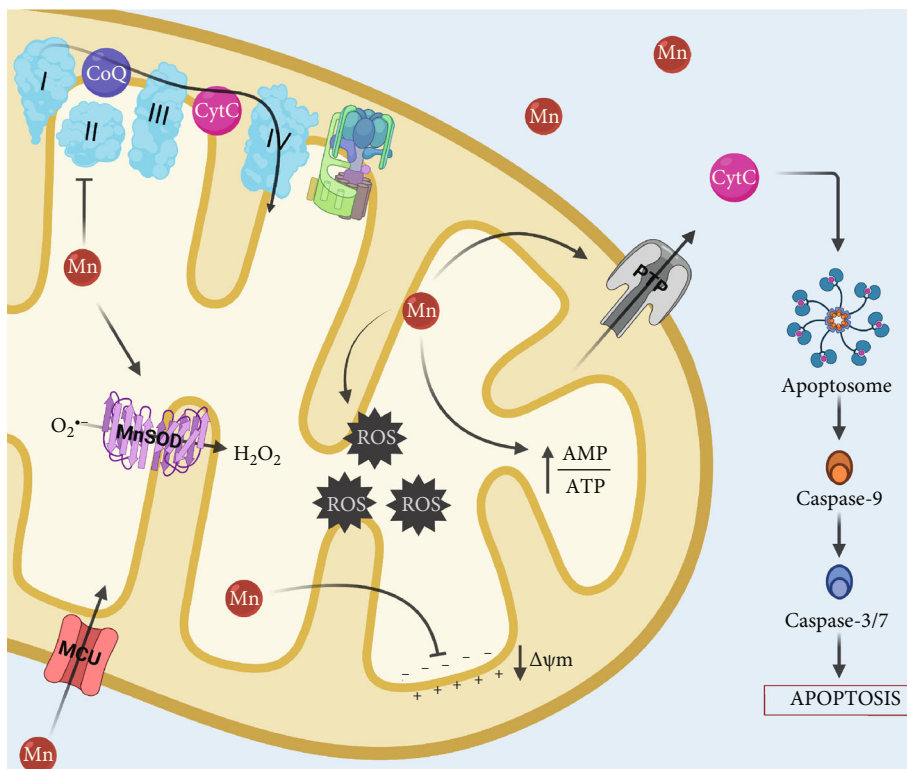
FIGURE 2: Effects of Mn exposure on mitochondrial function in glia. Once inside the cell, Mn is readily taken up by the mitochondria through the MCU, where exerts its toxic actions by producing free radicals and damaging the complex II of the electron transport chain, the excessive levels of Mn in the mitochondria can also affect Mn-SOD activity promoting hydrogen peroxide formation. Moreover, Mn depolarizes the mitochondrial membrane potential promoting the opening of the PTP, which allows the release of cytochrome C, triggering caspase-dependent apoptosis pathways.

along with the PPAR gamma coactivator-1 (PGC-1) [103]. The Mn-induced induction of oxidative stress proved to impair the ability of astrocytes to promote axonal and neurite outgrowth [104]. Recently, it has been shown that Mn alters glutathione (GSH) synthesis by inhibiting the glutamate/cystine antiporter (xCT) due to the induction of oxidative stress in striatum astrocytes [105].

### 3.4. Calcium Homeostasis.

An accumulating body of evidence indicates that dysregulation of calcium ($Ca^{2+}$) homeostasis is closely related to several neurodegenerative diseases, psychiatric disorders, and neurotoxic insults [106]. Even though glial cells do not fire action potentials, they are excitable in terms of intracellular signaling. $Ca^{2+}$ is an important second messenger that has a great variety of cellular functions. Notably, in astrocytes, neurotransmitters activate $Ca^{2+}$ signaling regulating glial processes such as energy expenditure *and* synaptic plasticity [107]. *D*ivalent metal cations tend to mimic some of the activities of $Ca^{2+}$, *and* Mn is one of these metals capable of competing for certain binding sites of $Ca^{2+}$ as well for transport systems, which makes it plausible that Mn interfere*s* in $Ca^{2+}$ regulation [108]. The exposure of astrocytes to Mn results in the sequestering of $Ca^{2+}$ within the mitochondria decreasing the available pool of releasable $Ca^{2+}$ from the endoplasmic reticulum (ER), ending with the inhibition of intercellular $Ca^{2+}$ waves, which are essential for purinergic signaling in

astrocytes [109]. In the same line of study, the inhibition of ATP-induced $Ca^{2+}$ waves and transients by Mn was mediated by the $Ca^{2+}$ entry via the transient receptor potential channel (TRPC3) in striatal astrocytes [110]. Recently, it has been demonstrated that astrocytes transfer functional mitochondria to the neurons in a $Ca^{2+}$-dependent manner during neuronal damage [111]. Moreover, several studies have described how Glu transport is coupled to $Ca^{2+}$ influx through the $Na^+/Ca^{2+}$ exchanger (NCX) [112]. These studies, in conjunction with the ones concerning Mn toxicity [108], demonstrate the crucial role of $Ca^{2+}$ dysregulation in glial cells after Mn exposure.

### 3.5. Autophagy.

In recent years, the role of autophagy in the context of Mn toxicity has attracted some attention [113]. Autophagy, which means self-eating in the Greek language, is an essential mechanism for the degradation of damaged subcellular components or protein aggregates. It is a highly regulated process consisting of several steps that could be summarized as the engulfment of bulk cytoplasm forming a double-membrane vacuole, namely, "autophagosome." Then, it is transported and fused to the lysosomes comprising the autolysosome, where finally, the degradation process takes place [114]. Either overactivation or suppression of autophagy can be involved in the pathogenesis of several neurodegenerative diseases [115]. Regarding the effects of Mn exposure in the process of autophagy, it has been
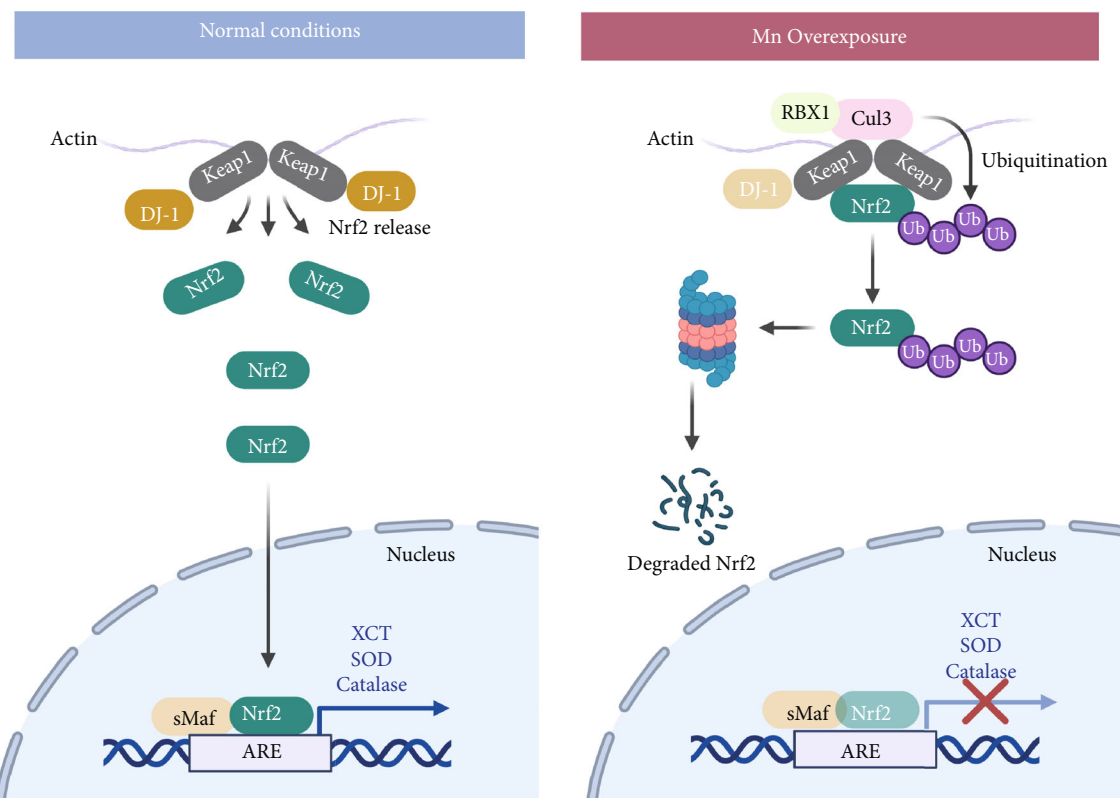
FIGURE 3: The role of Nrf2 in Mn-induced oxidative stress in glia. Nrf2 is a known regulator of the antioxidant response that translocates to the nucleus to act as a transcription factor binding to the antioxidant response element (ARE), enhancing the expression of antioxidant enzyme genes. For this to happen, it is necessary the release of Nrf2 from Keap1, such action is regulated by several effector proteins, DJ-1 is one of them. DJ-1 is downregulated in conditions of Mn overexposure, leading to the binding of Nrf2 to Keap1, promoting the degradation of Nrf2 by the ubiquitin proteasome impairing the expression of several antioxidant genes.

reported, in *in vitro* as well as *in vivo* models, that upon short-term Mn overexposure, there is an increase in the expression of proteins such as Beclin1, microtubule-associated protein 1 light chain 3 (LC3-II), and p62 which lead to the activation of autophagy as a mechanism of coping with the Mn insult. However, as the exposure to Mn progresses, the damage produced by this metal intensifies, suppressing the autophagic process triggering neuronal death [113]. Although most of these effects have been described in neuronal models, few studies have focused on the glia component concerning the role of autophagy in Mn neurodegeneration. The first study made in glia revealed that after Mn exposure, autophagy was activated to alleviate the toxic effects of this metal (Figure 4(a)) [116]. Moreover, this effect could be mediated, at least in part by heme oxygenase-1 (HO-1) [117]. In contrast, in a primary astrocyte culture, exposure to Mn decreased the autophagic influx by inhibiting transcription factor EB (TFEB) activity [118], since active TFEB leads to a global enhancement of lysosomal catabolic efficiency [119]. In microglia, it has also been described that Mn disrupts autophagy. It was demonstrated that through the Mn-induced upregulation of leucine-rich repeat kinase 2 (LRRK2), autophagy-related proteins were dysregulated and inflammation increased [120]. Furthermore, the disruption of the autophagic process by Mn leads to NLR family, pyrin domain containing 3- (NLRP3-) cas-

pase 1 inflammasome activation and the release of interleukin-1$\beta$ (IL-1$\beta$) [121], which is associated with declined autophagic capacity. Taken together, dysregulation of autophagy seems to ameliorate Mn cytotoxic effects by increasing the autophagic flux, as shown in BV-2 cells exposed to Mn, where a time-dependent increase in the expression of LC3-II and p62, delaying Mn cytotoxicity, however, prolonged exposure to Mn increases the amount of ROS inducing lysosomal alterations (Figure 4(b)), such as lysosomal membrane permeabilization (LMP) due to the presence of the proteolytic cleavage products of poly (ADP-ribose) polymerase 1 (PARP1) [46], promoting the release of cathepsins, leading to autophagosome accumulation and ultimately cell death (Figure 4(b)) [122].

3.6. *Neuroinflammation.* The first reports regarding Mn toxic effects in glial cells were related to the release of inflammatory mediators due to glia activation [33, 123] and remain one of the principal mechanisms of Mn-mediated toxicity. Glial cell activation is known as the hallmark of neuroinflammation in addition to peripheral immune cells and the release of proinflammatory mediators [124]. Mn-induced glial activation promotes gliosis in the basal ganglia [26], which increases neuronal damage, promoting the progression of the neurotoxicological disorder. Furthermore, exposure to Mn releases inflammatory intermediaries that
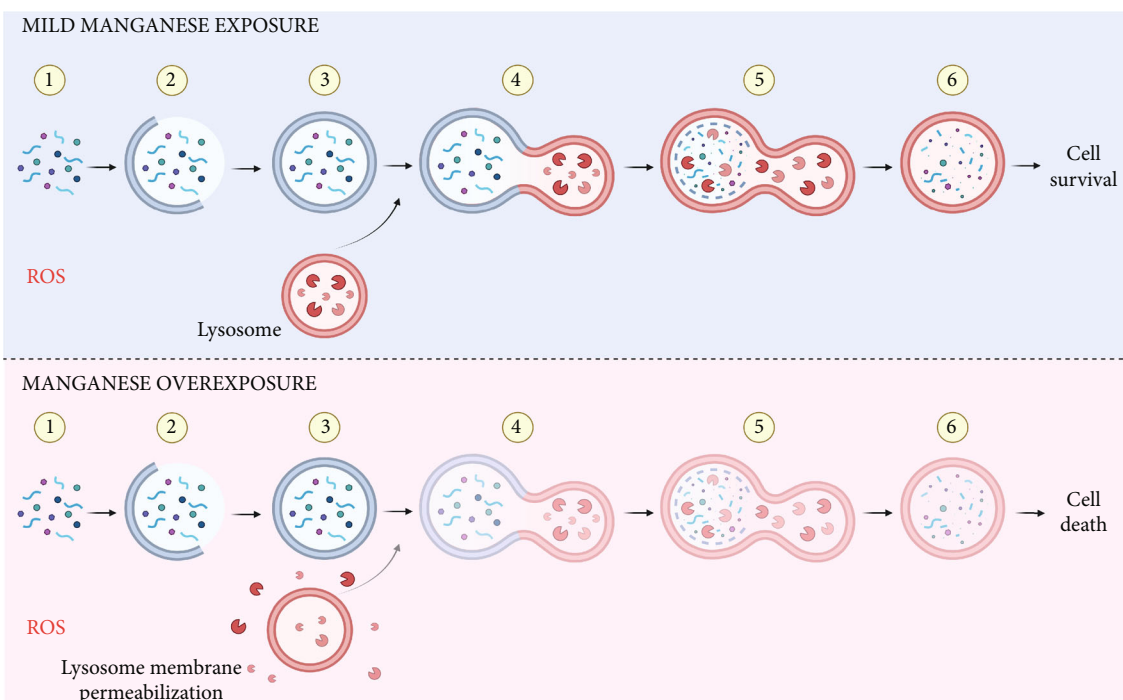
FIGURE 4: Effect of Mn exposure on autophagy in glia. Mn exposure induces ROS promoting organelle and protein damage (1). Under a "mild" Mn insult, glial cells increase their autophagic flux by increasing the expression of proteins such as Beclin1, LC3-II, and p62, the increase in these proteins would promote the initiation of the phagophore (2) and consequently the autophagosome (3). Then, after the fusion of the autophagosome with the lysosome (4), the autolysosome is created (5), allowing the degradation and recycling of damaged cellular components (6), to ameliorate Mn damage promoting cell survival. However, continuous overexposure to Mn disrupts this process by inducing lysosomal membrane permeabilization with the consequent release of cathepsins to the cytosol, leading to autophagosome accumulation and a truncated autophagic flux ending in cell death.

activate reactive astrocytes [99, 125]. In this regard, nuclear factor kappa B (NF-$\kappa$B) signaling in astrocytes has been implicated in the neuroinflammatory effects of Mn exposure. LRRK2 has also been implicated in Mn-induced microglia activation and consequent neuroinflammation [120, 126]. Mn exposure stimulates microglia to release hydrogen peroxide with the downstream activation of MAPK [127] and activation of NF-$\kappa$B signaling, promoting inflammatory responses by regulating cytokines and chemokines that amplify astrocytes' activation [128]. In addition, Mn also increases JAK2/STAT3 signaling in microglia increasing neuronal death due to the release of TNF-$\alpha$ and IL-1$\beta$ [43]. The NLRP3 inflammasome pathway has been suggested to play a critical role in Mn-induced neuroinflammation [121, 129, 130]. Moreover, Mn exposure induces aggregation of $\alpha$-synuclein-induced inflammation in astrocytes, impairing mitochondrial bioenergetics [131]. Further studies that take into consideration glial cells crosstalk during neuroinflammation are needed since it has been reported that activated microglia induce neurotic reactive astrocytes after acute CNS injury [132, 133].

## 4. Conclusion

A significant effort has been directed to dissect the functional and molecular events that Mn triggers in neurotoxicity development, but always taking the neuronal component as the main actor. Meanwhile, glia has always been relegated to a mere supporting role for neurons. In this contribution, we focused on the glial component as an important target of Mn deleterious effects. We provide herein an overview of the role of glial cells in Mn neurotoxicity, including the consequences on energy metabolism, redox homeostasis, Ca$^{2+}$ signaling, inflammation, and autophagia. Moreover, we detail the key findings in the Mn-induced disruption of the Glu/Gln shuttle.

Still, many questions remain to be answered regarding the role of glia in Mn neurotoxicity; the evidence so far demonstrates that these cells have a pivotal role in the management of the Mn insult and its relevance to the neuronal counterpart. It is time to reevaluate Mn neurotoxicity as a whole and consider both neurons and glia as targets. Further investigations are needed to take into consideration the close relationship that neurons and glia maintain. Cocultures of glial cells in physical contact with neurons or separated by a semipermeable membrane barrier would allow us to link the individual effects that had already been described in each cellular model and shed light on this health problem.

## Conflicts of Interest

The authors declare that there is no conflict of interest regarding the publication of this manuscript.

## Acknowledgments

## References

[1] L. Maiolo, V. Guarino, E. Saracino et al., "Glial interfaces: advanced materials and devices to uncover the role of astroglial cells in brain function and dysfunction," *Advanced Healthcare Materials*, vol. 10, no. 1, p. 2001268, 2021.

[2] C. S. von Bartheld, J. Bahney, and S. Herculano-Houzel, "The search for true numbers of neurons and glial cells in the human brain: a review of 150 years of cell counting," *The Journal of Comparative Neurology*, vol. 524, no. 18, pp. 3865–3895, 2016.

[3] J. Wahis, M. Hennes, L. Arckens, and M. G. Holt, "Star power: the emerging role of astrocytes as neuronal partners during cortical plasticity," *Current Opinion in Neurobiology*, vol. 67, pp. 174–182, 2021.

[4] F. He and Y. E. Sun, "Glial cells more than support cells?," *The International Journal of Biochemistry & Cell Biology*, vol. 39, no. 4, pp. 661–665, 2007.

[5] J. B. Zuchero and B. A. Barres, "Glia in mammalian development and disease," *Development*, vol. 142, no. 22, pp. 3805–3809, 2015.

[6] K. M. Erikson and M. Aschner, "10. Manganese: its role in disease and health," *Metal Ions in Life Sciences*, vol. 14, pp. 253–266, 2019.

[7] D. S. Avila, R. L. Puntel, and M. Aschner, "Manganese in health and disease," *Metal Ions in Life Sciences*, vol. 13, pp. 199–227, 2013.

[8] F. C. Wedler, "3 Biological Significance of Manganese in Mammalian Systems," *Progress in Medicinal Chemistry*, vol. 30, pp. 89–133, 1993.

[9] A. Takeda, "Manganese action in brain function," *Brain Research Reviews*, vol. 41, no. 1, pp. 79–87, 2003.

[10] K. V. Martin, D. Edmondson, K. M. Cecil et al., "Manganese exposure and neurologic outcomes in adult populations," *Neurologic Clinics*, vol. 38, no. 4, pp. 913–936, 2020.

[11] A. B. Bowman and M. Aschner, "Considerations on manganese (Mn) treatments for _in vitro_ studies," *Neurotoxicology*, vol. 41, pp. 141-142, 2014.

[12] R. C. Balachandran, S. Mukhopadhyay, D. McBride et al., "Brain manganese and the balance between essential roles and neurotoxicity," *The Journal of Biological Chemistry*, vol. 295, no. 19, pp. 6312–6329, 2020.

[13] P. Chen, M. Culbreth, and M. Aschner, "Exposure, epidemiology, and mechanism of the environmental toxicant manganese," *Environmental Science and Pollution Research*, vol. 23, pp. 13802–13810, 2016.

[14] I. Nyarko-Danquah, E. Pajarillo, A. Digman, K. F. A. Soliman, M. Aschner, and E. Lee, "Manganese accumulation in the brain via various transporters and its neurotoxicity mechanisms," *Molecules*, vol. 25, no. 24, p. 5880, 2020.

[15] P. Chen, J. Bornhorst, and M. Aschner, "Manganese metabolism in humans," *Frontiers in Bioscience*, vol. 23, no. 9, pp. 1655–1679, 2018.

[16] R. A. Yokel and J. S. Crossgrove, "Manganese toxicokinetics at the blood-brain barrier," *Research Report (Health Effects Institute)*, no. 119, pp. 7–73, 2004.

[17] P. Chen, S. Chakraborty, S. Mukhopadhyay et al., "Manganese homeostasis in the nervous system," *Journal of Neurochemistry*, vol. 134, pp. 601–610, 2015.

[18] I. Lago-Baldaia, V. M. Fernandes, and S. D. Ackerman, "More than mortar: glia as architects of nervous system development and disease," *Frontiers in Cell and Development Biology*, vol. 8, 2020.

[19] Y. Y. Jean, I. P. Bagayogo, and C. F. Dreyfus, "Release of trophic factors and immune molecules from astrocytes," *Astrocytes in (Patho) Physiology of the Nervous System*, vol. 11, pp. 351–381, 2009.

[20] A. Becerra-Calixto and G. P. Cardona-Gómez, "The role of astrocytes in neuroprotection after brain stroke: potential in cell therapy," *Frontiers in Molecular Neuroscience*, vol. 10, 2017.

[21] B. Stevens, "Glia: much more than the neuron's side-kick," *Current Biology*, vol. 13, no. 12, pp. R469–R472, 2003.

[22] L. Sancho, M. Contreras, and N. J. Allen, "Glia as sculptors of synaptic plasticity," *Neuroscience Research*, vol. 167, pp. 17–29, 2021.

[23] A. Semyanov, "Spatiotemporal pattern of calcium activity in astrocytic network," *Cell Calcium*, vol. 78, pp. 15–25, 2019.

[24] P. D. Blanc, "The early history of manganese and the recognition of its neurotoxicity, 1837-1936," *Neurotoxicology*, vol. 64, pp. 5–11, 2018.

[25] N. M. Filipov and C. A. Dodd, "Role of glial cells in manganese neurotoxicity," *Journal of Applied Toxicology*, vol. 32, no. 5, pp. 310–317, 2012.

[26] R. B. Tjalkens, K. A. Popichak, and K. A. Kirkley, "Inflammatory activation of microglia and astrocytes in manganese neurotoxicity," *Adv. Neurobiol.*, vol. 18, pp. 159–181, 2017.

[27] K. Ravi, M. J. Paidas, A. Saad, and A. R. Jayakumar, "Astrocytes in rare neurological conditions: morphological and functional considerations," *Journal of Comparative Neurology*, vol. 529, no. 10, pp. 2676–2705, 2021.

[28] B. Li, M. Xia, R. Zorec, V. Parpura, and A. Verkhratsky, "Astrocytes in heavy metal neurotoxicity and neurodegeneration," *Brain Research*, vol. 1752, p. 147234, 2021.

[29] F. C. Wedler, B. W. Ley, and A. A. Grippo, "Manganese (II) dynamics and distribution in glial cells cultured from chick cerebral cortex," *Neurochemical Research*, vol. 14, no. 11, pp. 1129–1135, 1989.

[30] G. Tholey, M. Ledig, P. Mandel et al., "Concentrations of physiologically important metal ions in glial cells cultured from chick cerebral cortex," *Neurochemical Research*, vol. 13, no. 1, pp. 45–50, 1988.

[31] E.-S. Y. Lee, M. Sidoryk, H. Jiang, Z. Yin, and M. Aschner, "Estrogen and tamoxifen reverse manganese-induced glutamate transporter impairment in astrocytes," *Journal of Neurochemistry*, vol. 110, pp. 530–544, 2009.

[32] E.-S. Y. Lee, Z. Yin, D. Milatovic, H. Jiang, and M. Aschner, "Estrogen and tamoxifen protect against Mn-induced toxicity in rat cortical primary cultures of neurons and astrocytes," *Toxicological Sciences*, vol. 110, pp. 156–167, 2009.

[33] M. Spranger, S. Schwab, S. Desiderato, E. Bonmann, D. Krieger, and J. Fandrey, "Manganese augments nitric oxide synthesis in murine astrocytes: a new pathogenetic mechanism in manganism?," *Experimental Neurology*, vol. 149, no. 1, pp. 277–283, 1998.

[34] A. Ledo, C. F. Lourenço, E. Cadenas, R. M. Barbosa, and J. Laranjinha, "The bioactivity of neuronal-derived nitric

oxide in aging and neurodegeneration: switching signaling to degeneration," *Free Radical Biology & Medicine*, vol. 162, pp. 500–513, 2021.

[35] M. Sidoryk-Wegrzynowicz and M. Aschner, "Manganese toxicity in the central nervous system: the glutamine/glutamate-γ-aminobutyric acid cycle," *Journal of Internal Medicine*, vol. 273, no. 5, pp. 466–477, 2013.

[36] M. Sild and E. S. Ruthazer, "Radial glia: progenitor, pathway, and partner," *The Neuroscientist*, vol. 17, no. 3, pp. 288–302, 2011.

[37] M. Escalante, J. Soto-Verdugo, L. C. Hernández-Kelly et al., "GLAST activity is modified by acute manganese exposure in Bergmann glial cells," *Neurochemical Research*, vol. 45, no. 6, pp. 1365–1374, 2020.

[38] L. Pellerin and P. J. Magistretti, "Sweet sixteen for ANLS," *Journal of Cerebral Blood Flow and Metabolism*, vol. 32, pp. 1152–1166, 2011.

[39] R. B. Hernández, M. Farina, B. P. Espósito, N. C. Souza-Pinto, F. Barbosa, and C. Suñol, "Mechanisms of manganese-induced neurotoxicity in primary neuronal cultures: the role of manganese speciation and cell type," *Toxicological Sciences*, vol. 124, no. 2, pp. 414–423, 2011.

[40] J. C. Savage, M. Carrier, and M. È. Tremblay, "Morphology of microglia across contexts of health and disease," *Methods Mol. O Biologico*, vol. 2034, pp. 13–26, 2019.

[41] F. Zhao, T. Cai, M. Liu, G. Zheng, W. Luo, and J. Chen, "Manganese induces dopaminergic neurodegeneration via microglial activation in a rat model of manganism," *Toxicological Sciences*, vol. 107, no. 1, pp. 156–164, 2009.

[42] E. Park and H. S. Chun, "Melatonin attenuates manganese and lipopolysaccharide-induced inflammatory activation of BV2 microglia," *Neurochemical Research*, vol. 42, pp. 656–666, 2017.

[43] L. Yin, Q. Dai, P. Jiang et al., "Manganese exposure facilitates microglial JAK2-STAT3 signaling and consequent secretion of TNF-a and IL-1β to promote neuronal death," *Neurotoxicology*, vol. 64, pp. 195–203, 2018.

[44] D. Peng, J. Li, Y. Deng et al., "Sodium para-aminosalicylic acid inhibits manganese-induced NLRP3 inflammasome-dependent pyroptosis by inhibiting NF-κB pathway activation and oxidative stress," *Journal of Neuroinflammation*, vol. 17, p. 343, 2020.

[45] Y. Fang, D. Peng, Y. Liang et al., "Sodium P-aminosalicylic acid inhibits manganese-induced neuroinflammation in BV2 microglial cells via NLRP3-CASP1 inflammasome pathway," *Biological Trace Element Research*, vol. 199, no. 9, pp. 3423–3432, 2021.

[46] S. Porte Alcon, R. M. Gorojod, and M. L. Kotler, "Regulated Necrosis Orchestrates Microglial Cell Death in Manganese-Induced Toxicity," *Neuroscience*, vol. 393, pp. 206–225, 2018.

[47] A. G. Rodríguez-Campuzano and A. Ortega, "Glutamate transporters: critical components of glutamatergic transmission," *Neuropharmacology*, vol. 192, p. 108602, 2021.

[48] Y. Zhou and N. C. Danbolt, "Glutamate as a neurotransmitter in the healthy brain," *Journal of Neural Transmission*, vol. 121, no. 8, pp. 799–817, 2014.

[49] S. Magi, S. Piccirillo, S. Amoroso, and V. Lariccia, "Excitatory amino acid transporters (Eaats): glutamate transport and beyond," *International Journal of Molecular Sciences*, vol. 20, no. 22, p. 5674, 2019.

[50] B. Weber and L. F. Barros, "The astrocyte: powerhouse and recycling center," *Cold Spring Harbor Perspectives in Biology*, vol. 7, no. 12, article a020396, 2015.

[51] A. Armada-Moreira, J. I. Gomes, C. C. Pina et al., "Going the extra (synaptic) mile: excitotoxicity as the road toward neurodegenerative diseases," *Frontiers in Cellular Neuroscience*, vol. 14, 2020.

[52] K. M. Erikson, D. C. Dorman, L. H. Lash, and M. Aschner, "Manganese inhalation by rhesus monkeys is associated with brain regional changes in biomarkers of neurotoxicity," *Toxicological Sciences*, vol. 97, no. 2, pp. 459–466, 2007.

[53] J. Wang, F. Wang, D. Mai, and S. Qu, "Molecular mechanisms of glutamate toxicity in Parkinson's disease," *Frontiers in Neuroscience*, vol. 14, 2020.

[54] A. S. Hazell and M. D. Norenberg, "Manganese decreases glutamate uptake in cultured astrocytes," *Neurochemical Research*, vol. 22, no. 12, pp. 1443–1447, 1997.

[55] L. Mutkus, J. L. Aschner, V. Fitsanakis, and M. Aschner, "The in vitro uptake of glutamate in GLAST and GLT-1 transfected mutant CHO-K1 cells is inhibited by manganese," *Biological Trace Element Research*, vol. 107, no. 3, pp. 221–230, 2005.

[56] K. M. Erikson, D. C. Dorman, L. H. Lash, and M. Aschner, "Duration of airborne-manganese exposure in rhesus monkeys is associated with brain regional changes in biomarkers of neurotoxicity," *Neurotoxicology*, vol. 29, no. 3, pp. 377–385, 2008.

[57] M. Sidoryk-Wegrzynowicz, E. Lee, N. Mingwei, and M. Aschner, "Disruption of astrocytic glutamine turnover by manganese is mediated by the protein kinase C pathway," *Glia*, vol. 59, no. 11, pp. 1732–1743, 2011.

[58] M. Sidoryk-Wegrzynowicz, E. Lee, and M. Aschner, "Mechanism of Mn(II)-mediated dysregulation of glutamine-glutamate cycle: focus on glutamate turnover," *Journal of Neurochemistry*, vol. 122, pp. 856–867, 2012.

[59] E. Lee, M. Sidoryk-Wegrzynowicz, Z. Yin, A. Webb, D. S. Son, and M. Aschner, "Transforming growth factor-α mediates estrogen-induced upregulation of glutamate transporter GLT-1 in rat primary astrocytes," *Glia*, vol. 60, no. 7, pp. 1024–1036, 2012.

[60] P. Karki, P. Hong, J. Johnson et al., "Arundic acid increases expression and function of astrocytic glutamate transporter EAAT1 via the ERK, Akt, and NF-κB pathways," *Molecular Neurobiology*, vol. 55, no. 6, pp. 5031–5046, 2018.

[61] P. Karki, C. Kim, K. Smith, D. S. Son, M. Aschner, and E. Lee, "Transcriptional Regulation of the Astrocytic Excitatory Amino Acid Transporter 1 (EAAT1) via NF-κB and Yin Yang 1 (YY1)," *The Journal of Biological Chemistry*, vol. 290, no. 39, pp. 23725–23737, 2015.

[62] E. Pajarillo, J. Johnson, A. Rizor et al., "Astrocyte-specific deletion of the transcription factor yin yang 1 in murine substantia nigra mitigates manganese-induced dopaminergic neurotoxicity," *The Journal of Biological Chemistry*, vol. 295, no. 46, pp. 15662–15676, 2020.

[63] P. Karki, A. Webb, K. Smith et al., "Yin yang 1 is a repressor of glutamate transporter EAAT2, and it mediates manganese-induced decrease of EAAT2 expression in astrocytes," *Molecular and Cellular Biology*, vol. 34, no. 7, pp. 1280–1289, 2014.

[64] Z. Qi, X. Yang, X. Sang et al., "Fluoxetine and riluzole mitigates manganese-induced disruption of glutamate transporters and excitotoxicity via ephrin-A3/GLAST-GLT-

1/Glu signaling pathway in striatum of mice," *Neurotoxicity Research*, vol. 38, no. 2, pp. 508–523, 2020.

[65] P. Karki, A. Webb, A. Zerguine, J. Choi, D. S. Son, and E. Lee, "Mechanism of raloxifene-induced upregulation of glutamate transporters in rat primary astrocytes," *Glia*, vol. 62, no. 8, pp. 1270–1283, 2014.

[66] J. Johnson, E. A. B. Pajarillo, E. Taka et al., "Valproate and sodium butyrate attenuate manganese-decreased locomotor activity and astrocytic glutamate transporters expression in mice," *Neurotoxicology*, vol. 64, pp. 230–239, 2018.

[67] J. Johnson, E. Pajarillo, P. Karki et al., "Valproic acid attenuates manganese-induced reduction in expression of GLT-1 and GLAST with concomitant changes in murine dopaminergic neurotoxicity," *Neurotoxicology*, vol. 67, pp. 112–120, 2018.

[68] Y. Deng, Z. Xu, B. Xu et al., "The protective effect of riluzole on manganese caused disruption of glutamate- glutamine cycle in rats," *Brain Research*, vol. 1289, pp. 106–117, 2009.

[69] Y. Deng, Z. Xu, B. Xu, D. Xu, Y. Tian, and W. Feng, "The protective effects of riluzole on manganese-induced disruption of glutamate transporters and glutamine synthetase in the cultured astrocytes," *Biological Trace Element Research*, vol. 148, no. 2, pp. 242–249, 2012.

[70] E. Pajarillo, J. Johnson, J. Kim et al., "17β-estradiol and tamoxifen protect mice from manganese-induced dopaminergic neurotoxicity," *Neurotoxicology*, vol. 65, pp. 280–288, 2018.

[71] Z. C. Li, F. Wang, S. J. Li et al., "Sodium para-aminosalicylic acid reverses changes of glutamate turnover in manganese-exposed rats," *Biological Trace Element Research*, vol. 197, no. 2, pp. 544–554, 2020.

[72] T. Eid, T. S. W. Lee, P. Patrylo, and H. P. Zaveri, "Astrocytes and glutamine synthetase in epileptogenesis," *Journal of Neuroscience Research*, vol. 97, no. 11, pp. 1345–1362, 2019.

[73] F. C. Wedler and R. B. Denman, "Glutamine synthetase: the major Mn(II) enzyme in mammalian brain," *Current Topics in Cellular Regulation*, vol. 24, pp. 153-154, 1984.

[74] M. Aschner and J. L. Aschner, "Manganese neurotoxicity: cellular effects and blood-brain barrier transport," *Neuroscience and Biobehavioral Reviews*, vol. 15, no. 3, pp. 333–340, 1991.

[75] G. Kim, H. S. Lee, J. S. Bang, B. Kim, D. Ko, and M. Yang, "A current review for biological monitoring of manganese with exposure, susceptibility, and response biomarkers," *Journal of Environmental Science and Health, Part C*, vol. 33, no. 2, pp. 229–254, 2015.

[76] D. Huyghe, Y. Nakamura, M. Terunuma et al., "Glutamine Synthetase Stability and Subcellular Distribution in Astrocytes Are Regulated by γ-Aminobutyric Type B Receptors," *The Journal of Biological Chemistry*, vol. 289, no. 42, pp. 28808–28815, 2014.

[77] N. C. Burton, J. S. Schneider, T. Syversen, and T. R. Guilarte, "Effects of chronic manganese exposure on glutamatergic and GABAergic neurotransmitter markers in the nonhuman primate brain," *Toxicological Sciences*, vol. 111, no. 1, pp. 131–139, 2009.

[78] K. M. Erikson, D. C. Dorman, V. Fitsanakis, L. H. Lash, and M. Aschner, "Alterations of oxidative stress biomarkers due to in utero and neonatal exposures of airborne manganese," *Biological Trace Element Research*, vol. 111, pp. 199–216, 2006.

[79] K. M. Erikson, D. C. Dorman, L. H. Lash, and M. Aschner, "Persistent alterations in biomarkers of oxidative stress resulting from combined in utero and neonatal manganese inhalation," *Biological Trace Element Research*, vol. 104, no. 2, pp. 151–164, 2005.

[80] C. J. Chen and S. L. Liao, "Oxidative stress involves in astrocytic alterations induced by manganese," *Experimental Neurology*, vol. 175, no. 1, pp. 216–225, 2002.

[81] H. C. Yoo, Y. C. Yu, Y. Sung, and J. M. Han, "Glutamine reliance in cell metabolism," *Experimental & Molecular Medicine*, vol. 52, no. 9, pp. 1496–1516, 2020.

[82] J. Albrecht and M. Zielińska, "Exchange-mode glutamine transport across CNS cell membranes," *Neuropharmacology*, vol. 161, p. 107560, 2019.

[83] D. Milatovic, Z. Yin, R. C. Gupta et al., "Manganese induces oxidative impairment in cultured rat astrocytes," *Toxicological Sciences*, vol. 98, no. 1, pp. 198–205, 2007.

[84] M. Sidoryk-Wecgrzynowicz, E. S. Lee, M. Ni, and M. Aschner, "Manganese-induced downregulation of astroglial glutamine transporter SNAT3 involves ubiquitin-mediated proteolytic system," *Glia*, vol. 58, no. 16, pp. 1905–1912, 2010.

[85] L. S. H. Nissen-Meyer, M. C. Popescu, E. H. Hamdani, and F. A. Chaudhry, "Protein kinase C-mediated phosphorylation of a single serine residue on the rat glial glutamine transporter SN1 governs its membrane trafficking," *The Journal of Neuroscience*, vol. 31, no. 17, pp. 6565–6575, 2011.

[86] C. E. Gavin, K. K. Gunter, and T. E. Gunter, "Manganese and calcium efflux kinetics in brain mitochondria. Relevance to manganese toxicity," *Biochemical Journal*, vol. 266, no. 2, pp. 329–334, 1990.

[87] C. E. Gavin, K. K. Gunter, and T. E. Gunter, "Manganese and calcium transport in mitochondria: implications for manganese toxicity," *Neurotoxicology*, vol. 20, no. 2–3, pp. 445–453, 1999.

[88] K. V. Rama Rao and M. D. Norenberg, "Manganese Induces the Mitochondrial Permeability Transition in Cultured Astrocytes," *The Journal of Biological Chemistry*, vol. 279, no. 31, pp. 32333–32338, 2004.

[89] Z. Yin, J. L. Aschner, A. P. dos Santos, and M. Aschner, "Mitochondrial-dependent manganese neurotoxicity in rat primary astrocyte cultures," *Brain Research*, vol. 1203, pp. 1–11, 2008.

[90] L. E. Gonzalez, A. A. Juknat, A. J. Venosa, N. Verrengia, and M. L. Kotler, "Manganese activates the mitochondrial apoptotic pathway in rat astrocytes by modulating the expression of proteins of the Bcl-2 family," *Neurochemistry International*, vol. 53, no. 6-8, pp. 408–415, 2008.

[91] Y. Liu, D. S. Barber, P. Zhang, and B. Liu, "Complex ii of the mitochondrial respiratory chain is the key mediator of divalent manganese-induced hydrogen peroxide production in microglia," *Toxicological Sciences*, vol. 132, no. 2, pp. 298–306, 2013.

[92] A. I. Ferger, L. Campanelli, V. Reimer et al., "Effects of mitochondrial dysfunction on the immunological properties of microglia," *Journal of Neuroinflammation*, vol. 7, p. 45, 2010.

[93] R. M. Gorojod, A. Alaimo, S. Porte Alcon, F. Saravia, and M. L. Kotler, "Interplay between lysosomal, mitochondrial and death receptor pathways during manganese-induced apoptosis in glial cells," *Archives of Toxicology*, vol. 91, no. 9, pp. 3065–3078, 2017.

[94] A. Alaimo, R. M. Gorojod, E. A. Miglietta, A. Villarreal, A. J. Ramos, and M. L. Kotler, "Manganese induces mitochondrial dynamics impairment and apoptotic cell death: A study in human Gli36 cells," *Neuroscience Letters*, vol. 554, pp. 76–81, 2013.

[95] Y. Chtourou, K. Trabelsi, H. Fetoui, G. Mkannez, H. Kallel, and N. Zeghal, "Manganese induces oxidative stress, redox state unbalance and disrupts membrane bound ATPases on murine neuroblastoma cells in vitro: protective role of silymarin," *Neurochemical Research*, vol. 36, pp. 1546–1557, 2011.

[96] J. Rose, C. Brian, J. Woods et al., "Mitochondrial dysfunction in glial cells: implications for neuronal homeostasis and survival," *Toxicology*, vol. 391, pp. 109–115, 2017.

[97] E. J. Martinez-Finley, C. E. Gavin, M. Aschner, and T. E. Gunter, "Manganese neurotoxicity and the role of reactive oxygen species," *Free Radical Biology & Medicine*, vol. 62, pp. 65–75, 2013.

[98] F. S. Archibald and C. Tyree, "Manganese poisoning and the attack of trivalent manganese upon catecholamines," *Archives of Biochemistry and Biophysics*, vol. 256, pp. 638–650, 1987.

[99] R. Barhoumi, J. Faske, X. Liu, and R. B. Tjalkens, "Manganese potentiates lipopolysaccharide-induced expression of NOS2 in C6 glioma cells through mitochondrial-dependent activation of nuclear factor kappaB," *Molecular Brain Research*, vol. 122, no. 2, pp. 167–179, 2004.

[100] G. Vavougios, S. G. Zarogiannis, and T. Doskas, "The putative interplay between DJ-1/NRF2 and dimethyl fumarate: a potentially important pharmacological target," *Multiple Sclerosis and Related Disorders*, vol. 21, pp. 88–91, 2018.

[101] E. Lee, Z. Yin, M. Sidoryk-Węgrzynowicz, H. Jiang, and M. Aschner, "15-Deoxy-$\Delta$12,14-prostaglandin J2 modulates manganese-induced activation of the NF-$\kappa$B, Nrf 2, and PI3K pathways in astrocytes," *Free Radical Biology & Medicine*, vol. 52, pp. 1067–1074, 2012.

[102] V. da Silva Santos, E. Bisen-Hersh, Y. Yu et al., "Anthocyanin-rich açaí (Euterpe oleracea Mart.) extract attenuates manganese-induced oxidative stress in rat primary astrocyte cultures," *Journal of Toxicology and Environmental Health. Part A*, vol. 77, no. 7, pp. 390–404, 2014.

[103] V. Exil, L. Ping, Y. Yu et al., "Activation of MAPK and FoxO by manganese (Mn) in rat neonatal primary astrocyte cultures," *PLoS One*, vol. 9, no. 5, p. e94753, 2014.

[104] G. Giordano, D. Pizzurro, K. VanDeMark, M. Guizzetti, and L. G. Costa, "Manganese inhibits the ability of astrocytes to promote neuronal differentiation," *Toxicology and Applied Pharmacology*, vol. 240, no. 2, pp. 226–235, 2009.

[105] X. Yang, H. Yang, F. Wu et al., "Mn inhibits GSH synthesis via downregulation of neuronal EAAC1 and astrocytic xCT to cause oxidative damage in the striatum of mice," *Oxidative Medicine and Cellular Longevity*, vol. 2018, 15 pages, 2018.

[106] E. Pchitskaya, E. Popugaeva, and I. Bezprozvanny, "Calcium signaling and molecular mechanisms underlying neurodegenerative diseases," *Cell Calcium*, vol. 70, pp. 87–94, 2018.

[107] S. Guerra-Gomes, N. Sousa, L. Pinto, and J. F. Oliveira, "Functional roles of astrocyte calcium elevations: from synapses to behavior," *Frontiers in Cellular Neuroscience*, vol. 11, 2018.

[108] O. M. Ijomone, O. M. Aluko, C. O. A. Okoh, A. C. Martins, and M. Aschner, "Role for calcium signaling in manganese neurotoxicity," *Journal of Trace Elements in Medicine and Biology*, vol. 56, pp. 146–155, 2019.

[109] R. B. Tjalkens, M. J. Zoran, B. Mohl, and R. Barhoumi, "Manganese suppresses ATP-dependent intercellular calcium waves in astrocyte networks through alteration of mitochondrial and endoplasmic reticulum calcium dynamics," *Brain Research*, vol. 1113, no. 1, pp. 210–219, 2006.

[110] K. M. Streifel, J. Miller, R. Mouneimne, and R. B. Tjalkens, "Manganese inhibits ATP-induced calcium entry through the transient receptor potential channel TRPC3 in astrocytes," *Neurotoxicology*, vol. 34, pp. 160–166, 2013.

[111] K. Hayakawa, E. Esposito, X. Wang et al., "Transfer of mitochondria from astrocytes to neurons after stroke," *Nature*, vol. 535, no. 7613, pp. 551–555, 2016.

[112] M. B. Robinson, M. L. Lee, and S. DaSilva, "Glutamate transporters and mitochondria: signaling, co-compartmentalization, functional coupling, and future directions," *Neurochemical Research*, vol. 45, no. 3, pp. 526–540, 2020.

[113] D.-Y. Yan and B. Xu, "The role of autophagy in manganese-induced neurotoxicity," *Frontiers in Neuroscience*, vol. 14, p. 959, 2020.

[114] A. Ortiz-Rodriguez and M. A. Arevalo, "The contribution of astrocyte autophagy to systemic metabolism," *International Journal of Molecular Sciences*, vol. 21, no. 7, p. 2479, 2020.

[115] C. T. Chu, "Mechanisms of selective autophagy and mitophagy: implications for neurodegenerative diseases," *Neurobiology of Disease*, vol. 122, pp. 23–34, 2019.

[116] R. M. Gorojod, A. Alaimo, S. Porte Alcon, C. Pomilio, F. Saravia, and M. L. Kotler, "The autophagic- lysosomal pathway determines the fate of glial cells under manganese-induced oxidative stress conditions," *Free Radical Biology & Medicine*, vol. 87, pp. 237–251, 2015.

[117] R. M. Gorojod, A. Alaimo, S. Porte Alcon et al., "Heme oxygenase-1 protects astroglia against manganese-induced oxidative injury by regulating mitochondrial quality control," *Toxicology Letters*, vol. 295, pp. 357–368, 2018.

[118] Z. Zhang, J. Yan, A. B. Bowman, M. R. Bryan, R. Singh, and M. Aschner, "Dysregulation of TFEB contributes to manganese-induced autophagic failure and mitochondrial dysfunction in astrocytes," *Autophagy*, vol. 16, no. 8, pp. 1506–1523, 2020.

[119] C. Di Malta, L. Cinque, and C. Settembre, "Transcriptional regulation of autophagy: mechanisms and diseases," *Frontiers in Cell and Development Biology*, vol. 7, p. 114, 2019.

[120] J. Chen, P. Su, W. Luo, and J. Chen, "Role of LRRK2 in manganese-induced neuroinflammation and microglial autophagy," *Biochemical and Biophysical Research Communications*, vol. 498, no. 1, pp. 171–177, 2018.

[121] D. Wang, J. Zhang, W. Jiang et al., "The role of NLRP3-CASP1 in inflammasome-mediated neuroinflammation and autophagy dysfunction in manganese-induced, hippocampal-dependent impairment of learning and memory ability," *Autophagy*, vol. 13, no. 5, pp. 914–927, 2017.

[122] S. Porte Alcon, R. M. Gorojod, and M. L. Kotler, "Kinetic and protective role of autophagy in manganese-exposed BV-2 cells," *Biochimica et Biophysica Acta-Molecular Cell Research*, vol. 1867, no. 10, p. 118787, 2020.

[123] J. Y. Chang and L. Z. Liu, "Manganese potentiates nitric oxide production by microglia," *Molecular Brain Research*, vol. 68, no. 1-2, pp. 22–28, 1999.

[124] S. Sarkar, E. Malovic, H. Jin, A. Kanthasamy, and A. G. Kanthasamy, "Chapter four-the role of manganese in neuroinflammation, in: M. Aschner, L.G.B.T.-a," in *Role Inflamm.*

*Environ. Neurotox*, N. Costa, Ed., pp. 121–131, Academic Press, 2019.

[125] K. A. Popichak, M. F. Afzali, K. S. Kirkley, and R. B. Tjalkens, "Glial-neuronal signaling mechanisms underlying the neuroinflammatory effects of manganese," *Journal of Neuroinflammation*, vol. 15, no. 1, p. 324, 2018.

[126] J. Kim, E. Pajarillo, A. Rizor et al., "LRRK2 kinase plays a critical role in manganese-induced inflammation and apoptosis in microglia," *PLoS One*, vol. 14, no. 1, article e0210248, 2019.

[127] P. Zhang, A. Hatter, and B. Liu, "Manganese chloride stimulates rat microglia to release hydrogen peroxide," *Toxicology Letters*, vol. 173, no. 2, pp. 88–100, 2007.

[128] K. S. Kirkley, K. A. Popichak, M. F. Afzali, M. E. Legare, and R. B. Tjalkens, "Microglia amplify inflammatory activation of astrocytes in manganese neurotoxicity," *Journal of Neuroinflammation*, vol. 14, no. 1, p. 99, 2017.

[129] S. Sarkar, D. Rokad, E. Malovic et al., "Manganese activates NLRP3 inflammasome signaling and propagates exosomal release of ASC in microglial cells," *Science Signaling*, vol. 12, no. 563, article eaat9900, 2019.

[130] X. Zhao, L. Yin, Y. Wu et al., "Manganese induces neuroinflammation via NF-$\kappa$B/ROS NLRP3 pathway in rat brain striatum and HAPI cells," *Molecular & Cellular Toxicology*, vol. 15, pp. 173–183, 2019.

[131] S. Sarkar, E. Malovic, D. S. Harischandra et al., "Manganese exposure induces neuroinflammation by impairing mitochondrial dynamics in astrocytes," *Neurotoxicology*, vol. 64, pp. 204–218, 2018.

[132] S. A. Liddelow, K. A. Guttenplan, L. E. Clarke et al., "Neurotoxic reactive astrocytes are induced by activated microglia," *Nature*, vol. 541, pp. 481–487, 2017.

[133] A. Bernaus, S. Blanco, and A. Sevilla, "Glia crosstalk in neuroinflammatory diseases," *Frontiers in Cellular Neuroscience*, vol. 14, p. 209, 2020.

[134] K. Erikson and M. Aschner, "Manganese causes differential regulation of glutamate transporter (GLAST) taurine transporter and metallothionein in cultured rat astrocytes," *Neurotoxicology*, vol. 23, no. 4-5, pp. 595–602, 2002.

[135] K. M. Erikson, R. L. Suber, and M. Aschner, "Glutamate/aspartate transporter (GLAST), taurine transporter and metallothionein mRNA levels are differentially altered in astrocytes exposed to manganese chloride, manganese phosphate or manganese sulfate," *Neurotoxicology*, vol. 23, no. 3, pp. 281–288, 2002.

[136] W. Zheng, Q. Zhao, V. Slavkovich, M. Aschner, and J. H. Graziano, "Alteration of iron homeostasis following chronic exposure to manganese in rats[1]," *Brain Research*, vol. 833, no. 1, pp. 125–132, 1999.

[137] S. Weber, D. C. Dorman, L. H. Lash, K. Erikson, K. E. Vrana, and M. Aschner, "Effects of manganese (Mn) on the developing rat brain: oxidative-stress related endpoints," *Neurotoxicology*, vol. 23, no. 2, pp. 169–175, 2002.

[138] A. W. Dobson, S. Weber, D. C. Dorman, L. K. Lash, K. M. Erikson, and M. Aschner, "Oxidative stress is induced in the rat brain following repeated inhalation exposure to manganese sulfate," *Biological Trace Element Research*, vol. 93, no. 1-3, pp. 113–126, 2003.

[139] K. M. Erikson, D. C. Dorman, L. H. Lash, A. W. Dobson, and M. Aschner, "Airborne manganese exposure differentially affects end points of oxidative stress in an age- and sex-dependent manner," *Biological Trace Element Research*, vol. 100, no. 1, pp. 049–062, 2004.

[140] M. Morello, P. Zatta, P. Zambenedetti et al., "Manganese intoxication decreases the expression of manganoproteins in the rat basal ganglia: an immunohistochemical study," *Brain Research Bulletin*, vol. 74, no. 6, pp. 406–415, 2007.

[141] B. Xu, Z. F. Xu, and Y. Deng, "Protective effects of MK-801 on manganese-induced glutamate metabolism disorder in rat striatum," *Experimental and Toxicologic Pathology*, vol. 62, no. 4, pp. 381–390, 2010.

[142] M. Sidoryk-Wegrzynowicz, E. Lee, J. Albrecht, and M. Aschner, "Manganese disrupts astrocyte glutamine transporter expression and function," *Journal of Neurochemistry*, vol. 110, no. 3, pp. 822–830, 2009.

# AMP-ACTIVATED PROTEIN KINASE ACTIVATION IN GLIAL CELLS EXPOSED TO MANGANESE

Jazmín Soto-Verdugo[1], Luisa Clara Regina Hernández-Kelly[1], Arturo Ortega[1]

[1]Centro de Investigación y de Estudios Avanzados del Instituto Politécnico Nacional, Toxicology Department, Mexico City, Mexico.

AMPK is an energy-sensing kinase that downregulates anabolic processes, such as protein synthesis to help to replenish the ATP stores in an energy-deprived cell. Thr$^{172}$ AMPK phosphorylation represents its activation hallmark, once phosphorylated, AMPK can disrupt translation through the inhibition of the mTOR signaling cascade inducing metabolic reprogramming. On the other hand, glial cells provide structural, trophic, and metabolic support to neurons. Glial cells play an active role in adult neurogenesis, regulation of synaptogenesis, and synaptic plasticity. Disturbances in glial physiology can lead to neurological disorders, including neurotoxicity-related diseases. In this regard, in high doses, Mn, an essential trace element, exerts serious oxidative and neurotoxic effects. Its main toxicity molecular mechanisms are mitochondrial impairment and metabolic stress. Hence, we decided to investigate the effect of short-term Mn exposure in signaling pathways involved in metabolic homeostasis. To this end, confluent Bergmann glial cells were exposed to 50-500 μM $MnCl_2$ for different periods, and the phosphorylation pattern of AMPK, and 4E-BP1 were measured. AMPK showed increased phosphorylation after 30 min of exposure to $MnCl_2$. These effects appear to be regulated by the Akt pathway since the inhibition of this protein with Akt IV, prevents AMPK phosphorylation after 30 min of exposure to $Mn^{2+}$, but after 60 min an opposite effect is present. Interestingly, the Mn treatment augmented 4E-BP1 phosphorylation up to 15 min of exposure but after 30 min, the effect was diminished, which was prevented by mTOR inhibition. Altogether, these results strongly suggest differential crosstalk between the AMPK and mTOR pathways upon $Mn^{2+}$ exposure. Furthermore, this metal exerts a biphasic effect on protein translation that might be related to a reduction in ATP levels and the resulting change in the protein *repertoire*. In conclusion, our findings strengthen the idea of the critical role of glial cell metabolism in neurotoxicity development.

# CROSSTALK BETWEEN AMPK AND AKT SIGNALING PATHWAYS IN GLIAL CELLS AFTER AN ACUTE NEUROTOXIC INSULT

Jazmin Soto-Verdugo, Mireya Castillo-Montesinos, Luis Mario Sánchez-Palestino, Jessica Gabriela Tovar-Ramírez, Luisa Clara Regina Hernández-Kelly, Arturo Ortega.

Centro de Investigación y de Estudios Avanzados del Instituto Politécnico Nacional, Toxicology Department, Mexico City, Mexico.

Glial cells provide structural, trophic, and metabolic support to neurons. These cells play an active role in adult neurogenesis, regulation of synaptogenesis, and synaptic plasticity. Disturbances in glial physiology can lead to neurological disorders, including neurotoxicity-related diseases. In this regard, in high doses, Manganese (Mn), an essential trace element, exerts serious oxidative and neurotoxic effects. Its main toxicity molecular mechanisms are mitochondrial impairment and metabolic stress. On the other hand, AMP-activated protein kinase (AMPK) and protein kinase B (Akt) are two primary effectors in response to metabolic stress. AMPK acts as an energy-sensing factor that downregulates anabolic processes, such as protein synthesis by inhibiting mTORC1 signaling to ameliorate the ATP deficit. Meanwhile, Akt promotes cell survival through apoptosis inhibition and protein synthesis up-regulation. In addition, AMPK and AKT also regulate their mutual phosphorylation directly or indirectly. Hence, we decided to investigate the effect of short-term Mn exposure in signaling pathways involved in metabolic homeostasis. To this end, we decided to use Bergmann glial cells (BGC) primary cultures, a well-established model of glial/neuronal interactions. Confluent BGC monolayers were exposed to 50-500 μM MnCl2 for different time periods, the phosphorylation patterns of AMPK and Akt, and the eukaryotic translation initiation factor 4E-binding protein 1 (4E-BP1) as a downstream effector, was measured. A time and dose-dependent increase in the phosphorylation status of these proteins was found. AMPK showed an increase in Thr172 phosphorylation after 30 min of exposure to MnCl2 (200 to 500 μM). These effects appear to be regulated by the Akt pathway since the inhibition of this protein with Akt IV, prevents AMPK phosphorylation after 30 min of exposure to Mn2+, but after 60 min an opposite effect is present with no effects at shorter exposure times. Interestingly, Akt phosphorylation increased as early as 5 min in a concentration-dependent manner returning to basal levels after 30 min. Mn treatment augmented 4E-BP1 phosphorylation up to 15 min of exposure, and this effect was prevented by mTORC1 inhibition. These results strongly suggest that differential crosstalk between the AMPK and PI3K/Akt pathways upon Mn2+ exposure. Furthermore, this metal exerts a biphasic effect on protein translation that might be related to a reduction in ATP levels and the resulting change in the protein repertoire of these cells. In conclusion, our findings strengthen the idea of the critical role of glial cells in neurotoxicity development.

# SHORT-TERM EXPOSURE TO MANGANESE MODIFIES PROTEIN TRANSLATION VIA PI3K/AKT SIGNALING IN GLIAL CELLS

Jazmin Soto Verdugo, Mireya Castillo-Montesinos, Luis Mario Sánchez-Palestino, Jessica Gabriela Tovar-Ramírez, Luisa Clara Regina Hernández-Kelly, Arturo Ortega

Centro de Investigación y de Estudios Avanzados del Instituto Politécnico Nacional, Toxicology, Mexico City, Mexico.

Glutamate (Glu), the major excitatory neurotransmitter in the nervous system, activates a wide variety of signal transduction cascades involved in the regulation of protein synthesis. Although protein translation is an exquisitely regulated process, translational dysregulation has been observed in many neurodegenerative disorders. Manganese (Mn) is an essential trace element, that in high doses exerts serious oxidative and neurotoxic effects. An established consequence of Mn neurotoxicity is the disruption of the glutamate/glutamine (Glu/Gln) cycle, leading to an excitotoxic insult. The molecular mechanisms mediating Mn-induced neurotoxicity, particularly in the context of the Glu/Gln cycle, are not yet fully understood. Hence, we decided to investigate the effect of Mn short-term exposure in signaling pathways involved in protein synthesis, such as the phosphatidylinositol 3 kinase (PI3K)/protein kinase B (Akt) cascade that regulates the Glu/Gln shuttle. To this end, we decided to use Bergmann glial cells (BGC) primary cultures, a well-established model of glial/neuronal interactions. Confluent BGC monolayers were exposed to $MnCl_2$ 50-500 μM for different periods and the phosphorylation patterns of Akt, the eukaryotic translation initiation factor 4E-binding protein 1 (4E-BP1), as well as the AMP-activated protein kinase (AMPK), were measured. A time and dose-dependent increase in the phosphorylation status of these proteins was found. An increase in Akt phosphorylation was observed as early as 5 min in a concentration-dependent manner. Pharmacological inhibition of PI3K and the sodium/calcium exchanger blocked these effects. Furthermore, Mn treatment augmented 4E-BP1 phosphorylation up to 15 min of exposure, and this effect was depleted by inhibition of mTORC1. The Mn-induced increase of AMPK phosphorylation suggests that Mn could exert a biphasic effect in protein synthesis that might be linked to a reduction in ATP levels and the resulting change in the protein repertoire of these cells. These findings strengthen the idea of the critical role that glial cells have in neurotoxicity development.

## WTH11-32

**3D ultrastructural morphology of mouse astrocytes in Alzheimer's disease**

A. Schober, J. Benjamin Kacerovsky, C. Salmon, N. Alivodej, A. Zhou, B. Phillips, T. Tibuleac, K. Murai

*Research Institute of McGill University Health Center, Centre for Research in Neuroscience, Montreal, Canada*

Astrocytes have long been simplistically characterized as a uniform cell population that take on the morphology of either protoplasmic or fibrous. However, emerging evidence indicates that astrocytes comprise a highly complex cell population with diverse morphology and function in both the healthy and diseased brain. Astrocytes have recently been implicated to play a major role in neurodegenerative diseases, including Alzheimer's disease (AD), however the highly specialized anatomical properties that are changed in these cells remains poorly understood. To better understand the morphology of astrocytes in normal and AD mice, we used a multi-level imaging approach with structured illumination microscopy (SIM) and focused ion beam high-resolution scanning electron microscopy (FIB-SEM). Both imaging techniques allow us to visualize astrocyte morphology at the subcellular resolution. Using SIM, we are able to not only visualize the complex branching pattern of whole astrocytes, but also to map the distribution of mitochondria throughout the whole cell. In order to further investigate astrocyte morphology in finer detail, we utilized FIB-SEM to three-dimensionally reconstruct astrocyte processes as well as their organelles throughout sections of brain tissue. Using both SIM and FIB-SEM allowed us to quantitatively compare the surface structure and organelle ultrastructure of astrocyte sub-compartments as well as to asses changes in healthy and diseased tissue. The data provided by these imaging techniques provide an important structural framework for understanding how the brain is organized in not only normal tissue, but also during Alzheimer's Disease and how this organization within astrocytes may relate to brain function.

## WTH11-33

**Modafinil regulates glutamine synthetase via PI3K-AKT signalling pathway in cerebellum**

J. Silva, L. Méndez, E. Bejarano-Pérez, L. C. H. Hérnandez-Kelly, A. Ortega

*Centro de Investigacion y de Estudios Avandos del IPN, Department of Toxicology, Mexico city, Mexico*

Glutamate is the major excitatory transmitter in the Central Nervous System (CNS) of vertebrates, exerts its actions through the activation of specific membrane receptors expressed in neurons and glial cells. Over-stimulation of glutamatergic receptors results in neuronal death, phenomena known as excitotoxicity. Extracellular glutamate levels are tightly regulated by a family high-affinity uptake systems expressed in neurons and glial cells. Most of the uptake process occurs in the glial compartment and is part of a biochemical glia/neuronal coupling known as the glutamate/glutamine shuttle by which this amino acid is recycled. Once internalized into glial cells, glutamate is metabolized to glutamine *via* Glutamine synthetase (GS) to be released to the vicinity of the presynaptic terminal, which takes it up and converts it back to glutamate, completing the cycle. Inhibition of GS blocks glutamatergic transmission. Among the great variety of CNS stimulants, modafinil is widely used as a wakefulness agent recommended for the treatment of excessive daytime sleepiness, fatigue, and impaired cognition. Despite the fact that the mechanism of action of this stimulant is still unclear, it increases glutamate extracellular levels. To establish a plausible involvement of glutamine synthetase in the effects of modafinil, we used the model of chick cerebellar Bergmann glia primary cultures. Acute treatment with modafinil results in an increase in GS activity as determined by g-glutamyl hydroxamate production. Moreover, using a PI3K block, we can determinate the participation of that signaling pathway in effect of modafinil. These results strengthen the notion of an important role of glial cells in glutamate-dependent neurotransmission through the regulation of its compulsory glia-mediated turnover.

## WTH11-35

**Exposure to manganese induces PI3K/AKT signaling in bergmann glial cells**

J. S. Verdugo, M. Castillo-Montesinos, L. M. Sánchez-Palestino, J. G. Tovar-Ramírez, L. C. R. Hernández-Kelly, A. Ortega

*Centro de Investigación y de Estudios Avanzados del Instituto Politécnico Nacional, Toxicología, Mexico City, Mexico*

Manganese (Mn) is an essential trace element that in high doses triggers serious oxidative and neurotoxic effects. An established consequence of Mn neurotoxicity is the disruption of the glutamate/glutamine (Glu/Gln) cycle, leading to an excitotoxic insult. Glu exerts its actions through the activation of specific plasma membrane receptors and transporters present in neurons and glial cells. Their over-activation is the biochemical hallmark of neuronal and oligodendrocyte cell death. The molecular mechanisms mediating Mn-induced neurotoxicity, particularly in the context of the Glu/Gln cycle, have yet to be completely understood. Hence, we decided to investigate the effect of Mn short-term exposure in signaling pathways, such as the phosphatidylinositol 3 kinase (PI3K)/protein kinase B (Akt) cascade that regulate the Glu/Gln shuttle in Bergmann glial cells (BGC) primary cultures, a well-established model of glial/neuronal interactions. Confluent BGC monolayers were exposed to subtoxic concentrations of Mn ($MnCl_2$: 50-500 μM) different time periods. Akt, as well as the eukaryotic translation initiation factor 4E-binding protein 1 (4E-BP1) phosphorylation patterns, were evaluated. Mn exposure increased Akt phosphorylation as early as 5 min exposure and lasted for 30 min in a concentration-dependent manner. Pharmacological PI3K inhibition blocked these effects. Also, the inhibition of the sodium-calcium exchanger diminished Akt phosphorylation induced by Mn. Finally, Mn treatment (200 μM) augmented 4E-BP1 phosphorylation after 10 to 30 min of exposure. Overall, these findings suggest that an altered intracellular PI3K/Akt signaling may represent an early event in Mn toxic mechanisms and suggest that protein synthesis could be severely affected by Mn. These results strengthen the idea of the critical role that glial cells have in neurotoxicity development.

# SHORT-TERM EXPOSURE TO MANGANESE ON BERGMANN GLIAL CELLS: RELEVANCE TO THE GLU/GLN CYCLE

Soto-Verdugo J., Hernández-Kelly L., López-Bayghen E., Ortega A.

Laboratory of Neurotoxicology, Toxicology Department, Cinvestav-IPN. Mexico City, Mexico.

Glutamate (Glu), the main excitatory neurotransmitter in the mammalian brain, it is cleared from the synaptic cleft by a family of sodium dependent Glu transporters. Inside the glial cell, it is metabolized by glutamine (Gln) synthetase to Gln and released to the neurons through sodium-dependent neutral amino acid carriers of the N system. Gln is taken up by neurons completing the Glu/Gln cycle. Bergmann glial cells (BGC) are a type of specialized radial glia that reside in the cerebellum. In this context, recent studies have shown that one of the targets for manganese accumulation is the cerebellum. Manganese (Mn) is an essential trace element that in high doses can exert serious oxidative and neurotoxic effects. Mn neurotoxicity is characterized by astrocytic impairment both in the expression and activity of Gln transporters. The N system is a major facilitator of Gln efflux from glial cells. Also, altered intracellular mitogen-activated protein kinases (MAPK) signaling pathways represent an early event linked to Mn exposure in the immature brain. The molecular mechanisms mediating Mn-induced neurotoxicity, particularly in the context of the Glu/Gln cycle, have yet to be completely understood. Hence, we decided to investigate the role of Mn short-term exposure on BGC, as a well-established model of glia/neuronal interactions. To thie end, primary cultures of chick cerebellar BGC were exposed to subtoxic concentrations of Mn (MnCl$_2$; 50-500 µM) from 15 minutes to 2 hours. The [$^3$H]-L-Gln release, as well as the extracellular signal-regulated kinase (ERK) 1/2 phosphorylation pattern were evaluated. Mn treatment caused a reduction in the Gln release after, although this effect was not sustained under a background of aspartate (Asp). Mn exposure increased ERK1/2 phosphorylation, from the lowest time and concentration tested. The effect was not potentiated on a co-exposure with Asp. Overall, these findings suggest that altered intracellular MAPKs signaling pathways may represent an early event concerning the effects of Mn and that the disruption of Glu homeostasis may lead to impairment of the glutamatergic neurotransmission.

# FICHA DE DATOS DE SEGURIDAD

## SECCIÓN 1. Identificación de la sustancia o la mezcla y de la sociedad o la empresa

### 1.1 Identificadores del producto

Nombre del producto : **MANGANESO(II) CLORURO PARA SINTESIS**

| | | |
|---|---|---|
| Referencia | : | 8.05930 |
| Artículo número | : | 805930 |
| Marca | : | Millipore |
| No. CAS | : | 7773-01-5 |

### 1.2 Usos pertinentes identificados de la sustancia o de la mezcla y usos desaconsejados

Usos identificados : Producto químico para síntesis

### 1.3 Datos del proveedor de la ficha de datos de seguridad

Compañía : Merck, S.A de C.V
Calle 5 No. 7 C.P.
53370 NAUCALPAN DE JUÁREZ, EDO. DE MÉXICO.
MEXICO

Teléfono : +52 (55)-2122-1600
Fax : +52 (55)-2122-1703

### 1.4 Teléfono de emergencia

Teléfono de Urgencia : 800-00-214-00 (SETIQ)
800-681-9531 (CHEMTREC)
(55) 55-59-15-88

## SECCIÓN 2. Identificación de los peligros

### 2.1 Clasificación de la sustancia o de la mezcla

**Clasificación SGA de acuerdo con 29 CFR 1910 (OSHA HCS).**

Toxicidad aguda, Oral (Categoría 3), H301
Lesiones oculares graves (Categoría 1), H318
Toxicidad específica en determinados órganos - exposiciones repetidas (Categoría 2), Cerebro, H373
Toxicidad específica en determinados órganos - exposiciones repetidas, Inhalación (Categoría 2), Cerebro, H373
Peligro a corto plazo (agudo) para el medio ambiente acuático (Categoría 2), H401
Peligro a largo plazo (crónico) para el medio ambiente acuático (Categoría 2), H411

Para el texto integro de las Declaraciones-H mencionadas en esta sección, véase la Sección 16.

### 2.2 Elementos de las etiquetas del SGA, incluidos los consejos de prudencia

| | Pictograma |  |
|---|---|---|

| | |
|---|---|
| Palabra de advertencia | Peligro |

**Indicación(es) de peligro**

| | |
|---|---|
| H301 | Tóxico en caso de ingestión. |
| H318 | Provoca lesiones oculares graves. |
| H373 | Puede provocar daños en los órganos (Cerebro) tras exposiciones prolongadas o repetidas. |
| H373 | Puede provocar daños en los órganos (Cerebro) tras exposiciones prolongadas o repetidas si se inhala. |
| H411 | Tóxico para los organismos acuáticos, con efectos nocivos duraderos. |

**Declaración(es) de prudencia**

| | |
|---|---|
| P260 | No respirar el polvo/ el humo/ el gas/ la niebla/ los vapores/ el aerosol. |
| P264 | Lavarse la piel concienzudamente tras la manipulación. |
| P270 | No comer, beber ni fumar durante su utilización. |
| P273 | Evitar su liberación al medio ambiente. |
| P280 | Llevar equipo de protección para los ojos/ la cara. |
| P301 + P310 + P330 | EN CASO DE INGESTIÓN: Llamar inmediatamente a un CENTRO DE TOXICOLOGÍA/ médico. Enjuagarse la boca. |
| P305 + P351 + P338 + P310 | EN CASO DE CONTACTO CON LOS OJOS: Enjuagar con agua cuidadosamente durante varios minutos. Quitar las lentes de contacto cuando estén presentes y pueda hacerse con facilidad. Proseguir con el lavado. Llamar inmediatamente a un CENTRO DE TOXICOLOGÍA/ médico. |
| P314 | Consultar a un médico en caso de malestar. |
| P391 | Recoger el vertido. |
| P405 | Guardar bajo llave. |
| P501 | Eliminar el contenido/ el recipiente en una planta de eliminación de residuos autorizada. |

**2.3   Peligros no clasificados de otra manera** - ninguno(a)

---

**SECCIÓN 3. Composición/información sobre los componentes**

**3.1   Sustancias**

| | | |
|---|---|---|
| Formula | : | MnCl2 |
| Peso molecular | : | 125.84 g/mol |
| No. CAS | : | 7773-01-5 |
| No. CE | : | 231-869-6 |

| Componente | Clasificación | Concentración |
|---|---|---|
| **Manganeso(II) cloruro** | | |
| | Acute Tox. 3; Eye Dam. 1; STOT RE 2; Aquatic Acute 2; Aquatic Chronic 2; H301, H318, H373, H373, H401, H411 | <= 100 % |

MilliporeSigma

Para el texto integro de las Declaraciones-H mencionadas en esta sección, véase la Sección 16.

---

## SECCIÓN 4. Primeros auxilios

### 4.1 Descripción de los primeros auxilios

**Recomendaciones generales**
Mostrar esta ficha de seguridad al doctor que esté de servicio.

**Si es inhalado**
Tras inhalación: aire fresco. Llamar al médico.

**En caso de contacto con la piel**
En caso de contacto con la piel: Quitar inmediatamente todas las prendas contaminadas. Aclararse la piel con agua/ducharse. Consultar a un médico.

**En caso de contacto con los ojos**
Tras contacto con los ojos: aclarar con abundante agua. Llamar inmediatamente al oftalmólogo. Retirar las lentillas.

**Por ingestión**
Tras ingestión: hacer beber agua (máximo 2 vasos). Consultar inmediatamente al médico. Solamente en casos excepcionales, si no es posible la asistencia médica dentro de una hora, provocar el vómito (solamente en personas plenamente despiertas y conscientes), administrar carbón activo (20 - 40 g en suspensión al 10%) y consultar al médico lo más rápidamente posible.

### 4.2 Principales síntomas y efectos, agudos y retardados
Los síntomas y efectos más importantes conocidos se describen en la etiqueta (ver sección 2.2) y / o en la sección 11

### 4.3 Indicación de toda atención médica y de los tratamientos especiales que deban dispensarse inmediatamente
Sin datos disponibles

---

## SECCIÓN 5. Medidas de lucha contra incendios

### 5.1 Medios de extinción

**Medios de extinción apropiados**
Usar medidas de extinción que sean apropiadas a las circunstancias del local y a sus alrededores.

**Medios de extinción no apropiados**
No existen limitaciones de agentes extinguidores para esta sustancia/mez cla.

### 5.2 Peligros específicos derivados de la sustancia o la mezcla
Gas cloruro de hidrógeno
Óxidos de Manganese/manganese
No combustible.
El fuego puede provocar emanaciones de:
Gas cloruro de hidrógeno
Posibilidad de formación de vapores peligrosos por incendio en el entorno.

124

## 5.3 Recomendaciones para el personal de lucha contra incendios

Permanencia en el área de riesgo sólo con sistemas de respiración artificiales e independientes del ambiente. Protección de la piel mediante observación de una distancia de seguridad y uso de ropa protectora adecuada .

## 5.4 Otros datos

Reprimir los gases/vapores/neblinas con agua pulverizada. Impedir la contaminación de las aguas superficiales o subterráneas por el agua que ha servido a la extinción de incendios.

---

## SECCIÓN 6. Medidas en caso de vertido accidental

## 6.1 Precauciones personales, equipo de protección y procedimientos de emergencia

Indicaciones para el personal que no forma parte de los servicios de emergencia: Evitar la inhalación de polvo. Evitar el contacto con la sustancia. Asegúrese una ventilación apropiada. Evacúe el área de peligro, respete los procedimientos de emergencia, con sulte con expertos.
Equipo de protección individual, ver sección 8.

## 6.2 Precauciones relativas al medio ambiente

No dejar que el producto entre en el sistema de alcantarillado.

## 6.3 Métodos y material de contención y de limpieza

Cubra las alcantarillas. Recoja, una y aspire los derrames. Observe posibles restricciones de materiales (véanse indicaciones en las secciónes 7 o 10). Recoger con precaución, proceder a su eliminación. Aclarar. Evitar le formación de polvo.

## 6.4 Referencia a otras secciones

Para eliminación de desechos ver sección 13.

---

## SECCIÓN 7. Manipulación y almacenamiento

## 7.1 Precauciones para una manipulación segura

### Consejos para una manipulación segura

Trabajar bajo campana extractora. No inhalar la sustancia/la mezcla.

### Medidas de higiene

Sustituir la ropa contaminada. Es recomendable una protección preventiva de la piel. Lavar las manos al término del trabajo.
Ver precauciones en la sección 2.2

## 7.2 Condiciones de almacenamiento seguro, incluidas posibles incompatibilidades

### Condiciones de almacenamiento

No usar recipientes de metálicos o metales ligeros.
Bien cerrado. Seco. Manténgase el recipiente en un lugar bien ventilado. Mantenerlo encerrado en una zona unicamente accesible por las personas autorizadas o calificadas.

Temperatura de almacenaje recomendada indicada en la etiqueta del producto.

### Clase de almacenamiento

Clase de almacenamiento (TRGS 510): 6.1D: Materiales tóxicos peligrosos o materiales peligrosos que causan efectos crónicos/No combustibles, tóxicos agudos Cat.3

## 7.3 Usos específicos finales

Aparte de los usos mencionados en la sección 1.2 no se estipulan otros usos específicos

MilliPORe
SiGMa

125

**8.1 Parámetros de control**

**Componentes con valores límite ambientales de exposición profesional.**

| Componente | No. CAS | Valor | Parámetros de control | Base |
|---|---|---|---|---|
| Manganeso(II) cloruro | 7773-01-5 | C | 5 mg/m3 | Límites de Exposición Ocupacional (OSHA),EE.UU - Tabla Z-1 Límites para los contaminantes del aire |
| | | TWA | 0.1 mg/m3 | Valores límite (TLV) de la ACGIH,USA |
| | Observaciones | No clasificados como cancerigenos en humanos | | |
| | | TWA | 0.02 mg/m3 | Valores límite (TLV) de la ACGIH,USA |
| | | No clasificados como cancerigenos en humanos | | |
| | | C | 5 mg/m3 | OSHA - Tabla Z-1 Límites para los contaminantes del aire - 1910.1000, EE.UU. |
| | | TWA | 1 mg/m3 | Límites de exposición recomendados de NIOSH, EE.UU. |
| | | ST | 3 mg/m3 | Límites de exposición recomendados de NIOSH, EE.UU. |
| | | PEL | 0.2 mg/m3 | California: Límites de exposición permisibles para contaminantes químicos Title 8, Article 107) |

**8.2 Controles de la exposición**

**Controles técnicos apropiados**
Sustituir la ropa contaminada. Es recomendable una protección preventiva de la piel.
Lavar las manos al término del trabajo.

**Protección personal**

**Protección de los ojos/ la cara**
Use equipo de protección para los ojos probado y aprobado según las normas gubernamentales correspondientes, tales como NIOSH (EE.UU.) o EN 166 (UE). Gafas de seguridad ajustadas al contorno del rostro

**Protección de la piel**
Esta recomendación solo es válida para el producto mencionado en la ficha de datos de seguridad, suministrado por nosotros y para el fin indicado. Al disolver o mezclar en otras sustancias y cuando las condiciones difieran de las indicadas en EN374, debe dirigirse al suministrador de guantes con distintivo CE (por ejem. KCL GmbH, D-36124 Eichenzell, Internet: www.kcl.de)
Sumerción
Material: Caucho nitrílo
espesura minima de capa: 0.11 mm
Tiempo de penetración: 480 min
Material probado:KCL 741 Dermatril® L

Esta recomendación solo es válida para el producto mencionado en la ficha de datos de seguridad, suministrado por nosotros y para el fin indicado. Al disolver o mezclar en otras sustancias y cuando las condiciones difieran de las indicadas en EN374, debe dirigirse al suministrador de guantes con distintivo CE (por ejem. KCL GmbH, D-36124 Eichenzell, Internet: www.kcl.de)
Salpicaduras
Material: Caucho nitrílo
espesura minima de capa: 0.11 mm
Tiempo de penetración: 480 min
Material probado:KCL 741 Dermatril® L

**Protección Corporal**
prendas de protección

**Protección respiratoria**
necesaria en presencia de polvo.
Nuestras recomendaciones sobre protección respiratoria se basan en las normas siguientes: DIN EN 143, DIN 14387 y otras normas relativas al uso de la protección respiratoria usada.

**Control de exposición ambiental**
No dejar que el producto entre en el sistema de alcantarillado.

---

## SECCIÓN 9. Propiedades físicas y químicas

### 9.1 Información sobre propiedades físicas y químicas básicas

| | | |
|---|---|---|
| a) | Aspecto | Forma: escamas |
| | | Color: rosa |
| b) | Olor | Sin datos disponibles |
| c) | Umbral olfativo | Sin datos disponibles |
| d) | pH | 5.5 a 25 g/l a 20 °C (68 °F) |
| e) | Punto de fusión/ punto de congelación | Punto/intervalo de fusión: 652 °C (1206 °F) |
| f) | Punto inicial de ebullición e intervalo de ebullición | 1,190 °C 2,174 °F a 1,013 hPa |
| g) | Punto de inflamación | Sin datos disponibles |
| h) | Tasa de evaporación | Sin datos disponibles |
| i) | Inflamabilidad (sólido, gas) | El producto no es inflamable. |
| j) | Inflamabilidad superior/inferior o límites explosivos | Sin datos disponibles |
| k) | Presión de vapor | Sin datos disponibles |
| l) | Densidad de vapor | Sin datos disponibles |
| m) | Densidad | 2.980 gcm3 |
| | Densidad relativa | Sin datos disponibles |
| n) | Solubilidad en agua | 757 g/l a 20 °C (68 °F) |

127

| o) | Coeficiente de reparto n-octanol/agua | Sin datos disponibles |
| p) | Temperatura de auto-inflamación | Sin datos disponibles |
| q) | Temperatura de descomposición | Sin datos disponibles |
| r) | Viscosidad | Sin datos disponibles |
| s) | Propiedades explosivas | Sin datos disponibles |
| t) | Propiedades comburentes | ningún |

**9.2 Otra información de seguridad**
Sin datos disponibles

---

## SECCIÓN 10. Estabilidad y reactividad

**10.1 Reactividad**
Sin datos disponibles

**10.2 Estabilidad química**
El producto es químicamente estable bajo condiciones normales (a tempera tura ambiental).

**10.3 Posibilidad de reacciones peligrosas**
Sin datos disponibles

**10.4 Condiciones que deben evitarse**
Evitar la humedad.
información no disponible

**10.5 Materiales incompatibles**
Cinc, Óxidos de sodio/sodio, Potasio, Ácidos fuertes, Peróxido de hidrógeno

**10.6 Productos de descomposición peligrosos**
En caso de incendio: véase sección 5

---

## SECCIÓN 11. Información toxicológica

**11.1 Información sobre los efectos toxicológicos**

**Toxicidad aguda**
DL50 Oral - Ratón - macho - 1,330 mg/kg
DL50 Oral - Rata - hembra - 236 mg/kg
Inhalación: Sin datos disponibles
Cutáneo: Sin datos disponibles
Sin datos disponibles

**Corrosión o irritación cutáneas**
Piel - Conejo
Resultado: No irrita la piel - 4 h

Millipore - 8.05930

128

(Directrices de ensayo 404 del OECD)

**Lesiones o irritación ocular graves**
Ojos - Conejo
Resultado: irritante
(Directrices de ensayo 405 del OECD)

**Sensibilización respiratoria o cutánea**
Local lymph node assay (LLNA) - Ratón
Resultado: negativo
(Directrices de ensayo 429 del OECD)

**Mutagenicidad en células germinales**
Sin datos disponibles

**Carcinogenicidad**
Sin datos disponibles

IARC:     No se identifica ningún componente de este producto, que presente niveles mayores que o igual a 0,1% como agente carcinógeno humano probable, posible o confirmado por la (IARC) Agencia Internacional de Investigaciones sobre Carcinógenos.

NTP:      En este producto no se identifica ningún componente, que presente niveles mayores que o iguales a 0.1%, como agente carcinógeno conocido o anticipado por el (NTP) Programa Nacional de Toxicología.

OSHA:     Ningún componente de este producto está presente en niveles superiores o iguales al 0,1 % por lo que no se encuentra en la lista de OSHA de carcinógenos regulados.

**Toxicidad para la reproducción**
Sin datos disponibles
Sin datos disponibles

**Toxicidad específica en determinados órganos - exposición única**
Sin datos disponibles

**Toxicidad específica en determinados órganos - exposiciones repetidas**
Puede provocar daños en los órganos tras exposiciones prolongadas o repetidas. - Cerebro

**Peligro de aspiración**
Sin datos disponibles

## 11.2 Información Adicional

Se observó un descenso de la fertilidad entre los sujetos masculinos expuestos a polvos de manganeso. El envenenamiento crónico por manganeso afecta principalmente al sistema nervioso central. Entre los primeros síntomas figuran languidez, sensación de sueño y debilidad en las piernas. En los casos más avanzados se han descrito aspecto inexpresivo de la cara, como de máscara, trastornos emocionales como risa incontrolable y marcha espástica con tendencia a las caídas al andar. Se ha observado una alta incidencia de neumonía en trabajadores expuestos a polvo o humo de algunos compuestos de manganeso., Según nuestras informaciones, creemos que no se han investigado adecuadamente las propiedades químicas, físicas y toxicológicas.

## SECCIÓN 12. Información ecológica

### 12.1 Toxicidad

MilliPORE
SiGMA

129

| Toxicidad para las dafnias y otros invertebrados acuáticos | CE50 - Daphnia magna (Pulga de mar grande) - 9.8 mg/l - 48 h |
|---|---|
| Toxicidad para las algas | Inhibición del crecimiento CE50 - Pseudokirchneriella subcapitata - 3.83 mg/l - 72 h<br>(Directrices de ensayo 201 del OECD) |

**12.2 Persistencia y degradabilidad**
Sin datos disponibles

**12.3 Potencial de bioacumulación**
Sin datos disponibles

**12.4 Movilidad en el suelo**
Sin datos disponibles

**12.5 Resultados de la valoración PBT y mPmB**
La valoración de PBT / mPmB no está disponible ya que la evaluación de la seguridad química no es necesaria / no se ha realizado

**12.6 Otros efectos adversos**
Evitar su liberación al medio ambiente.

---

## SECCIÓN 13. Consideraciones relativas a la eliminación

**13.1 Métodos para el tratamiento de residuos**

### Producto
Los residuos deben eliminarse de acuerdo con normativas locales y nacion a originales. No los mezcle con otros residuos. Maneje los recipientes sucios como el propio producto. Consulte en www.retrologistik.com sobre procesos relativos a la devolución de productos químicos o recipientes, o contáctenos si tiene más preguntas.

---

## SECCIÓN 14. Información relativa al transporte

### DOT (US)
UN number: 3288    Class: 6.1             Packing group: III
Proper shipping name: Toxic solid, inorganic, n.o.s. (manganese(II) chloride)
Reportable Quantity (RQ):
Poison Inhalation Hazard: No

### IMDG
Número ONU: 3288 Clase: 6.1              Grupo de embalaje: III   EMS-No: F-A, S-A
Designación oficial de transporte de las Naciones Unidas: TOXIC SOLID, INORGANIC, N.O.S. (Manganeso(II) cloruro)
Contaminante marino : no
### IATA
Número ONU: 3288 Clase: 6.1             Grupo de embalaje: III
Designación oficial de transporte de las Naciones Unidas: Sólido tóxico, inorgánico, n.e.p. (Manganeso(II) cloruro)

**MilliPORE SiGMa**

130

## SECCIÓN 15. Información reglamentaria

**SARA 302 Componentes**
Este material no contiene componentes con una sección 302 EHS TPQ.

**SARA 313 Componentes**
Los siguientes componentes están sujetos a los niveles de referencia establecidos por SARA Título III, Sección 313:

| | No. CAS | Fecha de revisión |
|---|---|---|
| Manganeso(II) cloruro | 7773-01-5 | 2015-07-08 |

**Massachusetts Right To Know Componentes**
No hay componentes sujetos al Acta de Derecho a Saber de Massachusetts.

## SECCIÓN 16. Otra información

**Otros datos**
La información indicada arriba se considera correcta pero no pretende ser exhaustiva y deberá utilizarse únicamente como orientación. La información contenida en este documento esta basada en el presente estado de nuestro conocimiento y es aplicable a las precauciones de seguridad apropiadas para el producto. No representa ninguna garantía de las propiedades del producto. La Corporación Sigma-Aldrich y sus Compañías Afiliadas, no responderán por ningún daño resultante de la manipulación o contacto con el producto indicado arriba. Dirijase a www.sigma-aldrich.com y/o a los términos y condiciones de venta en el reverso de la factura o de la nota de entrega. Copyright 2020 Sigma-Aldrich Co. LLC. Se autoriza la reproducción en número ilimitado de copias para uso exclusivamente interno.
La marca que aparece en el encabezado y/o el pie de página de este documento puede no coincidir visualmente con el producto adquirido mientras hacemos la transición de nuestra marca. Sin embargo, toda la información del documento relativa al producto permanece sin cambios y coincide con el producto solicitado. Para más información, póngase en contacto con mlsbranding@sial.com

| Versión: 8.5 | Fecha de revisión: 09/11/2021 | Fecha de impresión: 09/11/2021 |
|---|---|---|

MilliPORe SiGMa

131